

DIPARTIMENTO INTERATENEO DI FISICA DELL' UNIVERSITÀ DI BARI
VIA AMENDOLA 173, 70126, BARI

DISSERTATION IN PHYSICS

SATELLITE LASER RANGING
AND GENERAL RELATIVITY

Supervisors **Ph. D.**
L. GUERRIERO, I. CIUFOLINI, E.C. PAVLIS L. IORIO

XIV CICLO 1999-2001

“INTENTIO VERO NOSTRA EST
MANIFESTARE [...] EA, QUE SUNT, SICUT SUNT.”
(In fact our intention is to represent what is as it is)
Friedrich II von Hohenstaufen,
in *De Arte venandi cum avibus*,
< P.I, 3 > < *De intentione* >

Contents

1	Introduction	11
1.1	The Lense-Thirring drag of inertial frames	12
1.2	The gravitomagnetic clock effect	16
1.3	The gravitoelectric pericenter shift	16
1.4	The LARES mission	17
1.5	Conclusions	17
2	The Lense-Thirring effect on the orbit of a test body	18
2.1	Introduction	18
2.2	The gravitomagnetic potential	19
2.3	The rate equations for the Keplerian orbital elements	21
2.4	Secular gravitomagnetic effects on the Keplerian orbital elements: spherical central source	24
2.5	Secular gravitomagnetic effects on the Keplerian orbital elements: non-spherical central source	26
2.6	Figures	32
3	Orbital perturbations induced by solid Earth and ocean tides	33
3.1	Introduction	33
3.2	The tide generating potential	35

3.3	Solid Earth tidal perturbations	40
3.3.1	Discussion of the numerical results	47
3.3.2	The mismodelling in the nodes and the perigee	50
3.3.3	The mean anomaly and the inclination	51
3.4	Tables	52
3.5	Gravitational potential of the ocean Earth tides	58
3.6	Ocean tidal orbital perturbations	64
3.6.1	Discussion of the numerical results	68
3.6.2	Comparison between solid and ocean tidal perturbations	71
3.6.3	The mismodelling in the nodes and the perigee	72
3.6.4	The mean anomaly and the inclination	73
3.7	Tables	75
3.8	Indirect tidal perturbations	79
3.9	Tables	82
3.10	Conclusions	83
4	The impact of the Earth tides on the determination of the Lense-Thirring effect	85
4.1	Introduction	85
4.2	Systematic error due to the zonal tides on the measurement of the Lense-Thirring effect	87
4.3	The simulated residual signal	90
4.4	Sensitivity analysis	93
4.5	The effect of the very long periodic harmonics	96
4.6	The error due to the inclination	99
4.7	Conclusions	100

4.8	Tables	103
4.9	Figures	104
5	The gravitomagnetic clock effect	112
5.1	Introduction	112
5.2	The electromagnetic scenario	113
5.3	The gravitational scenario	115
6	Satellite gravitational orbital perturbations and the gravitomagnetic clock effect	117
6.1	Introduction	117
6.2	The radial error induced by the solid Earth and ocean tides	118
6.3	The azimuthal error induced by the solid Earth and ocean tides	120
6.4	Static geopotential perturbations	122
6.5	Discussion and conclusions	124
6.6	Figures	127
7	Satellite orbital non-gravitational perturbations and the gravitomagnetic clock effect	131
7.1	Introduction	131
7.2	The radial position	133
7.2.1	The radiative perturbations	134
7.2.2	The thermal perturbations	135
7.2.3	Other perturbations	136
7.3	The azimuthal position	136
7.3.1	The radiative perturbations	137
7.3.2	The thermal perturbations	137

7.3.3	Other perturbations	138
7.4	Conclusions	138
8	On the possibility of measuring the PPN parameters β and γ with LAGEOS and LAGEOS II	140
8.1	The relativistic perigee precession of LAGEOS type satellites	143
8.2	The systematic errors	144
8.2.1	Tides and other disturbing harmonics	146
8.2.2	Errors in the inclination	147
8.3	Numerical simulations	148
8.4	Discussion and conclusions	149
8.5	Tables	150
8.6	Figures	151
9	The LARES mission revisited: some alternative scenarios	154
9.1	Introduction	154
9.2	The impact of the even zonal harmonics of the geopotential on the original LARES mission	155
9.3	An alternative LARES scenario	156
9.4	The POLARES	158
9.5	Conclusions	159
9.6	Figures	161
10	Conclusions and recommendations for future work	164
10.1	Summary of the obtained results	164
10.2	Recommendations for future work	168
A	The classical precessions of the node and the perigee	170

A.1	The nodal coefficients	171
A.2	The perigee coefficients	173
A.3	The mismodelled classical precessions of the SLR satellites	176
B	The systematic zonal error	179
C	Some useful parameters used in the text	181
	Acknowledgements	183
	References	184
	Web resources	200

List of Figures

2.1	Keplerian orbital elements for an elliptical orbit	32
4.1	Simulated combined residuals of the nodes of LAGEOS and LAGEOS II and the perigee of LAGEOS II for the gravitomagnetic experiment.	105
4.2	Systematic error induced by Earth's solid and ocean tides on the determination of Lense-Thirring trend over various time spans.	106
4.3	Simulated combined residuals and their fit for the gravitomagnetic experiment.	107
4.4	Error induced by $K_1 l = 3 p = 1$ tide on the detection of the Lense-Thirring trend.	108
4.5	Error induced by SRP(4,241) harmonic on the detection of the Lense-Thirring trend.	109
4.6	Error induced by the 18.6-year tide on the detection of the Lense-Thirring trend.	110
4.7	Percent error induced by the mismodelling in the inclination on the detection of the Lense-Thirring trend.	111
6.1	Errors in the radial and azimuthal positions for the gravitomagnetic clock effect.	127

6.2	Mismodeled azimuthal perturbation induced by the 18.6-year tide for the gravitomagnetic clock effect.	128
6.3	Mismodeled azimuthal rate per revolution induced by the C_{20} geopotential coefficient for the gravitomagnetic clock effect.	129
6.4	Period of the K_1 $l = 3$ $p = 1$ $q = -1$ radial tidal perurbation for the gravitomagnetic clock effect.	130
8.1	Systematic relative error induced by harmonic perturbations on the PPN parameters measurement	151
8.2	Systematic relative error induced by the mismodelling in the inclinations on the PPN parameters measurement	152
8.3	Simulated standard statistical error in the PPN parameters measurement	153
9.1	Original LARES mission: sensitivity to inclination.	161
9.2	Original LARES mission: sensitivity to semimajor axis.	162
9.3	Alternative LARES mission: sensitivity to inclination.	162
9.4	Alternative LARES mission: sensitivity to semimajor axis.	163
9.5	POLARES configuration: sensitivity to inclination.	163

List of Tables

3.1	Solid Earth tidal perturbations on the node Ω of LAGEOS	52
3.2	Solid Earth tidal perturbations on the node Ω of LAGEOS II.	53
3.3	Solid Earth tidal perturbations on the perigee ω of LAGEOS II.	54
3.4	Corrections due to Earth's flattening and rotation to solid tidal perturbations.	54
3.5	Solid Earth tidal perturbations on the mean anomaly \mathcal{M} of LAGEOS. .	55
3.6	Solid Earth tidal perturbations on the mean anomaly \mathcal{M} of LAGEOS II. .	56
3.7	Solid Earth tidal perturbations on the inclination i of LAGEOS.	57
3.8	Solid Earth tidal perturbations on the inclination i of LAGEOS II. . . .	58
3.9	Mismodeled solid tidal perturbations on nodes of LAGEOS and LAGEOS II and perigee of LAGEOS II.	58
3.10	Ocean tidal perturbations on the node Ω of LAGEOS.	75
3.11	Ocean tidal perturbations on the node Ω of LAGEOS II.	75
3.12	Ocean tidal perturbations on the perigee ω of LAGEOS II.	75
3.13	Ocean tidal perturbations on the mean anomaly \mathcal{M} of LAGEOS. . . .	76
3.14	Ocean tidal perturbations on the mean anomaly \mathcal{M} of LAGEOS II. . .	76

A.1 Mismodelled classical nodal precessions and predicted Lense-Thirring nodal precessions of the existing spherical passive geodetic laser-ranged satellites and of LARES	177
A.2 Mismodelled classical perigee precessions and predicted Lense-Thirring perigee precessions of the existing spherical passive geodetic laser-ranged satellites and of LARES	177
A.3 Orbital parameters of the existing spherical passive geodetic laser- ranged satellites other than LAGEOS and LARES.	178
C.1 Earth's and LAGEOS parameters used in the text.	182

Chapter 1

Introduction

The last decade can be characterized by an impressive diversity of techniques monitoring the artificial and natural satellite dynamics, as well as the Earth rotation: improved laser technology, renewed Doppler techniques, satellite radar altimetry, massive usage of the Global Positioning System (GPS), etc. Each of these techniques is optimally tailored to a specific type of application or scientific problem. For example, it appears that laser tracking (SLR: see on the WEB: <http://ilrs.gsfc.nasa.gov>) of passive geodynamics satellites (LAGEOS, LAGEOS II, Starlette, Stella, Ajisai, Etalon I and II) over relatively long time intervals provides an excellent method for determining the long-term variations of the geopotential [Kaula, 1966] (including tidal effects) and many small non-gravitational phenomena [Milani *et al.*, 1987]. In <http://earth.agu.org/revgeophys/marsha01/node1.html> it can be found that the precision reached in the latest years by such technique in measuring the position of the passive laser-ranged geodetic satellites LAGEOS and LAGEOS II amounts to 1 cm or better¹.

Such astonishing levels of accuracy have disclosed an unexpectedly wide field of research in space geodesy, geophysics and fundamental physics. E.g., now it is possible to plan satellite-based experiments devoted to the experimental control even of some tiny post-Newtonian features of the Earth's gravitational field predicted by Einstein's General Relativity [Lämmerzahl *et al.*, 2001]. They are usually expressed in terms of certain solve-for least squares fits' parameters. In evaluating the precision

¹In August 2001 the single-shot accuracy in tracking LAGEOS at Matera amounts to 5 mm

of the results of these experiments it must be considered that, in general, the main error does not consist of the standard statistical error of the fits but of the various systematic errors. They are induced by a complete set of other physical effects acting upon the satellites to be employed [*Montenbruck and Gill*, 2000]. Such perturbations are often quite larger than the relativistic effects investigated and induce systematic errors to be correctly evaluated and assessed. Many of these aliasing effects are traditionally investigated by geophysics and space geodesy, so that such experiments are multidisciplinary efforts which cover many scientific areas until now separated [*Soffel*, 1989; *Graffarend and Joos*, 1992]. Indeed, the expansion of the SLR network, together with improved system accuracies, has enabled the laser data to contribute directly to improving orbit force models. It allows one to calculate more accurately, among other things, the error budget of many space-based general relativistic experiments: this is the main topic of the present work. It does not treat the measurement modelling errors specifically related to the laser-ranging technique.

1.1 The Lense-Thirring drag of inertial frames

One of the most interesting topic in General Relativity is the structure of the spacetime around a spherically symmetric rotating mass-energy distribution. Indeed, in the slow-motion and weak-field approximation, it exhibits the characteristic feature of exerting a non-central force on a test particle due to the total angular momentum of the central object, contrary to Newtonian mechanics in which the gravitational action of a body is caused only by its mass, regardless to its rotational motion. Because of the formal analogies with the electrodynamics, this effect, deduced from the equations of Einstein for the first time by Lense and Thirring in 1918 [*Lense and Thirring*, 1918], is also defined as gravitomagnetism. A comprehensive review of its properties can be found in [*Ciufolini and Wheeler*, 1995; *Mashhoon et al.*, 2001; *Mashhoon*, 2001].

In the past few years we have seen increasing efforts, both from a theoretical and an experimental point of view, devoted to the measurement of the Lense-Thirring effect in the weak gravitational field of the Earth by means of artificial satellites. At present, there are two main proposals which point towards the implementation

of this goal: the Gravity Probe-B mission [Everitt *et al.*, 2001], and the approach proposed by *Ciufolini* [1986] which consists in using the actually orbiting LAGEOS laser-ranged satellite and launching another satellite of LAGEOS type, the LARES, with the same orbital parameters of LAGEOS except for the inclination, which should be supplementary with respect to it, the eccentricity which should be one order of magnitude larger, and the area-to-mass ratio which should be smaller so to reduce the impact of the non-gravitational orbital perturbations (see Appendix C for the LAGEOS type satellites' data). The observable would be a secular linear trend built up with the sum of the residuals of the longitudes of the ascending nodes Ω of LARES and LAGEOS (see chapter 2 and Fig. (2.1) for an explanation of the Keplerian orbital elements in terms of which the orbit of a satellite can be parameterized). The proposed orbital geometry would allow one to minimize the impact of the aliasing trend due to the mismodelling in the classical nodal precessions generated by the oblateness of the Earth, which would represent the main systematic error.

The GP-B mission is aimed to the detection of the motion of a spinning particle. The precise evolution of a spinning object (gyroscope) is usually determined via the classic Papapetrou equations. However, there is ongoing discussion, even within the context of General Relativity, of the applicability of the Papapetrou equations. Thus the gyroscope measurement tests both the gravitational field and the accuracy of description of the motion of a spinning object. The Lense-Thirring frame dragging can be computed completely in terms of geodesic equations, and so its observation will provide an unambiguous control of the predictions of Einstein's equations [*Ciufolini and Matzner*, 1998]. At present, both the GP-B and the LARES have not yet been launched: however, while the GP-B is scheduled to fly in 2002, the fate of LARES project is still uncertain.

Recently *Ciufolini* [1996] has put forward an alternative strategy based on the utilization of the already existing LAGEOS and LAGEOS II which allowed the detection of the Lense-Thirring drag at a precision level of the order of 20% [*Ciufolini et al.*, 1998]. While the GP-B mission is focused on the gravitomagnetic dragging of the spin of a freely falling body, in the LAGEOS experiment it is the entire orbit of the satellite which is considered to undergo the secular Lense-Thirring precession. More exactly,

among the Keplerian orbital elements [*Sterne*, 1960; *Allison and Ashby*, 1993], the node Ω and the perigee ω are affected by the gravitomagnetic perturbation. For LAGEOS and LAGEOS II it amounts to

$$\dot{\Omega}_{\text{LT}}^{\text{LAGEOS}} \simeq 31 \text{ mas/y}, \quad (1.1)$$

$$\dot{\Omega}_{\text{LT}}^{\text{LAGEOS II}} \simeq 31.5 \text{ mas/y}, \quad (1.2)$$

$$\dot{\omega}_{\text{LT}}^{\text{LAGEOS}} \simeq 31.6 \text{ mas/y}, \quad (1.3)$$

$$\dot{\omega}_{\text{LT}}^{\text{LAGEOS II}} \simeq -57 \text{ mas/y}, \quad (1.4)$$

where mas/y stands for milliarcseconds per year.

- In chapter 2 a brief derivation of such results is presented. It follows ordinary linear satellite perturbation theory. Indeed, in the slow-motion and weak-field approximation, the gravitomagnetic potential is treated as a classical disturbing term with respect to the Newtonian gravitoelectric monopole. The effect of the non-sphericity of the central source on the Lense-Thirring rate equations is also worked out and the possibility of detecting it by means of LAGEOS and LAGEOS II in the terrestrial field is explored.

The observable quantity proposed in [*Ciufolini*, 1996] is a suitable combination of the orbital residuals of the nodes of LAGEOS and LAGEOS II and the perigee of LAGEOS II

$$\dot{y} \equiv \delta\dot{\Omega}_{\text{exp}}^{\text{I}} + c_1 \times \delta\dot{\Omega}_{\text{exp}}^{\text{II}} + c_2 \times \delta\dot{\omega}_{\text{exp}}^{\text{II}} = \mu_{\text{LT}} \times 60.2. \quad (1.5)$$

In it $c_1 = 0.295$, $c_2 = -0.35$, μ_{LT} is the scaling, solve-for parameter, equal to 1 in General Relativity and 0 in classical mechanics, to be determined and $\delta\dot{\Omega}_{\text{exp}}^{\text{I}}$, $\delta\dot{\Omega}_{\text{exp}}^{\text{II}}$, $\delta\dot{\omega}_{\text{exp}}^{\text{II}}$ are the orbital residuals, in mas, calculated with the aid of some orbit determination software like UTOPIA or GEODYN, of the nodes of LAGEOS and LAGEOS II and the perigee of LAGEOS II. The residuals account for any unmodelled or mismodelled physical phenomena acting on the observable analyzed. By dealing with the gravitomagnetism as an unmodelled physical effect, General Relativity predicts a linear trend with a slope of 60.2 mas/y

$$\dot{y}_{\text{LT}} \equiv (31 \text{ mas/y}) + c_1 \times (31.5 \text{ mas/y}) + c_2 \times (-57 \text{ mas/y}) \simeq 60.2 \text{ mas/y}. \quad (1.6)$$

The coefficients c_1 and c_2 of eq. (1.5) depend on the orbital parameters of LAGEOS and LAGEOS II (see [*Ciufolini*, 1996] and Appendix A) and are built up so to cancel

out all the static and dynamical contributions of degree $l = 2, 4$ and order $m = 0$ of the Earth's gravitational field. This cancellation is required to reduce especially the impact of the first two even ($l = 2, 4$) zonal ($m = 0$) harmonics of the static geopotential. Indeed, at the present level of accuracy of the terrestrial gravitational field [Lemoine *et al.*, 1998], the mismodelled parts of the classical orbital precessions of the node and the perigee, caused by the Earth's oblateness and parameterized with the first two even zonal coefficients J_2 and J_4 (see Appendix A and [Kaula, 1966]), for a single satellite amount to a significative part of the corresponding Lense-Thirring effect itself on the considered orbital element (see Tab. A.1 and Tab. A.2 of Appendix A). The combined residuals of eq. (1.5) are affected by a complete set of gravitational and non-gravitational perturbations; among the former ones those generated by the solid Earth and ocean tides [Melchior, 1983; Cartwright, 2000] play an important role.

- In chapter 3 the amplitudes and the periods of the most relevant tidal perturbations acting upon the Keplerian orbital elements of LAGEOS and LAGEOS II have been worked out. This analysis covers both the solid $l = 2$ and the ocean $l = 2, 3, 4$ part of the tidal spectrum, includes both the first order and the second order contributions, in the sense of the Kaula's theory of perturbations [Kaula, 1966], and, for the nodes of LAGEOS and LAGEOS II and the perigee of LAGEOS II, also a calculation of the mismodelling in the first order perturbative amplitudes compared to the Lense-Thirring drag over 4 years.
- Chapter 4 is devoted to the study of the impact of the solid Earth and ocean tidal perturbations on eq. (1.5) with particular care to the systematic errors induced by them on the measurement of μ_{LT} . The left hand side of eq. (1.5) has been calculated by adopting the nominal values of the perturbative amplitudes worked out in chapter 3 in order to test if the first two even degree zonal tidal lines do not really affect the combined residuals. This is particularly important for the 18.6-year tidal constituent whose period is that of the longitude of the ascending node of the Moon, i.e. 18.6 years. Indeed, over observational time spans of few years it could resemble a trend as well and its mismodelled part, accounted for by the residuals combination, could corrupt the measurement of μ_{LT} . The results obtained in chapter 3 have been employed also in order to obtain a simulated residual curve on which several tests

have been performed for the various tesseral ($m = 1$) and sectorial ($m = 2$) tidal constituents, not cancelled out by the combined residuals, with the aim of assessing their contribution on the systematic uncertainty in the measurement of μ_{LT} .

1.2 The gravitomagnetic clock effect

The other investigated effect is the so called gravitomagnetic “clock effect” [*Vladimirov et al.*, 1987; *Mashhoon et al.*, 1999; *Tartaglia*, 2000a] which consists of a difference in the orbital periods of two counter-orbiting test particles on circular equatorial geodesic orbits around a central spinning body. Studies conducted up to now on the feasibility and the error budget of such an experiment in the field of Earth can be found in [*Gronwald et al.*, 1997; *Mashhoon et al.*, 2001; *Tartaglia*, 2000b; *Lichtenegger et al.*, 2000; 2001; *Iorio*, 2001b; 2001c; 2001d].

- The possibility of detecting this effect using artificial Earth satellites has led to develop a more intuitive approach to its derivation in chapter 5.
- In chapter 6 the influence of the orbital gravitational perturbations on the detection of this general relativistic feature has been worked out.
- Chapter 7 is devoted to the non-gravitational perturbations and to the constraints posed by them on the feasibility of such demanding experiment.

1.3 The gravitoelectric pericenter shift

- In chapter 8 the experience gained in the Lense-Thirring LAGEOS experiment is used to propose a possible experiment for measuring accurately the general relativistic pericenter shift of a test body due to the Schwarzschild’s gravitoelectric part of the terrestrial gravitational field by means of the SLR data to LAGEOS and LAGEOS II. The approach is similar to that of the current Lense-Thirring LAGEOS experiment and it is based on another suitable combination of orbital residuals of the nodes of LAGEOS and LAGEOS II and the perigee of LAGEOS II. The possibility of adopting

different observables is examined as well.

1.4 The LARES mission

- In chapter 9 we reanalyze the original LARES mission from the point of view of the sensitivity of the related observable to the departures of the LARES orbital parameters from their nominal values due to the orbital injection errors. Moreover, we propose an alternative combination of orbital residuals involving also the LAGEOS II which would yield to a smaller and more stable value of the error due to the mismodelling in the even zonal harmonics of the geopotential which turns out to be the main source of systematic error.

1.5 Conclusions

- Chapter 10 is devoted to the conclusions and to the recommendations for future work.

Chapter 2

The Lense-Thirring effect on the orbit of a test body

2.1 Introduction

In this chapter an alternative strategy is presented in order to derive the Lense-Thirring effect [Iorio, 2001e]. It reveals itself useful especially in the prediction of the behavior of all the Keplerian orbital elements of the test body in the gravitational field of different kinds of rotating sources. Indeed, the calculations involve not only the secular effects for a perfectly spherical source, but also for a central body with departures from sphericity. Until now the latter effects have been treated only in the context of the GP-B mission [Teyssandier, 1977a; 1977b; Adler and Silbergleit, 2000]. Our calculations are based on the Lagrangian planetary equations [Kaula, 1966; Bertotti and Farinella, 1990; Vinti, 1998] and a non-central hamiltonian term whose existence, if from one hand can be rigorously deduced, from the other hand can be intuitively guessed by analogy from the corresponding term in electrodynamics for the Lagrangian of a charged particle acted upon by electric and magnetic fields.

For a perfectly spherical source the well known Lense-Thirring rate equations for the secular precessions of the node and the perigee are reobtained. In the case of a central body with axial symmetry around the rotation axis the calculations show that, again, only the node and the perigee of the test body are affected by secular, tiny precessions. The results obtained have been applied to the LAGEOS satellites in

the field of the Earth: it turns out that the quadrupole mass moment of our planet induces corrections to the usual Lense-Thirring rate equations too small in order to be detected with the actual sensitivity of laser-ranging technique.

2.2 The gravitomagnetic potential

In general, it can be proved [Mashhoon *et al.*, 2001] that the general relativistic equations of motion of a test particle of mass m freely falling in a stationary gravitational field, in the weak-field and slow-motion approximation, are given by

$$m \frac{d^2 \mathbf{r}}{dt^2} \simeq m \left(\mathbf{E}_g + \frac{\mathbf{v}}{c} \times \mathbf{B}_g \right). \quad (2.1)$$

In eq. (2.1) \mathbf{E}_g and \mathbf{B}_g are the gravitoelectric and gravitomagnetic fields, respectively. If a perfectly spherically symmetric rotating body is assumed as gravitational source, in eq. (2.1) $\mathbf{E}_g = -GM\mathbf{i}_r/r^2 + \mathcal{O}(c^{-2})$ is the Newtonian gravitational field of a spherical body, with M its mass and G the Newtonian gravitational constant¹, while \mathbf{B}_g is given by [Mashhoon *et al.*, 2001]

$$\mathbf{B}_g = \nabla \times \mathbf{A}_g \simeq 2 \frac{G}{c} \left[\frac{\mathbf{J} - 3(\mathbf{J} \cdot \mathbf{i}_r)\mathbf{i}_r}{r^3} \right], \quad (2.2)$$

in which

$$\mathbf{A}_g(\mathbf{r}) \simeq -2 \frac{G}{c} \frac{\mathbf{J} \times \mathbf{r}}{r^3}. \quad (2.3)$$

In eq. (2.3) \mathbf{J} is the angular momentum of the central body. The field $\mathbf{A}_g \equiv (h_{01}, h_{02}, h_{03})$, named gravitomagnetic potential, is due to the off-diagonal components of the spacetime metric tensor

$$g_{\mu\nu} = \eta_{\mu\nu} + h_{\mu\nu}, \quad \mu, \nu = 0, 1, 2, 3, \quad (2.4)$$

where $\eta_{\mu\nu}$ is the Minkowski metric tensor. In obtaining eq. (2.3) a non-rotating reference frame $K\{x, y, z\}$ with the z axis directed along the intrinsic angular momentum of the central spinning body \mathbf{J} and the $\{x, y\}$ plane coinciding with its equatorial plane has been used. The origin is located at the center of mass of the central body. Eq. (2.1) holds if \mathbf{A}_g is not time-varying.

¹The terms of order $\mathcal{O}(c^{-2})$ are the post-Newtonian corrections due to the static Schwarzschild part of the metric.

The gravitomagnetic potential generates a non-central gravitational contribute due uniquely to the angular momentum of the gravitational source that the Newtonian mechanics does not predict, though the conditions of validity of eq. (2.1) are the same for which the latter holds as well.² So it is possible to speak of mass-energy currents whose motion exerts a non-central gravitational force on a test massive body analogous to the Lorentz force felt by a charged particle when it is moving in a magnetic field. Indeed, its equations of motions

$$m \frac{d^2 \mathbf{r}}{dt^2} \simeq q \left(\mathbf{E} + \frac{\mathbf{v}}{c} \times \mathbf{B} \right) \quad (2.5)$$

are formally analogous to eq. (2.1). Eq. (2.5) can be derived by means of the Lagrangian

$$\mathcal{L}_{e.m.} = \frac{1}{2} m v^2 - qV + \frac{q}{c} (\mathbf{v} \cdot \mathbf{A}). \quad (2.6)$$

where \mathbf{v} is the velocity of the particle and V is its scalar potential.

Since one of the most promising ways to detect the gravitomagnetic precession consists of employing artificial Earth satellites, it would be helpful to derive the rate equations for the change in the parameters that characterize their orbits. To this aim one could introduce “by hand” a perturbative term $k (\mathbf{v} \cdot \mathbf{A}_g)$ in the gravitational Lagrangian of the particle and use it in some particular perturbative scheme; the constant k would be determined by means of dimensional considerations and taking into account that it should be built up of universal constants. In fact it is possible to show that a non-central term analogous to $\frac{q}{c} (\mathbf{v} \cdot \mathbf{A})$ can be rigorously deduced in the Lagrangian of a test body in the gravitational field of a spinning mass-energy distribution, and that it can be exploited in deriving straightforwardly the effect of the gravitomagnetic potential on the Keplerian orbital elements of the test body.

²Incidentally, it may be interesting to notice that eq. (2.1) are consistent with the fundamental Einstein assumption [Einstein, 1975] that a non-accelerated reference frame with a gravitational field is equivalent, within certain limits, to an accelerated one without any gravitational field. Indeed, if a reference frame solidal with the rotating body is assumed, the equations of motion for a test particle are formally identical to eq. (2.1): the gravitomagnetic force term $\frac{m}{c} (\mathbf{v} \times \mathbf{B}_g)$ is substituted by the Coriolis force term $2m(\mathbf{v} \times \boldsymbol{\Omega})$ where $\boldsymbol{\Omega}$ is the angular velocity vector of the rotating body [Vladimirov *et al.*, 1987]. See also [Mashhoon, 1993].

2.3 The rate equations for the Keplerian orbital elements

The relativistic Lagrangian for a free particle in a gravitational field can be cast into the form:

$$\mathcal{L} = \mathcal{L}^{(0)} + \mathcal{L}^{(1)}. \quad (2.7)$$

In eq. (2.7) the term $\mathcal{L}^{(1)}$ is to be intended as containing the contributions of the off-diagonal terms of the metric

$$\mathcal{L}^{(1)} = \frac{m}{c} g_{0k} \dot{x}^0 \dot{x}^k. \quad (2.8)$$

In this case, recalling that the slow motion approximation is used, the eq. (2.8) becomes

$$\mathcal{L}^{(1)} \equiv \mathcal{L}_{gm} = \frac{m}{c} (\mathbf{A}_g \cdot \mathbf{v}). \quad (2.9)$$

For different derivations of \mathcal{L}_{gm} see also [Landau and Lifshitz, 1979; Misner *et al.*, 1973; Bertotti and Farinella, 1990]. In this chapter it is proposed to adopt \mathcal{L}_{gm} in order to deriving the Lense-Thirring effect on the orbital elements of a particle in the field of a rotating gravitational source.

To this aim it must be assumed that under the gravitomagnetic force the departures of the test body's trajectory from the unperturbed Keplerian ellipse are very small in time. This allows to introduce the concept of osculating ellipse. It means that, at a given instant of time, the particle may be assumed to lie on the Keplerian ellipse determined by the position and velocity at that instant thought as initial conditions for an unperturbed motion; at the next instant of time the particle will be at a point of another Keplerian ellipse, slightly different with respect to the previous one and determined by the real position and velocity of the test body at the new instant of time thought as new initial conditions for an unperturbed Keplerian orbit. In other words, the real trajectory of the test body at every instant may be approximated by an osculating Keplerian ellipse. So the perturbed motion can be described in terms of unperturbed Keplerian elements varying in time. See Fig. (2.1). Consider the frame $K\{x, y, z\}$ previously defined and a frame $K'\{X, Y, Z\}$ with the Z axis directed along the orbital angular momentum \mathbf{l} of the test body, the plane $\{X, Y\}$ coinciding

with the orbital plane of the test particle and the X axis directed toward the pericenter. K and K' have the same origin located in the center of mass of the central body. The Keplerian orbital elements are [Kaula, 1966]:

- a, e , the semimajor axis and the ellipticity which define the size and the shape of the orbit in its plane
- Ω, i , the longitude of the ascending node and the inclination which fix the orientation of the orbit in the space, i.e. of K' with respect to K . The longitude of the ascending node Ω is the angle in the equatorial plane of $K\{x, y, z\}$ between the x axis and the line of nodes in which the orbital plane intersects the equatorial plane. The inclination i is the angle between the z and Z axis
- ω, \mathcal{M} , the argument of pericenter and the mean anomaly. The argument of pericenter ω is the angle in the orbital plane between the line of nodes and the X axis; it defines the orientation of the orbit in its plane. The mean anomaly \mathcal{M} specifies the motion of the test particle on its orbit. It is related to the mean motion $n = (GM)^{1/2}a^{-3/2}$, where M is the mass of the gravitating central source, through $\mathcal{M} = n(t - t_p)$ in which t_p is the time of pericenter passage

It is customary to define also:

- $\varpi = \Omega + \omega$, the longitude of pericenter
- $u = \omega + f$, the argument of latitude where f is the angle, called true anomaly, which in the orbital plane determines the position of the test particle with respect to the pericenter
- $\varepsilon = \varpi + n(t_0 - t_p)$, the mean longitude at the epoch t_0 . If $t_0 = 0$, it is customary to write ε as $L_0 = \varpi - nt_p$.

The matrix \mathbf{R}_{xX} for the change of coordinates from K' to K is [Kaula, 1966]

$$\begin{pmatrix} \cos \Omega \cos \omega - \sin \Omega \cos i \sin \omega & -\cos \Omega \sin \omega - \sin \Omega \cos i \cos \omega & \sin \Omega \sin i \\ \sin \Omega \cos \omega + \cos \Omega \cos i \sin \omega & -\sin \Omega \sin \omega + \cos \Omega \cos i \cos \omega & -\cos \Omega \sin i \\ \sin i \sin \omega & \sin i \cos \omega & \cos i \end{pmatrix}. \quad (2.10)$$

Using eq. (2.10) and $X = r \cos f$, $Y = r \sin f$, $Z = 0$ it is possible to express the geocentric rectangular Cartesian coordinates of the orbiter in terms of its Keplerian elements

$$\begin{cases} x = r(\cos u \cos \Omega - \sin u \cos i \sin \Omega) \\ y = r(\cos u \sin \Omega + \sin u \cos i \cos \Omega) \\ z = r \sin u \sin i. \end{cases} \quad (2.11)$$

Redefining suitably the origin of the angle Ω so that $\cos \Omega = 1$, $\sin \Omega = 0$, the previous equations become

$$\begin{cases} x = r \cos u \\ y = r \sin u \cos i \\ z = r \sin u \sin i. \end{cases} \quad (2.12)$$

Considering for the test particle the total mechanical energy with the sign reversed, according to [Vinti, 1998], $\mathcal{F} \equiv -\mathcal{E}_{tot} = -(\mathcal{T} + \mathcal{U})$, where \mathcal{T} and \mathcal{U} are the kinetic and potential energies per unit mass, it is possible to work out the analytical expressions for the rate of changes of a , e , i , Ω , ω , \mathcal{M} due to any non-central gravitational contribution. To this aim it is useful to isolate in \mathcal{U} the central part $-\mathcal{C}$ of the gravitational field from the terms $-\mathcal{R}$ which may cause the Keplerian orbital elements to change in time: $\mathcal{U} = -\mathcal{C} - \mathcal{R}$. For a spherically symmetric body, \mathcal{F} becomes

$$\mathcal{F} = \frac{GM}{r} + \mathcal{R} - \mathcal{T} = \frac{GM}{2a} + \mathcal{R}. \quad (2.13)$$

Concerning the perturbative scheme to be employed, the well known Lagrange planetary equations are adopted. At first order, they are:

$$\frac{da}{dt} = \frac{2}{na} \frac{\partial \mathcal{R}}{\partial \mathcal{M}}, \quad (2.14)$$

$$\frac{de}{dt} = \frac{1 - e^2}{na^2 e} \frac{\partial \mathcal{R}}{\partial \mathcal{M}} - \frac{(1 - e^2)^{1/2}}{na^2 e} \frac{\partial \mathcal{R}}{\partial \omega}, \quad (2.15)$$

$$\frac{di}{dt} = \cos i \frac{1}{na^2 (1 - e^2)^{1/2} \sin i} \frac{\partial \mathcal{R}}{\partial \omega} - \frac{1}{na^2 (1 - e^2)^{1/2} \sin i} \frac{\partial \mathcal{R}}{\partial \Omega}, \quad (2.16)$$

$$\frac{d\Omega}{dt} = \frac{1}{na^2 (1 - e^2)^{1/2} \sin i} \frac{\partial \mathcal{R}}{\partial i}, \quad (2.17)$$

$$\frac{d\omega}{dt} = -\cos i \frac{1}{na^2 (1 - e^2)^{1/2} \sin i} \frac{\partial \mathcal{R}}{\partial i} + \frac{(1 - e^2)^{1/2}}{na^2 e} \frac{\partial \mathcal{R}}{\partial e}, \quad (2.18)$$

$$\frac{d\mathcal{M}}{dt} = n - \frac{1 - e^2}{na^2 e} \frac{\partial \mathcal{R}}{\partial e} - \frac{2}{na} \frac{\partial \mathcal{R}}{\partial a}. \quad (2.19)$$

The idea of this work consists of using \mathcal{L}_{gm} to obtain a suitable non-central term \mathcal{R}_{gm} to be employed in these equations. This can be done considering the Hamiltonian for the test particle

$$\mathcal{H} = \mathbf{p} \cdot \mathbf{v} - \mathcal{L}. \quad (2.20)$$

Inserting eq. (2.7) in eq. (2.20) one has

$$\mathcal{H} = \mathcal{H}^{(0)} + \mathcal{H}_{gm}, \quad (2.21)$$

with $\mathcal{H}_{gm} = -\frac{m}{c}(\mathbf{A}_g \cdot \mathbf{v})$. So it can be posed

$$\mathcal{R}_{gm} = -\frac{\mathcal{H}_{gm}}{m} = \frac{(\mathbf{A}_g \cdot \mathbf{v})}{c}. \quad (2.22)$$

Now it is useful to express eq. (2.22) in terms of the Keplerian elements. Referring to eq. (2.3), eq. (2.12), and recalling that in the frame $K\{x, y, z\} \mathbf{J} = (0, 0, J)$ and that for an unperturbed Keplerian motion

$$\frac{1}{r} = \frac{(1 + e \cos f)}{a(1 - e^2)}, \quad (2.23)$$

it is possible to obtain, for a perfectly spherical central body

$$\mathcal{R}_{gm} = -\frac{2G}{c^2} \frac{J \cos i}{r} \dot{u} = -\frac{2GJ \cos i}{c^2} \frac{(1 + e \cos f)}{a(1 - e^2)} \dot{u}. \quad (2.24)$$

In eq. (2.24) $\dot{u} \simeq \dot{f}$ is assumed due to the fact that the osculating element ω may be retained almost constant on the temporal scale of variation of the true anomaly of the test body.

2.4 Secular gravitomagnetic effects on the Keplerian orbital elements: spherical central source

The secular effects can be worked out by adopting the same strategy followed, e.g., in [Vinti, 1998] for a similar kind of perturbing functions. By using averaging we implicitly make several assumptions about the system that may restrict the validity and applicability of our result. Averaging is generally applied to systems where the perturbing force is sufficiently small so that, over one orbital period, the deviations of the true trajectory from the Keplerian trajectory are relatively small. This perturbation can generally be related to the magnitude of the perturbing acceleration as compared to the central-body attraction [Scheeres and Hu, 2001]. In this case, clearly, we can view the application of the averaging approach as valid. When eq.

(2.24) is mediated over one orbital period of the test body, a , e , i , Ω and ω are to be considered constant:

$$\langle \mathcal{R} \rangle_{2\pi} = -\frac{1}{P} \int_0^P \frac{G}{c^2} \frac{2J}{r} \cos i du = -n \frac{G}{c^2} \frac{2J \cos i}{2\pi} \int_0^{2\pi} \frac{df}{r} = -n \frac{G}{c^2} \frac{2J \cos i}{a(1-e^2)}. \quad (2.25)$$

The relation $du = d\omega + df = df$ has been used in eq. (2.25). Eq. (2.25) can now be used in determining the secular changes of the Keplerian orbital elements of the test body. From it one gets:

$$\frac{\partial \langle \mathcal{R} \rangle_{2\pi}}{\partial \mathcal{M}} = 0, \quad (2.26)$$

$$\frac{\partial \langle \mathcal{R} \rangle_{2\pi}}{\partial \omega} = 0, \quad (2.27)$$

$$\frac{\partial \langle \mathcal{R} \rangle_{2\pi}}{\partial \Omega} = 0, \quad (2.28)$$

$$\frac{\partial \langle \mathcal{R} \rangle_{2\pi}}{\partial i} = \frac{G}{c^2} \frac{2nJ \sin i}{a(1-e^2)}, \quad (2.29)$$

$$\frac{\partial \langle \mathcal{R} \rangle_{2\pi}}{\partial e} = -\frac{G}{c^2} \frac{4nJe \cos i}{a(1-e^2)^2}. \quad (2.30)$$

A particular care is needed for the treatment of n when the derivative of $\langle \mathcal{R} \rangle_{2\pi}$ with respect to a is taken; indeed, it must be posed as:

$$\frac{\partial \langle \mathcal{R} \rangle_{2\pi}}{\partial a} = \frac{\partial \langle \mathcal{R} \rangle_{2\pi}}{\partial a} \Big|_n + \frac{\partial \langle \mathcal{R} \rangle_{2\pi}}{\partial n} \Big|_a \frac{\partial n}{\partial a}. \quad (2.31)$$

In eq. (2.31)

$$\frac{\partial \langle \mathcal{R} \rangle_{2\pi}}{\partial a} \Big|_n = \frac{G}{c^2} \frac{2nJ \cos i}{a^2(1-e^2)}, \quad (2.32)$$

and

$$\frac{\partial \langle \mathcal{R} \rangle_{2\pi}}{\partial n} \Big|_a \frac{\partial n}{\partial a} = \frac{G}{c^2} \frac{3nJ \cos i}{a^2(1-e^2)}. \quad (2.33)$$

From eq. (2.14) and eq. (2.26) it appears that there are no secular changes in the semimajor axis³, and so the orbital period of the test body, related to the mean motion by $P = 2\pi/n$, can be considered constant. So in eq. (2.31) only eq. (2.32) must be retained. Using eqs. (2.26)-(2.31) in eqs. (2.14)-(2.19) one obtains for the averaged rates

$$\frac{da}{dt} \Big|_{LT} = 0, \quad (2.34)$$

$$\frac{de}{dt} \Big|_{LT} = 0, \quad (2.35)$$

³Here only the effect of the off-diagonal gravitomagnetic components of the metric tensor is considered, neglecting any other physical influence of gravitational and non gravitational origin.

$$\left. \frac{di}{dt} \right|_{LT} = 0, \quad (2.36)$$

$$\left. \frac{d\Omega}{dt} \right|_{LT} = \frac{G}{c^2} \frac{2J}{a^3(1-e^2)^{3/2}}, \quad (2.37)$$

$$\left. \frac{d\omega}{dt} \right|_{LT} = -\frac{G}{c^2} \frac{6J \cos i}{a^3(1-e^2)^{3/2}}, \quad (2.38)$$

$$\left. \frac{d\mathcal{M}}{dt} \right|_{LT} = 0. \quad (2.39)$$

They are the well known Lense-Thirring equations [*Lense and Thirring*, 1918; *Ciufolini and Wheeler*, 1995]. In deriving them it has been assumed that the spatial average over f yields the same results for the time average [*Arnold*, 1983; 1989; *Milani et al.*, 1987].

2.5 Secular gravitomagnetic effects on the Keplerian orbital elements: non-spherical central source

In this section we shall deal with a non-spherical central rotating source endowed with axial symmetry around the rotation axis.

In classical electrodynamics the potential vector for a generic steady current distribution can be written as

$$\mathbf{A}(\mathbf{r}) = \frac{1}{c} \int \frac{\rho(\mathbf{r}') \mathbf{v}}{|\mathbf{r} - \mathbf{r}'|} d\mathbf{r}'. \quad (2.40)$$

The quantity ρ is the charge density which, in general, depends on \mathbf{r} , but, in this case, not on time. If we assume that the current distribution rotates uniformly around an axis, chosen as z axis, then, since for any current element $\mathbf{v} = \alpha \mathbf{i}_z \times \mathbf{r}$, with α angular velocity of the current distribution, eq. (2.40) becomes

$$\mathbf{A}(\mathbf{r}) = \frac{\alpha}{c} \int \frac{\rho(\mathbf{r}') \mathbf{i}_z \times \mathbf{r}}{|\mathbf{r} - \mathbf{r}'|} d\mathbf{r}'. \quad (2.41)$$

For an axisymmetrical, stationary current distribution, it can be shown [*Jackson*, 1962] that the lines of the potential vector are circles around the z axis, and its modulus is

a cylindrical symmetric function of ξ and z , where:

$$\begin{aligned} x &= \xi \cos \phi \\ y &= \xi \sin \phi \\ z &= z, \end{aligned} \quad (2.42)$$

$\xi \geq 0$, $0 \leq \phi < 2\pi$, define the cylindrical coordinates. So, eq. (2.41) reduces to:

$$\mathbf{A}(\mathbf{r}) = \frac{\alpha}{c} H(\xi, z) \mathbf{i}_\phi. \quad (2.43)$$

The function $H(\xi, z)$ remains unchanged under rotations around the z axis. Passing from cylindrical to rectangular Cartesian coordinates, the components of the potential vector become

$$A_1 = -\frac{\alpha}{c} H(\xi, z) y, \quad (2.44)$$

$$A_2 = \frac{\alpha}{c} H(\xi, z) x, \quad (2.45)$$

$$A_3 = 0. \quad (2.46)$$

Recalling that, in the linear approximation, the general relativistic gravitomagnetic potential can be obtained from the vector potential of electromagnetism times $-4G$ [*Ciufolini and Wheeler, 1995*], eqs. (2.44)-(2.46) lead to

$$h_{01} = \frac{4G\alpha}{c} H(\xi, z) y, \quad (2.47)$$

$$h_{02} = -\frac{4G\alpha}{c} H(\xi, z) x, \quad (2.48)$$

$$h_{03} = 0. \quad (2.49)$$

Obviously, eqs. (2.47)-(2.49) can be rigorously obtained solving the linearized Einstein field equation, written in the Lorentz gauge, for a localized ($g_{\mu\nu} \rightarrow \eta_{\mu\nu}$ at spatial infinity), axisymmetrical, stationary mass distribution in the weak-field and slow-motion approximation:

$$\Delta h_{0k} = 0 \quad (2.50)$$

$$\Delta h_{0k} = \frac{16\pi G}{c^4} T_{0k}. \quad (2.51)$$

The quantites T_{0k} are the $\{0k\}$ components of the stress-energy tensor for the matter; in deriving eq. (2.51) the internal stresses have been neglected. Eq. (2.51) is valid inside the matter, while eq. (2.50) holds in the free space outside the central body and tells us that $H(\xi, z)y$ and $H(\xi, z)x$ are harmonic functions. This feature was used

by Teyssandier in obtaining a multipolar expansion of $H(\xi, z)$ [Teyssandier, 1977a]. Introducing in the frame K the usual spherical coordinates $\{r, \theta, \phi\}$, if r_e is the radius of the smallest sphere centered on the origin of the coordinates containing the whole body (in practice, it should be the equatorial radius, R_\oplus in the case of the Earth), in the region $r \geq r_1 > r_e$ $H(r, \theta)$ is given by

$$H(r, \theta) = \frac{I}{2r^3} \left[1 - \sum_{l=1}^{\infty} K_l \left(\frac{r_e}{r} \right)^l P'_{l+1}(\cos \theta) \right], \quad (2.52)$$

with

$$K_l = \frac{2}{2l+3} \frac{Mr_e^2}{I} (L_l - J_{l+2}), \quad (2.53)$$

$$L_l = -\frac{1}{Mr_e^{l+2}} \int \rho(r', \theta') r'^{l+2} P_l(\cos \theta') d\mathbf{r}'. \quad (2.54)$$

In eqs. (2.57)-(2.54) I is the moment of inertia of the body about the z axis, M is the total mass of the central body, ρ is its density, $P'_{l+1}(\cos \theta)$ is the first derivative of the Legendre polynomial of degree $l+1$ and J_l is the Newtonian multipole moment of degree l , given by

$$J_l = -\frac{1}{Mr_e^l} \int \rho(r', \theta') r'^l P_l(\cos \theta') d\mathbf{r}'. \quad (2.55)$$

It is interesting to notice that, if in eq. (2.57) only the spherical symmetric term

$$H^{(0)}(r) = \frac{I}{2r^3} \quad (2.56)$$

is retained, as it would be the case for a perfectly spherical central body, eqs. (2.47)-(2.49) reduce to

$$h_{01}^{(0)} = \frac{2GI\alpha}{c} \frac{y}{r^3}, \quad (2.57)$$

$$h_{02}^{(0)} = -\frac{2GI\alpha}{c} \frac{x}{r^3}, \quad (2.58)$$

$$h_{03}^{(0)} = 0. \quad (2.59)$$

For a spherical rotating body $J = I\alpha$, and so eqs. (2.57)-(2.59) can be cast into the familiar form

$$\mathbf{A}_g^{(0)} = -\frac{2G}{c} \frac{\mathbf{J} \times \mathbf{r}}{r^3}. \quad (2.60)$$

The correction of order l to the gravitomagnetic potential due to the non-sphericity of the central rotating body is given by

$$h_{01}^{(l)} = -\frac{2GI\alpha}{r^3 c} y K_l \left(\frac{r_e}{r} \right)^l P'_{l+1}(\cos \theta), \quad (2.61)$$

$$h_{02}^{(l)} = \frac{2GI\alpha}{r^3 c} x K_l \left(\frac{r_e}{r}\right)^l P'_{l+1}(\cos\theta), \quad (2.62)$$

$$h_{03}^{(l)} = 0. \quad (2.63)$$

modelling the central body as a spheroid stratified into ellipsoidal shells, in [Teyssandier, 1977b] is shown that all the relativistic coefficients K_l vanish, except K_2 ; if we consider our planet, from the analysis of Teyssandier of various models of Earth's interior, it turns out to be positive and of $\mathcal{O}(10^{-3})$.

The starting point in deriving the relativistic multipole corrections of degree l to eqs. (2.34)-(2.39) is the perturbative lagrangian term

$$\mathcal{L}_{gm}^{(l)} = \frac{m}{c} (\mathbf{A}_g^{(l)} \cdot \mathbf{v}), \quad (2.64)$$

where m is the mass of the point particle and \mathbf{v} is its velocity. In the case $l = 2$, in eqs. (2.61)-(2.63) the first derivative of the Legendre polynomial of degree 3 appear;

$$P_3(\psi) = \frac{1}{2} (5\psi^3 - 3\psi), \quad \psi = \cos\theta, \quad (2.65)$$

$$P'_3(\psi) = \frac{1}{2} (15\psi^2 - 3), \quad \psi = \cos\theta. \quad (2.66)$$

Inserting eq. (2.66) in eqs. (2.61)-(2.63) leads to

$$\mathcal{L}_{gm}^{(2)} = -m \frac{GI\alpha}{c^2 r^3} \frac{(y\dot{x} - x\dot{y})}{r^2} r_e^2 K_2 (15 \cos^2 \theta - 3). \quad (2.67)$$

Such a perturbative term must be expressed in terms of the Keplerian orbital elements in order to be employed in the first order Lagrange planetary equations. In this case \mathcal{R} is $\mathcal{R}^{(2)} = \frac{(\mathbf{A}_g^{(2)} \cdot \mathbf{v})}{c}$. Using eq. (2.11) and recalling that $z = r \cos\theta$ it is possible to obtain

$$\frac{(y\dot{x} - x\dot{y})}{r^2} = -\dot{u} \cos i \quad (2.68)$$

$$\cos\theta = \sin u \sin i. \quad (2.69)$$

Neglecting terms of order $\mathcal{O}(e^n)$, $n \geq 2$, we can write

$$\frac{1}{r^3} \simeq \frac{1 + 3e \cos f}{a^3 (1 - e^2)^3}, \quad (2.70)$$

having assumed

$$\frac{1}{r} = \frac{1 + e \cos f}{a(1 - e^2)}. \quad (2.71)$$

Eqs. (2.68)-(2.70) in eq. (2.67) give

$$\mathcal{R}^{(2)} = \frac{G}{c^2} \frac{I\alpha r_e^2 K_2 \cos i}{a^3(1-e^2)^3} (1 + 3e \cos f) (15 \sin^2 u \sin^2 i - 3) \dot{u}. \quad (2.72)$$

If we want to investigate the secular trends of the orbital elements, we must average eq. (2.72) over an orbital period of the test body, as done in the previous section. It is straightforward to obtain

$$\langle (1 + 3e \cos f) (15 \sin^2 u \sin^2 i - 3) \dot{u} \rangle_{2\pi} = \frac{n}{2} (9 - 15 \cos^2 i). \quad (2.73)$$

In deriving eq. (2.73) we have adopted the reasonable assumption that the pericenter of the test body remains almost unchanged during an orbital revolution, i. e. $du = d\omega + df \simeq df$. So we have

$$\langle \mathcal{R}^{(2)} \rangle_{2\pi} = \frac{G}{c^2} \frac{nI\alpha r_e^2 K_2}{2a^3(1-e^2)^3} (9 \cos i - 15 \cos^3 i). \quad (2.74)$$

Eq. (2.74) can be considered as the 2nd order correction to the gravitomagnetic perturbing function given in eq. (2.25). Eq. (2.74) yields

$$\frac{\partial \langle \mathcal{R}^{(2)} \rangle_{2\pi}}{\partial \mathcal{M}} = 0, \quad (2.75)$$

$$\frac{\partial \langle \mathcal{R}^{(2)} \rangle_{2\pi}}{\partial \omega} = 0, \quad (2.76)$$

$$\frac{\partial \langle \mathcal{R}^{(2)} \rangle_{2\pi}}{\partial \Omega} = 0, \quad (2.77)$$

$$\frac{\partial \langle \mathcal{R}^{(2)} \rangle_{2\pi}}{\partial i} = \frac{G}{c^2} \frac{nI\alpha r_e^2 K_2}{2a^3(1-e^2)^3} \sin i (45 \cos^2 i - 9), \quad (2.78)$$

$$\frac{\partial \langle \mathcal{R}^{(2)} \rangle_{2\pi}}{\partial e} = \frac{G}{c^2} \frac{3neI\alpha r_e^2 K_2}{2a^3(1-e^2)^4} (9 \cos i - 15 \cos^3 i), \quad (2.79)$$

$$\left. \frac{\partial \langle \mathcal{R}^{(2)} \rangle_{2\pi}}{\partial a} \right|_n = -\frac{G}{c^2} \frac{3nI\alpha r_e^2 K_2}{2a^4(1-e^2)^3} (9 \cos i - 15 \cos^3 i). \quad (2.80)$$

By inserting eqs. (2.75)-(2.80) in eqs. (2.14)-(2.19) it can be obtained for the averaged rates

$$\left. \frac{da}{dt} \right|_{LT}^{(2)} = 0, \quad (2.81)$$

$$\left. \frac{de}{dt} \right|_{LT}^{(2)} = 0, \quad (2.82)$$

$$\left. \frac{di}{dt} \right|_{LT}^{(2)} = 0, \quad (2.83)$$

$$\frac{d\Omega}{dt} \bigg|_{\text{LT}}^{(2)} = \frac{G}{c^2} \frac{I\alpha r_e^2 K_2}{2a^5(1-e^2)^{7/2}} (45 \cos^2 i - 9), \quad (2.84)$$

$$\frac{d\omega}{dt} \bigg|_{\text{LT}}^{(2)} = -\cos i \frac{d\Omega}{dt} \bigg|_{\text{LT}}^{(2)} + \frac{G}{c^2} \frac{3I\alpha r_e^2 K_2}{a^5(1-e^2)^{7/2}} (9 \cos i - 15 \cos^3 i), \quad (2.85)$$

$$\frac{d\mathcal{M}}{dt} \bigg|_{\text{LT}}^{(2)} = 0. \quad (2.86)$$

Eqs. (2.81)-(2.86) yield the corrections to the precessional rate Lense-Thirring equations when the central rotating body is not perfectly spherical.

If we use in eqs. (2.84)-(2.85) the values $r_e = R_{\oplus} \simeq 6,378$ km, $K_2 = 0.874 \times 10^{-3}$ [Teyssandier, 1977b] we can obtain an estimate of the sensitivity of LAGEOS and LAGEOS II to the relativistic Earth's quadrupole correction to the Lense-Thirring precessional rates. The results ⁴are:

$$\dot{\Omega}_{\text{LAGEOS}}^{(2)} = -6.7 \times 10^{-1} \text{ mas/century}, \quad (2.87)$$

$$\dot{\Omega}_{\text{LAGEOS II}}^{(2)} = 2.8 \text{ mas/century}, \quad (2.88)$$

$$\dot{\omega}_{\text{LAGEOS II}}^{(2)} = 5.4 \text{ mas/century}. \quad (2.89)$$

The present accuracy in the measurement of the LAGEOS rates of the node and the perigee is of the order of 1 mas/y. This implies that such tiny corrections do not affect the current efforts in detecting the Lense-Thirring drag.

⁴The perigee of LAGEOS is not considered here since its rate is very difficult to measure. Indeed, the observable quantity for this orbital element is the product $e\omega$, and $e_{\text{LAGEOS}} = 0.0045$.

2.6 Figures

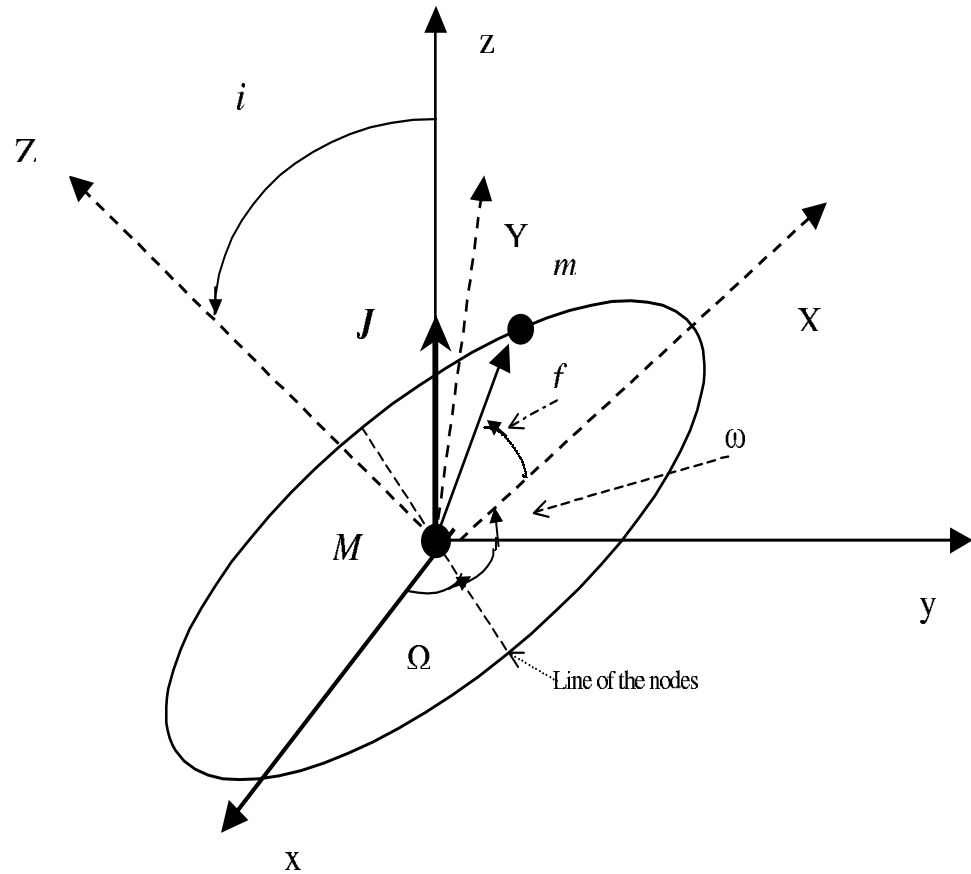


Figure 2.1: Orbital elements for a general Keplerian osculating ellipse.

Chapter 3

Orbital perturbations induced by solid Earth and ocean tides

3.1 Introduction

In this chapter the problem of calculating the gravitational time-dependent perturbations induced by solid Earth and ocean tides on the Keplerian orbital elements of LAGEOS and LAGEOS II is addressed. The focus of the analysis, although the calculations involve the inclination, the node, the perigee and the mean anomaly, is on the nodes of LAGEOS and LAGEOS II and the perigee of LAGEOS II in view of their close connection to the measurement of the Lense-Thirring effect. The perturbative scheme adopted, both for the first order and for the second order perturbations, is that based on the Lagrange's planetary equations [Kaula, 1966; Dow, 1988; Christodoulidis *et al.*, 1988; Casotto, 1989].

An evaluation from first principles of the amplitudes, the periods and the initial phases of the tidal perturbations on the nodes of LAGEOS and LAGEOS II and the perigee of LAGEOS II is useful, in the present context, for the following reasons.

- It allows one to point out which tidal constituents the Lense-Thirring shift is mainly sensitive to, so that people can focus the researches on them
- It allows one to get insight in how to update the orbit determination softwares.

In this way the impact on the time series of those tidal constituents which will turn

out to be more effective could be reduced along with the number of the parameters to be included in the least-squares solution

- For a given observational time span T_{obs} it allows one to find those constituents whose periods are longer than it and consequently may act like superimposed bias (e.g. the 18.6-year and 9.3-year zonal tides and the $K_1 l = 3 p = 1 q = -1$ ocean diurnal tide on the perigee of LAGEOS II) corrupting the detection of the gravitomagnetic shift. In these cases, if we know their amplitudes, periods and initial phases we could fit and remove them from the time series¹ or, at least, it should be possible to assess the mismodelling level induced by them on the detection of the Lense-Thirring trend. So, also these estimates can be included in the final error budget. (See chapter 4)
- It can be used as starting point for numerical simulations of the combined residual data in order to check, e. g., the impact of the diurnal ($m=1$) and semidiurnal ($m=2$) tidal perturbations (not cancelled out by the Ciufolini's observable), as done in chapter 4
- The calculations for the mean anomaly and the inclination are motivated by the following reasons. In [Ciufolini, 2000] a possible use of the mean anomaly in the gravitomagnetic LAGEOS experiment is reported. Regarding the inclination, in fact, the combined residuals actually used are affected not only by the remaining even zonal harmonics of the geopotential but also by the residuals of this orbital element [Ciufolini *et al.*, 1997]. In chapter 4 the results obtained for the tidal perturbations of the inclination will be used in assessing quantitatively the impact of this source of systematic error.

The chapter is organized as follows. In Sec. 2 the essential features of the tide generating potential, from which the tidal forces are traditionally derived, are reviewed.

The solid Earth tidal perturbations are worked out in Sec. 3-4. An evaluation of their mismodelling and a comparison with the Lense-Thirring perturbations on the nodes of LAGEOS and LAGEOS II and the perigee of LAGEOS II over 4 years are

¹If the period of the disturbing harmonic, assumed to be known, is shorter than the time series length the perturbation can be viewed as an empirically fit quantity. But if its period is longer than the time series length it is not possible to fit and remove the harmonic from the data without removing also the true trend, unless we know the initial phase.

also presented.

Sec. 5-7 are devoted to the orbital perturbations due to the ocean tides and their mismodelling in connection with the Lense-Thirring drag. They are treated in detail because the ocean tides are known less accurately than the solid ones, so that the impact of their mismodelling on the gravitomagnetic trend is more relevant.

In Sec. 8-9 the second order effects [*Balmino*, 1974; *Dow*, 1988; *Christodoulidis et al.*, 1988; *Casotto*, 1989;] on the node, the perigee and the mean anomaly of LAGEOS and LAGEOS II, due to the oblateness of the Earth, are worked out.

Sec. 10 is devoted to the conclusions.

3.2 The tide generating potential

On the scale of the Earth's dimensions the gravitational field of any not too far astronomical body B cannot be considered uniform so that the various points of our planet are acted upon by a differential gravitational pull in the external field of B . This is the origin of the Earth's solid, ocean and atmospheric tides, mainly due to the Moon and the Sun. It is customary to derive the tidal forces acting on a point on the Earth's surface from the so called tide generating potential which, in its most general form, for a perturbing body B can be written as [*Dronkers*, 1964; *Lambeck*, 1977; *Melchior*, 1983]

$$\begin{aligned} \Phi_B &= \frac{GM_B}{d_B} \sum_{l=2}^{\infty} \left(\frac{r}{d_B} \right)^l P_l(\cos z) = \\ &= \frac{3}{4} GM_B \frac{R^2}{c_B^3} \left(\frac{r}{R} \right)^2 \left(\frac{c_B}{d_B} \right)^3 \left[\frac{4}{3} P_2(\cos z) + \frac{4}{3} \frac{r}{d_B} P_3(\cos z) + \dots \right]. \end{aligned} \quad (3.1)$$

In eq. (3.1) the following quantities appear

- R mean Earth's equatorial radius
- M_B mass of the perturbing body
- d_B instantaneous distance between the Earth and the perturbing body B

- r distance between the center of mass of the Earth and a point on its surface
- $P_l(x)$ Legendre polynomials of degree l :

$$P_l(x) = \frac{(-1)^l}{l!2^l} \frac{d^l}{dx^l} (1-x^2)^l \quad (3.2)$$

- z geocentric zenithal distance of the perturbing body
- c_B mean distance between the Earth and the perturbing body

The factor

$$\frac{3}{4} GM_B \frac{R^2}{c_B^3} \left(\frac{r}{R} \right)^2 \quad (3.3)$$

is often rewritten as

$$D_B(r) = \frac{M_B}{M_M} \frac{c_M^3}{c_B^3} D(r), \quad (3.4)$$

with

$$D(r) = \frac{3}{4} GM_M \frac{R^2}{c_M^3} \left(\frac{r}{R} \right)^2 = D_1 \left(\frac{r}{R} \right)^2 \quad (3.5)$$

in which

$$D_1 = \frac{3}{4} GM_M \frac{R^2}{c_M^3} \quad (3.6)$$

is the Doodson constant for the Moon, having the dimension of an energy per unit mass, and M_M is the Moon's mass. Thus the tide generating potential outside of the Earth Φ_B^l is a harmonic function of degree l and can be written in the form $\Phi_B^l = r^l Y_l(\phi, \lambda)$ where $Y_l(\phi, \lambda)$ is a surface harmonic, with ϕ and λ the terrestrial latitude and East longitude. At the Earth's surface it becomes $\Phi_B^l(\mathbf{R}) = (R/r)^l \Phi_B^l(\mathbf{r})$.

It is useful to express eq. (3.1) in terms of the geocentric equatorial coordinates $\{\phi, \delta_B, H_B\}$ of an Earth-fixed frame where

- δ_B declination of the perturbing body
- H_B hour angle of the perturbing body

This can be done by means of the following spherical trigonometric formula

$$\cos z = \sin \phi \sin \delta_B + \cos \phi \cos \delta_B \cos H_B. \quad (3.7)$$

The result is the Laplace's tidal development: it consists of a sum of terms each of which is the product of a factor depending only on the latitude of a given place on the Earth (the geodetic coefficient) and a time-dependent factor which depends on the astronomical coordinates δ_B and H_B of the perturbing body. E.g., the term of degree $l = 2$ becomes

$$\begin{aligned}\Phi_B^2 = D_B(r) \left(\frac{c_B}{d_B}\right)^3 & \left[\left(\frac{1 - 3 \sin^2 \phi}{2}\right) \left(\frac{1}{3} - \sin^2 \delta_B\right) + \right. \\ & \left. + \sin 2\phi \sin 2\delta_B \cos H_B + \cos^2 \phi \cos^2 \delta_B \cos 2H_B \right].\end{aligned}\quad (3.8)$$

In this sum the quantities c_B/d_B , δ_B , H_B exhibit a very complex behavior in time due to the astronomical motions of the perturbing body B . They must be carefully expanded in periodic components in order to obtain an expression for the tidal potential as a sum of harmonic terms. This can be done by using the ephemerides tables for the perturbing bodies. Obviously, the most relevant are the Moon and the Sun. Since the ephemerides refer to the ecliptic and not to the celestial equator, it is necessary to express δ_B and H_B in terms of ecliptical coordinates. Spherical trigonometry gives

$$\sin \delta_B = \sin \varepsilon \cos \beta_B \sin \lambda_B + \cos \varepsilon \sin \lambda_B, \quad (3.9)$$

$$\cos \delta_B \cos H_B = \cos \beta_B \cos \lambda_B \cos \theta + (\cos \varepsilon \cos \beta_B \sin \lambda_B - \sin \varepsilon \sin \beta_B) \sin \theta, \quad (3.10)$$

where:

- ε inclination of the ecliptic to the celestial equator
- λ_B , β_B ecliptical longitude and latitude of the perturbing body, respectively
- θ sidereal time

The lunar and solar ephemerides express d_B , λ_B , β_B in terms of time-dependent series of sines and cosines whose arguments are linear combinations of the mean Lunar time τ and other astronomical quantities of the Moon and the Sun ². Among them the most useful are the mean ecliptical lunisolar variables s , h , p , N' , p_s [Dronkers, 1964]. They are

²The most recent developments take in account also the influence of other planets like Venus and Jupiter [Roosbeek, 1996].

- s mean ecliptical longitude of the Moon with period $P_s = 27.32$ days
- h mean ecliptical longitude of the Sun with period $P_h = 365.2422$ days
- p mean ecliptical longitude of the Moon's perigee with period $P_p = 3,232$ days (8.84 years)
- $N' = -N$ mean ecliptical longitude of the Moon's node with the sign reversed, with period $P_N = 6,798.38$ days (18.61 years). The lunar node, moving in the Earth-fixed frame from East to West counterclockwise, is retrograde with respect to the other lunisolar longitudes
- p_s mean ecliptical longitude of the perihelion with period $P_{p_s} = 7.65 \times 10^6$ days (20,953 years)

Putting eqs. (3.9)-(3.10) in the Laplace's tidal development, with the ephemerides expansions for d_B , λ_B , β_B , allows one to obtain the harmonic expansion of the tide generating potential Φ_B [Doodson, 1921; Cartwright and Tayler, 1971; Cartwright and Edden, 1973; Buellsfeld, 1985; Tamura, 1987; Xi, 1987 ; Hartmann and Wenzel, 1995; Roosbeek, 1996]. It consists of a sum of terms, the constituents, with sinusoidal time dependence where the sines and cosines have arguments involving linear combinations σt of the previously defined orbital longitudes of the Sun and the Moon

$$\sigma t = j_1\tau + j_2s + j_3h + j_4p + j_5N' + j_6p_s. \quad (3.11)$$

The circular frequency of the tidal bulge generated by the corresponding constituent, viewed in the terrestrial frame, is then given by

$$\sigma \equiv 2\pi f = j_1\dot{\tau} + j_2\dot{s} + j_3\dot{h} + j_4\dot{p} + j_5\dot{N}' + j_6\dot{p}_s; \quad (3.12)$$

by considering that $\tau = \theta - s$, eq. (3.12) becomes

$$\sigma = j_1\dot{\theta} + (j_2 - j_1)\dot{s} + j_3\dot{h} + j_4\dot{p} + j_5\dot{N}' + j_6\dot{p}_s. \quad (3.13)$$

The coefficients j_k , $k = 1, \dots, 6$ are small integers which can assume negative, positive or null values. The advantage of using such lunisolar ecliptical variables relies in the fact that they, over an interval of a century or so, are practically linear increasing with time. This feature will reveal itself very useful in integrating the equations for

the orbital perturbations. Each tidal constituent is identified by the set of the six integers j_k , $k = 1, \dots, 6$ arranged in the so called Doodson number:

$$j_1(j_2 + 5)(j_3 + 5).(j_4 + 5)(j_5 + 5)(j_6 + 5). \quad (3.14)$$

In it the integer j_1 classifies the tides in long period or zonal ($j_1 = 0$), diurnal or tesseral ($j_1 = 1$) and semidiurnal or sectorial ($j_1 = 2$).

The tide generating potential is the cornerstone for every calculation of tidal perturbations on the satellites' Keplerian orbital elements. Indeed, if the Earth, globally modeled as a nonrigid body, is acted upon by a tidal potential Φ_l harmonic in degree, it deforms itself giving rise, among other things, to a periodic redistribution of the masses within its volume. This deformation acts upon a point in the external space surrounding the Earth by means of an additional potential [Love, 1926]

$$\phi_l(\mathbf{r}) = k_l \left(\frac{R}{r} \right)^{l+1} \Phi_l(R) = k_l \left(\frac{R}{r} \right)^{2l+1} \Phi_l(r) \quad (3.15)$$

where k_l is one of the so called Love numbers (they will be defined precisely in the following sections). A close orbiting satellite is perturbed by such an additional potential and senses the global effect of the solid and fluid mass redistribution in the Earth. This means that if one wish to employ a pool of satellites in order to recover the tidal parameters, like the Love numbers, entering the tidal perturbations and wants to use the so obtained values to predict the perturbations on some particular satellite, he or she must be very careful. Indeed, such values are aliased by the whole of the effects sensed by the measuring satellites; it is as if they would be "tailored" for the satellites used in their recovery. So, these "effective" tidal parameters neither can be directly compared to those measured on the Earth's surface or predicted by any theoretical model and related to the physical properties of the Earth, nor can be used in calculating *a priori* the tidal perturbations on the satellites of interest for some particular application, as is the case for the detection of the Lense-Thirring effect. Differently stated, when the tidal perturbations are to be predicted for a given satellite, it is incorrect to use for it the "effective" values of the geophysical parameters recovered by other satellites. It is so customary to split the analytical expressions of the tidal perturbations into a part due to the solid Earth tides and another one which accounts for the effects of the oceans [Lambeck *et al.*, 1974]. After this step, their effects on the

satellite of interest must be analytically predicted using for the various parameters the values theoretically calculated or measured in such a way that they reflect the effective Earth's properties.

3.3 Solid Earth tidal perturbations

Concerning the solid Earth tides [*Wang*, 1997], as in [*Dow*, 1988] and [*Bertotti and Carpino*, 1989], the starting point is the frequency-dependent model of *Wahr* [1981b]. It is based on the assumption of a perfectly elastic, hydrostatically prestressed, ellipsoidal rotating Earth acted upon by the lunisolar tidal potential. The interior of our planet is thought to be made of a solid inner core, a fluid outer core, and a solid mantle capped by a thin continental crust, without oceans and atmosphere. Substantially, the Earth is thought as a set of coupled harmonic oscillators showing a variety of resonant frequencies, the normal modes, which can be excited by the external forcing constituents of the tide generating potential [*Wahr*, 1981a].

The expansion adopted for it is that of *Cartwright and Tayler* [1971] in terms of harmonic constituents of degree l , order m and circular frequency σ

$$\Phi = g \sum_{l=2}^{\infty} \sum_{m=0}^l \left(\frac{r}{R}\right)^l Y_l^m(\phi, \lambda) \sum_f H_l^m(f) e^{i(\sigma t + c_{lm})}. \quad (3.16)$$

Only the real part of eq. (3.16) has to be retained. The quantities entering eq. (3.16) are

- Y_l^m spherical harmonics

$$Y_l^m(\phi, \lambda) = \sqrt{\frac{2l+1}{4\pi} \frac{(l-m)!}{(l+m)!}} P_l^m(\sin \phi) e^{im\lambda}, \quad (3.17)$$

in which the Condon-Shortley phase factor $(-1)^m$ has been neglected in order to compare our results to those of [*Bertotti and Carpino*, 1989]

- $H_l^m(f)$ coefficients of the harmonic expansion. They contain the lunisolar ephemerides information and define the modulus of the vertical shift V/g in the equipotential surface at the Earth's surface for $r = R_{\oplus}$ with respect to the case

in which only proper Earth's gravity is considered. The values used in the present calculation are those recently released by *Roosbeek* [1996] using the ELP2000-85 series for the ecliptical coordinates of the Moon [*Chapront-Touzé*, 1988] and the VSOP87 series for those of the Sun [*Bretagnon and Francou*, 1988]. Their accuracy is of the order of 10^{-7} m. In order to use them in place of the coefficients of *Cartwright and Edden* [1973], which have a different normalization, a multiplication for a suitable conversion factor [*McCarthy*, 1996] has been performed. Due to the extreme smallness of the $H_l^m(f)$ for $l \geq 3$, in the following summations only the term of degree $l = 2$ are to be considered

- c_{lm} additive constant. It is equal to $-\pi/2$ in order to generate sines for the $l - m$ odd constituents, while it is equal to 0 in order to yield cosines for the $l - m$ even constituents.

The Earth free space potential under the action of the tidal constituent of degree l , order m and circular frequency σ , dropping the time dependence due to $e^{i\sigma t}$, can be written as

$$\phi_l^m = \text{Re } g H_l^m \left[k_{lm}^{(0)} \left(\frac{R}{r} \right)^{l+1} Y_l^m + k_{lm}^+ \left(\frac{R}{r} \right)^{l+3} Y_{l+2}^m \right], \quad (3.18)$$

in which

- r distance from the Earth's center of mass and a point in the space outside of the Earth

- The parameter

$$k_{lm}^{(0)}(f) = \sqrt{k_{lm}^R(f)^2 + k_{lm}^I(f)^2}, \quad (3.19)$$

is the modulus of the Love number k [*Love*, 1926; *Mathews et al.*, 1995] for a static, spherical Earth. In general, it is defined as the ratio of the free space gravitational potential $\phi(\mathbf{r})$, evaluated at the Earth's equator, and the tide generating potential $\Phi(\mathbf{r})$ calculated at the mean equatorial radius. If the rotation and non-sphericity of the Earth are accounted for, there are different values of k for any l, m and f . In general, they are evaluated by convolving, in the frequency domain, the tide generating potential with the transfer function for a non rigid Earth [*Dahlen*, 1972; *Smith*, 1974]. There are several theoretical calculations for the Love numbers k [*Wahr*, 1981b; *Wang*,

1994; *Mathews et al.*, 1995; *McCarthy*, 1996; *Dehant et al.*, 1999]. They differ in the choice of the Earth's interior models [*Gilbert and Dziewonski*, 1975; *Dziewonski and Anderson*, 1981] adopted for the calculation of the transfer function and the departure from elasticity of the mantle's behavior. Particularly important is also if they account for, or not, the normal modes in the diurnal band. In eq. (3.19) the IERS conventions [*McCarthy*, 1996] have been used for $k_{lm}^{(0)}(f)$:

$$k_{lm}^I(f) = \text{Im } k_{lm} + \delta k_f^{\text{anel}}, \quad (3.20)$$

$$k_{lm}^R(f) = \text{Re } k_{lm} + \delta k_f^{\text{el}}, \quad (3.21)$$

where $\text{Im } k_{lm}$ and $\text{Re } k_{lm}$ are the frequency-independent parts of Love numbers, and δk_f^{anel} , δk_f^{el} are the frequency-dependent corrections. They are important in the diurnal band, through δk_f^{el} , and in the zonal band with δk_f^{anel} due to the anelasticity of the mantle. The $k_{lm}^+(f)$ account for the rotation and ellipticity of our planet. In the present analysis for the latitude dependent Love numbers $k_{lm}^+(f)$ the values quoted in [*Dehant et al.*, 1999] have been adopted.

Neglecting, in this first step, their tiny contribution, the free space potential by means of which the Earth responds to the forcing lunisolar tidal potential can be written, in the time domain, as

$$\phi = \frac{GM}{R} \sum_{l=2}^{\infty} \sum_{m=0}^l \sqrt{\frac{2l+1}{4\pi} \frac{(l-m)!}{(l+m)!}} \frac{1}{r} \left(\frac{R}{r}\right)^l \times \sum_f k_{lm}^{(0)} H_l^m P_l^m(\sin \phi) \begin{bmatrix} \cos(\sigma t + m\lambda) \\ \sin(\sigma t + m\lambda) \end{bmatrix}. \quad (3.22)$$

Here and in the following, the upper expressions refer to $l - m$ even while the lower ones refer to $l - m$ odd. Eq. (3.22) can be put into the form

$$\phi = \frac{GM}{R} \sum_{l=2}^{\infty} \sum_{m=0}^l \frac{1}{r} \left(\frac{R}{r}\right)^l (C_{lm} \cos m\lambda + S_{lm} \sin m\lambda) P_l^m(\sin \phi), \quad (3.23)$$

in which, assuming temporarily for the sake of simplicity that the Love numbers are not frequency-dependent, the coefficients C_{lm} and S_{lm} are:

$$C_{lm} = A_{lm} k_{lm}^{(0)} \sum_f H_l^m \begin{bmatrix} \cos \sigma t \\ \sin \sigma t \end{bmatrix}, \quad (3.24)$$

$$S_{lm} = A_{lm} k_{lm}^{(0)} \sum_f H_l^m \begin{bmatrix} -\sin \sigma t \\ \cos \sigma t \end{bmatrix}, \quad (3.25)$$

with

$$A_{lm} = \sqrt{\frac{2l+1}{4\pi} \frac{(l-m)!}{(l+m)!}}. \quad (3.26)$$

The C_{lm} and S_{lm} have the dimensions of lengths. Eq. (3.23) is formally equal to the well known expression of the static geopotential worked out by *Kaula* [1966]

$$\phi = \frac{GM}{r} \left\{ 1 + \sum_{l=2}^{\infty} \sum_{m=0}^l \left(\frac{R}{r} \right)^l P_{lm}(\sin \phi) [C_{lm} \cos m\lambda + S_{lm} \sin m\lambda] \right\}. \quad (3.27)$$

By means of the transformation:

$$\frac{1}{r} \left(\frac{R}{r} \right)^l P_l^m(\sin \phi) e^{im\lambda} = \frac{1}{a} \left(\frac{R}{a} \right)^l \sum_{p=0}^l F_{lmp}(i) \sum_{q=-\infty}^{+\infty} G_{lpq}(e) \begin{bmatrix} e^{i\psi_{lmpq}} \\ -ie^{i\psi_{lmpq}} \end{bmatrix}, \quad (3.28)$$

with

$$\psi_{lmpq} = (l - 2p)\omega + (l - 2p + q)\mathcal{M} + m(\Omega - \theta), \quad (3.29)$$

it can be cast into the familiar form

$$\phi = \frac{GM}{R} \sum_{l=2}^{\infty} \sum_{m=0}^l \frac{1}{a} \left(\frac{R}{a} \right)^l \sum_{p=0}^l \sum_{q=-\infty}^{+\infty} F_{lmp}(i) G_{lpq}(e) S_{lmpq}(\omega, \Omega, \mathcal{M}, \theta), \quad (3.30)$$

where $F_{lmp}(i)$ and $G_{lpq}(e)$ are the inclination and eccentricity functions respectively [*Kaula*, 1966]. The S_{lmpq} is given by

$$S_{lmpq} = \begin{bmatrix} C_{lm} \\ -S_{lm} \end{bmatrix} \cos \psi_{lmpq} + \begin{bmatrix} S_{lm} \\ C_{lm} \end{bmatrix} \sin \psi_{lmpq}. \quad (3.31)$$

Eq. (3.31) in our case becomes

$$S_{lmpq} = A_{lm} k_{lm}^{(0)} \sum_f H_l^m \cos(\sigma t + \psi_{lmpq}). \quad (3.32)$$

It is worthwhile noting that eq. (3.28) expresses a transformation of coordinates from the geocentric equatorial frame rotating with the Earth to the geocentric inertial frame $K\{x, y, z\}$. This fact will reveal itself of paramount importance in evaluating the frequencies of the tidal perturbations on the Keplerian elements.

Up to now the response of the Earth to the forcing tidal potential has been considered as perfectly elastic; if it had been so, there would be no delay between the Earth's tidal bulge and the Moon in the sense that when the latter passes at the observer's meridian, say, at A the tidal bulge reaches A at exactly the same time. The reality is quite different since complicated mechanisms of energy dissipation in the interior of the Earth [*Lambeck*, 1975; *Varga*, 1998] makes its response to depart from the perfectly elastic behavior previously sketched. A phase lag with respect to the external

lunisolar potential must be introduced in the sense that the tidal bulge reaches the observer's meridian at A after a certain time Δt with respect to the passage at A of Moon. It is generally assumed that it is the Earth's mantle to exhibit an anelastic behavior at the various frequencies of the tide generating potential; this topic is not yet well understood, but if one wants to account for the phase lag introduced by it, he or she has to adopt complex frequency-dependent Love numbers [Mathews *et al.*, 1995]. In order to give a quantitative estimation also of the lag angle it has been decided to adopt the values of Mathews *et al.* [1995] quoted in [McCarthy, 1996]; indeed, Dehant *et al.* [1999] do not quote the imaginary part of $k_{lm}^{(0)}(f)$ and the discrepancies with their values for $|k_{lm}^{(0)}(f)|$ amount to only 0.1 %. Moreover, concerning the effects of mantle's anelasticity, the results of Dehant *et al.* [1999] are not less uncertain than the other ones.

An equivalent form of eq. (3.24) and eq. (3.25), for a single constituent of frequency σ , which reveals useful in handling with complex quantities is:

$$C_{lmf} - iS_{lmf} = \eta A_{lm} k_{lm}^{(0)} H_l^m(f) e^{i\sigma t}, \quad (3.33)$$

with $\eta = -i$ if $l - m$ is odd and $\eta = 1$ if $l - m$ is even. If the anelasticity of the Earth's mantle is to be accounted for writing $k_{lm}^{(0)}(f) = k_{lm}^R(f) + ik_{lm}^I(f)$, eq. (3.33) becomes

$$\begin{aligned} C_{lmf} - iS_{lmf} = \eta A_{lm} H_l^m(f) \times & \left[(k_{lm}^R \cos \sigma t - k_{lm}^I \sin \sigma t) + \right. \\ & \left. + i(k_{lm}^R \sin \sigma t + k_{lm}^I \cos \sigma t) \right], \end{aligned} \quad (3.34)$$

or:

$$C_{lm} = A_{lm} \sum_f H_l^m \left[\begin{array}{c} k_{lm}^R \cos \sigma t - k_{lm}^I \sin \sigma t \\ k_{lm}^R \sin \sigma t + k_{lm}^I \cos \sigma t \end{array} \right], \quad (3.35)$$

$$S_{lm} = A_{lm} \sum_f H_l^m \left[\begin{array}{c} -k_{lm}^R \sin \sigma t - k_{lm}^I \cos \sigma t \\ k_{lm}^R \cos \sigma t - k_{lm}^I \sin \sigma t \end{array} \right], \quad (3.36)$$

If eq. (3.35) and eq. (3.36) are put into eq. (3.31), it is straightforward to obtain for it:

$$S_{lmpq} = A_{lm} \sum_f H_l^m k_{lm}^{(0)}(f) \cos(\sigma t + \psi_{lmpq} - \delta_{lmf}), \quad (3.37)$$

with:

$$k_{lm}^{(0)}(f) = \sqrt{k_{lm}^R(f)^2 + k_{lm}^I(f)^2}, \quad (3.38)$$

$$\tan \delta_{lmf} = \frac{k_{lm}^I(f)}{k_{lm}^R(f)}. \quad (3.39)$$

The factor δ_{lmf} is the phase lag of the response of the solid Earth with respect to the tidal constituent of degree l , order m and circular frequency σ induced by the anelasticity in the mantle: notice that if $k_{lm}^I(f) = 0$, also $\tan \delta_{lmf} = 0$. An inspection of the values quoted in [McCarthy, 1996] shows that, at the low frequencies of the zonal constituents of the tide generating potential, the role played by the mantle's anelasticity is more relevant than in the diurnal and semidiurnal bands. Indeed, while for the tesseral and sectorial tides one finds $k_{21}^I = -0.00144$ and $k_{22}^I = -0.00130$ for all the frequencies, in the zonal band $k_{20}^I(f)$ varies from -0.00541 to -0.00192 .

Eq. (3.30), with the S_{lmpq} given by eq. (3.37), is the dynamical, non-central part of the geopotential due to the response of the solid Earth to the forcing lunisolar tidal action. In the linear Lagrange equations of perturbation theory for the rates of change of the Keplerian elements it can play the role of the perturbative term \mathcal{R} . It is an observed fact that the secular motions are the dominant perturbation in the elements ω , Ω , \mathcal{M} of geodetically useful satellites. So, taking as constants a , e , i and consider as linearly variable in time ω , Ω , \mathcal{M} and θ , apart from σt , the following expressions, at first order, may be worked out

$$\begin{aligned} \Delta\Omega_f &= \frac{g}{na^2\sqrt{1-e^2}\sin i} \sum_{l=0}^{\infty} \sum_{m=0}^l \left(\frac{R}{r}\right)^{l+1} \times \\ &\times A_{lm} \sum_{p=0}^l \sum_{q=-\infty}^{+\infty} \frac{dF_{lmp}}{di} G_{lpq} \frac{1}{f_p} k_{lm}^{(0)} H_l^m \sin \gamma_{flmpq}, \end{aligned} \quad (3.40)$$

$$\begin{aligned} \Delta\omega_f &= \frac{g}{na^2\sqrt{1-e^2}} \sum_{l=0}^{\infty} \sum_{m=0}^l \left(\frac{R}{r}\right)^{l+1} \times \\ &\times A_{lm} \sum_{p=0}^l \sum_{q=-\infty}^{+\infty} \left[\frac{1-e^2}{e} F_{lmp} \frac{dG_{lpq}}{de} - \frac{\cos i}{\sin i} \frac{dF_{lmp}}{di} G_{lpq} \right] \frac{1}{f_p} k_{lm}^{(0)} H_l^m \sin \gamma_{flmpq}, \end{aligned} \quad (3.41)$$

$$\begin{aligned} \Delta\mathcal{M}_f &= \frac{g}{na^2} \sum_{l=0}^{\infty} \sum_{m=0}^l \left(\frac{R}{r}\right)^{l+1} \times \\ &\times A_{lm} \sum_{p=0}^l \sum_{q=-\infty}^{+\infty} F_{lmp} \left[2(l+1)G_{lpq} - \frac{1-e^2}{e} \frac{dG_{lpq}}{de} \right] \frac{1}{f_p} k_{lm}^{(0)} H_l^m \sin \gamma_{flmpq}, \end{aligned} \quad (3.42)$$

$$\Delta i_f = \frac{g}{na^2\sqrt{1-e^2}\sin i} \sum_{l=0}^{\infty} \sum_{m=0}^l \left(\frac{R}{r}\right)^{l+1} \times$$

$$\times A_{lm} \sum_{p=0}^l \sum_{q=-\infty}^{+\infty} F_{lmp} G_{lpq} [(l-2p) \cos i - m] \frac{1}{f_p} k_{lm}^{(0)} H_l^m \cos \gamma_{flmpq}, \quad (3.43)$$

with

$$\gamma_{flmpq} = (l-2p)\omega + (l-2p+q)\mathcal{M} + m(\Omega - \theta) + \sigma t - \delta_{lmf}, \quad (3.44)$$

$$f_p = (l-2p)\dot{\omega} + (l-2p+q)\dot{\mathcal{M}} + m(\dot{\Omega} - \dot{\theta}) + \sigma. \quad (3.45)$$

The indirect, second order effects due to the oblateness of the Earth [Balogh *et al.*, 2000] have been neglected in this section. Due to the secular trend of the Lense-Thirring effect, only the perturbations whose periods are much longer than those of the orbital satellites motions, which, typically, amount to a few hours, are to be considered. This implies that in such terms the rate of the mean anomaly does not appear and the condition

$$l - 2p + q = 0 \quad (3.46)$$

must hold. Moreover, if the effect of Earth's diurnal rotation, which could introduce periodicities of the order of 24 hours, is to be neglected, one must retain only those terms in which the non-negative multiplicative coefficient j_1 of the Greenwich sidereal time in σt coincides to the order m of the tidal constituent considered: in this way in f_p the contributions of $\dot{\theta}$ are equal and opposite, and cancel out. With these bounds on l , m , p and q the circular frequencies of the perturbations of interest become

$$f_p = \dot{\Gamma}_f + (l-2p)\dot{\omega} + m\dot{\Omega} \quad (3.47)$$

in which

$$\dot{\Gamma}_f = (j_2 - m)\dot{s} + j_3\dot{h} + j_4\dot{p} + j_5\dot{N}' + j_6\dot{p}_s. \quad (3.48)$$

In the performed calculation only the degree $l = 2$ constituents have been considered due to the smallness of the $k_{3m}^{(0)}$ and $H_3^m(f)$. For $l = 2$, p runs from 0 to 2, and so, in virtue of the condition $l - 2p + q = 0$, q assumes the values $-2, 0, 2$. From an inspection of the table of the eccentricity functions $G_{lpq}(e)$ in [Kaula, 1966] it turns out that $G_{20-2} = G_{222} = 0$, while $G_{210} = (1 - e^2)^{-3/2}$. For this combination of l , p and q the condition $l - 2p = 0$ holds: the frequencies of the perturbations are, in this case, given by

$$f_p = \dot{\Gamma}_f + m\dot{\Omega}. \quad (3.49)$$

Passing from σ to $\dot{\Gamma}_f + m\dot{\Omega}$, as previously noticed, is equivalent to leaving the Earth-fixed frame of reference for the inertial one, in which the relevant physical feature

is the orientation of the tidal bulges with respect to the orbital plane of satellite. Indeed, $\dot{\Gamma}_f + m\dot{\Omega}$ could be considered as the relative frequency of motions of the tidal bulge and the orbital plane, both viewed in the inertial frame. $\dot{\Gamma}_f$ is the opposite of the inertial rate of the tidal bulge obtained from the Earth-fixed one subtracting the Earth's rotation rate $\dot{\theta}$ times m in order to account for the symmetry of the bulges. The periodicities introduced in the perturbations by eq. (3.49) are, in general, much longer than the ones present in the tidal potential because, while the latter are dominated by $j_1\dot{\theta}$ due to the rotation of the Earth-fixed frame, the former are mainly determined by the precessional rates $m\dot{\Omega}$ of the orbital frames of the different satellites in the inertial frame. This explains the major variety of periodicities in the orbital elements' perturbations of the near-Earth's satellites with respect to the tides sensed by an observer on the Earth surface which are mainly concentrated in the diurnal and semidiurnal bands. In eqs. (3.40)-(3.43) it is worthwhile noting that the amplitudes of the perturbations are inversely proportional to the frequency of the perturbation f_p . This implies that some tidal constituent which in the Earth-fixed frame has a high frequency, in the inertial frame may induce relevant perturbations because its frequency greatly decreases; this fact could compensate an eventual small value of its coefficient in the harmonic expansion of the tide generating potential (calculated in the terrestrial frame). In other words, constituents which on the Earth's surface would produce small tides may become important in perturbing the orbits of near-Earth's satellites due to the changes in their frequencies when viewed in the inertial frame.

3.3.1 Discussion of the numerical results

In view of their direct implication in eq. (1.5), in the following we shall focus our attention to the nodes of LAGEOS and LAGEOS II and the perigee of LAGEOS II. In Tab. 3.1, Tab. 3.2, and Tab. 3.3 the results for them are shown; since the observable quantity for ω is $e\omega$ [Ciufolini, 1996], the calculation for the perigee of LAGEOS, due to the notable smallness of the eccentricity of its orbit, have not been performed. The tidal lines for which the analysis was performed have been chosen also in order to make a comparison with the perturbative amplitudes of the ocean tides based on the results of EGM96 gravity model [Lemoine *et al.*, 1998] which will

be shown in the next sections. It is interesting to notice that the periods of many of these tidal perturbations are almost equal to or longer than an year, a time interval in which their effect may alias the Lense-Thirring effect, if the observations are taken on a such temporal scale; indeed, only if the data were acquired on time intervals of the order of many years it should be possible to clearly resolve the action of these tidal lines with respect to the secular Lense-Thirring trend. And also in this case, it could remain the aliasing effect of the 18.6-year and 9.3-year tides. Up to now, in [Ciufolini *et al.*, 1997, 1998] the authors have analyzed the data acquired on a 4 years interval for a suitable combination of residuals showing that many tidal signals with periods shorter than it can be resolved by means of suitable fits.

The results presented in Tab. 3.1, Tab. 3.2 and Tab. 3.3 can be compared to those of Dow [1988] and Carpino [Bertotti and Carpino, 1989]. See also [Christodoulidis, 1978]. In doing so it must be kept in mind that both these authors have neglected not only the contribution of k_{lm}^+ but also the anelasticity and the frequency dependence of the Love numbers $k_{lm}^{(0)}$. Moreover, Dow includes in his analysis also the indirect influences of the oblateness of the Earth for O_1 , Q_1 , M_2 and N_2 . Obviously, in their analyses the LAGEOS II is not present since it was launched only in 1992. Another important factor to be considered is the actual sensitivity in measurements of Ω and ω , in the sense that the eventual discrepancies between the present results and the other ones must be not smaller than the experimental error in the Keplerian elements if one wish to check the theoretical assumptions behind the different models adopted. Carpino has analyzed the inclination and the node of LAGEOS only. His value for the important zonal 18.6-year tide is -1087.24 mas, while Tab. 3.1 gives $-1,079.38$ mas; the difference amounts to 7.86 mas, the 0.72% of the “elastic”, frequency-independent Carpino’s value. Considering that for the node Ω of LAGEOS the present accuracy is of the order of the mas, 7.86 mas could be in principle detected, allowing for a discrimination between the different models adopted in the calculation. For the K_1 tide, one of the most powerful constituent in perturbing the satellites’ orbits, Tab. 3.1 quotes $1,744.38$ mas against 2144.46 mas of Carpino’s result; the gap is 400.08 mas, the 18.6% of Carpino. In the sectorial band, the present analysis quotes for the K_2 -92.37 mas and Carpino -97.54 mas; there is a difference of 5.17 mas, the 5.3% of the Carpino’s value. It must pointed out that there are other tidal lines for which the

difference falls below the mas level, as is the case for the 9.3-year tide. As it could be expected, the major differences between the present “anelastic”, frequency-dependent calculations and the other ones based on a single, real value for the Love number k_2 lie in the diurnal band: in it the contribution of anelasticity is not particularly relevant, but, as already pointed out, the elastic part of $k_{21}^{(0)}$ is strongly dependent on frequencies of the tidal spectrum. May be interesting to notice that when the calculation have been repeated with the same value $k_2 = 0.317$ adopted by Carpino, his results have been obtained again.

Another feature which characterizes this study is the calculation of the phase lag of the solid Earth’s response with respect to the tide generating potential. In Tab. 3.1, Tab. 3.2 and Tab. 3.3 $\tan \delta_{lmf}$ is always negative and does not exceed 10^{-2} in absolute value showing that the response of the Earth is slightly retarded with respect to the forcing lunisolar tidal potential. In absolute value, $\tan \delta_{20f}$ is greater than $\tan \delta_{21f}$ and $\tan \delta_{22f}$ of one order of magnitude, confirming that the behavior of the solid Earth’s response is more influenced by the anelasticity in the zonal band that in the diurnal and semidiurnal ones.

Up to now the effects induced by the Earth’s flattening and the Earth’s rotation have been neglected. If they have to be analyzed it is necessary to take in eq. (3.18) the part

$$\text{Re } g \sum_{l=2}^{\infty} \sum_{m=0}^l \sum_f H_l^m(f) \left(\frac{R}{r}\right)^{l+3} k_{lm}^+(f) Y_{l+2}^m(\phi, \lambda) \quad (3.50)$$

and work out it in the same manner as done for the spherical non-rotating Earth’s contribution. In applying the transformation to the orbital elements given by eq. (3.28) one has to substitute everywhere l with $l + 2$. So the equations for the perturbations on the node and the perigee become

$$\begin{aligned} \Delta\Omega_f^+ &= \frac{g}{na^2\sqrt{1-e^2}\sin i} \sum_{l=0}^{\infty} \sum_{m=0}^l \left(\frac{R}{r}\right)^{l+3} A_{l+2} \, {}_m H_l^m \times \\ &\quad \times k_{lm}^+ \frac{1}{f_p} \sum_{p=0}^l \sum_{q=-\infty}^{+\infty} \frac{dF_{l+2} \, {}_{mp}}{di} G_{l+2} \, {}_{pq} \sin \gamma_{fl+2 \, {}_{mpq}}, \end{aligned} \quad (3.51)$$

$$\begin{aligned} \Delta\omega_f^+ &= \frac{g}{na^2\sqrt{1-e^2}} \sum_{l=0}^{\infty} \sum_{m=0}^l \left(\frac{R}{r}\right)^{l+3} A_{l+2} \, {}_m k_{lm}^+ H_l^m \frac{1}{f_p} \times \\ &\quad \times \sum_{p=0}^l \sum_{q=-\infty}^{+\infty} \left[\frac{1-e^2}{e} F_{l+2} \, {}_{mp} \frac{dG_{l+2} \, {}_{pq}}{de} - \frac{\cos i}{\sin i} \frac{dF_{l+2} \, {}_{mp}}{di} G_{l+2} \, {}_{pq} \right] \sin \gamma_{fl+2 \, {}_{mpq}}. \end{aligned} \quad (3.52)$$

The corrections induced by the Earth's flattening and rotation, due to the smallness of k_{lm}^+ , have been calculated only for those tidal lines which turned out to be the most effective in perturbing the node and the perigee of LAGEOS and LAGEOS II, i.e. the zonal 18.6-year tide and the K_1 . Adopting the values quoted in [Dehant *et al.*, 1999] for k_{lm}^+ and eqs. (3.51)-(3.52) it is possible to obtain the results summarized in Tab. 3.4. The quoted values, with the exception of the node of LAGEOS II, fall below the mas level turning out, at the present, undetectable.

3.3.2 The mismodelling in the nodes and the perigee

Concerning the errors in the values released in Tab. 3.1, Tab. 3.2, and Tab. 3.3, the major source of uncertainty in the perturbative amplitudes lies in the Love numbers $k_{2m}^{(0)}(f)$, and the orbital injection errors δi affecting the inclination i .

About the latter, by assuming $\delta i = 0.5$ mas [Ciufolini, 1989], we have calculated $\left| \frac{\partial A(\Omega)}{\partial i} \right| \delta i$ and $\left| \frac{\partial A(\omega)}{\partial i} \right| \delta i$ for 055.565, K_1 , and S_2 which are the most powerful tidal constituents in perturbing LAGEOS and LAGEOS II orbits. The results are of the order of 10^{-6} mas, so that we can neglect the effect of uncertainties in the inclination determination.

Concerning the Love numbers $k_{2m}^{(0)}(f)$, from a preliminary point of view, theoreticians claim that they are able to compute them with an accuracy of 10^{-4} using the specified Earth model. But the Earth models may differ. Probably uncertainty in Earth models may bring errors in computation of the Love numbers of the second order about 10^{-3} [L. Petrov, private communication, 1999]. First of all, this means that the level of accuracy of 1 mas, i.e. 10^{-9} rad, on Ω and ω given by eq. (3.40) and eq. (3.41) can be well reached, since the uncertainty in $H_l^m(f)$ amounts to 10^{-7} m. Second, assuming a mean value of 0.3 for k_2 , it can be stated that the uncertainty in the solid Earth tidal perturbation due to a single tide generating potential's constituent amount to almost 0.3 % for Ω and ω .

More specifically, we have assessed the uncertainties in them by calculating for certain tidal constituents the factor $\delta k_2/k_2$; k_2 is the average on the values released

by the most reliable models and δk_2 is its standard deviation. According to the recommendations of the Working Group of Theoretical Tidal Model of the Earth Tide Commission ([http://www.astro.oma.be/D1/EARTH\\$_TIDES/wgtide.html](http://www.astro.oma.be/D1/EARTH$_TIDES/wgtide.html)), in the diurnal band we have chosen the values released by *Mathews et al.* [1995], *McCarthy* [1996] and the two sets by *Dehant et al.* [1999]. For the zonal and sectorial bands we have included also the results of *Wang* [1994]. The uncertainties calculated in the Love numbers k_2 span from 0.5% to 1.5% for the tides of interest. However, it must be noticed that the worst known Love numbers are those related to the zonal band of the tidal spectrum due to the uncertainties in the anelasticity of the Earth's mantle. These results have been obtained in order to calculate the mismodelled amplitudes of the solid tidal perturbations $\delta\Omega^I$, $\delta\Omega^{II}$ and $\delta\omega^{II}$ for the nodes of LAGEOS and LAGEOS II and the perigee of LAGEOS II; they have been subsequently compared with the gravitomagnetic precessions over 4 years $\Delta\Omega_{LT}^I = 124$ mas, $\Delta\Omega_{LT}^{II} = 126$ mas and $\Delta\omega_{LT}^{II} = -228$ mas. In Tab. 3.9 we have quoted only those tidal lines whose mismodelled perturbative amplitudes are greater than 1% of the gravitomagnetic perturbations. It turns out that only 055.565 18.6-year and K_1 exceed this cutoff.

3.3.3 The mean anomaly and the inclination

In Tab. 3.5 and Tab. 3.6 the results for the mean anomaly are quoted, while Tab. 3.7 and Tab. 3.8 are devoted to the inclination.

Concerning the mean anomaly, in general LAGEOS is more sensitive than LAGEOS II. The 18.6-year tide and the K_1 induce perturbations of the order of 10^3 mas.

Regarding the inclination, by inspecting eq. (3.43) it can be noticed that the $m = 0$ zonal tidal perturbations vanish. Among the tesseral and sectorial constituents K_1 , K_2 and S_2 are the most effective in perturbing the inclination at a level of 10^2 mas.

3.4 Tables

Table 3.1: Perturbative amplitudes on the node Ω of LAGEOS due to solid Earth tides for $l = 2$, $p = 1$, $q = 0$. In the first column the Doodson number of each constituent is quoted followed by the Darwin's name, when it is present. The tidal lines are listed in order of decreasing periods. The coefficients $H_l^m(f)$ are those recently calculated by Roosbeek and multiplied by suitable normalization factors (IERS standards) in order to make possible a comparison with those of Cartwright and Edden. $\tan \delta_{lmf}$ expresses the phase lag of the solid Earth response with respect to the tidal potential due to the anelasticity in the mantle. The periods are in days, the amplitudes in mas and the $H_l^m(f)$ in meters.

Tide	Period	Amplitude	k_2 Love number	$H_l^m(f)$	$\tan \delta_{lmf}$
055.565	6,798.38	-1,079.38	0.315	0.02792	-0.01715
055.575	3,399.19	5.23	0.313	0.000272	-0.015584
056.554 S_a	365.27	9.96	0.307	-0.00492	-0.01135
057.555 S_{sa}	182.62	31.21	0.305	-0.03099	-0.01029
065.455 M_m	27.55	5.28	0.302	-0.03518	-0.00782
075.555 M_f	13.66	4.94	0.301	-0.06659	-0.007059
165.545	1232.94	-41.15	0.259	-0.007295	-0.00554
165.555 K_1	1,043.67	1,744.38	0.257	0.3687012	-0.0055933
165.565	904.77	203.02	0.254	0.050028	-0.005653
163.555 P_1	-221.35	136.44	0.286	-0.12198	-0.005017
145.555 O_1	-13.84	19	0.297	-0.26214	-0.00484
135.655 Q_1	-9.21	2.42	0.297	-0.05019	-0.00483
274.556	-1,217.55	1.68	0.301	0.000625	-0.00431
274.554	-1,216.73	-6.63	0.301	-0.00246	-0.00431
275.555 K_2	521.835	-92.37	0.301	0.0799155	-0.00431
273.555 S_2	-280.93	182.96	0.301	0.2940	-0.00431
272.556 T_2	-158.80	6.04	0.301	0.0171884	-0.00431
255.555 M_2	-14.02	19.63	0.301	0.6319	-0.00431
245.655 N_2	-9.29	2.49	0.301	0.12099	-0.00431

Table 3.2: Perturbative amplitudes on the node Ω of LAGEOS II due to solid Earth tides for $l = 2$, $p = 1$, $q = 0$. In the first column the Doodson number of each constituent is quoted followed by the Darwin's name, when it is present. The tidal lines are listed in order of decreasing periods. The coefficients $H_l^m(f)$ are those recently calculated by Roosbeek and multiplied by suitable normalization factors (IERS standards) in order to make possible a comparison with those of Cartwright and Edden. $\tan \delta_{lmf}$ expresses the phase lag of the solid Earth response with respect to the tidal potential due to the anelasticity in the mantle. The periods are in days, the amplitudes in mas and the $H_l^m(f)$ in meters.

Tide	Period	Amplitude	k_2 Love number	$H_l^m(f)$	$\tan \delta_{lmf}$
055.565	6,798.38	1,982.16	0.315	0.02792	-0.01715
055.575	3,399.19	-9.61	0.313	-0.000272	-0.015584
056.554 S_a	365.27	-18.28	0.307	-0.00492	-0.01135
057.555 S_{sa}	182.62	-57.31	0.305	-0.03099	-0.01029
065.455 M_m	27.55	-9.71	0.302	-0.03518	-0.00782
075.555 M_f	13.66	-9.08	0.301	-0.06659	-0.007059
165.565	-621.22	-58.31	0.254	0.050028	-0.005653
165.555 K_1	-569.21	-398	0.257	0.3687012	-0.0055933
165.545	-525.23	7.33	0.259	-0.007295	-0.005541
163.555 P_1	-138.26	35.65	0.286	-0.1219	-0.005017
145.555 O_1	-13.33	7.66	0.297	-0.26214	-0.00484
135.655 Q_1	-8.98	0.98	0.297	-0.05019	-0.00483
275.555 K_2	-284.6	-92.51	0.301	0.079915	-0.004318
274.556	-159.96	-0.40	0.301	0.000625	-0.00431
274.554	-159.95	1.6	0.301	-0.00246	-0.0043
273.555 S_2	-111.24	-133.04	0.301	0.29402	-0.00431
272.556 T_2	-85.27	-5.96	0.301	0.017188	-0.00431
255.555 M_2	-13.03	-33.05	0.301	0.6319	-0.004318
245.655 N_2	-8.84	-4.35	0.301	0.12099	-0.00431

Table 3.3: Perturbative amplitudes on the perigee ω of LAGEOS II due to solid Earth tides for $l = 2$, $p = 1$, $q = 0$. In the first column the Doodson number of each constituent is quoted followed by the Darwin's name, when it is present. The tidal lines are listed in order of decreasing periods. The coefficients $H_l^m(f)$ are those recently calculated by Roosbeek and multiplied by suitable normalization factors (IERS standards) in order to make possible a comparison with those of Cartwright and Edden. $\tan \delta_{lmf}$ expresses the phase lag of the solid Earth response with respect to the tidal potential due to the anelasticity in the mantle. The periods are in days, the amplitudes in mas and the $H_l^m(f)$ in meters.

Tide	Period	Amplitude	k_2 Love number	$H_l^m(f)$	$\tan \delta_{lmf}$
055.565	6,798.38	-1,375.58	0.315	0.02792	-0.01715
055.575	3,399.19	6.66	0.313	-0.000272	-0.015584
056.554 S_a	365.27	12.69	0.307	-0.00492	-0.01135
057.555 S_{sa}	182.62	39.77	0.305	-0.03099	-0.01029
065.455 M_m	27.55	6.74	0.302	-0.03518	-0.00782
075.555 M_f	13.66	6.30	0.301	-0.06659	-0.007059
165.565	-621.22	290.43	0.254	0.050028	-0.005653
165.555 K_1	-569.21	1,982.14	0.257	0.3687012	-0.0055933
165.545	-525.23	-36.52	0.259	-0.007295	-0.005541
163.555 P_1	-138.26	-177.56	0.286	-0.1219	-0.005017
145.555 O_1	-13.33	-38.16	0.297	-0.26214	-0.00484
135.655 Q_1	-8.98	-4.92	0.297	-0.05019	-0.00483
275.555 K_2	-284.6	-88.19	0.301	0.079915	-0.004318
274.556	-159.96	-0.38	0.301	0.000625	-0.00431
274.554	-159.95	1.52	0.301	-0.00246	-0.0043
273.555 S_2	-111.24	-126.83	0.301	0.29402	-0.00431
272.556 T_2	-85.27	-5.68	0.301	0.017188	-0.00431
255.555 M_2	-13.03	-31.9	0.301	0.6319	-0.004318
245.655 N_2	-8.84	-4.15	0.301	0.12099	-0.00431

Table 3.4: Corrections, in mas, to the Earth solid tidal perturbations on the nodes of LAGEOS and the perigee of LAGEOS II due to the Earth's flattening and Earth's rotation for $l = 2$, $p = 2$, $q = 0$. The values adopted for k_{2m}^+ are those quoted by Dehant [1999].

Tide	$\Delta\Omega_{\text{LAGEOS}}$	$\Delta\Omega_{\text{LAGEOS II}}$	$\Delta\omega_{\text{LAGEOS II}}$	k_{2m}^+
055.565	0.43	1.28	0.19	-0.00094
165.555 K_1	-0.97	-9.49	0.85	-0.00074

Table 3.5: Perturbative amplitudes on the mean anomaly \mathcal{M} of LAGEOS due to solid Earth tides for $l = 2$, $p = 1$, $q = 0$. In the first column the Doodson number of each constituent is quoted followed by the Darwin's name, when it is present. The tidal lines are listed in order of decreasing periods. The Love numbers k_2 have been calculated using the IERS standards. The coefficients $H_l^m(f)$ are those recently calculated by Roosbeek and multiplied by suitable normalization factors (IERS standards) in order to make possible a comparison with those of Cartwright and Edden. $\tan \delta_{lmf}$ expresses the phase lag of the solid Earth response with respect to the tidal potential due to the anelasticity in the mantle. The periods are in days, the amplitudes in mas and the $H_l^m(f)$ in meters.

Tide	Period	Amplitude	k_2	Love number	$H_l^m(f)$	$\tan \delta_{lmf}$
055.565	6,798.38	1,029.90	0.315		0.02792	-0.01715
055.575	3,399.19	-4.99	0.313		0.000272	-0.015584
056.554 S_a	365.27	-9.5	0.307		-0.00492	-0.01135
057.555 S_{sa}	182.62	-29.78	0.305		-0.03099	-0.01029
065.455 M_m	27.55	-5.04	0.302		-0.03518	-0.00782
075.555 M_f	13.66	-4.72	0.301		-0.06659	-0.007059
165.545	1232.94	-48.50	0.259		-0.007295	-0.00554
165.555 K_1	1,043.67	2,055.72	0.257		0.3687012	-0.0055933
165.565	904.77	239.26	0.254		0.050028	-0.005653
163.555 P_1	-221.35	160.80	0.286		-0.12198	-0.005017
145.555 O_1	-13.84	22.39	0.297		-0.26214	-0.00484
135.655 Q_1	-9.21	2.85	0.297		-0.05019	-0.00483
274.554	-1,216.73	25.76	0.301		-0.00246	-0.00431
274.556	-1,217.55	-6.55	0.301		0.000625	-0.00431
275.555 K_2	521.8	358.93	0.301		0.0799155	-0.00431
273.555 S_2	-280.93	-710.96	0.301		0.0171884	-0.00431
272.556 T_2	-158.80	-23.49	0.301		0.0171884	-0.00431
255.555 M_2	-14.02	-76.3	0.301		0.6319	-0.00431
245.655 N_2	-9.29	-9.68	0.301		0.12099	-0.00431

Table 3.6: Perturbative amplitudes on the mean anomaly \mathcal{M} of LAGEOS II due to solid Earth tides for $l = 2$, $p = 1$, $q = 0$. In the first column the Doodson number of each constituent is quoted followed by the Darwin's name, when it is present. The tidal lines are listed in order of decreasing periods. The Love numbers k_2 have been calculated using the IERS standards. The coefficients $H_l^m(f)$ are those recently calculated by Roosbeek and multiplied by suitable normalization factors (IERS standards) in order to make possible a comparison with those of Cartwright and Edden. $\tan \delta_{lmf}$ expresses the phase lag of the solid Earth response with respect to the tidal potential due to the anelasticity in the mantle. The periods are in days, the amplitudes in mas and the $H_l^m(f)$ in meters.

Tide	Period	Amplitude	k_2	Love number	$H_l^m(f)$	$\tan \delta_{lmf}$
055.565	6,798.38	-172.28	0.315		0.02792	-0.01715
055.575	3,399.19	0.83	0.313		-0.000272	-0.015584
056.554 S_a	365.27	1.58	0.307		-0.00492	-0.01135
057.555 S_{sa}	182.62	4.98	0.305		-0.03099	-0.01029
065.455 M_m	27.55	0.84	0.302		-0.03518	-0.00782
075.555 M_f	13.66	0.78	0.301		-0.06659	-0.007059
165.565	-621.22	255	0.254		0.050028	-0.005653
165.555 K_1	-569.21	1,740.36	0.257		0.3687012	-0.0055933
165.545	-525.23	-32.07	0.259		-0.007295	-0.005541
163.555 P_1	-138.26	-155.90	0.286		-0.1219	-0.005017
145.555 O_1	-13.33	-33.5	0.297		-0.26214	-0.00484
135.655 Q_1	-8.98	-4.32	0.297		-0.05019	-0.00483
275.555 K_2	-284.6	-144.34	0.301		0.079915	-0.00431
274.556	-159.96	-0.63	0.301		0.000625	-0.00431
274.554	-159.95	2.49	0.301		-0.00246	-0.00431
273.555 S_2	-111.24	-207.57	0.301		0.29402	-0.00431
272.556 T_2	-85.27	-9.3	0.301		0.017188	-0.00431
255.555 M_2	-13.03	-52.28	0.301		0.6319	-0.00431
245.655 N_2	-8.84	-6.79	0.301		0.12099	-0.00431

Table 3.7: Perturbative amplitudes on the inclination i of LAGEOS due to solid Earth tides for $l = 2$, $p = 1$, $q = 0$. In the first column the Doodson number of each constituent is quoted followed by the Darwin's name, when it is present. The tidal lines are listed in order of decreasing periods. The Love numbers k_2 have been calculated using the IERS standards. The coefficients $H_l^m(f)$ are those recently calculated by Roosbeek and multiplied by suitable normalization factors (IERS standards) in order to make possible a comparison with those of Cartwright and Edden. $\tan \delta_{lmf}$ expresses the phase lag of the solid Earth response with respect to the tidal potential due to the anelasticity in the mantle. The periods are in days, the amplitudes in mas and the $H_l^m(f)$ in meters.

Tide	Period	Amplitude	k_2	Love number	$H_l^m(f)$	$\tan \delta_{lmf}$
165.545	1,232.94	17.19	0.259		-0.007295	-0.00554
165.555 K_1	1,043.67	-728.96	0.257		0.3687012	-0.0055933
165.565	904.77	-84.84	0.254		0.050028	-0.005653
163.555 P_1	-221.35	-57.02	0.286		-0.12198	-0.005017
145.555 O_1	-13.84	-7.94	0.297		-0.26214	-0.00484
135.655 Q_1	-9.21	-1.01	0.297		-0.05019	-0.00483
274.554	-1,216.73	-18.27	0.301		-0.00246	-0.00431
274.556	-1,217.55	4.64	0.301		0.000625	-0.00431
275.555 K_2	521.8	-254.55	0.301		0.0799155	-0.00431
273.555 S_2	-280.93	504.21	0.301		0.2940	-0.00431
272.556 T_2	-158.80	16.66	0.301		0.0171884	-0.00431
255.555 M_2	-14.02	54.11	0.301		0.6319	-0.00431
245.655 N_2	-9.29	6.86	0.301		0.12099	-0.00431

Table 3.8: Perturbative amplitudes on the inclination i of LAGEOS II due to solid Earth tides for $l = 2$, $p = 1$, $q = 0$. In the first column the Doodson number of each constituent is quoted followed by the Darwin's name, when it is present. The tidal lines are listed in order of decreasing periods. The Love numbers k_2 have been calculated using the IERS standards. The coefficients $H_l^m(f)$ are those recently calculated by Roosbeek and multiplied by suitable normalization factors (IERS standards) in order to make possible a comparison with those of Cartwright and Edden. $\tan \delta_{lmf}$ expresses the phase lag of the solid Earth response with respect to the tidal potential due to the anelasticity in the mantle. The periods are in days, the amplitudes in mas and the $H_l^m(f)$ in meters.

Tide	Period	Amplitude	k_2	Love number	$H_l^m(f)$	$\tan \delta_{lmf}$
165.565	-621.22	-106.97	0.254		0.050028	-0.005653
165.555 K_1	-569.21	-730.09	0.257		0.3687012	-0.0055933
165.545	-525.23	13.45	0.259		-0.007295	-0.005541
163.555 P_1	-138.26	65.04	0.286		-0.1219	-0.005017
145.555 O_1	-13.33	14.05	0.297		-0.26214	-0.00484
135.655 Q_1	-8.98	1.81	0.297		-0.05019	-0.00483
275.555 K_2	-284.6	121.1	0.301		0.079915	-0.00431
274.556	-159.96	0.53	0.301		0.000625	-0.00431
274.554	-159.95	-2.09	0.301		-0.00246	-0.0043
273.555 S_2	-111.24	174.15	0.301		0.29402	-0.00431
272.556 T_2	-85.27	7.8	0.301		0.017188	-0.00431
255.555 M_2	-13.03	43.86	0.301		0.6319	-0.00431
245.655 N_2	-8.84	5.7	0.301		0.12099	-0.00431

Table 3.9: Mismodeled solid tidal perturbations on the nodes Ω of LAGEOS and LAGEOS II and the perigee ω of LAGEOS II compared to their gravitomagnetic precessions over 4 years $\Delta\Omega_{LT}^I = 124$ mas $\Delta\Omega_{LT}^II = 126$ mas $\Delta\omega_{LT}^I = -228$ mas. Only those constituents which exceed the 1 % cutoff have been quoted. The ratios are in percent and the δX in mas.

Tide	$\frac{\delta k_2}{k_2}$	$\delta\Omega^I$	$\frac{\delta\Omega^I}{\Delta\Omega_{LT}^I}$	$\delta\Omega^{II}$	$\frac{\delta\Omega^{II}}{\Delta\Omega_{LT}^{II}}$	$\delta\omega^{II}$	$\frac{\delta\omega^{II}}{\Delta\omega_{LT}^{II}}$
055.565	1.5	-16.5	13.3	30.3	24	-21	9.2
165.555 K_1	0.5	9	7.2	-2	1.6	10.2	4.4

3.5 Gravitational potential of the ocean Earth tides

One of the early attempts to explain the phenomenon of fluid tides [Zahel, 1997] in its globality is the equilibrium theory [Defant, 1961; Melchior, 1983] by Newton. It is based on the assumption that at every time the free water surface of the oceans coincides exactly with the spheroidal equipotential surface at $r = R$ due to the combined action of the Earth's proper gravity and the lunisolar tidal potential. Differently stated, the oceanic tidal bulge at every instant coincides exactly with the envelope of

the forces produced by the tide generating potential at the Earth's surface. At every tidal constituents $\Phi(f)$ corresponds an equilibrium partial tide η_f . Referring to eq. (3.16) it can be write:

$$\eta_f = \frac{\Phi_f(R)}{g} = A_{lm} H_l^m P_l^m(\sin \phi) \cos(\sigma t + m\lambda + c_{lm}). \quad (3.53)$$

For $l = 2$ and $m = 0$ eq. (3.53) represents a standing wave which crests at $t = 0$, while for $l = 2$ and $m = 1, 2$ it refers to running waves around the oceans from East to West. If the equilibrium theory had been valid, it would mean that the water masses acted upon by the tidal potential are deprived almost entirely of their inertia in the sense that they would adapt instantaneously to their equilibrium positions on the equipotential surface which, in fact, changes in time at the frequencies of the lunisolar tidal potential. The reality is quite different, because of the complex hydrodynamical behavior of the oceans; at every equilibrium partial tide η_f corresponds an effective partial tide [Hendershott and Munk, 1970]

$$\zeta_f = \xi_f(\vartheta, \lambda) \cos [\sigma t - \delta_f(\vartheta, \lambda)], \quad (3.54)$$

where $\xi_f(\vartheta, \lambda)$ and $\delta_f(\vartheta, \lambda)$ [Schwiderski, 1980] are defined as harmonic constants: $\xi_f(\vartheta, \lambda)$ is half the difference between high water and low water for a given place while $\delta_f(\vartheta, \lambda)$ is the phase lag of the ocean tide with respect to the equilibrium one when the phase of the latter is calculated at Greenwich meridian $\lambda = 0$: the delay at any other meridian is obtained simply adding $m\lambda$ to $\delta_f(\vartheta, \lambda)$. Moreover, ζ_f at every time \bar{t} crests on the “cotidal” line $\sigma\bar{t} = \delta_f(\vartheta, \lambda)$; in general, referring to a given point (ϑ, λ) , e.g., on the shoreline, the cotidal lines related to two consecutive instants may depart from the shore into the sea or vice versa, giving rise to outcoming and incoming waves with respect to that place.

Such departures from the equilibrium theory are due to several reasons. First of all, the fluid elements can freely flow and once they had been put in motion, their notable inertia prevent them to change instantaneously their state of motion making them stop at the equipotential surface. Second, dissipative phenomena and non-linear interactions among the various partial tides and other ocean currents must be taken in account. This implies that the response of the water masses to the forcing lunisolar potential presents a phase lag with respect to it: the sea surface is not an equipotential

one so that tangential forces acts on the water particles generating tidal currents. The equilibrium theory may be considered an almost good approximation to the reality only at very low frequencies of the tidal potential, like as the Moon and the Sun would remain fix in the space with respect to the Earth.

The equations of motion governing the complex hydrodynamics of the tidal currents are the so called Lagrange Tidal Equations (LTE) [Neumann, 1966; Pekeris and Akkad, 1969; Hendershott, 1972; Hendershott, 1973; Gill, 1982], which, in general, are not linear. The simplest form for them is obtained considering a spherical, rotating Earth entirely covered by an ocean made of a perfect and incompressible fluid; if only the tangential motion is considered, neglecting the squares and the cross products of the velocity field's components, it is possible to obtain the following linearized LTE:

$$\frac{\partial v_\vartheta}{\partial t} = +2\omega_\oplus v_\lambda \cos \vartheta - \frac{g}{R} \frac{\partial(\zeta - \eta)}{\partial \vartheta}, \quad (3.55)$$

$$\frac{\partial v_\lambda}{\partial t} = -2\omega_\oplus v_\vartheta \cos \vartheta - \frac{g}{R \sin \vartheta} \frac{\partial(\zeta - \eta)}{\partial \lambda}, \quad (3.56)$$

$$\frac{\partial \zeta}{\partial t} = -\frac{1}{R \sin \vartheta} \left[\frac{\partial(hv_\lambda)}{\partial \lambda} + \frac{\partial(h \sin \vartheta v_\vartheta)}{\partial \vartheta} \right], \quad (3.57)$$

in which

ϑ terrestrial colatitude.

h depth of the ocean, $h = h(\vartheta, \lambda)$, m.

ζ non-equilibrium, ocean partial tide, m.

v_ϑ and v_λ tangential components of the water's velocity field.

The LTE are linear, and so each ocean partial tide ζ_f can be treated independently of the other ones. The fundamental problem of the ocean tides consists of the determination of the harmonic constants for every place on the Earth: this can be obtained, in principle, resolving the LTE for a given constituent, but this task is in many cases prohibitive due to the great calculational complexity needed to obtain realistic results. Another strategy consists of employing geodetic artificial satellites, as is done in the realization of the various Earth Gravity Model of the Goddard Space Flight Center among which EGM96 [Lemoine *et al.*, 1998] is the most recent, or in altimetric measurements [Shum *et al.*, 1995].

In order to calculate the gravitational effect of the water masses raised by the tidal forces of a given constituent $\Phi_l^m(f)$ it can be considered a spherical layer with radius

R endowed with a bidimensional surface mass density $\mu_f(\vartheta, \lambda) = \rho\zeta_f(\vartheta, \lambda)$, where ρ is the volumetric ocean water density assumed constant, and calculate its potential as:

$$U_f = G \int \frac{\mu_f(\vartheta', \lambda')}{|\mathbf{r} - \mathbf{r}'|} d\Sigma' = G \int \frac{\rho\zeta_f(\vartheta', \lambda')}{|\mathbf{r} - \mathbf{r}'|} d\Sigma'. \quad (3.58)$$

In eq. (3.58) the geodetic convention for the potential is used [Kaula, 1966]: in it U is the potential usually defined in physics with the sign reversed. Let us rewrite ζ_f as:

$$\zeta_f = \xi_f \cos(\sigma t - \delta_f) = \xi_f \cos \delta_f \cos \sigma t + \xi_f \sin \delta_f \sin \sigma t. \quad (3.59)$$

The following step consists of expanding eq. (3.59) in spherical harmonics [Dow, 1988; Christodoulidis *et al.*, 1988]:

$$\xi_f \cos \delta_f = \sum_{l=0}^{\infty} \sum_{m=0}^l (a_{lmf} \cos m\lambda + b_{lmf} \sin m\lambda) P_l^m(\sin \phi), \quad (3.60)$$

$$\xi_f \sin \delta_f = \sum_{l=0}^{\infty} \sum_{m=0}^l (c_{lmf} \cos m\lambda + d_{lmf} \sin m\lambda) P_l^m(\sin \phi). \quad (3.61)$$

The coefficients of the harmonic expansion, which have the dimension of lengths, can be calculated if the harmonic constants are known by means of the following formulas

$$a_{lmf} = \frac{(2l+1)(2-\delta_{0m})}{4\pi} \frac{(l-m)!}{(l+m)!} \times \int \xi_f \cos \delta_f \cos m\lambda P_l^m(\sin \phi) d\Sigma, \quad (3.62)$$

$$b_{lmf} = \frac{(2l+1)(2-\delta_{0m})}{4\pi} \frac{(l-m)!}{(l+m)!} \times \int \xi_f \cos \delta_f \sin m\lambda P_l^m(\sin \phi) d\Sigma, \quad (3.63)$$

$$c_{lmf} = \frac{(2l+1)(2-\delta_{0m})}{4\pi} \frac{(l-m)!}{(l+m)!} \times \int \xi_f \sin \delta_f \cos m\lambda P_l^m(\sin \phi) d\Sigma, \quad (3.64)$$

$$d_{lmf} = \frac{(2l+1)(2-\delta_{0m})}{4\pi} \frac{(l-m)!}{(l+m)!} \times \int \xi_f \sin \delta_f \sin m\lambda P_l^m(\sin \phi) d\Sigma. \quad (3.65)$$

Eqs. (3.62)-(3.65) are the connection between the harmonic constants obtained through oceanographic models and the data acquired by geodetic satellites, in the sense that if the coefficients a_{lmf} , b_{lmf} , c_{lmf} , d_{lmf} , for a given tidal line, are known from orbital analysis, by means of eq. (3.62)-eq. (3.65), the essential features of that partial tide may be recovered. With eqs. (3.60)-(3.61) eq. (3.59) becomes

$$\zeta_f = \sum_{l=0}^{\infty} \sum_{m=0}^l (C_{lmf} \cos m\lambda + S_{lmf} \sin m\lambda) P_l^m(\sin \phi) \quad (3.66)$$

in which

$$C_{lmf} = a_{lmf} \cos \sigma t + c_{lmf} \sin \sigma t, \quad (3.67)$$

$$S_{lmf} = b_{lmf} \cos \sigma t + d_{lmf} \sin \sigma t. \quad (3.68)$$

By inserting eq. (3.66) in eq. (3.58) and expanding in spherical harmonics also the term $1/|\mathbf{r} - \mathbf{r}'|$, it can be obtained

$$U_f = 4\pi G R \rho \sum_{l=0}^{\infty} \sum_{m=0}^l \frac{1}{2l+1} \left(\frac{R}{r}\right)^{l+1} (C_{lmf} \cos m\lambda + S_{lmf} \sin m\lambda) P_l^m(\sin \phi). \quad (3.69)$$

In eq. (3.69), using eq. (3.67)-eq. (3.68), one can further expand $(C_{lmf} \cos m\lambda + S_{lmf} \sin m\lambda)$ by introducing the prograde (westwards) and retrograde waves [Schwiderski, 1980]

$$C_{lmf} \cos m\lambda + S_{lmf} \sin m\lambda = \sum_{\pm} K_{lmf}^{\pm} \cos(m\lambda \pm \sigma t) \pm S_{lmf}^{\pm} \sin(m\lambda \pm \sigma t). \quad (3.70)$$

In eq. (3.70) and in the following, expressions like $\sum_{\pm} A^{\pm} \cos(a \pm b)$ must be interpreted as $A^+ \cos(a+b) + A^- \cos(a-b)$. The sign $+$ refers to the progressive (westwards) waves while the sign $-$ is for the waves moving from West to East. From eqs. (3.67)-(3.68) and eq. (3.70) one has

$$a_{flm} = K_{flm}^+ + K_{flm}^-, \quad (3.71)$$

$$b_{flm} = S_{flm}^+ - S_{flm}^-, \quad (3.72)$$

$$c_{flm} = S_{flm}^+ + S_{flm}^-, \quad (3.73)$$

$$d_{flm} = -K_{flm}^+ + K_{flm}^-. \quad (3.74)$$

From these equations, by defining

$$K_{lmf}^{\pm} = C_{lmf}^{\pm} \cos \varepsilon_{flm}^{\pm}, \quad (3.75)$$

$$S_{lmf}^{\pm} = C_{lmf}^{\pm} \sin \varepsilon_{flm}^{\pm}, \quad (3.76)$$

it is possible to express the coefficients of the expansion of the harmonic constants a_{lmf} , b_{lmf} , c_{lmf} , d_{lmf} in terms of C_{lmf}^{\pm} , ε_{lmf}^{\pm} which can be recovered by geodetic satellites

$$C_{lmf}^+ \cos \varepsilon_{lmf}^+ = \frac{a_{lmf} - d_{lmf}}{2}, \quad (3.77)$$

$$C_{lmf}^- \cos \varepsilon_{lmf}^- = \frac{a_{lmf} + d_{lmf}}{2}, \quad (3.78)$$

$$C_{lmf}^+ \sin \varepsilon_{lmf}^+ = \frac{c_{lmf} + b_{lmf}}{2}, \quad (3.79)$$

$$C_{lmf}^- \sin \varepsilon_{lmf}^- = \frac{-b_{lmf} + c_{lmf}}{2}. \quad (3.80)$$

Eq. (3.63) and eq. (3.65) show that, for $m = 0$, it turns out $b_{l0f} = d_{l0f} = 0$ identically; this implies through eqs. (3.77)-(3.80) that

$$C_{l0f}^+ = C_{l0f}^-, \quad (3.81)$$

$$\varepsilon_{l0f}^+ = \varepsilon_{l0f}^-. \quad (3.82)$$

Eqs. (3.81)-(3.82) will be used in the next section. It is interesting to notice that eqs. (3.77)-(3.80), or also eqs. (3.71)-(3.74), show that if it were $c_{lmf} = d_{lmf} = 0$, the distinction between the prograde and retrograde waves would disappear and only one kind of waves would remain, as in the equilibrium theory. Indeed, eqs. (3.64)-(3.65) point out that $c_{lmf} = d_{lmf} = 0$ if and only if $\delta_f = 0$, where δ_f is the phase lag of the ocean response with respect to the lunisolar tidal constituent due to the ocean hydrodynamics.

Eq. (3.69), with eq. (3.70) and eqs. (3.75)-(3.76), becomes

$$U_f = 4\pi G R \rho \sum_{l=0}^{\infty} \sum_{m=0}^l \sum_{+} \left(\frac{R}{r}\right)^{l+1} \frac{C_{lmf}^{\pm}}{2l+1} \cos(\sigma t \pm m\lambda - \varepsilon_{lmf}^{\pm}) P_l^m(\sin \phi). \quad (3.83)$$

Eq. (3.83) expresses the gravitational potential of the Earth's ocean waters, thought as a spherical layer of mass $\rho \zeta_f$ raised by the action of a given lunisolar tidal constituent of circular frequency σ .

But these enormous water masses act upon the sea floor and the whole of the solid Earth which are deformed and attracted by them. This effect has also to be considered. It can be done according to eq. (3.15) and introducing the so called load Love numbers k'_l [Farrell, 1972; Dow, 1988; Pagiatakis, 1990]. The global response of the Earth oceans to the forcing tidal constituent of frequency σ can be written as

$$U_f = U_{\text{oc}} + U_{\text{load}} = 4\pi G R \rho \sum_{l=0}^{\infty} \sum_{m=0}^l \sum_{+} \left(\frac{R}{r}\right)^{l+1} \frac{(1+k'_l)}{2l+1} \times \\ \times C_{lmf}^{\pm} \cos(\sigma t \pm m\lambda - \varepsilon_{lmf}^{\pm}) P_l^m(\sin \phi), \quad (3.84)$$

with $U_f < U_{\text{oc}}$, i.e. $k' < 0$. This fact can be intuitively guessed by thinking about U in terms of shift of the equipotential surfaces $h = U/g$: if the sea floor is raised by the tidally driven water masses the total shift is smaller than it would be if we considered the solid Earth as completely rigid.

3.6 Ocean tidal orbital perturbations

Eq. (3.84) can be fruitfully rewritten in a form more suitable for calculating the perturbations induced on the Keplerian orbital elements of artificial satellites [*Felsen-treger and Marsh, 1978; Goad and Douglas, 1978*]. To this aim the following quantities are defined

$$A_{lmf}^{\pm} = 4\pi GR\rho \frac{(1+k_l')}{2l+1} C_{lmf}^{\pm}, \quad (3.85)$$

$$C_{lmf}^{\pm} = A_{lmf}^{\pm} \cos(\mp\sigma t \pm \varepsilon_{lmf}^{\pm}), \quad (3.86)$$

$$S_{lmf}^{\pm} = A_{lmf}^{\pm} \sin(\mp\sigma t \pm \varepsilon_{lmf}^{\pm}). \quad (3.87)$$

U_f becomes

$$U_f = \sum_{l=0}^{\infty} \sum_{m=0}^l \sum_{+}^{\pm} \left(\frac{R}{r}\right)^{l+1} (C_{lmf}^{\pm} \cos m\lambda + S_{lmf}^{\pm} \sin m\lambda) P_l^m(\sin \phi). \quad (3.88)$$

Eq. (3.88) is formally equal to the expression of the static gravitational potential of the Earth worked out by Kaula. So, with the same mathematical menagerie used for the geopotential in [*Kaula, 1966*], it is possible to write eq. (3.88) in terms of the Keplerian orbital elements of a test body in the field of the Earth as

$$U_f = \sum_{l=0}^{\infty} \sum_{m=0}^l \sum_{+}^{\pm} \left(\frac{R}{r}\right)^{l+1} A_{lmf}^{\pm} \sum_{p=0}^l \sum_{q=-\infty}^{+\infty} F_{lmp}(i) G_{lpq}(e) \begin{bmatrix} \cos \gamma_{flmpq}^{\pm} \\ \sin \gamma_{flmpq}^{\pm} \end{bmatrix}, \quad (3.89)$$

in which

$$\gamma_{flmpq}^{\pm} = (l-2p)\omega + (l-2p+q)\mathcal{M} + m(\Omega - \theta) \pm (\sigma t - \varepsilon_{lmf}^{\pm}). \quad (3.90)$$

The equations for the tidal ocean perturbations may be worked out as already done for the solid Earth tides in Sec. 4. At first order, one obtains

$$\begin{aligned} \Delta\Omega_f &= \frac{1}{na^2\sqrt{1-e^2}\sin i} \sum_{l=0}^{\infty} \sum_{m=0}^l \sum_{+}^{\pm} \left(\frac{R}{r}\right)^{l+1} A_{lmf}^{\pm} \times \\ &\quad \times \sum_{p=0}^l \sum_{q=-\infty}^{+\infty} \frac{dF_{lmp}}{di} G_{lpq} \frac{1}{f_p} \begin{bmatrix} \sin \gamma_{flmpq}^{\pm} \\ -\cos \gamma_{flmpq}^{\pm} \end{bmatrix}_{l-m \text{ odd}}^{l-m \text{ even}}, \end{aligned} \quad (3.91)$$

$$\begin{aligned} \Delta\omega_f &= \frac{1}{na^2\sqrt{1-e^2}} \sum_{l=0}^{\infty} \sum_{m=0}^l \sum_{+}^{\pm} \left(\frac{R}{r}\right)^{l+1} A_{lmf}^{\pm} \times \\ &\quad \times \sum_{p=0}^l \sum_{q=-\infty}^{+\infty} \left[\frac{1-e^2}{e} F_{lmp} \frac{dG_{lpq}}{de} - \frac{\cos i}{\sin i} \frac{dF_{lmp}}{di} G_{lpq} \right] \frac{1}{f_p} \begin{bmatrix} \sin \gamma_{flmpq}^{\pm} \\ -\cos \gamma_{flmpq}^{\pm} \end{bmatrix}_{l-m \text{ odd}}^{l-m \text{ even}}, \end{aligned} \quad (3.92)$$

$$\begin{aligned} \Delta \mathcal{M}_f &= \frac{1}{na^2} \sum_{l=0}^{\infty} \sum_{m=0}^l \sum_{+} \left(\frac{R_{\oplus}}{r} \right)^{l+1} A_{lmf}^{\pm} \times \\ &\times \sum_{p=0}^l \sum_{q=-\infty}^{+\infty} F_{lmp}(i) \left[2(l+1)G_{lpq}(e) - \frac{1-e^2}{e} \frac{dG_{lpq}}{de} \right] \frac{1}{f_p} \begin{bmatrix} \sin \gamma_{flmpq}^{\pm} \\ -\cos \gamma_{flmpq}^{\pm} \end{bmatrix}_{l-m \text{ odd}}^{l-m \text{ even}}, \end{aligned} \quad (3.93)$$

$$\begin{aligned} \Delta i_f &= \frac{1}{na^2 \sqrt{1-e^2} \sin i} \sum_{l=0}^{\infty} \sum_{m=0}^l \sum_{+} \left(\frac{R_{\oplus}}{r} \right)^{l+1} A_{lmf}^{\pm} \times \\ &\times \sum_{p=0}^l \sum_{q=-\infty}^{+\infty} F_{lmp}(i) G_{lpq}(e) [(l-2p) \cos i - m] \frac{1}{f_p} \begin{bmatrix} \cos \gamma_{flmpq}^{\pm} \\ \sin \gamma_{flmpq}^{\pm} \end{bmatrix}_{l-m \text{ odd}}^{l-m \text{ even}}, \end{aligned} \quad (3.94)$$

in which

$$f_p = (l-2p)\dot{\omega} + (l-2p+q)\dot{\mathcal{M}} + m(\dot{\Omega} - \dot{\theta}) \pm \sigma. \quad (3.95)$$

It should be noticed that the frequencies of the perturbations given by eq. (3.95) are different, in general, from the frequencies of the solid Earth tidal perturbations given by eq. (3.45). While for the solid tides the diurnal modulation due to $\dot{\theta}$ cancels out automatically if one considers those terms in which $j_1 = m$, for the ocean tides, in general, this does not happen because of the presence of the Eastwards waves due to the non-equilibrium pattern of the ocean tidal bulge.

Long periodicities can be obtained considering those combinations of l , p and q for which $l-2p+q=0$ holds and retaining the Westward prograde terms with $j_1 = m$. Only in this way in eq. (3.95) the contributions of $\dot{\theta}$ are equal and opposite, and cancel out. With these bounds on l , m , p and q the frequencies of the perturbations of interest become

$$f_p = \dot{\Gamma}_f + (l-2p)\dot{\omega} + m\dot{\Omega}. \quad (3.96)$$

It is worthwhile noting that the frequencies f_p are identical to those of solid tidal perturbations [Dow, 1988; Bertotti and Carpino, 1989], so that the satellites cannot distinguish one effect from the other, a feature which will turn out to be important in the recovery of the coefficients C_{lmf}^{\pm} .

For $l=2$, as for the solid tides, $l-2p=0$ holds. The frequencies of the perturbations are, in this case, given by

$$f_p = \dot{\Gamma}_f + m\dot{\Omega}. \quad (3.97)$$

If l is odd the situation is different because now all the terms with p running from 0 to l must be considered and q is different from zero: $q = 2p - l$. So, the rates of the perturbations include the contribute of $\dot{\omega}$.

Up to now the prograde wave terms only have been considered in order to deal with long period perturbations. Yet, there is a case in which also the retrograde terms fit into this scheme; it is possible to show that for l even and $m = 0$ the frequencies of prograde and retrograde terms coincide, in absolute values, and the perturbation amplitudes are twice the amplitudes of the prograde terms only. Indeed, according to eqs. (3.91)-(3.93), $\Delta\Omega_f$, $\Delta\omega_f$ are proportional to

$$\sum_{+}^{\pm} A_{flm}^{\pm} \frac{1}{f_p} \left[\begin{array}{c} \sin \gamma_{flmpq}^{\pm} \\ -\cos \gamma_{flmpq}^{\pm} \end{array} \right]; \quad (3.98)$$

in this case $l - m$ is even and retaining only those terms for which $l - 2p = 0$ one has:

$$\gamma_{fl0\frac{l}{2}0}^{\pm} = \pm(\sigma t - \varepsilon_{fl0}^{\pm}), \quad (3.99)$$

$$f_p = \pm\sigma. \quad (3.100)$$

Expanding eq. (3.98) it can be obtained

$$\begin{aligned} A_{fl0}^+ \frac{1}{\sigma} \sin(\sigma t - \varepsilon_{fl0}^+) + A_{fl0}^- \frac{1}{-\sigma} \sin[-(\sigma t - \varepsilon_{fl0}^-)] &= \\ = A_{fl0}^+ \frac{1}{\sigma} \sin(\sigma t - \varepsilon_{fl0}^+) + A_{fl0}^- \frac{1}{\sigma} \sin(\sigma t - \varepsilon_{fl0}^-). \end{aligned} \quad (3.101)$$

Since $A_{fl0}^+ = A_{fl0}^-$ and $\varepsilon_{fl0}^+ = \varepsilon_{fl0}^-$, as shown by eq. (3.81) and eq. (3.82), eq. (3.101) becomes

$$\frac{2A_{fl0}^+}{\sigma} \sin(\sigma t - \varepsilon_{fl0}^+). \quad (3.102)$$

Eqs. (3.91)-(3.92) have been adopted in order to compute the amplitudes of the ocean tidal perturbations on the Keplerian elements Ω for LAGEOS and LAGEOS II and ω for LAGEOS II which pertain directly the Lense-Thirring experiment. Also in this section the perturbations of second order [Balogh *et al.*, 2000] due to the oblateness of the Earth have not been considered, as already done for the solid tides. The inclination and eccentricity functions used are those quoted in [Kaula, 1966]. For the numerical values of the various geophysical parameters which figure in eqs. (3.91)-(3.92) the IERS standards [McCarthy, 1996] have been used, while the EGM96 gravity

model [Lemoine *et al.*, 1998] has been adopted for the choice of the tidal constituents and their coefficients C_{lm}^\pm in the ocean tidal potential U_f . The calculation have been performed, considering only the progressive waves, for the following tidal lines:

M_m (065.455), S_a (056.554), M_f (075.555), S_{sa} (057.555);

K_1 (165.555), O_1 (145.555), P_1 (163.555), Q_1 (135.655);

K_2 (275.555), M_2 (255.555), S_2 (273.555), N_2 (245.655), T_2 (272.556).

For each of these tidal constituents the following terms have been calculated:

$l = 2$, $p = 1$, $q = 0$ because the eccentricity functions $G_{lpq}(e)$ for $p = 0$, $q = -2$ and $p = 2$, $q = 2$ vanish.

$l = 3$, $p = 1$, $q = -1$ and $l = 3$, $p = 2$, $q = 1$ because G_{30-3} and G_{333} are not quoted in [Kaula, 1966] due to their smallness: indeed, the $G_{lpq}(e)$ are proportional to $e^{|q|}$.

$l = 4$, $p = 2$, $q = 0$ because the other admissible combinations of l , p and q give rise to negligible eccentricity functions. So, also for $l = 4$ the condition $l - 2p = 0$, in practice, holds and the constituents of degree $l = 2$ and $l = 4$ generate detectable perturbations with identical periods.

Similar analysis can be found in [Christodoulidis, 1978; Dow, 1988]. It should be noticed that when Christodoulidis performed his study, which is relative to only five constituents, neither the LAGEOS nor the LAGEOS II were in orbit, while Dow has sampled the tidal spectrum for LAGEOS in a poorer manner with respect to this study in the sense that, for each constituent, only the terms of degree $l = 2$ have been considered with the exception of the K_1 whose $l = 4$ contribution has been also analyzed. Moreover, when these work have been realized there were a few coefficients C_{lmf}^+ available with relevant associated errors.

Some explanations are needed about the determination of the coefficients C_{lmf}^\pm . In EGM96 the geopotential is recovered through both altimeter and surface gravity information, and satellites data. The pool of near-Earth satellites employed, in general, are not perceptibly perturbed by the entire tidal spectrum, but they are sensitive only to some certain tidal lines, depending on the features of their orbits. Moreover, on a large enough temporal scale they cannot distinguish between solid and prograde ocean tidal perturbations because their frequencies are the same. Finally, there are also other periodic physical phenomena different from the tides that affect the orbits

of the geodetic satellites; in many cases their periodicities are similar to that of the tides, particularly in the zonal band. These facts imply that in the analytical expressions of the perturbations it is necessary to assume as known *a priori* from various reliable models some solid or ocean tidal terms and consider variable the other ones in order to adjust them by means of the experimentally determined values of the perturbations; all the constituents considered, both those held fixed and the other recovered, must be capable to influence perceptibly the satellites employed. The strategy followed in EGM96 has consisted in adopting the frequency-dependent Wahr model for the solid tides [Wahr, 1981b] with its values for the Love numbers and the $H_l^m(f)$ of Cartwright and Edden, calculating a certain number of ocean tidal terms by means of oceanographic models [Schwiderski, 1981], when it has been possible to solve the LTE, or by means of other algorithms [Casotto, 1989], considering also the retrograde waves, and choosing the 13 ocean tidal terms listed above to be adjusted. The values recovered for the coefficients C_{20f}^+ account for also the retrograde terms because, as previously noticed, their periods are equal to those of prograde ones. The terms whose value has been considered given *a priori* constitute the so called background; it necessarily contains terms up to sixth degree because the attenuation due to altitude makes the near-Earth satellites almost insensitive to larger degree terms: indeed, in eqs. (3.91)-(3.92) the A_{lmf}^\pm are proportional to:

$$\left(\frac{R}{r}\right)^{l+1} \frac{1}{2l+1}. \quad (3.103)$$

The values obtained for the coefficients C_{lmf}^+ are, in general, biased by the effects of the anelasticity of the solid Earth's mantle and by all other phenomena which have not been explicitly modeled in the background. For example, in the values recovered for the S_a are included climatological effects which have not gravitational origin; in the S_2 coefficients are also included the variations of the atmospheric pressure due to the atmospheric tides.

3.6.1 Discussion of the numerical results

In Tab. 3.10, Tab. 3.11 and Tab. 3.12 the present results for the nodes Ω of LAGEOS and LAGEOS II, and the argument of perigee ω for LAGEOS II are quoted.

From an accurate inspection of Tab. 3.10, Tab. 3.11 it is possible to notice that, for the nodes Ω , only the even degree terms give an appreciable contribute; the $l = 3$ terms are totally negligible. This so because $\Delta\Omega_f$ is proportional to the $G_{lpq}(e)$ functions which, in turn, are, in general, proportional to $e^{|q|}$: in this case the eccentricity functions are $G(e)_{31-1} = e(1 - e^2)^{-5/2} = G(e)_{321}$ and the eccentricities of LAGEOSsatellites are of the order of 10^{-2} or less.

Among the long period zonal tides, the Solar annual tide S_a (056.554) exerts the most relevant action on the nodes, with an associated percent error in the amplitudes of 6.7 %. It is interesting to compare for this tidal line the ocean tidal perturbations of degree $l = 2$ $A_{\text{LAGEOS}}^{\text{ocean}}(\Omega) = -20.55$ mas, $A_{\text{LAGEOS II}}^{\text{ocean}}(\Omega) = 37.7$ mas, with those due to the solid Earth tides $A_{\text{LAGEOS}}^{\text{solid}}(\Omega) = 9.96$ mas, $A_{\text{LAGEOS II}}^{\text{solid}}(\Omega) = -18.28$ mas. The ocean amplitudes amount to 204 % of the solid ones, while for the other zonal constituents they vary from 9.9 % for the M_m to the 18.5 % of the S_{sa} . This seems to point toward that the recovered value of C_{20f}^+ for the S_a is biased by other climatological effects than the tides; indeed, for all the other tidal lines, zonal or not, the ocean tidal perturbations of degree $l = 2$ amount to almost 10 % of the solid Earth tides perturbations.

The terms of degree $l = 2$ of the tesseral tides K_1 (165.555) and O_1 (145.555) induce very large perturbations on the node of LAGEOS and, to a lesser extent, of LAGEOS II; Tab. 3.10 and Tab. 3.11 quote 156.55 mas, 151.02 mas for the former and -35.69 mas, -34.43 mas for the latter. The associated percent errors are 3.8 % and 2.9 %, respectively. For the terms of degree $l = 4$, which have the same periods of those of degree $l = 2$, the situation is reversed: Tab. 3.10 and Tab. 3.11 quote 4.63 mas and 3.54 mas for LAGEOS and 41.58 and 31.81 mas for LAGEOS II. The percent errors associated with K_1 and O_1 , for $l = 4$, are 3.9 % and 5.7 % respectively. For all the tesseral lines investigated the ocean tidal perturbations of degree $l = 2$ are, in general, the 10 % of the solid tidal perturbations.

Among the sectorial tides, the most relevant in perturbing the nodes of LAGEOS satellites, on large temporal scales, is the M_2 (255.555): Tab. 3.10 and Tab. 3.11 quote -75.59 mas ($l = 2$) and -77.40 mas ($l = 4$) for LAGEOS, and -75.65 mas ($l = 2$) and -48.07 mas ($l = 4$) for LAGEOS II. The associated percent errors are 0.9

% for $l = 2$ and 42.8 % for $l = 4$. The M_2 ocean perturbation of degree $l = 2$ amounts to 10.3 % of the corresponding solid tide. The same holds for the other sectorial tides of degree $l = 2$.

About the periodicities of these perturbations in relation to the detection of Lense-Thirring effect, the same considerations already exposed for the solid tides hold also in this case. Moreover, it must be pointed out the aliasing role played by the zonal 18.6-year and 9.3-year tides in the extracting any secular effect, like the gravitomagnetic precession, from a record whose duration is shorter than their very long periods. Recently both Starlette and LAGEOS SLR satellites passed their 19th year in orbit and this span of time is now adequate to get reliable information about these tides [Cheng, 1995; Eanes, 1995] due to their slow frequencies they can be correctly modeled in terms of the equilibrium theory through the H_l^m coefficients and a complex Love number accounting for the anelasticity of the mantle. So, concerning them the results quoted for the solid tides can be considered adequately representative. In Tab. 3.12 the amplitudes of the perturbations on the argument of perigee ω for LAGEOS II are quoted. For this orbital element the factor

$$\frac{1 - e^2}{e} F_{lmp} \frac{dG_{lpq}}{de} - \frac{\cos i}{\sin i} \frac{dF_{lmp}}{di} G_{lpq} \quad (3.104)$$

to which $\Delta\omega_f$ is proportional makes the contributions of the $l = 3$ terms not negligible. For the even degree terms the situation is quite similar to that of Ω in the sense that the most influent tidal lines are the S_a , K_1 , O_1 and M_2 .

Once again, among the long period tides the S_a exhibits a characteristic behavior. Indeed, its $l = 3$ contributions are much stronger than those of the other zonal tides. This fact could be connected to the large values obtained in its C_{30f}^+ coefficient and people believe that it partially represents north to south hemisphere mass transport effects with an annual cycle nontidal in origin. The $l = 3$ terms present, in general, for the perigee of LAGEOS II a very interesting spectrum also for the tesseral and sectorial bands: for LAGEOS II there are lots of tidal lines which induce, on large temporal scales, very relevant perturbations on ω , with periods of the order of an year or more. In particular, it must be quoted the effect of K_1 line for $p = 1$, $q = -1$: the perturbation induced amount to -1,136 mas with period of -1,851.9 days. These values are comparable to the effects induced by the solid Earth tidal constituent of degree $l = 2$ on the node Ω of LAGEOS. Comparing the degree $l = 2$ terms with

those of the solid tides, it can be noticed that also for the perigee the proportions are the same already seen for the nodes.

3.6.2 Comparison between solid and ocean tidal perturbations

In general it is possible to state that, as far as the terms of degree $l = 2$ are concerned, the ocean tides affect the satellites' orbits more weakly than the solid Earth tides. To this aim, may be interesting an inspection of eq. (3.40) and eq. (3.91), or eq. (3.41) and eq. (3.92). Assuming for the sake of simplicity a spherical elastic Earth with frequency-independent real Love numbers and only prograde waves for the ocean tides, it turns out that for any Keplerian element, the amplitudes of the perturbations, for a given constituent of degree l , order m and circular frequency σ , can be written as

$$A_{lmf}^{\text{solid}} \propto A_{lm} k_{lm}^{(0)} g H_l^m = \frac{A_{lm} k_{lm}^{(0)}}{3} 4\pi G \rho^{\text{solid}} R H_l^m \equiv Q^{\text{solid}} 4\pi G \rho^{\text{solid}} R H_l^m, \quad (3.105)$$

$$A_{lmf}^{\text{ocean}} \propto \left(\frac{1+k'_l}{2l+1}\right) 4\pi G \rho^{\text{water}} R C_{lmf}^+ \equiv Q^{\text{water}} 4\pi G \rho^{\text{water}} R C_{lmf}^+. \quad (3.106)$$

So it is possible to obtain:

$$\frac{A_{lmf}^{\text{ocean}}}{A_{lmf}^{\text{solid}}} = \frac{Q^{\text{ocean}}}{Q^{\text{solid}}} \frac{\rho^{\text{ocean}}}{\rho^{\text{solid}}} \frac{C_{lmf}^+}{H_l^m}. \quad (3.107)$$

Assuming $\rho^{\text{solid}} = 5.5 \text{ g cm}^{-3}$ and $\rho^{\text{water}} = 1.025 \text{ g cm}^{-3}$, $\rho^{\text{water}}/\rho^{\text{solid}} = 0.1836$ and the eq. (3.107) becomes

$$\frac{A_{lmf}^{\text{ocean}}}{A_{lmf}^{\text{solid}}} = \frac{Q^{\text{ocean}}}{Q^{\text{solid}}} \times 0.1836 \times \frac{C_{lmf}^+}{H_l^m}. \quad (3.108)$$

For zonal and tesseral tides, using the nominal value for the Love number $k_2 = 0.317$ used by Carpino, one has:

$$\frac{A_{\text{zon}}^{\text{ocean}}}{A_{\text{zon}}^{\text{solid}}} = 0.3875 \frac{C_{lmf}^+}{H_l^m}, \quad (3.109)$$

$$\frac{A_{\text{tess}}^{\text{ocean}}}{A_{\text{tess}}^{\text{solid}}} = 0.9524 \frac{C_{lmf}^+}{H_l^m}. \quad (3.110)$$

For the S_{sa} the ratio $C_{lmf}^+ / H_l^m(f)$ amounts to 0.477, while for the K_1 it is equal to 0.0767. So, $A^{\text{ocean}}(S_{sa}) = 18.5\% A^{\text{solid}}(S_{sa})$, and $A^{\text{ocean}}(K_1) = 7.31\% A^{\text{solid}}(K_1)$. This examples show that the different values of the densities for the ocean water and the

solid Earth and the behavior of the ratio $C_{lmf}^+/H_l^m(f)$ for different frequencies of the tidal spectrum play a determinant role in fixing the relative strength of the ocean and solid tidal perturbations of degree $l = 2$.

Concerning the ratio $C_{lmf}^+/H_l^m(f)$, an extensive analysis has pointed out the following features: the C_{lmf}^+ are, in general, smaller than the $H_l^m(f)$ and the ratio $C_{lmf}^+/H_l^m(f)$ tends to increase with the periods of the tidal constituents (viewed in the terrestrial frame). These facts could be explained by noting that the $H_l^m(f)$ coefficients refer to the shift from the unperturbed, self-gravitational-centrifugal geoid to the tidally corrected one of the equilibrium theory, while the C_{lmf}^+ , related to the effective ocean tidal hydrodynamics, represent the real, vertical shift of the free water surface with respect to the unperturbed equipotential level (the mean geoid). Since the water masses freely flow with respect to the time-varying equipotential surface, it becomes clear that the size of the C_{lmf}^+ is smaller than that of the $H_l^m(f)$ which refer to the unrealistic situation in which there are no tidal currents pushing away the oceans from their equilibrium tidal bulge. But if the tidal equipotential surface changes slowly in time, the water masses have the possibility of adapting to it and “accumulating” in their almost steady equilibrium level surface. In other words, the lower the frequencies of the tidal constituents are, the higher the validity of the equilibrium theory is also for the oceans so that at the longer periods of the zonal constituents the solid Earth and its oceans tend to behave similarly according to the equilibrium theory.

3.6.3 The mismodelling in the nodes and the perigee

Concerning the mismodelling on the ocean tidal perturbations, the main source of uncertainties in them is represented by the load Love numbers k_l' and the coefficients C_{lmf}^+ . Regarding the ocean loading, the first calculations of the load Love numbers k_l' are due to *Farrell* [1972]. *Pagiatakis* [1990] in a first step has recalculated k_l' for an elastic, isotropic and non-rotating Earth: for $l < 800$ he claims that his estimates differ from those by *Farrell* [1972], calculated with the same hypotheses, of less than 1%. Subsequently, he added to the equations, one at a time, the effects of anisotropy, rotation and dissipation; for low values of l their effects on the results of the calcu-

lations amount to less than 1%. It has been decided to calculate $\left| \frac{\partial A(\omega)}{\partial k'_l} \right| \delta k'_l$ of the perigee of LAGEOS II for $K_1 l = 3 p = 1$ which turns out to be the most powerful ocean tidal constituent acting upon this orbital element. First, we have calculated mean and standard deviation of the values for k'_3 by Farrell and Pagiatakis obtaining $\delta k'_3/k'_3 = 0.9\%$, in according to the estimates by Pagiatakis. Then, by assuming in a pessimistic way that the global effect of the departures from these symmetric models yield to a total $\delta k'_3/k'_3 = 2\%$, we have obtained $\delta\omega^{\text{II}} = 5.5$ mas which corresponds to 2% of $\Delta\omega_{\text{LT}}^{\text{II}}$ over 4 years. Subsequently, for this constituent and for all other tidal lines we have calculated the effect of the mismodelling of C_{lmf}^+ as quoted in EGM96 [Lemoine *et al.* 1998]. In Tab. 3.17 we compare the so obtained mismodelled ocean tidal perturbations to those generated over 4 years by the Lense-Thirring effect. It turns out that the perigee of LAGEOS II is more sensitive to the mismodelling of the ocean part of the Earth response to the tide generating potential. In particular, the effect of $K_1 l = 3 p = 1 q = -1$ is relevant with a total $\delta\omega = \left| \frac{\partial A(\omega)}{\partial C_{lmf}^+} \right| \delta C_{lmf}^+ + \left| \frac{\partial A(\omega)}{\partial k'_l} \right| \delta k'_l$ of 64.5 mas amounting to 28.3 % of $\Delta\omega_{\text{LT}}^{\text{II}}$ over 4 years.

3.6.4 The mean anomaly and the inclination

In Tab. 3.13 and Tab. 3.14 the results for the mean anomaly are quoted, while Tab. 3.15 and Tab. 3.16 are devoted to the inclination.

In general, the mean anomaly of LAGEOS is more sensitive than that of LAGEOS II. The most striking feature of the ocean tidal perturbative spectrum of the LAGEOS' mean anomalies is that the $l = 3, p = 1, 2, q = \pm 1$ perturbations are, for many constituents, larger than the $l = 2, 4$ ones. Indeed, among the $l = 2$ terms, only K_1 induce perturbations of the order of 10^2 mas. Moreover, the odd degree ocean tidal perturbations are of the same order of magnitude, or even larger, than the $l = 2$ solid tidal perturbations. The most effective constituents in generating the $l = 3$ perturbations, with amplitudes of the order of $10^2 - 10^3$ mas, are S_a, K_1, P_1, K_2 and S_2 . It is worthwhile noting that, among the $l = 2$ solid tidal perturbations, only the 18.6-year tide and the K_1 reach the 10^3 mas level.

Regarding the inclination, the situation is quite different. The odd degree ocean

tidal perturbations are totally negligible. The even degree ocean tidal perturbations amount to few dozens mas. Also for the ocean tides, the $m = 0$ zonal constituents do not induce perturbations on the inclination.

3.7 Tables

Table 3.10: Perturbative amplitudes on the node Ω of LAGEOS due to ocean tides. P indicates the periods in days, A the amplitudes in mas and E the percent error in the C_{lmf}^+ . The values employed for them and the related errors are those quoted in EGM96 model.

Tide	$l = 2, p = 1, q = 0$			$l = 3, p = 1, q = -1$			$l = 3, p = 2, q = 1$			$l = 4, p = 2, q = 0$		
	P	A	E	P	A	E	P	A	E	P	A	E
065.455 M_m	27.55	-0.54	14.4	28	-10^{-4}	66.6	27.11	10^{-4}	66.6	-	-	-
056.554 S_a	365.27	-20.55	6.7	464.67	-10^{-2}	10	300.91	10^{-2}	10	-	-	-
075.555 M_f	13.66	-0.62	7.8	13.77	-10^{-4}	112	13.55	10^{-4}	112	-	-	-
057.555 S_{sa}	182.62	-5.98	9.4	204.5	-10^{-3}	27.2	164.9	10^{-3}	27.2	-	-	-
165.555 K_1	1,043.67	156.55	3.8	2,684.2	-0.36	5.2	647.76	10^{-2}	5.2	1,043.67	4.63	3.9
163.555 P_1	-221.35	-11.49	8.1	-195.95	10^{-3}	18.5	-254.3	-10^{-3}	18.5	-221.35	-0.32	8
145.555 O_1	-13.84	-2	2.9	-13.72	10^{-3}	3.2	-13.95	10^{-4}	3.2	-13.84	10^{-2}	5.7
135.655 Q_1	-9.21	-0.28	13.5	-9.16	10^{-4}	25	-9.26	10^{-5}	25	-9.21	-10^{-3}	20
275.555 K_2	521.83	-6.24	11.1	751.5	-10^{-2}	5.5	399.7	10^{-2}	5.5	521.83	-9.58	15.4
273.555 S_2	-280.93	9.45	3.9	-241.24	10^{-3}	7.1	-336.25	-10^{-2}	7.1	-280.93	15.08	5.2
272.556 T_2	-158.8	0.28	75	-145.3	10^{-4}	50	-175	-10^{-3}	50	-158.8	0.44	100
255.555 M_2	-14.02	2.03	0.9	-13.9	-10^{-4}	7.4	-14.14	10^{-3}	7.4	-14.02	2.08	2.8
245.655 N_2	-9.29	0.3	4.6	-9.2	10^{-5}	12.5	-9.3	10^{-4}	12.5	-9.29	0.3	8.3

Table 3.11: Perturbative amplitudes on the node Ω of LAGEOS II due to ocean tides. P indicates the periods in days, A the amplitudes in mas and E the percent error in the C_{lmf}^+ . The values employed for them and the related errors are those quoted in EGM96 model.

Tide	$l = 2, p = 1, q = 0$			$l = 3, p = 1, q = -1$			$l = 3, p = 2, q = 1$			$l = 4, p = 2, q = 0$		
	P	A	E	P	A	E	P	A	E	P	A	E
065.455 M_m	27.55	1	14.4	26.65	10^{-3}	66.6	28.5	-10^{-3}	66.6	-	-	-
056.554 S_a	365.27	37.71	6.7	252.8	0.13	10	657.5	-0.35	10	-	-	-
075.555 M_f	13.6	1.13	7.8	13.43	10^{-4}	112	13.89	-10^{-4}	112	-	-	-
057.555 S_{sa}	182.62	10.98	9.4	149.41	10^{-2}	27.2	234.8	-10^{-2}	27.2	-	-	-
165.555 K_1	-569.21	-35.69	3.8	-1,851.9	-1.02	5.2	-336.3	-10^{-3}	5.2	-569.21	41.58	3.9
163.555 P_1	-138.26	-3	8.1	-166.23	-10^{-2}	18.5	-118.35	-10^{-4}	18.5	-138.26	3.29	8
145.555 O_1	-13.3	-0.8	2.9	-13.5	-10^{-2}	3.2	-13.12	-10^{-4}	3.2	-13.3	0.7	5.7
135.655 Q_1	-8.98	-0.11	13.5	-9.08	-10^{-3}	25	-8.89	10^{-5}	25	-8.98	0.11	20
275.555 K_2	-284.6	-6.24	11.1	-435.38	-0.13	5.5	-211.4	10^{-2}	5.5	-284.6	-5.95	15.4
273.555 S_2	-111.2	-6.87	3.9	-128.6	-10^{-2}	7.1	-97.9	10^{-2}	7.1	-111.2	-6.79	5.2
272.556 T_2	-85.27	-0.277	75	-95.14	-10^{-3}	50	-77.25	10^{-3}	50	-85.27	-0.274	100
255.555 M_2	-13.03	-3.46	0.9	-13.2	-10^{-3}	7.4	-12.83	10^{-3}	7.4	-13.03	-2.2	2.8
245.655 N_2	-8.8	-0.46	4.6	-8.9	-10^{-3}	12.5	-8.7	10^{-4}	12.5	-8.8	-0.34	8.3

Table 3.12: Perturbative amplitudes on the perigee ω of LAGEOS II due to ocean tides. P indicates the periods in days, A the amplitudes in mas and E the percent error in the C_{lmf}^+ . The values employed for them and the related errors are those quoted in EGM96 model.

Tide	$l = 2, p = 1, q = 0$			$l = 3, p = 1, q = -1$			$l = 3, p = 2, q = 1$			$l = 4, p = 2, q = 0$		
	P	A	E	P	A	E	P	A	E	P	A	E
065.455 M_m	27.55	-0.69	14.4	26.65	-1.53	66.6	28.5	1.64	66.6	-	-	-
056.554 S_a	365.27	-26.17	6.7	252.8	-114.35	10	657.5	297.34	10	-	-	-
075.555 M_f	13.66	-0.78	7.8	13.43	-0.58	112	13.89	0.60	112	-	-	-
057.555 S_{sa}	182.6	-7.62	9.4	149.41	-22.95	27.2	234.8	36.07	27.2	-	-	-
165.555 K_1	-569.21	177.76	3.8	-1,851.9	-1.136	5.2	-336.28	346.6	5.2	-569.21	-3.95	3.9
163.555 P_1	-138.26	14.95	8.1	-166.2	-28.97	18.5	-118.35	34.67	18.5	-138.2	-0.31	8
145.555 O_1	-13.3	4	2.9	-13.55	-13.7	3.2	-13.12	22.3	3.2	-13.3	-10^{-2}	5.7
135.655 Q_1	-8.98	0.58	13.5	-9.08	-1.17	25	-8.89	1.92	25	-8.98	-10^{-2}	20
275.555 K_2	-284.6	-5.95	11.1	-435.3	214.23	5.5	-211.4	87.3	5.5	-284.6	-2.49	15.3
273.555 S_2	-111.2	-6.55	3.9	-128.6	98.47	7.1	-97.9	62.9	7.1	-111.2	-2.85	5.2
272.556 T_2	-85.2	-0.26	75	-95.1	5.2	50	-77.2	3.54	50	-85.2	-0.11	100
255.555 M_2	-13.03	-3.3	0.9	-13.2	9.7	7.4	-12.83	7.9	7.4	-13.03	-0.92	2.8
245.655 N_2	-8.48	-0.44	4.6	-8.94	1.95	12.5	-8.75	1.6	12.5	-8.84	-0.14	8.3

Table 3.13: Perturbative amplitudes on the mean anomaly \mathcal{M} of LAGEOS due to ocean tides. P indicates the periods in days, A the amplitudes in mas. The percent error in the C_{lmf}^+ and the values employed for them are those quoted in EGM96 model. The terms of degree $l = 4$ give totally negligible contributions.

Tide	$l = 2, p = 1, q = 0$		$l = 3, p = 1, q = -1$		$l = 3, p = 2, q = 1$	
	P	A	P	A	P	A
065.455 M_m	27.55	0.52	28	-2.82	27.11	2.73
056.554 S_a	365.27	19.6	464.67	-368.36	300.91	238.54
075.555 M_f	13.66	0.59	13.77	-1.05	13.55	1.03
057.555 S_{sa}	182.62	5.7	204.5	-55.07	164.9	44.43
165.555 K_1	1,043.67	184.5	2,684.2	5,436.73	647.76	-1,712.74
145.555 O_1	-13.84	-2.36	-13.72	-45.9	-13.95	60.97
163.555 P_1	-221.35	-13.55	-195.95	-112.8	-254.3	191.11
135.655 Q_1	-9.21	-0.33	-9.16	-3.9	-9.26	5.15
275.555 K_2	521.83	24.25	751.5	-1,319.7	399.7	-16.4
255.555 M_2	-14.02	-7.89	-13.9	36.6	-14.14	0.87
273.555 S_2	-280.93	-36.75	-241.24	659.03	-336.25	21.54
245.655 N_2	-9.29	-1.04	-9.24	7.21	-9.34	0.17
272.556 T_2	-158.8	-1.09	-145.3	28.35	-175	0.8

Table 3.14: Perturbative amplitudes on the mean anomaly \mathcal{M} of LAGEOS II due to ocean tides. P indicates the periods in days, A the amplitudes in mas. The percent error in the C_{lmf}^+ and the values employed for them are those quoted in EGM96 model. The terms of degree $l = 4$ give totally negligible contributions.

Tide	$l = 2, p = 1, q = 0$		$l = 3, p = 1, q = -1$		$l = 3, p = 2, q = 1$	
	P	A	P	A	P	A
065.455 M_m	27.55	10^{-2}	26.65	1.53	28.5	-1.63
056.554 S_a	365.27	-3.27	252.8	114.07	657.5	-296.6
075.555 M_f	13.6	-10^{-2}	13.43	0.58	13.89	-0.6
057.555 S_{sa}	182.62	-0.95	149.41	22.9	234.8	-35.9
165.555 K_1	-569.21	156.08	-1,851.9	1,134.74	-336.3	-346
145.555 O_1	-13.33	3.52	-13.55	13.73	-13.12	-22.32
163.555 P_1	-138.26	13.12	-166.23	28.9	-118.35	-34.6
135.655 Q_1	-8.98	0.5	-9.08	1.17	-8.89	-1.92
275.555 K_2	-284.6	-9.74	-435.38	-213.78	-211.4	-87.19
255.555 M_2	-13.03	-5.4	-13.24	-9.75	-12.83	-7.93
273.555 S_2	-111.2	-10.72	-128.6	-98.27	-97.9	-62.86
245.655 N_2	-8.84	-0.72	-8.94	-1.95	-8.75	-1.6
272.556 T_2	-85.27	-0.4	-95.14	-5.19	-77.25	-3.54

Table 3.15: Perturbative amplitudes on the inclination i of LAGEOS due to ocean tides. P indicates the periods in days, A the amplitudes in mas and E the percent error in the C_{lmf}^+ . The values employed for them and the related errors are those quoted in EGM96 model. The terms of degree $l = 3$ give totally negligible contributions.

Tide	$l = 2, p = 1, q = 0$			$l = 4, p = 2, q = 0$		
	P	A	E	P	A	E
165.555 K_1	1,043.67	-65.42	3.8	1,043.67	-13.66	3.9
145.555 O_1	-13.8	0.83	2.9	-13.8	0.13	5.7
163.555 P_1	-221.35	4.8	8.1	-221.35	0.9	8
135.655 Q_1	-9.21	0.12	13.5	-9.21	2×10^{-2}	20
275.555 K_2	521.83	-17.2	11.1	521.83	-8.3	15.3
255.555 M_2	-14.02	5.6	0.9	-14.02	1.8	2.8
273.555 S_2	-280.93	26.06	3.9	-280.93	13.11	5.2
245.655 N_2	-9.29	0.7	4.6	-9.29	0.27	8.3
272.556 T_2	-158.8	0.77	75	-158.8	0.39	100

Table 3.16: Perturbative amplitudes on the inclination i of LAGEOS II due to ocean tides. P indicates the periods in days, A the amplitudes in mas and E the percent error in the C_{lmf}^+ . The values employed for them and the related errors are those quoted in EGM96 model. The terms of degree $l = 3$ give totally negligible contributions.

Tide	$l = 2, p = 1, q = 0$			$l = 4, p = 2, q = 0$		
	P	A	E	P	A	E
165.555 K_1	-569.21	-65.47	3.8	-569.21	-2.67	3.9
145.555 O_1	-13.3	-1.48	2.9	-13.3	-4×10^{-2}	5.7
163.555 P_1	-138.26	-5.5	8.1	-138.2	-0.21	8
135.655 Q_1	-8.9	-0.21	13.5	-8.9	-7×10^{-3}	20
275.555 K_2	-284.6	8.17	11.1	-284.6	1.53	15.3
255.555 M_2	-13.03	4.53	0.9	-13.03	0.56	2.8
273.555 S_2	-111.2	8.99	3.9	-111.2	1.75	5.2
245.655 N_2	-8.8	0.6	4.6	-8.8	8×10^{-2}	8.3
272.556 T_2	-85.2	0.36	75	-85.2	7×10^{-2}	100

Table 3.17: Mismodeled ocean tidal perturbations on the nodes Ω of LAGEOS and LAGEOS II and the perigee ω of LAGEOS II compared to their gravitomagnetic precessions over 4 years $\Delta\Omega_{LT}^I = 124$ mas $\Delta\Omega_{LT}^{II} = 126$ mas $\Delta\omega_{LT}^{II} = -228$ mas. The effect of the ocean loading has been neglected. When the 1% cutoff has not been reached a - has been inserted. The values quoted for $K_1 l = 3 p = 1$ includes also the mismodelling in the ocean loading coefficient k'_3 assumed equal to 2%. The ratios are in percent and the mismodelled amplitudes δX in mas.

Tide	$\frac{\delta C^+}{C^+}$	$\delta\Omega^I$	$\frac{\delta\Omega^I}{\Delta\Omega_{LT}^I}$	$\delta\Omega^{II}$	$\frac{\delta\Omega^{II}}{\Delta\Omega_{LT}^{II}}$	$\delta\omega^{II}$	$\frac{\delta\omega^{II}}{\Delta\omega_{LT}^{II}}$
$S_a l=2 p=1 q=0$	6.7	1.37	1.1	2.5	1.9	-	-
$S_a l=3 p=1 q=-1$	10	-	-	-	-	11.4	5
$S_a l=3 p=2 q=1$	10	-	-	-	-	29.7	13
$S_{sa} l=3 p=1 q=-1$	27.2	-	-	-	-	6.2	2.7
$K_1 l=2 p=1 q=0$	3.8	5.9	4.7	1.3	1	6.75	2.9
$K_1 l=3 p=1 q=-1$	5.2	-	-	-	-	64.5	28.3
$K_1 l=3 p=2 q=1$	5.2	-	-	-	-	18	7.9
$K_1 l=4 p=2 q=0$	3.9	-	-	1.6	1.2	-	-
$P_1 l=3 p=1 q=-1$	18.5	-	-	-	-	5.3	2.3
$P_1 l=3 p=2 q=1$	18.5	-	-	-	-	6.4	2.8
$K_2 l=3 p=1 q=-1$	5.5	-	-	-	-	11.7	5
$K_2 l=3 p=2 q=1$	5.5	-	-	-	-	4.8	2
$S_2 l=3 p=1 q=-1$	7.1	-	-	-	-	6.9	3
$S_2 l=3 p=2 q=1$	7.1	-	-	-	-	4.4	1.9
$T_2 l=3 p=1 q=-1$	50	-	-	-	-	2.6	1.1

3.8 Indirect tidal perturbations

The most relevant part of the observed secular precessional rates of Ω , ω and \mathcal{M} of LAGEOS and LAGEOS II are due to the first even zonal coefficient of the static, centrifugal component of the geopotential [Kaula, 1966] (see Appendix A)

$$\dot{\Omega}_{\text{obl}} = -\frac{3}{2} \frac{nJ_2}{(1-e^2)^2} \left(\frac{R_{\oplus}}{a} \right)^2 \cos i, \quad (3.111)$$

$$\dot{\omega}_{\text{obl}} = -\frac{3}{4} \frac{nJ_2}{(1-e^2)^2} \left(\frac{R_{\oplus}}{a} \right)^2 (1 - 5 \cos^2 i), \quad (3.112)$$

$$\dot{\mathcal{M}}_{\text{obl}} = \frac{3}{4} \frac{nJ_2 \sqrt{1-e^2}}{(1-e^2)^2} \left(\frac{R_{\oplus}}{a} \right)^2 (3 \cos^2 i - 1), \quad (3.113)$$

in which $J_2 = 1.0826266836 \times 10^{-3}$ [Lemoine *et al.*, 1998]. From an inspection of eqs. (3.111)-(3.113) it appears that, if the Keplerian elements a , e , i are perturbed by any physical cause, like the solid and fluid tides, there is a cross-coupling between such perturbations and the $\dot{\Omega}_{\text{obl}}$, $\dot{\omega}_{\text{obl}}$, $\dot{\mathcal{M}}_{\text{obl}}$ [Dow, 1988] giving rise to second order perturbations on the node, perigee and mean anomaly. It is possible to express them in the following way

$$\Delta\Omega^{(2)} = \frac{\partial\dot{\Omega}_{\text{obl}}}{\partial a} \int \Delta a dt + \frac{\partial\dot{\Omega}_{\text{obl}}}{\partial e} \int \Delta e dt + \frac{\partial\dot{\Omega}_{\text{obl}}}{\partial i} \int \Delta i dt, \quad (3.114)$$

$$\Delta\omega^{(2)} = \frac{\partial\dot{\omega}_{\text{obl}}}{\partial a} \int \Delta a dt + \frac{\partial\dot{\omega}_{\text{obl}}}{\partial e} \int \Delta e dt + \frac{\partial\dot{\omega}_{\text{obl}}}{\partial i} \int \Delta i dt, \quad (3.115)$$

$$\Delta\mathcal{M}^{(2)} = \frac{\partial\dot{\mathcal{M}}_{\text{obl}}}{\partial a} \int \Delta a dt + \frac{\partial\dot{\mathcal{M}}_{\text{obl}}}{\partial e} \int \Delta e dt + \frac{\partial\dot{\mathcal{M}}_{\text{obl}}}{\partial i} \int \Delta i dt. \quad (3.116)$$

In eq. (3.114)-eq. (3.116) the quantities Δa , Δe , Δi denote the first order tidal perturbations on the semimajor axis, the eccentricity and inclination. It turns out that

$$\Delta a \propto (l - 2p + q), \quad (3.117)$$

$$\Delta e \propto (l - 2p + q)(1 - e^2)^{1/2} - (l - 2p), \quad (3.118)$$

$$\Delta i \propto (l - 2p) \cos i - m. \quad (3.119)$$

According to the condition $l - 2p + q = 0$, eq. (3.117)-eq. (3.119) show that, in this case, only the perturbations on the eccentricity and the inclination are to be considered. Moreover, since for the solid Earth tides the relation $l - 2p = 0$ is also fulfilled, the second order perturbations due to eccentricity are only those related to

the $l = 3$ part of the ocean tidal spectrum. They turn out to be totally negligible, so that only the cross-coupling due to solid and fluid tidal perturbations on inclination is to be considered. As a consequence, the second order zonal tidal perturbations vanish.

It turns out that

$$\frac{\partial \dot{\Omega}_{\text{obl}}}{\partial i} = - \frac{3}{2} \frac{nC_{20}}{(1-e^2)^2} \left(\frac{R_{\oplus}}{a} \right)^2 \sin i, \quad (3.120)$$

$$\frac{\partial \dot{\omega}_{\text{obl}}}{\partial i} = \frac{3}{4} \frac{nC_{20}}{(1-e^2)^2} \left(\frac{R_{\oplus}}{a} \right)^2 10 \cos i \sin i, \quad (3.121)$$

$$\frac{\partial \dot{\mathcal{M}}_{\text{obl}}}{\partial i} = \frac{3}{4} \frac{nC_{20} \sqrt{1-e^2}}{(1-e^2)^2} \left(\frac{R_{\oplus}}{a} \right)^2 6 \cos i \sin i. \quad (3.122)$$

According to eq. (3.114)-eq. (3.116), eq. (3.120)-eq. (3.122) and to eq. (3.43), for the solid tides the second order perturbations due to the tidal constituent of frequency f are

$$\begin{aligned} \Delta\Omega_f^{(2)} = & - \frac{3}{2} \frac{nC_{20}}{(1-e^2)^2} \left(\frac{R_{\oplus}}{a} \right)^2 \frac{g}{na^2 \sqrt{1-e^2}} \sum_{l=0}^{\infty} \sum_{m=0}^l \left(\frac{R_{\oplus}}{r} \right)^{l+1} A_{lm} \times \\ & \times \sum_{p=0}^l \sum_{q=-\infty}^{+\infty} F_{lmp}(i) G_{lpq}(e) [(l-2p) \cos i - m] \frac{1}{f_p^2} k_{lm}^{(0)} H_l^m \sin \gamma_{flmpq}, \end{aligned} \quad (3.123)$$

$$\begin{aligned} \Delta\omega_f^{(2)} = & \frac{3}{4} \frac{nC_{20}}{(1-e^2)^2} \left(\frac{R_{\oplus}}{a} \right)^2 10 \cos i \frac{g}{na^2 \sqrt{1-e^2}} \sum_{l=0}^{\infty} \sum_{m=0}^l \left(\frac{R_{\oplus}}{r} \right)^{l+1} A_{lm} \times \\ & \times \sum_{p=0}^l \sum_{q=-\infty}^{+\infty} F_{lmp}(i) G_{lpq}(e) [(l-2p) \cos i - m] \frac{1}{f_p^2} k_{lm}^{(0)} H_l^m \sin \gamma_{flmpq}, \end{aligned} \quad (3.124)$$

$$\begin{aligned} \Delta\mathcal{M}_f^{(2)} = & \frac{3}{4} \frac{nC_{20} \sqrt{1-e^2}}{(1-e^2)^2} \left(\frac{R_{\oplus}}{a} \right)^2 6 \cos i \frac{g}{na^2 \sqrt{1-e^2}} \sum_{l=0}^{\infty} \sum_{m=0}^l \left(\frac{R_{\oplus}}{r} \right)^{l+1} A_{lm} \times \\ & \times \sum_{p=0}^l \sum_{q=-\infty}^{+\infty} F_{lmp}(i) G_{lpq}(e) [(l-2p) \cos i - m] \frac{1}{f_p^2} k_{lm}^{(0)} H_l^m \sin \gamma_{flmpq}. \end{aligned} \quad (3.125)$$

Concerning the ocean tides, eq. (3.94) leads to

$$\begin{aligned} \Delta\Omega_f^{(2)} = & \frac{3}{2} \frac{nC_{20}}{(1-e^2)^2} \left(\frac{R_{\oplus}}{a} \right)^2 \frac{1}{na^2 \sqrt{1-e^2}} \sum_{l=0}^{\infty} \sum_{m=0}^l \sum_{\pm} \left(\frac{R_{\oplus}}{r} \right)^{l+1} A_{lmf}^{\pm} \times \\ & \times \sum_{p=0}^l \sum_{q=-\infty}^{+\infty} F_{lmp}(i) G_{lpq}(e) [(l-2p) \cos i - m] \frac{1}{f_p^2} \left[\begin{array}{c} \sin \gamma_{flmpq}^{\pm} \\ -\cos \gamma_{flmpq}^{\pm} \end{array} \right]_{l-m}^{\text{even}}_{\text{odd}}, \end{aligned} \quad (3.126)$$

$$\Delta\omega_f^{(2)} = \frac{3}{4} \frac{nC_{20}}{(1-e^2)^2} \left(\frac{R_{\oplus}}{a} \right)^2 10 \cos i \frac{1}{na^2 \sqrt{1-e^2}} \sum_{l=0}^{\infty} \sum_{m=0}^l \sum_{\pm} \left(\frac{R_{\oplus}}{r} \right)^{l+1} A_{lmf}^{\pm} \times$$

$$\times \sum_{p=0}^l \sum_{q=-\infty}^{+\infty} F_{lmp}(i) G_{lpq}(e) [(l-2p) \cos i - m] \frac{1}{f_p^2} \begin{bmatrix} \sin \gamma_{flmpq}^{\pm} \\ -\cos \gamma_{flmpq}^{\pm} \end{bmatrix}_{l-m \text{ odd}}^{l-m \text{ even}}, \quad (3.127)$$

$$\begin{aligned} \Delta \mathcal{M}_f^{(2)} = & \frac{3}{4} \frac{n C_{20} \sqrt{1-e^2}}{(1-e^2)^2} \left(\frac{R_{\oplus}}{a} \right)^2 6 \cos i \frac{1}{na^2 \sqrt{1-e^2}} \left(\frac{R_{\oplus}}{r} \right)^{l+1} A_{lmf}^{\pm} \times \\ & \times \sum_{p=0}^l \sum_{q=-\infty}^{+\infty} F_{lmp}(i) G_{lpq}(e) [(l-2p) \cos i - m] \frac{1}{f_p^2} \begin{bmatrix} \sin \gamma_{flmpq}^{\pm} \\ -\cos \gamma_{flmpq}^{\pm} \end{bmatrix}_{l-m \text{ odd}}^{l-m \text{ even}}. \end{aligned} \quad (3.128)$$

In Tab. 3.18 and Tab. 3.19 the results for LAGEOS and LAGEOS II are released. Concerning the ocean tidal spectrum, it turns out that only the $l = 2$ part of it induces contributions of appreciable magnitude to the amplitudes; they have been quoted in parentheses. The fact that the second order tidal perturbations depend on $1/f_p^2$, contrary to the direct ones depending only on $1/f_p$, makes their spectrum really interesting, since it is in several cases of the same order of magnitude of the direct tidal spectrum summarized in Tab. 3.1-Tab. 3.6. It is instructive to consider the K_1 tidal line. For LAGEOS, Tab. 3.1 quotes $\Delta\Omega^{(1)} = 1,744.38$ mas, while Tab. 3.18 has $\Delta\Omega^{(2)} = -2,044.19$ mas; $\Delta\mathcal{M}^{(2)} = -2,050.89$ mas in Tab. 3.18 is to be compared to $\Delta\mathcal{M}^{(1)} = 2,055.72$ mas of Tab. 3.5. Concerning LAGEOS II, Tab. 3.19 quotes $\Delta\Omega^{(2)} = 954.96$ mas, while Tab. 3.2 has $\Delta\Omega^{(1)} = -398$ mas; $\Delta\omega^{(2)} = -2,898.55$ mas of Tab. 3.19 has as counterpart $\Delta\omega^{(1)} = 1,982.14$ mas in Tab. 3.3; Tab. 3.6 quotes $\Delta\mathcal{M}^{(1)} = 1,740.36$ mas, while Tab. 3.19 has the value $\Delta\mathcal{M}^{(2)} = -1,738.96$ mas. Such results show that, in the tesseral and sectorial bands, the effective magnitude of the tidal perturbations on Ω , ω , \mathcal{M} can be very different, in amplitudes and phases, from those due to only the direct effects of tides.

3.9 Tables

Table 3.18: Perturbative amplitudes on the node, perigee and mean anomaly of LAGEOS due to the indirect effect of the solid Earth tidal perturbations on the inclination i of degree $l = 2$, $p = 1$, $q = 0$. $A(X)$ denotes the amplitude, in mas, of the perturbation on the Keplerian element X . In parentheses the main contributions due to ocean tidal perturbation on the inclination i of degree $l = 2$ are quoted. The value employed for the unnormalized Stokes coefficient C_{20} is -0.0010827.

Tide	P (days)	$A(\Omega)$ (mas)	$A(\omega)$ (mas)	$A(\mathcal{M})$ (mas)
135.655 Q_1	-9.21	2×10^{-2}	4×10^{-2}	2×10^{-2}
165.565	904.77	-202.22	-344.89	-206.93
165.555 K_1	1,043.67	-2,004.19 (-179.8)	-3,418.2 (-306.7)	-2,050.89 (-184.06)
145.555 O_1	-13.84	0.28	0.49	0.29
165.545	1,232.94	55.86	95.27	57.16
163.555 P_1	-221.35	33.24	56.7	34.02
245.655 N_2	-9.29	-0.16	-0.28	-0.17
255.555 M_2	-14.02	-1.99	-3.41	-2.04
275.555 K_2	521.83	-349.93 (-23.6)	-596.82 (-40.3)	-358.08 (-24.2)
274.556	-1,217.55	-14.9	-25.42	-15.25
274.554	-1,216.73	58.56	99.88	59.92
273.555 S_2	-280.93	-373.16 (-19.3)	-636.43 (-32.9)	-381.85 (-19.7)
272.556 T_2	-158.8	-6.9	-11.8	-7.13

Table 3.19: Perturbative amplitudes on the node, perigee and mean anomaly of LAGEOS II due to the indirect effect of the solid Earth tidal perturbations on the inclination i of degree $l = 2$, $p = 1$, $q = 0$. $A(X)$ denotes the amplitude, in mas, of the perturbation on the Keplerian element X . In parentheses the main contributions due to ocean tidal perturbation on the inclination i of degree $l = 2$ are quoted. The value employed for the unnormalized Stokes coefficient C_{20} is -0.0010827.

Tide	P (days)	$A(\Omega)$ (mas)	$A(\omega)$ (mas)	$A(\mathcal{M})$ (mas)
135.655 Q_1	-8.98	-3×10^{-2}	0.11	6×10^{-2}
165.565	-621.22	152.71	-463.51	-278
165.555 K_1	-569.21	954.96 (85.6)	-2,898.55 (-259.9)	-1,738.96 (-155.9)
145.555 O_1	-13.33	-0.43	1.3	0.78
165.545	-525.23	-16.23	49.2	29.57
163.555 P_1	-138.26	-20.78	63.07	37.84
245.655 N_2	-8.84	-0.11	0.35	0.21
255.555 M_2	-13.03	-1.31	3.98	2.39
275.555 K_2	-284.6	-79.2 (-5.3)	240.39 (16.2)	144.22 (9.7)
274.556	-159.96	-0.19	0.59	0.35
274.554	-159.95	0.77	-2.33	-1.4
273.555 S_2	-111.24	-44.51 (-2.3)	135.12 (6.9)	81.06 (4.2)
272.556 T_2	-85.27	-1.52	4.64	2.78

3.10 Conclusions

Concerning the orbital tidal perturbations on LAGEOS and LAGEOS II the following improvements with respect to the previous works have been reached:

- The inclination, the node, the perigee and the mean anomaly have been considered
- The analysis has been extended also to LAGEOS II, launched in 1992
- Concerning the solid tides, the most recent available frequency-dependent Love numbers k_2 have been used instead of a single-valued Love number $k_2 = 0.317$. Moreover, the latitude-dependence of the Love number k^+ has been considered for some selected tidal lines
- About the ocean tides, their orbital perturbations have been extensively calculated for $l = 2, 3, 4$ by using the most recent available model EGM 96. Interesting are the results obtained for the K_1 , $l = 3$ $m = 1$ $p = 1$ $q = -1$ oceanic constituent. Indeed it induces on the perigee of LAGEOS II and the mean anomalies of both LAGEOS perturbations whose amplitudes are of the order of thousands of mas and the periods amounts to some years as the solid tidal perturbations
- An evaluation of the mismodelling on such orbital perturbations, for certain tidal constituents, have been performed
- The indirect solid and ocean tidal perturbations due to the cross-coupling with the secular rates of the node, the perigee and the mean anomaly have been worked out

The calculations performed here have a general validity because they can be extended to any artificial satellite. The results presented here for the LAGEOS can be used, from one hand, in improving the modelling of their orbital perturbations and, from another hand, for the correct evaluation of the error budget in any space-based experiment devoted to the measurement of some particular feature of the Earth's gravitational field like that proposed in chapter 8 in order to measure the PPN pa-

rameters β and γ .

In the context of the general relativistic Lense-Thirring experiment, the calculations performed here have been used, in view of a refinement of the error budget, in order to check preliminarily which tidal constituents are really important in perturbing the combined residuals so to fit and remove them from the data, if possible, or, at least, to evaluate the systematic error induced by them. Tab. 5 and Tab. 9 show that, over a 4 years time span the nodes of the two LAGEOS are sensitive to the even components of the 18.6-year line, the K_1 and the S_a at a 1% level at least. Moreover, the perigee of LAGEOS II turns out to be very sensitive to the $l = 3$ part of the ocean tidal spectrum.

The results obtained in this chapter for the nodes of LAGEOS and LAGEOS II and the perigee of LAGEOS II will be the starting point for the numerical simulations with MATLAB, described in chapter 4 and chapter 8, performed to assess quantitatively the direct impact of the tidal perturbations on the gravitomagnetic Lense-Thirring experiment, currently implemented, and on the proposed gravitoelectric experiment. Moreover, the results obtained for the inclination will be used for the evaluation of the systematic error induced by the mismodelling of this orbital element in both the experiments.

Chapter 4

The impact of the Earth tides on the determination of the Lense-Thirring effect

4.1 Introduction

According to [Ciufolini, 1996], the Lense-Thirring effect could be detected, in the field of the Earth, by analyzing the orbits of the two laser-ranged LAGEOS and LAGEOS II satellites. The observable adopted is the combination of orbital residuals of eq. (1.5): the determination of the scaling parameter μ_{LT} , 1 in General Relativity and 0 in Newtonian mechanics, is influenced by a great number of gravitational and non-gravitational perturbations acting upon LAGEOS and LAGEOS II. Among the perturbations of gravitational origin a primary role is played by the solid Earth and ocean tides. Their effects on the orbital elements of LAGEOS and LAGEOS II has been extensively analyzed in chapter 3.

In [Ciufolini, 1996] it is claimed the combined residuals $y \equiv \delta\Omega_{\text{exp}}^{\text{I}} + c_1\delta\Omega_{\text{exp}}^{\text{II}} + c_2\delta\omega_{\text{exp}}^{\text{II}}$ allow one to cancel out the static and dynamical perturbations of degree $l = 2, 4$ and order $m = 0$ of the terrestrial gravitational field; however, this is not so for the tesseral ($m = 1$) and sectorial ($m = 2$) tides. This chapter aims to assess quantitatively how the solid and ocean Earth tides of order $m = 0, 1, 2$ affect the recovery of μ_{LT} in view of a refinement of the error budget of the gravitomagnetic LAGEOS experiment.

Concerning the zonal tides, the results obtained in chapter 3 for the amplitudes of their perturbations have been used directly in eq. (1.5) in order to test in a preliminary way if the $l = 2, 4$ $m = 0$ tidal perturbations cancel out.

Regarding the tesseral and sectorial tides the analysis of their impact on the Lense-Thirring measurement is done by simulating the real residual curve and analyzing it. The T_{obs} chosen span ranges from 4 years to 8 years. This is so because 4 years is the length of the latest time series actually analyzed in [Ciufolini *et al.*, 1998] and 8 years is the maximum length obtainable today because LAGEOS II has been launched in 1992. The analysis includes also the long-period signals due to solar radiation pressure and the J_3 geopotential zonal harmonic acting on the perigee of LAGEOS II. In our case we have a signal built up with the secular Lense-Thirring trend¹ and a certain number of long-period harmonics, i.e. the tesseral and sectorial tidal perturbations and the other signals with known periodicities. The part of interest for us is the secular trend while the harmonic part represents the noise. We address the problem of how the harmonics affect the recovery of the secular trend on given time spans T_{obs} and various samplings Δt .

Among the long-period perturbations we distinguish between those signals whose periods are shorter than T_{obs} and those signals with periods longer than T_{obs} . While the former average out if T_{obs} is an integer multiple of their periods, the action of the latter is more subtle since they could resemble a trend over temporal intervals too short with respect to their periods. They must be considered as biases on the Lense-Thirring determination affecting its recovery by means of their mismodelling. Thus, it is of the utmost importance that we reliably assess their effect on the determination of the trend of the gravitomagnetic effect. It would be useful to direct the efforts of the community (geophysicists, astronomers and space geodesists) towards the improvement of our knowledge of those tidal constituents to which μ_{LT} turns out to be particularly sensitive (for the LAGEOS orbits).

This investigation will quantify unambiguously what one means with statements like: $\Delta\mu_{\text{tides}} \leq X\%\mu_{\text{LT}}$. In this chapter we shall try to put forward a simple and

¹In fact, the combined residuals are affected also by the secular contribution due to $l = 6, 8, \dots$ zonal terms of the geopotential. Their effect amounts to almost 10% of the Lense-Thirring trend [Radicchio, 1998].

meaningful approach. It must be pointed out though that it is not a straightforward application of any exact or rigorously proven method; on the contrary, it is, at a certain level, heuristic and intuitive, but it has the merit of yielding reasonable and simple answers and allowing for their critical discussion.

The chapter is organized as follows. In section 2 the effects of the $l = 2, 4 m = 0$ constituents on the combined residuals is examined; it turns out that, not only they affect it at a level $<< 1\%$, but this feature also extends, within certain limits, to the $l = 3, m = 0$ part of the tidal spectrum. In section 3 the features of the simulation procedure of the observable curve are outlined. In section 4 the effects of the harmonics of the order $m = 1, 2$ with period shorter than 4 years are examined by comparing the least squares fitted values of μ_{LT} in two different scenarios: in the first one the simulated curve is complete and the fitting model contains all the most relevant signals plus a straight line, while in the second one some selected harmonics are removed from the simulated curve which is fitted by means of the straight line only. section 5 address the topic of the harmonics with periods longer than 4 years. In section 6 the evaluation of the systematic error induced by the mismodelling in the inclination is assessed. section 7 is devoted to the conclusions.

4.2 Systematic error due to the zonal tides on the measurement of the Lense-Thirring effect

The combined residuals by Ciufolini are useful since they should vanish if calculated for the even zonal contributions $C_{2,0}$ and $C_{4,0}$ of the geopotential [Ciufolini, 1996]. More precisely, the right side of eq. (1.5) should become equal to zero if the left side were calculated for any of these two even zonal contributions, both of static and dynamical origin; the nearer to zero is the right side, the smaller is the systematic uncertainty in μ_{LT} due to the contribution considered.

In order to test this important feature for the case of tides, in a very conservative way the results obtained in chapter 3, Tab. 3.1, Tab. 3.2, Tab. 3.3 for the solid tides and Tab. 3.10, Tab. 3.11, Tab. 3.12 for the ocean tides, have been used in eq. (1.5)

by assuming, for the sake of clarity and in order to make easier the comparison with [Ciufolini *et al.*, 1997], an observational period of 1 year and the nominal values of the calculated tidal perturbative amplitudes, as if the zonal solid and ocean tides were not at all included in the GEODYN II dynamical models so that the residuals should account entirely for them.

The results are released in Tab. 4.1 and Tab. 4.2. The values of $\Delta\mu_{LT}$ quoted there for the various zonal tidal lines may be considered as the systematic error in μ_{LT} due to the chosen constituents, if considered one at a time by neglecting any possible reciprocal correlation among the other tidal lines. Tab. 4.1 and Tab. 4.2 show that the percent error in the general relativistic value of μ_{LT} due to the 18.6-year tide, the most dangerous one in recovering the LT since it superimposes to the gravitomagnetic trend over time spans of a few year, amounts to 21.9 %, while for all the other zonal tides it decreases to 0.1 % or less. This means that, even if neglected in the satellite orbit determination models, the $l = 2 m = 0$ tides, with the exception of the 18.6-year tide, do not affect the recovery of μ_{LT} by means of the combined residuals.

It is interesting to compare the present results to those released in [Ciufolini *et al.*, 1997] for the 18.6-year tide. The value -0.219 due to the solid component for μ_{LT} quoted in Tab. 4.1 must be compared to -0.361 in [Ciufolini *et al.*, 1997], with an improvement of 39.3 %. In the cited work there is no reference to any estimate of the mismodelling of the 18.6-year tide, so that we have used the nominal tidal perturbative amplitudes released in it: $A(\Omega^I) = -997$ mas, $A(\Omega^{II}) = 1,805$ mas and $A(\omega^{II}) = -1,265$ mas. These figures for the perturbative amplitudes due to the solid Earth tide of 18.6-year are notably different from those quoted in the present study. In [Ciufolini *et al.*, 1997] the theoretical framework in which they have been calculated (F. Vespe, private communication, 1999) is based on the assumption of a spherical, static, elastic Earth with a single nominal value of $k_2 = 0.317$ used for the entire tidal spectrum. The inclusion of the tiny corrections due to the Earth's flattening and rotation on the perturbative amplitudes of Ω and ω for the 18.6-year tide could allow one to slightly improve the related uncertainty in μ_{LT} ; it would amount to 20.6 %. But since the present-day accuracy in laser ranging measurements could hardly allow one to detect these small effects, their utilization in eq. (1.5) is debatable.

Remember that the result quoted for the 18.6-year tide is obtained in the worst possible case, i.e. a time span of only 1 year and the assumption that the residuals have been built up by neglecting completely the zonal tides in the dynamical models used. If, more realistically, we calculate eq. (1.5) with the mismodelled amplitudes quoted in the first row of Tab. 3.9 for the 18.6-year tide we obtain, over 1 year, $\Delta\mu = -3.51 \times 10^{-3}$. This strongly highlights that many efforts, either theoretical or experimental, must be done in order to modelling the more accurately as possible such a constituent so that it can be included in the nominal background of the orbital determination softwares like GEODYN II at a satisfactory level of accuracy. The calculations performed in this work point toward this goal in the sense that, if we put our values for the perturbative amplitudes due to the 18.6-year tide in the models of, e.g., GEODYN II and subsequently build up the orbital residuals, we expect that the contribution of such semisecular constituent to $\Delta\mu_{\text{LT}}$ amounts to the value quoted here.

Even though a cancellation is not expected as for the first two even zonal constituents, by calculating the left hand side of eq. (1.5) for the other tides yields, at least, an order of magnitude of their effect on μ_{LT} . An interesting, unpredicted feature stands out for the odd zonal ocean tides. The contribution of $l = 3$ zonal ocean tidal nominal perturbations over 1 year to $\Delta\mu_{\text{LT}}$ can be found in Tab. 4.3 and Tab. 4.4. By inspecting them it is clear that the sensitivity of perigee of LAGEOS II to the $l = 3$ part of the ocean tidal spectrum may affect the recovery of the Lense-Thirring parameter μ_{LT} by means of the proposed combined residuals, especially as far as S_a and S_{sa} are concerned. This fact agrees with the results of Tab. 3.17 which tells us that the mismodelled parts of S_a and S_{sa} are not negligible fractions of $\Delta\omega_{\text{LT}}^{\text{II}}$. However, if the mismodelled amplitudes are employed in eq. (1.5) it can be seen that, over 1 year, a cancellation of the order of 10^{-1} (S_a $l = 3$ $p = 2$) and 10^{-2} (S_a $l = 3$ $p = 1$; S_{sa} $l = 3$ $p = 1, 2$) takes place. The contributions of the mismodelling on M_m and M_f are completely negligible. So, we can conclude that also the $l = 3$ part of the zonal ocean tidal spectrum may not affect the combined residuals in a notable manner if the $l = 3$ part of S_a and S_{sa} is properly accounted for.

4.3 The simulated residual signal

The first step of our strategy was to generate with MATLAB a time series which simulates, at the same length and resolution, the real residual curve obtainable from $y = \delta\Omega_{\text{exp}}^{\text{I}} + c_1\delta\Omega_{\text{exp}}^{\text{II}} + c_2\delta\omega_{\text{exp}}^{\text{II}}$ through, e.g., GEODYN. This simulated curve (“Input Model” - IM in the following) was constructed with:

- The secular Lense-Thirring trend as predicted by the General Relativity²
- A certain number of sinusoids of the form $\delta A_k \cos(\frac{2\pi}{P_k}t + \phi_k)$ with known periods P_k , $k = 1,..N$ simulating the mismodelled tides and other long-period signals which, to the level of assumed mismodelling, affect the combined residuals
- A noise of given amplitude which simulates the experimental errors in the laser-ranged measurements and, depending on the characteristics chosen for it, some other physical forces.

In a nutshell

$$\text{IM} = \text{LT} + [\text{mismodelled tides}] + [\text{other mismodelled long period signals}] + [\text{noise}]. \quad (4.1)$$

The harmonics included in the IM are the following:

- K_1 , $l = 2$ solid and ocean; node of LAGEOS ($P=1,043.67$ days)
- K_1 , $l = 2$ solid and ocean; node and perigee of LAGEOS II ($P=-569.21$ days)
- K_1 , $l = 3$, $p = 1$ ocean; perigee of LAGEOS II ($P=-1,851.9$ days)
- K_1 , $l = 3$, $p = 2$ ocean; perigee of LAGEOS II ($P=-336.28$ days)
- K_2 , $l = 3$, $p = 1$ ocean; perigee of LAGEOS II ($P=-435.3$ days)
- K_2 , $l = 3$, $p = 2$ ocean; perigee of LAGEOS II ($P=-211.4$ days)
- 165.565 , $l = 2$ solid; node of LAGEOS ($P=904.77$ days)
- 165.565 , $l = 2$ solid; node and perigee of LAGEOS II ($P=-621.22$ days)
- S_2 , $l = 2$ solid and ocean; node of LAGEOS ($P=-280.93$ days)
- S_2 , $l = 2$ solid and ocean; node and perigee of LAGEOS II ($P=-111.24$ days)
- S_2 , $l = 3$, $p = 1$ ocean; perigee of LAGEOS II ($P=-128.6$ days)

²Remember that in the dynamical models of GEODYN II it was set purposely equal to 0 so that the residuals absorbed (contained) entirely the relativistic effect [Ciufolini *et al.*, 1997].

- $S_2, l = 3, p = 2$ ocean; perigee of LAGEOS II ($P=-97.9$ days)
- $P_1, l = 2$ solid and ocean; node of LAGEOS ($P=-221.35$ days)
- $P_1, l = 2$ solid and ocean; node and perigee of LAGEOS II ($P=-138.26$ days)
- $P_1, l = 3, p = 1$ ocean; perigee of LAGEOS II ($P=-166.2$ days)
- $P_1, l = 3, p = 2$ ocean; perigee of LAGEOS II ($P=-118.35$ days)
- Solar Radiation Pressure, perigee of LAGEOS II ($P=-4,241$ days)
- Solar Radiation Pressure, perigee of LAGEOS II ($P=657$ days)
- perigee odd zonal C_{30} , perigee of LAGEOS II ($P=821.79$)

In the following the signals due to solar radiation pressure will be denoted as $\text{SRP}(P)$ where P is their period; the effects of the eclipses and Earth penumbra have not been accounted for. Many of the periodicities listed above have been actually found in the Fourier spectrum of the real residual curve [*Ciufolini et al.*, 1997]. Concerning $K_1 l = 3 p = 1$ and $\text{SRP}(4,241)$, see section 5.

When the real data are collected they refer to a unique, unrepeatable situation characterized by certain starting and ending dates for T_{obs} . This means that each analysis which could be carried out in the real world necessarily refers to a given set of initial phases and noise for the residual curve corresponding to the chosen observational period; if the data are collected over the same T_{obs} shifted backward or forward in time, in general, such features of the curve will change. We neither know a priori when the next real experiment will be performed, nor which will be the set of initial phases and the level of experimental errors accounted for by the noise. Moreover, maybe the dynamical models of the orbit determination software employed are out of date in regard to the perturbations acting upon satellites' orbits or do not include some of them at all. Consequently, it would be incorrect to work with a single simulated curve, fixed by an arbitrary set of δA_k , ϕ_k and noise, because it could refer to a situation different from that in which, in the real world, the residuals will actually correspond.

The need for great flexibility in generating the IM becomes apparent: to account for the entire spectrum of possibilities occurring when the real analysis will be carried out. We therefore decided to build into the MATLAB routine the capability to vary randomly the initial phases ϕ_k , the noise and the amplitude errors δA_k . Concerning

the error amplitudes of the harmonics, they can be randomly varied so that δA_k spans $[0, \delta A_k^{\text{nom}}]$ where δA_k^{nom} is the nominal mismodelled amplitude calculated taking into account Tab. 3.9 and Tab. 3.17; it means that we assume they are reliable estimates of the differences between the real data and the dynamical models of the orbital determination softwares, i.e. of the residuals. The MATLAB routine allows also the user to decide which harmonic is to be included in the IM; it is also possible to choose the length of the time series T_{obs} , the sampling step Δt and the amplitude of the noise. Fig. (4.1) shows a typical simulation over 3.1 years with $\Delta t = 15$ days and a given set of random initial phases and noise: all the long period signals have been included with $\delta A_k = \delta A_k^{\text{nom}}$. It can be compared to the real residual curve released in [Ciufolini *et al.*, 1997] for the same time step and time span going from November 1992 to December 1995: qualitatively they agree very well. We also calculated the root mean square for the IM simulated data, of 9 mas.

In order to assess quantitatively this feature we proceeded as follows. First, over a time span of 3.1 years, we fitted the IM with a straight line only, finding for a choice of random phases and noise which qualitatively reproduces the curve shown in [Ciufolini *et al.*, 1997], the value of 38.25 mas for the root mean square of the post fit IM. The value quoted in [Ciufolini *et al.*, 1997] is 43 mas. Second, as done in the cited paper, we fitted the complete IM with the LT plus a set of long-period signals (see section 4) and then we subtracted the so adjusted harmonics from the original IM obtaining a “residual” simulated signal curve. The latter was subsequently fitted with a straight line only, finding a rms post fit of 12.3 mas (it is nearly independent of the random phases and the noise) versus 13 mas quoted in [Ciufolini *et al.*, 1997]. A uniformly distributed noise with nonzero average and amplitude of 50 mas was used (see section 4). These considerations suggest that the simulation procedure adopted is reliable, replicates the real world satisfactorily and yields a good starting point for conducting our sensitivity analysis.

4.4 Sensitivity analysis

A preliminary analysis was carried out in order to evaluate the importance of the mismodelled solid tides on the recovery of μ_{LT} . We calculated the average

$$\frac{1}{T_{obs}} \int_0^{T_{obs}} [\text{solid tides}] dt, \quad (4.2)$$

where $[\text{solid tides}]$ denotes the analytical expressions of the mismodelled solid tidal perturbations as given by eqs. (3.40)-(3.41). Subsequently, we compared it to the value of the gravitomagnetic trend for the same T_{obs} . The tests were repeated by varying Δt , T_{obs} and the initial phases. They have shown that the mismodelled part of the solid Earth tidal spectrum is entirely negligible with respect to the LT signal, falling always below 1% of the gravitomagnetic shift of the combined residuals accumulated over the examined T_{obs} .

For the ocean tides and the other long-period signals the problem was addressed in a different way. First, for a given Δt and different time series lengths, we included in the IM the effects of LT, the noise and the solid tides only: subsequently we fitted it simply by means of a straight line. In a second step we have simultaneously added, both to the IM and the fitting model (FM hereafter), all the ocean tides, the solar radiation pressure SRP(657) signal and the odd zonal geopotential harmonic. We then compared the fitted values of μ_{LT} and $\delta\mu_{LT}$ recovered from both cases in order to evaluate $\Delta\mu_{LT}$ and $\Delta\delta\mu_{LT}$. The least squares fits [Bard, 1974; Draper and Smith, 1981] were performed by means of the MATLAB routine “nlleasqr” (see, e.g., <http://www.ill.fr/tas/matlab/doc/mfit.html>); as $\delta\mu_{LT}$ we have assumed the square root of the diagonal covariance matrix element relative to the slope parameter. It simulates the formal experimental error which, in the context of the gravitomagnetic LAGEOS experiment, is far smaller than the systematic errors which, consequently, must be carefully assessed. Notice that the SRP(4,241) has never been included in the FM (See section 5), while $K_1 l = 3 p = 1$ has been included for $T_{obs} > 5$ years. For both of the described scenarios we have taken the average for μ_{LT} and $\delta\mu_{LT}$ over 1,500 runs performed by varying randomly the initial phases, the noise and the amplitudes of the mismodelled signals in order to account for all possible situations occurring in the real world, as pointed out in the previous section. The

large number of repetitions was chosen in order to avoid that statistical fluctuations in the results could “leak” into $\Delta\overline{\mu_{LT}}$ and $\Delta\overline{\delta\mu_{LT}}$ and corrupt them at the level of 1%. With 1,500 runs the standard deviations on $\overline{\mu_{LT}}$ and $\overline{\delta\mu_{LT}}$ are of the order of 10^{-3} or less, so that we can reliably use the results of such averages for our comparisons of $\overline{\mu_{LT}}$ (no tides) vs $\overline{\mu_{LT}}$ (all tides).

Before implementing such strategy for different T_{obs} , Δt and noise we carefully analyzed the $\Delta t = 15$ days, $T_{obs}=4$ years experiment considered in [Ciufolini *et al.*, 1998] by trying to obtain the quantitative features outlined there, so that we start from a firm and reliable basis. This goal was achieved by proceeding as outlined in the previous section and adopting a uniformly distributed random noise with an amplitude of 35 mas.

Fig. 4.2 shows the results for $\Delta\overline{\mu_{LT}}$ obtained with $\Delta t = 15$ days and a uniform random noise with amplitudes of 50 mas and 35 mas corresponding to the characteristics of the real curves in [Ciufolini *et al.*, 1997; 1998]. Notice that our estimates for the case $T_{obs} = 4$ years almost coincide with those by Ciufolini *et al.* [1998] who claim $\Delta\mu_{tides} \leq 4\%$. Notice that for $T_{obs} > 7$ years the effect of tidal perturbations errors falls around 2%. By choosing different Δt does not introduce appreciable modifications to the results presented here. This fact was tested by repeating the set of runs with $\Delta t = 7$ and 22 days.

Up to this point we dealt with the entire set of long-period signals affecting the combined residuals; now we ask if it is possible to assess individually the influence of each tide on the recovery of LT. We shall focus our attention on the case $\Delta t = 15$ days, $T_{obs}=4$ years.

In order to evaluate the influence of each tidal constituent on the recovery of μ_{LT} two complementary approaches could be followed in principle. The first one consists of starting without any long-period signal either in the IM or in the FM, and subsequently adding to them one harmonic at a time, while neglecting all the others. In doing so it is implicitly assumed that each constituent is mutually uncorrelated with any other one present in the signal. In fact, the matter is quite different since if for the complete model case we consider the covariance and correlation matrices of the

FM adjusted parameters it turns out that the LT is strongly correlated, at a level of $|Corr(i, j)| > 0.9$, with certain harmonics, which happen to be mutually correlated too. These are:

- K_1 , $l = 2$ ($P=1,043.67$ days; 1.39 cycles completed)
- K_1 , $l = 2$ ($P=-569.21$ days; 2.56 cycles completed)
- K_1 , $l = 3$, $p = 2$ ($P=-336.28$ days; 4.34 cycles completed)
- K_2 , $l = 3$, $p = 1$ ($P=-435.3$ days; 3.35 cycles completed)
- Solar Radiation Pressure, ($P=657$ days; 2.22 cycles completed)
- perigee odd zonal C_{30} , ($P=821.79$; 1.77 cycles completed)

Their FM parameters are indeterminate in the sense that the values estimated are smaller than the relative uncertainties assumed to be $\sqrt{Cov(i, i)}$. On the contrary, there are other signals which are poorly correlated to the LT and whose reciprocal correlation too is very low and that are well determined. These are:

- K_2 , $l = 3$, $p = 2$ ($P=-211.4$ days; 6.91 cycles completed)
- S_2 , $l = 3$, $p = 1$ ($P=-128.6$ days; 11.3 cycles completed)
- S_2 , $l = 3$, $p = 2$ ($P=-97.9$ days; 14.9 cycles completed)
- P_1 , $l = 3$, $p = 1$ ($P=-166.2$ days; 8.78 cycles completed)
- P_1 , $l = 3$, $p = 2$ ($P=-118.35$ days; 12.3 cycles completed)

In Fig. (4.3) the complete IM and FM are shown for a given choice of the initial phases, uniform noise with amplitude of 50 mas, $T_{\text{obs}} = 4$ years and $\Delta t = \text{days}$. It is interesting to notice that over $T_{\text{obs}} = 4$ years the signals uncorrelated with the LT have in general described many complete cycles, contrary to these correlated with LT. This means that the signals that average out over T_{obs} decorrelate with LT, allowing the gravitomagnetic trend to emerge clearly against the background, almost not affecting the LT recovery. This feature has been tested as follows. In a first step, all the uncorrelated tides have been removed from both the IM (50 mas uniform random noise) and the FM, leaving only the correlated tides in. The runs were then repeated, all other things being equal, the following values were recorded: $\overline{\mu_{\text{LT}}} = 1.2104$, $\overline{\delta\mu_{\text{LT}}} = 0.1006$ with a variation with respect to the complete model case ($\overline{\mu_{\text{LT}}} = 1.2073$, $\overline{\delta\mu_{\text{LT}}} = 0.1295$) of: $\Delta\overline{\mu_{\text{LT}}} \simeq 0.3\%$, $\Delta\overline{\delta\mu_{\text{LT}}} \simeq 2.9\%$. Conversely, if all the signals with strong correlation are removed from the simulated data and from the FM, leaving only the uncorrelated ones in, we obtain: $\overline{\mu_{\text{LT}}} = 1.1587$, $\overline{\delta\mu_{\text{LT}}} = 0.0186$ with $\Delta\overline{\mu_{\text{LT}}} \simeq 4.8\%$, $\Delta\overline{\delta\mu_{\text{LT}}} \simeq 11\%$. Notice that the sum of both contributions for

$\Delta\overline{\mu_{LT}}$ yields exactly the overall value $\Delta\overline{\mu_{LT}} = 5.2\%$ as obtained in the previous analysis (cf. Fig. 4.2 for $T_{\text{obs}} = 4$ years). This highlights the importance of certain long period signals in affecting the recovery of LT and justify the choice of treating them simultaneously as it was done in obtaining Fig. 4.2. Moreover, it clearly indicates that the efforts of the scientific community should be focused on the improvement of the knowledge of these tidal constituents. It has been tested that for $T_{\text{obs}} = 8$ years all such “geometrical” correlations among the LT and the harmonics nearly disappear, as it would be intuitively expected.

4.5 The effect of the very long periodic harmonics

In this section we shall deal with those signals whose periods are longer than 4 years which could corrupt the recovery of LT resembling superimposed trends if their periods are considerably longer than the adopted time series length.

In chapter 3 we have shown the existence of a very long periodic ocean tidal perturbation acting upon the perigee of LAGEOS II. It is the K_1 $l = 3$ $p = 1$ $q = -1$ constituent with period $P = 1,851.9$ days (5.07 years) and nominal amplitudes of $-1,136$ mas. In [Lucchesi, 2001], for the effect of the direct solar radiation pressure on the perigee of LAGEOS II, it has been explicitly calculated, by neglecting the effects of the eclipses, a signal SRP(4,241) with $P = 4,241$ days (11.6 years) and nominal amplitude of 6400 mas. The mismodelling on these harmonics, both of the form $\delta A \sin(\frac{2\pi}{P}t + \phi)$, amounts to 64.5 mas for the tidal constituent, as shown in section 3.6, and to 32 mas for SRP(4,241), according to [Lucchesi, 2001].

About the actual presence of such semisecular harmonics in the spectrum of the real combined residuals, it must be pointed out that, over $T_{\text{obs}} = 3.1$ years [Ciufolini *et al.*, 1997], it is not possible that so low frequencies could be resolved by Fourier analysis. Indeed, according to [Godin, 1972; Priestley, 1981], when a signal is sampled over a finite time interval T_{obs} it induces a sampling also in the spectrum. The lowest frequency that can be resolved is

$$f_{\text{min}} = \frac{1}{2T_{\text{obs}}}, \quad (4.3)$$

i.e. a harmonic must describe, at least, half a cycle over T_{obs} in order to be detected in the spectrum. f_{min} is called elementary frequency band and it also represents the minimum separation between two frequencies in order to be resolved. For our two signals we have $f(K_1) = 5.39 \times 10^{-4}$ cycles per day (cpd) and $f(\text{SRP}) = 2.35 \times 10^{-4}$ cpd; over 3.1 years $f_{\text{min}} = 4.41 \times 10^{-4}$ cpd. This means that the two harmonics neither can be resolved as distinct nor they can be found in the spectrum at all. In order to resolve them we should wait for $T_{\text{obs}} = 4.5$ years which corresponds to their separation $\Delta f = 3.04 \times 10^{-4}$ cpd, according to eq. (4.3). In view of the potentially large aliasing effect of these two harmonics on the LT it was decided to include both $K_1 l = 3 p = 1$ and SRP(4,241) in the simulated residual curve at the level of mismodelling claimed before.

In order to obtain an upper bound of their contribution to the systematic uncertainty in μ_{LT} we proceeded as follows. First, we calculated the temporal average of the perturbations induced on the combined residuals by the two harmonics over different T_{obs} according to

$$I = \frac{1}{T_{\text{obs}}} \int_0^{T_{\text{obs}}} c_2 \delta A \sin\left(\frac{2\pi}{P}t + \phi\right) dt = c_2 \frac{\delta A}{\tau} (\cos \phi + \sin \phi \sin \tau - \cos \phi \cos \tau), \quad (4.4)$$

with $\tau = 2\pi \frac{T_{\text{obs}}}{P}$. The results are shown in Fig. 4.4 and Fig. 4.5. It can be seen that, for given T_{obs} , the averages are periodic functions of the initial phases ϕ with period 2π . Since the gravitomagnetic trend is positive and growing in time, we shall consider only the positive values of the temporal averages corresponding to those portions of sinusoid which are themselves positive. Moreover, notice that, in this case, one should consider if the perturbation's arc is rising or falling over the considered T_{obs} : indeed, even though the corresponding averages could be equal, it is only in the first case that the sinusoid has an aliasing effect on the LT trend. The values of ϕ which maximize the averages were found numerically and for such values the maxima of the averages were calculated. Subsequently, these results in mas were compared to the amount of the predicted gravitomagnetic shift accumulated over the chosen T_{obs} by the combined residuals $y_{\text{LT}} = 60.2 \text{ (mas/y)} \times T_{\text{obs}} \text{ (y)}$. The results are shown in Tab. 4.5 and Tab. 4.6 and, as previously outlined, represent a pessimistic estimate. It is interesting to notice that an analysis over $T_{\text{obs}} = 5$ years, that should not be much more demanding than the already performed works, could cancel out the effect of the $K_1 l = 3 p = 1$ tide; in this scenario the effect of SRP(4,241) should amount, at most to 2.6% of the

LT effect. Notice also that for $T_{\text{obs}} = 7$ years, a time span sufficient for the LT to emerge on the background of most of the other tidal perturbations, the estimates of Fig. 4.2 are compatible with those of Tab. 4.5 and Tab. 4.6 which predict an upper contribution of 1.1% from the $K_1 l = 3 p = 1$ and 1.3% from SRP(4,241) on the LT parameter μ_{LT} .

An approach, similar to that used in [Vespe, 1999] in order to assess the influence of the eclipses and Earth penumbra effects on the perigee of LAGEOS II has been applied also to our case. It consists of fitting with a straight line only the mismodelled perturbation to be considered and, subsequently, comparing the slope of such fits to that due to gravitomagnetism which is equal to 1 in units of 60.2 mas/y. We have applied this method to $K_1 l = 3 p = 1$ and SRP(4,241) with the already cited mismodelled amplitudes and by varying randomly the initial phases ϕ within $[-2\pi, 2\pi]$. The mean value of the fit's slope, in units of 60.2 mas/y, over 1,500 runs is very close to zero. This agrees with Fig. 4.4 and Fig. 4.5 which tell us that the temporal averages of $K_1 l = 3 p = 1$ and SRP(4,241) are periodic functions of ϕ with period of 2π and, consequently, have zero mean value. Concerning the upper limits of $\Delta\mu_{\text{LT}}$ derived from these runs, they agree with those released in Tab. 4.5 and Tab. 4.6 up to 1-2 %.

The method of temporal averages can be successfully applied also for the $l = 2 m = 0$ 18.6-year tide. It is a very long period zonal tidal perturbation which could potentially reveal itself as the most dangerous in aliasing the results for μ_{LT} since its nominal amplitude is very large and its period is much longer than the T_{obs} which could be adopted for real analysis. Ciufolini [1996] claims that the combined residuals have the merit of cancelling out all the static and dynamical geopotential's contributions of degree $l = 2, 4$ and order $m = 0$, so that the 18.6-year tide would not create problems. This topic was quantitatively addressed in a preliminary way. Indeed, in order to make comparisons with other works, we have simply calculated for $T_{\text{obs}} = 1$ year the combined residuals with only the mismodelled amplitudes of the 18.6-year tidal perturbations on the nodes of LAGEOS and LAGEOS II and the perigee of LAGEOS II. This means that the dynamical pattern over the time span of such important tidal perturbation was not investigated. We did this by calculating

the average over different T_{obs} . The results are in Fig. 4.6 which shows clearly that the 18.6-year tide does not affect at all the estimation of μ_{LT} if we adopt as observable the combined residuals proposed by Ciufolini. Indeed, for $T_{\text{obs}} = 4$ years, the average effect will reach, at most, 0.08% of the gravitomagnetic shift over the same time span.

This feature of the 18.6-year tide is confirmed also by fitting with a straight line only the sinusoid of this perturbation on the combined residual: the adjusted slope amounts, at most, to less than 1% of the gravitomagnetic effect for different T_{obs} .

4.6 The error due to the inclination

The combined residuals by Ciufolini allow one to cancel out the effect of the mismodelling in J_2 and J_4 but are affected by the higher degree even zonal harmonics of the geopotential and by the residuals of the inclination angle [Ciufolini *et al.*, 1996; 1997] according to

$$\delta\mu_{\text{inclination}} = \frac{\partial\dot{\Omega}^{\text{I}}}{\partial i}\delta i^{\text{I}} + 0.295 \frac{\partial\dot{\Omega}^{\text{II}}}{\partial i}\delta i^{\text{II}} - 0.35 \frac{\partial\dot{\omega}^{\text{II}}}{\partial i}\delta i^{\text{II}}, \quad (4.5)$$

in which, by considering only the J_2 contribution to the classical precessions, $\frac{\partial\dot{\Omega}^{\text{I}}}{\partial i} = 6$ rad/y, $\frac{\partial\dot{\Omega}^{\text{II}}}{\partial i} = 5.3$ rad/y and $\frac{\partial\dot{\omega}^{\text{II}}}{\partial i} = -16$ rad/y.

An assessment of eq. (4.5) requires an inspection of the residuals of the inclination over the considered time spans. To this aim we have simulated with MATLAB the time series of the mismodelled parts of the inclinations of LAGEOS and LAGEOS II for different time spans. We have included the solid Earth and ocean tides, as worked out in chapter 3, and the solar radiation pressure [Lucchesi, 2001]. Subsequently, at fixed T_{obs} , we have performed 5,000 runs by varying the initial phases and for each run we have calculated $\langle\delta i^{\text{I}}\rangle$ and $\langle\delta i^{\text{II}}\rangle$ in mas; then we have inserted them in eq. (4.5) and we have taken the ratios of such values to the general relativistic shift for the given time span. We have so obtained a vector of 5,000 figures, for any given T_{obs} , depending on the initial phases which represent the systematic errors induced by the mismodelling in the inclination. Such values turn out to be normally distributed, so that we have chosen their standard deviation to represent $\delta\mu_{\text{incl}}$ for the various T_{obs} chosen. The results are shown in Fig. 4.7.

Our estimates predicts a systematic error induced by the mismodelling in the inclination of almost 3.8% over 4 years and of almost 1.5% over 8 years. Notice that the estimates released in [*Ciufolini et al.*, 1997] over 3.1 years, $\delta\mu_{\text{incli}} \simeq 10\%\mu_{\text{LT}}$, seem to be too pessimistic, while those quoted in [*Ciufolini et al.*, 1998], $\delta\mu_{\text{incli}} \simeq 5\%\mu_{\text{LT}}$, are in agreement with our estimates.

4.7 Conclusions

The detection of the Lense-Thirring effect can be achieved by means of the eq. (1.5). *Ciufolini* [1996] claims that the static and dynamical terms of degree $l = 2, 4$ and order $m = 0$ of the geopotential do not affect his proposed combined residuals.

In this chapter we have tested this statement in regard not only to the $l = 2, 4$ $m = 0$ solid and ocean Earth tides, but also to the $m = 1, 2$ ones and to the other long-period perturbations which affect the combined residuals.

Concerning the zonal tides, in order to compare our results to those released in [*Ciufolini et al.*, 1997], we have preliminarily used the nominal perturbative amplitudes by calculating eq. (1.5) on a time span of 1 year. As far as the $l = 2$ $m = 0$ tides are concerned, the 18.6-year tide cancels out at a level of 10^{-1} only. But if we repeat the calculations with the mismodelled amplitudes over 1 year the accuracy of the cancellation grows to 10^{-3} . This shows that the more accurate the dynamical models employed in building up the orbital residuals are, the more accurate the recovery of the Lense-Thirring becomes. The $l = 4$ zonal tides do not create problems. Also the $l = 3$ $m = 0$ tides, and this is an unpredicted feature, although at a lesser extent, cancel out at a level ranging from 10^{-1} - 10^{-2} if they are properly accounted in the residuals' construction. This points towards a better understanding, from both a theoretical and experimental point of view, of the $l = 3$, $m = 0$ part of the tidal spectrum. The results presented in this chapter not only confirm the usefulness of the formula by Ciufolini for the $l = 2, 4$ $m = 0$ tides, but also extend its validity to the $l = 3$ $m = 0$ part of the tidal response spectrum.

Regarding the tesseral and sectorial tides, on one hand, by simulating the real

residual curve in order to reproduce as closely as possible the results obtained for the $\Delta t = 15$ days $T_{\text{obs}} = 4$ years scenario published in [Ciufolini *et al.*, 1998] it has been possible to refine and detail the estimates for it. On the other hand, this procedure also extends them to longer observational periods in view of new, more sophisticated analysis to be completed in the near future based on real data analyzed with the orbit determination software GEODYN II in collaboration with the teams from the Joint Center for Earth Systems Technology at NASA Goddard Space Flight Center and at the University of Rome La Sapienza. Since such numerical analysis is very demanding in terms of both time employed and results analysis burden, it should be very useful to have a priori estimates which could better direct the work. This could be done, e.g., by identifying which tidal constituents μ_{LT} is more or less sensitive to in order to seek improved dynamical models for use in GEODYN.

As far as the perturbations generated by the solid Earth tides, the high level of accuracy with which they are known has yielded a contribution to the systematic errors in μ_{LT} which falls well below 1%, so that they are of no concern at present.

Concerning the ocean tidal perturbations and the other long-period harmonics, for those whose periods are shorter than 4 years, the role played by T_{obs} , Δt and the noise has been investigated. It turned out that Δt has no discernible effect on the adjusted value of μ_{LT} , while T_{obs} is very important and so is the noise. The main results for these are summarized in Fig. 4.2, which tells us that the entire set of long-period signals, if properly accounted for in building up the residuals, affect the recovery of the Lense-Thirring effect at a level not worse than 4% – 5% for $T_{\text{obs}} = 4$ years; the error contribution diminishes to about 2% after 7 years of observations.

We have also shown which tides are strongly anticorrelated and correlated with the gravitomagnetic trend over 4 years of observations. The experimental and theoretical efforts should concentrate on improving these constituents in particular. This geometrical correlation tends to diminish as T_{obs} grows. This can be intuitively recognized by noting that the longer T_{obs} is, the larger the number of cycles these periodic signals are sampled over and cleaner the way in which the secular Lense-Thirring trend emerges against the background “noise”.

The ocean tide constituents K_1 $l = 3$ $p = 1$ and the solar radiation pressure harmonic SRP(4,241) generate perturbations on the perigee of LAGEOS II with periods of 5.07 years and 11.6 years respectively, so that they act on the Lense-Thirring effect as biases and corrupt its determination with the related mismodelling: indeed they may resemble trends if T_{obs} is shorter than their periods. They were included in the simulated residual curve and their effect was evaluated in different ways with respect to the other tides. An upper bound was calculated for their action and it turns out that they contribute to the systematic uncertainty in the recovery of μ_{LT} at a level of less than 4% depending on T_{obs} and the initial phases ϕ . The results are summarized in Tab. 4.5 and Tab. 4.6. An observational period of 5 years, which seems to be a reasonable choice in terms of time scale and computational burden, allows one to average out the effect of the K_1 $l = 3$ $p = 1$.

The strategy followed for the latter harmonics has been extended also to the $l = 2$ $m = 0$ zonal 18.6-year tide. Fig. 4.6 confirms the claim in [Ciufolini, 1996] that it does not affect the combined residuals.

In conclusion, the strategy presented here could be used as follows. Starting from a simulated residual curve based on the state of art of the real analysis performed until now, it provides helpful indications in order to improve the force models of the orbit determination software as far as tidal perturbations are concerned and to perform new analysis with real residuals. Moreover, when real data will be collected for a given scenario it will be possible to use them in our software in order to adapt the simulation procedure to the new situation; e.g. it is expected that the noise level in the near future will diminish in view of improvements in laser ranging technology and modelling. Thus, we shall repeat our analysis for $\Delta\mu_{\text{tides}}$ when these new results become available.

4.8 Tables

Table 4.1: Contribution of the even zonal solid tidal constituents to $\Delta\mu_{\text{LT}}$ by means of the formula $\delta\dot{\Omega}^{\text{II}} + \delta\dot{\Omega}^{\text{II}} \times 0.295 - \delta\dot{\omega}^{\text{II}} \times 0.35 = 60.2 \times \mu_{\text{LT}}$ for $l = 2$, $m = 0$, $p = 1$, $q = 0$.

Tide	$A(\Omega_{\text{I}})$ (mas)	$A(\Omega_{\text{II}})$ (mas)	$A(\omega_{\text{II}})$ (mas)	$\Delta\mu_{\text{LT}}$
055.565	-1,079.38	1,982.16	-1,375.58	-0.219
055.575	5.23	-9.61	6.66	1.06×10^{-3}
056.554 S_a	9.95	-18.28	12.69	2.02×10^{-3}
057.555 S_{sa}	31.21	-57.31	39.77	6.33×10^{-3}
065.455 M_m	5.28	-9.71	6.74	1.07×10^{-3}
075.555 M_f	4.94	-9.08	6.3	1×10^{-3}

Table 4.2: Contribution of the even zonal ocean tidal constituents to $\Delta\mu_{\text{LT}}$ by means of the formula $\delta\dot{\Omega}^{\text{II}} + \delta\dot{\Omega}^{\text{II}} \times 0.295 - \delta\dot{\omega}^{\text{II}} \times 0.35 = 60.2 \times \mu_{\text{LT}}$ for $l = 2$, $m = 0$, $p = 1$, $q = 0$.

Tide	$A(\Omega_{\text{I}})$ (mas)	$A(\Omega_{\text{II}})$ (mas)	$A(\omega_{\text{II}})$ (mas)	$\Delta\mu_{\text{LT}}$
056.554 S_a	-20.55	37.71	-26.17	-3.68×10^{-3}
057.555 S_{sa}	-5.98	10.98	-7.62	-1.28×10^{-3}
065.455 M_m	-0.54	1	-0.69	-8.78×10^{-5}
075.555 M_f	-0.62	1.13	-0.78	-1.73×10^{-4}

Table 4.3: Contribution of the odd zonal ocean tidal constituents to $\Delta\mu_{\text{LT}}$ by means of the formula $\delta\dot{\Omega}_{\text{I}} + \delta\dot{\Omega}^{\text{II}} \times 0.295 - \delta\dot{\omega}^{\text{II}} \times 0.35 = 60.2 \times \mu_{\text{LT}}$ for $l = 3$, $m = 0$, $p = 1$, $q = -1$.

Tide	$A(\Omega_{\text{I}})$ (mas)	$A(\Omega_{\text{II}})$ (mas)	$A(\omega_{\text{II}})$ (mas)	$\Delta\mu_{\text{LT}}$
056.554 S_a	-0.063	0.13	-114.35	0.66
057.555 S_{sa}	-9×10^{-3}	0.028	-22.95	0.133
065.455 M_m	-4×10^{-4}	1×10^{-3}	-1.53	-8.93×10^{-3}
075.555 M_f	-1×10^{-4}	7×10^{-4}	-0.58	3.41×10^{-3}

Table 4.4: Contribution of the odd zonal ocean tidal constituents to $\Delta\mu_{\text{LT}}$ by means of the formula $\delta\dot{\Omega}^{\text{I}} + \delta\dot{\Omega}^{\text{II}} \times 0.295 - \delta\dot{\omega}^{\text{II}} \times 0.35 = 60.2 \times \mu_{\text{LT}}$ for $l = 3$, $m = 0$, $p = 2$, $q = 1$.

Tide	$A(\Omega_{\text{I}})$ (mas)	$A(\Omega_{\text{II}})$ (mas)	$A(\omega_{\text{II}})$ (mas)	$\Delta\mu_{\text{LT}}$
056.554 S_a	0.047	-0.36	297.34	-1.72
057.555 S_{sa}	7×10^{-3}	-0.044	36.07	-0.209
065.455 M_m	4×10^{-4}	-2×10^{-3}	1.642	-9.55×10^{-3}
075.555 M_f	1.79×10^{-4}	-7×10^{-4}	-0.60	-3.52×10^{-3}

Table 4.5: Effect of the averaged mismodelled harmonic $K_1 l = 3 p = 1$ on the Lense-Thirring trend for different T_{obs} . In order to obtain upper limits the maximum value for the average of the tidal constituent has been taken, while for the gravitomagnetic effect it has been simply taken the value $y_{\text{LT}} \times T_{\text{obs}}$.

T_{obs} (years)	$\max c_2 \langle \delta\omega^{\text{II}} \rangle$ (mas)	y_{LT} (mas)	$\max c_2 \langle \delta\omega^{\text{II}} \rangle / y_{\text{LT}}$ (%)
4	5.6	240.8	2.3
5	0.3	301	0.09
6	3.3	361.2	0.9
7	4.8	421.4	1.1

Table 4.6: Effect of the averaged mismodelled harmonic SRP(4, 241) on the Lense-Thirring trend for different T_{obs} . In order to obtain upper limits the maximum value for the average of the radiative harmonic has been taken, while for the gravitomagnetic effect it has been simply taken the value $y_{\text{LT}} \times T_{\text{obs}}$.

T_{obs} (years)	$\max c_2 \langle \delta\omega^{\text{II}} \rangle$ (mas)	y_{LT} (mas)	$\max c_2 \langle \delta\omega^{\text{II}} \rangle / y_{\text{LT}}$ (%)
4	9.1	240.8	3.7
5	8	301	2.6
6	6.8	361.2	1.8
7	5.6	421.4	1.3

4.9 Figures

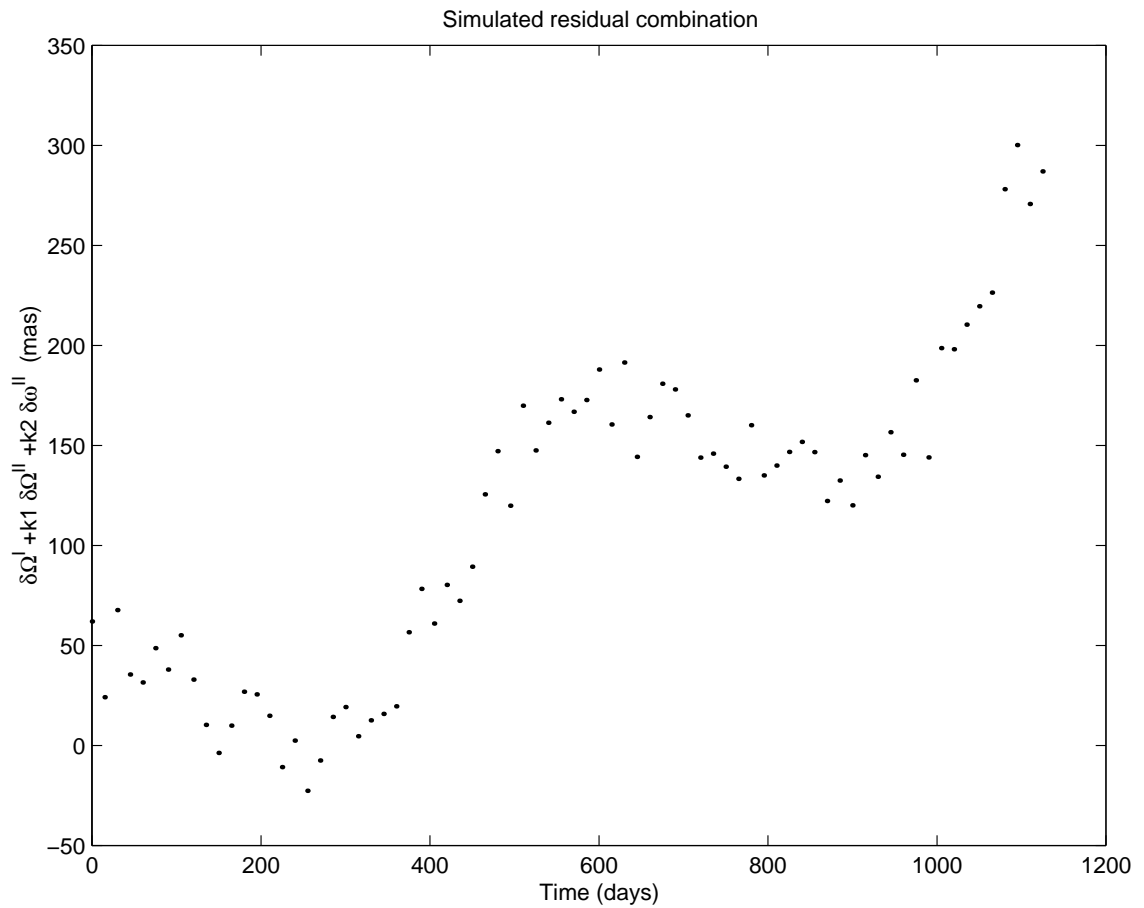


Figure 4.1: Simulated residual curve. The time span is 3.1 years, the time step is 15 days and all the long period signals are included. The random initial phases and the noise have been chosen in order to reproduce as closely as possible the residual curve of [Ciufolini *et al.*, 1997]. The rms of the simulated data amounts to almost 9 mas, the 5% of the predicted gravitomagnetic value for the combined residuals.

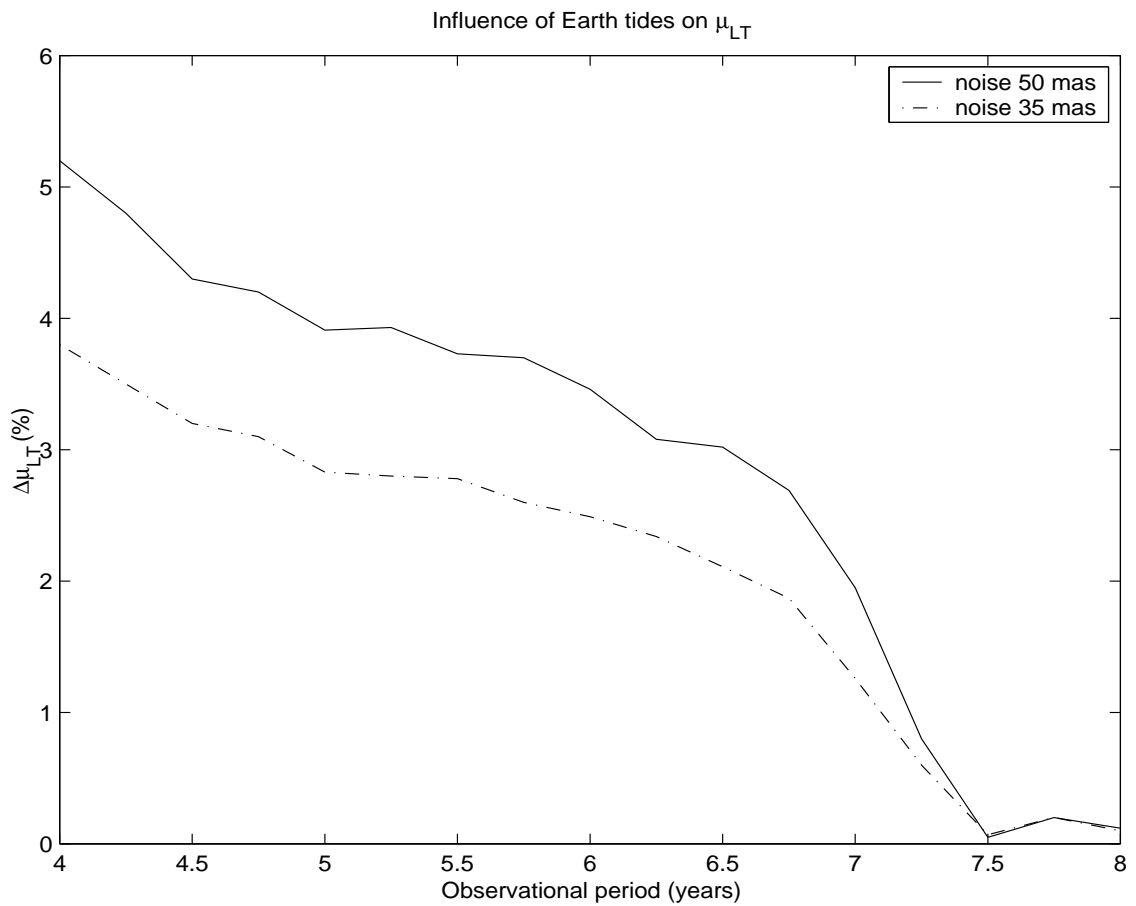


Figure 4.2: Effects of the long period signals on the recovery of μ_{LT} for $\Delta t=15$ days and different choice of uniform random noise. Each point in the curves represents an average over 1,500 runs performed by varying randomly the initial phases and the noise's pattern. $\Delta\mu_{LT}$ is the difference between the least squares fitted value of μ_{LT} when both the IM and the FM includes the LT plus all the harmonics and that obtained without any harmonic both in the IM and in the FM.

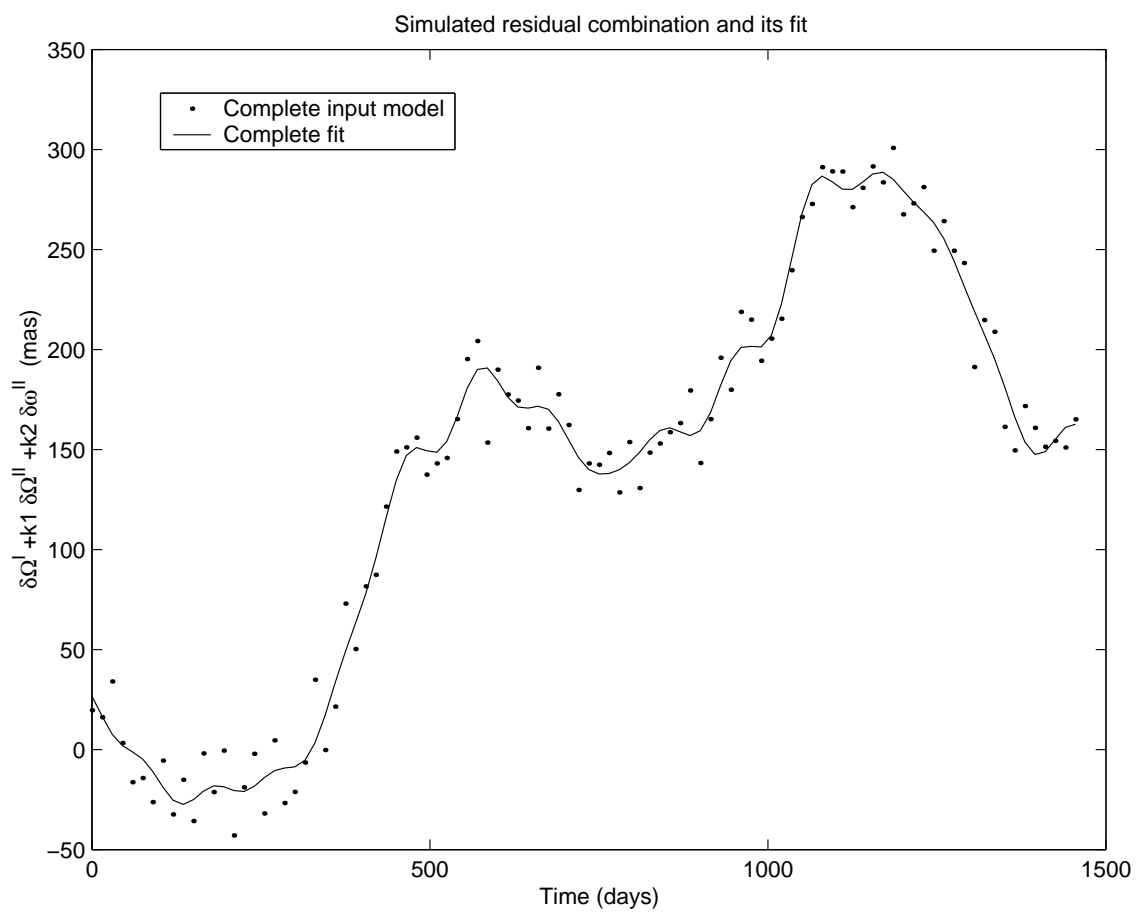


Figure 4.3: Simulated residual curve and related fit. The time span is 4 years, the time step is 15 days, the simulated data RMS amounts to 9 mas and all the long period signals are included in the simulated data. The initial phases and the noise are random.

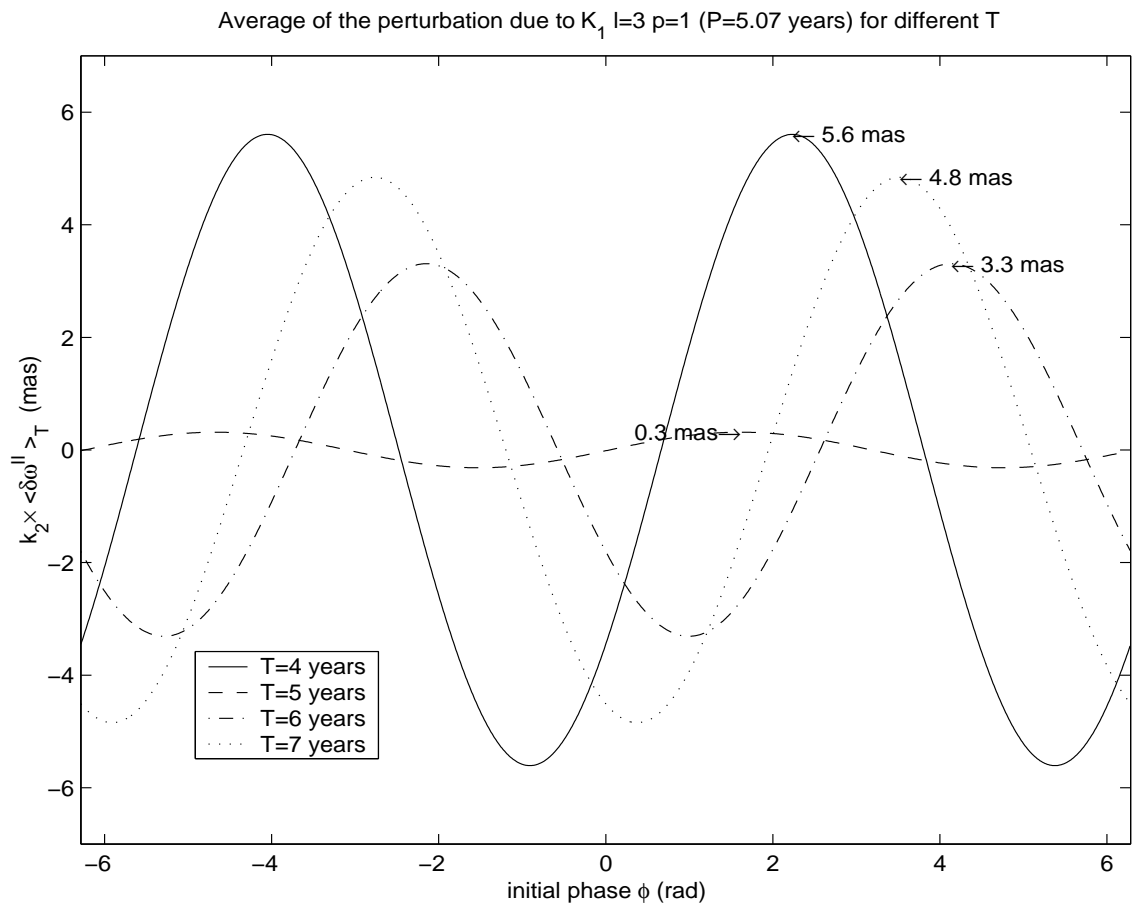


Figure 4.4: Average $c_2 \langle \delta\omega^{\text{II}} \rangle_T$ over different T_{obs} of the perturbation induced on the combined residuals by the mismodelled harmonic K_1 $l = 3$ $p = 1$. In general, it depends on the initial phase ϕ . It has been calculated a mismodelling of 64.5 mas from a nominal amplitude of 1,136 mas. It is mainly due to the C_{31f}^+ ocean tidal coefficient and the load Love number k'_3 .

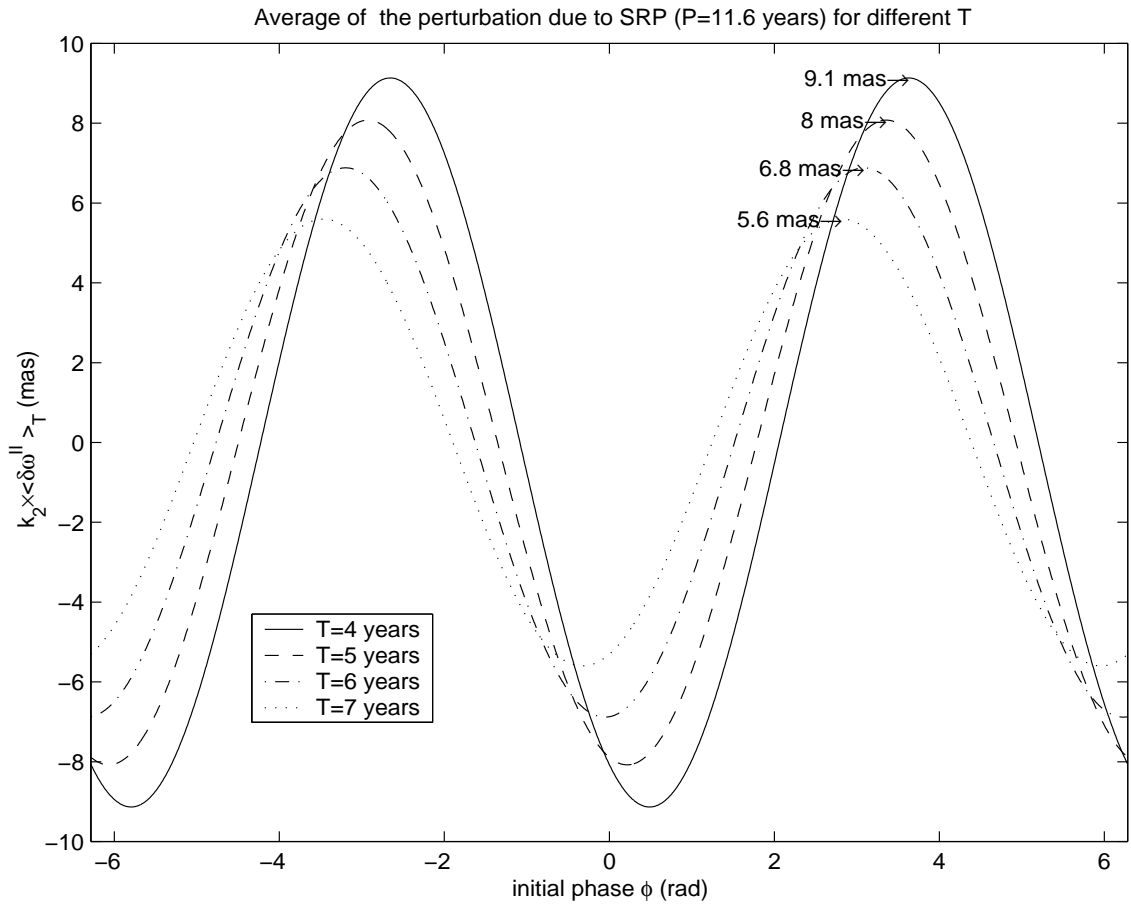


Figure 4.5: Average $c_2 \langle \delta\omega^{\text{II}} \rangle_T$ over different T_{obs} of the perturbation induced on the combined residuals by the mismodelled harmonic SRP(4,241). In general, it depends on the initial phase ϕ . It has been assumed a 0.5% level of mismodelling mainly due to the reflectivity coefficient C_R of LAGEOS II. The effects of the eclipses have been neglected.

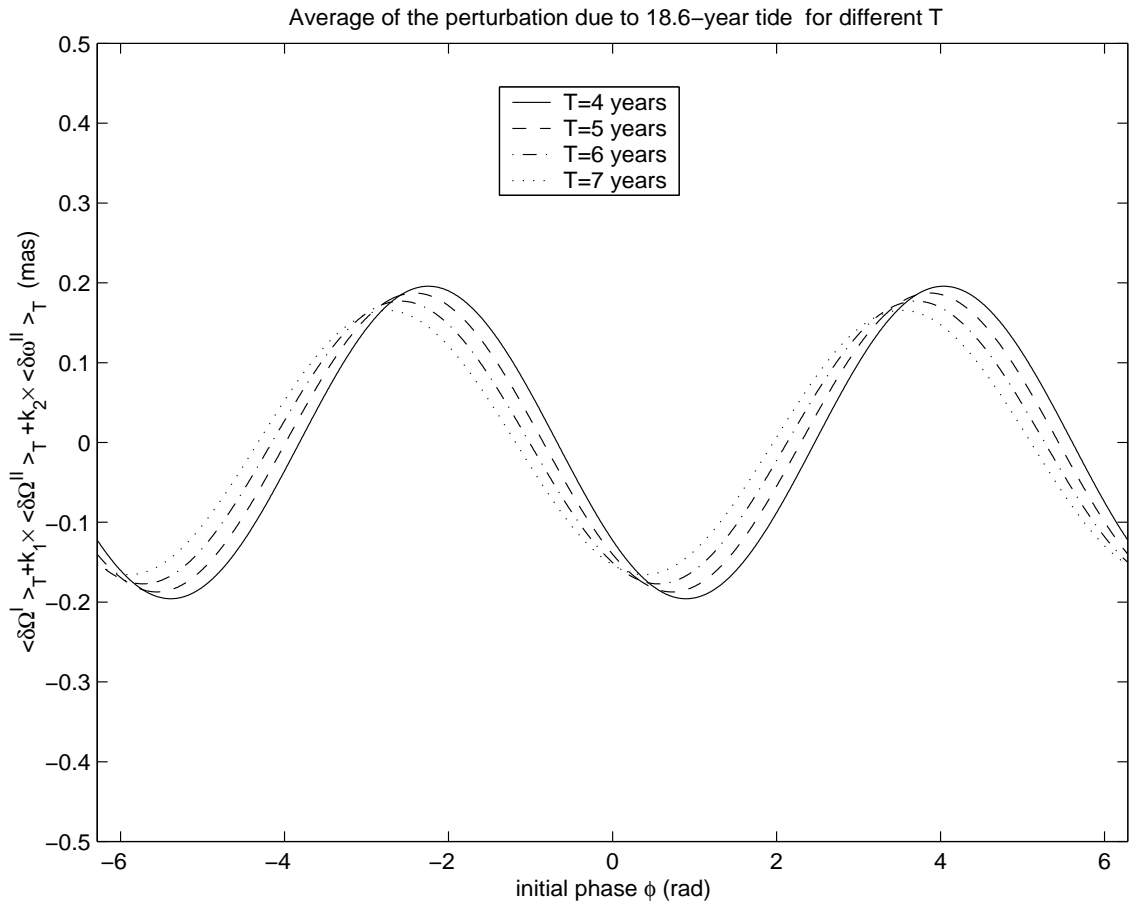


Figure 4.6: Average $\langle \delta\Omega^I \rangle_T + c_1 \langle \delta\Omega^{II} \rangle_T + c_2 \langle \delta\omega^{II} \rangle_T$ over different T_{obs} of the perturbation induced on the combined residuals by the mismodelled 18.6-year tide. In general, it depends on the initial phase ϕ . It has been assumed a 1.5% level of mismodelling on the Love number k_2 mainly due to the anelasticity of the Earth's mantle behavior.

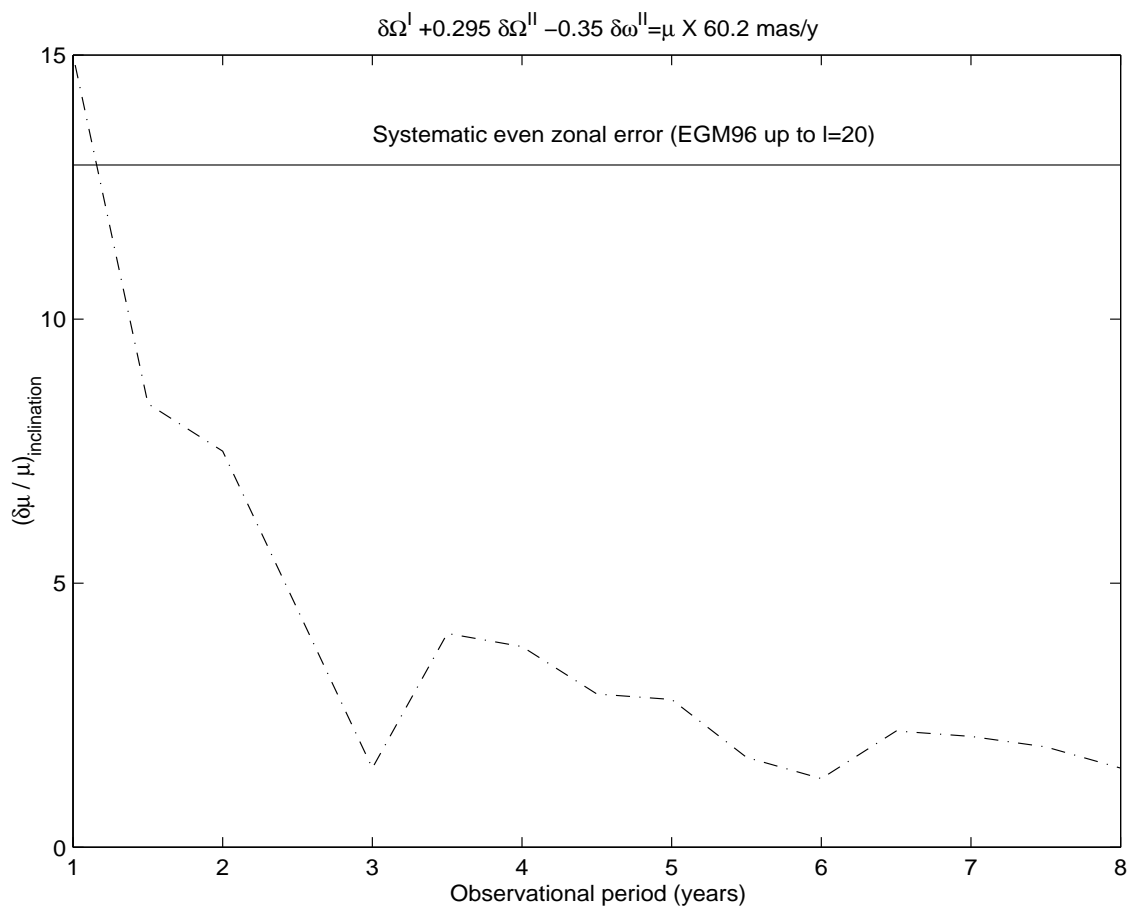


Figure 4.7: Systematic percent error induced on the measurement of the Lense-Thirring trend by the mismodelling in the inclination angle.

Chapter 5

The gravitomagnetic clock effect

5.1 Introduction

Among the satellite-based experiments recently proposed to measure the gravitomagnetic force in the field of the Earth one of the most interesting is devoted to the detection of the the gravitomagnetic clock effect [*Cohen and Mashhoon, 1993; Mashhoon et al., 1999; Lichtenegger et al., 2000; Mashhoon et al., 2001*]. It consists of the fact that two clocks moving along pro- and retrograde circular equatorial orbits, respectively, about a central rotating mass M with proper angular momentum J exhibit a difference in their proper times which, if calculated after some fixed angular interval, say 2π , amounts to

$$(\tau_+ - \tau_-)_{\phi=2\pi} = 4\pi \frac{J}{Mc^2}. \quad (5.1)$$

Eq. (5.1) holds at first order in J and at distances much larger than the gravitational radius $r_g = \frac{2GM}{c^2}$ of the central body so to neglect terms of order $\mathcal{O}(c^{-4})$. Moreover, it is equal to the difference in the orbital periods T_{\pm} of the two clocks as viewed by an asymptotic inertial observer. For the Earth eq. (5.1) yields a time difference of 1.3×10^{-7} s.

The chapter is organized as follows. We first consider in section 2 two test electric charges moving on the same circular orbit but in opposite directions in orthogonal electric and magnetic fields and show that the particles take different times in describing a full orbit. The expression for the time difference is completely analogous to that of

the general relativistic gravitomagnetic clock effect in the weak-field and slow-motion approximation. The latter is obtained in section 3 by considering the gravitomagnetic force as a small classical non-central perturbation of the main central Newtonian monopole force. This formula differs from the general relativistic expression by terms of order c^{-4} .

5.2 The electromagnetic scenario

Let us consider two point charges q of mass m orbiting a central spherically symmetric distribution of total charge Q of opposite sign, e.g. $Q < 0$ and $q > 0$: we will suppose that the two charges move along identical circular orbits but in opposite directions. We will denote q_+ the charge moving counterclockwise and q_- the charge moving clockwise and will assume as positive the counterclockwise direction. By adopting cylindrical coordinates let us assume that the motion of the two charges occurs in the equatorial plane of Q chosen as $\{r, \phi\}$ coordinate plane. The equation of motion reads

$$m \frac{v_\pm^2}{r} = |q|E, \quad (5.2)$$

so that

$$T^{(0)} = \frac{2\pi r}{v_\pm} = 2\pi \sqrt{\frac{mr}{|q|E}} : \quad (5.3)$$

both the two moving charges describe a complete orbit of radius r in the same times $T^{(0)} = \frac{2\pi}{n}$ with the mean motion given by $n = \sqrt{|q|E/mr}$. It should be noticed that it depends on the charge-to-mass ratio.

If we switch on a magnetic field $\mathbf{B} = Bi_z$ orthogonal to the plane of motion, the two charges will experience an additional Lorentz force $\mathbf{F}_L = (q/c)\mathbf{v} \times \mathbf{B}$, which for $q > 0$ will be antiparallel to the electric field for the counterclockwise moving charge and parallel to the electric field for the clockwise moving charge. Hence the equation of motion for $q > 0$ becomes

$$m \frac{v_\pm^2}{r} = qE \mp \frac{q}{c}v_\pm B, \quad (5.4)$$

and therefore

$$\left(v_\pm \pm \frac{qB}{2mc}r\right)^2 = \left(n^2 + \frac{q^2B^2}{4m^2c^2}\right)r^2. \quad (5.5)$$

We assume that the magnetic field is weak; therefore, we can neglect the square of the Larmor frequency $q^2 B^2 / 4m^2 c^2$ in comparison with the square of the orbital frequency n^2 in eq. (5.5) and obtain $v_{\pm} = (n \mp qB/2mc)r$, i.e.

$$\left(\frac{d\phi}{dt} \right)_{\pm} = \pm \left(n \mp \frac{qB}{2mc} \right), \quad (5.6)$$

or

$$dt_{\pm} = \pm \frac{d\phi}{n \left(1 \mp \frac{qB}{2mcn} \right)} \simeq \pm \frac{d\phi}{n} \left(1 \pm \frac{qB}{2mcn} \right). \quad (5.7)$$

By integrating eq. (5.7) from 0 to 2π for the counterclockwise orbit and 2π to 0 for the clockwise orbit, we find the orbital periods of the two charges

$$T_{\pm} = \frac{2\pi}{n} \left(1 \pm \frac{qB}{2mcn} \right) = T^{(0)} \pm \frac{\pi B}{c E} r, \quad (5.8)$$

and hence their difference after one revolution

$$T_+ - T_- = \frac{2\pi B}{c E} r. \quad (5.9)$$

By inspection of eq. (5.8) we see that the magnetic correction to the orbital period is independent of the charge-to-mass ratio of the orbiting electric charges, in contrast to the unperturbed period $T^{(0)}$. Indeed we could have started section 2 with the less restrictive assumption that the two charges only have the same charge-to-mass ratio.

Let us now assume that the two charges are far away from the central charge and current distributions so that the magnetic field can be considered to be generated by a magnetic dipole $\mathbf{m} = -\mu \mathbf{i}_z$ of magnitude $\mu = IS/c$, where S is the surface area of the loop enclosed by the current I and therefore

$$B = \frac{\mu}{r^3}, \quad E = \frac{|Q|}{r^2}, \quad (5.10)$$

which, upon inserting into eq. (5.9) yield

$$T_+ - T_- = \frac{2\pi}{c} \frac{\mu}{|Q|}. \quad (5.11)$$

This time difference depends on both the sign of the charges and on the direction of the magnetic field. Upon exchanging the signs of Q and q , i.e. $Q > 0$ and $q < 0$, the counterclockwise revolving charge will move faster while the clockwise moving charge will move slower. However, as expected by charge symmetry, eq. (5.11) will be unaffected if the signs of the charges and of the magnetic field are reversed simultaneously.

Further, we notice that the radius of the orbit does not appear in eq. (5.11) and that this time difference can be interpreted as a consequence of the fact that the speed of light has a finite value; indeed, for $c \rightarrow \infty$, $T_+ - T_- \rightarrow 0$.

5.3 The gravitational scenario

The electromagnetic scenario previously described is analogous to the following gravitational one. Let us consider a central spherically symmetric rotating mass M with its proper angular momentum directed along the z axis $\mathbf{J} = J\mathbf{i}_z$ and a pair of test bodies orbiting it along circular equatorial orbits in opposite directions: we will denote m_+ the mass evolving in the same sense of the central body and m_- the mass orbiting in the opposite sense. We will assume that the radius r of the orbits is much larger than the Schwarzschild radius r_g of the central body, as it would happen for an experiment in the field of the Earth. It is well known that in the weak-field and slow-motion approximation the stationary spacetime metric of an axially symmetric mass-energy distribution generates the so called gravitoelectric and gravitomagnetic fields (see chapter 2, eqs. (2.2)-(2.3))

$$\mathbf{E}_g = -\frac{GM}{r^2}\mathbf{i}_r, \quad (5.12)$$

$$\mathbf{B}_g = \nabla \times \mathbf{A}_g, \quad (5.13)$$

In our case, for circular equatorial orbits eq. (2.3) becomes

$$\mathbf{A}_g = A_\phi \mathbf{i}_\phi = -\frac{2G}{c} \frac{J}{r^2} \mathbf{i}_\phi, \quad (5.14)$$

so that, in cylindrical coordinates

$$\mathbf{B}_g = \frac{1}{r} \frac{\partial(rA_\phi)}{\partial r} \mathbf{i}_z = B_g \mathbf{i}_z = \frac{2G}{c} \frac{J}{r^3} \mathbf{i}_z. \quad (5.15)$$

At this point the calculations follow closely those of the electromagnetic case previously examined because the equation of motion of a test body in the weak gravitational field of a stationary axisymmetric mass-energy distribution is analogous to that of a point charge q acted upon by an electric and magnetic field \mathbf{E} and \mathbf{B} , as shown by eq. (2.1). By inserting the expressions of B_g and E_g in eq. (5.9) we obtain the well known expression

$$T_+ - T_- = 4\pi \frac{J}{c^2 M}. \quad (5.16)$$

Notice that the mass moving in the same sense of rotation of the central mass moves slower than the mass moving in the opposite sense. If we reversed the sense of rotation of the central gravitating source, the clockwise mass m_- would be slower. In this way the sense of rotation of the central mass is no more matter of convention but could be related to a physical phenomenon, i.e. the mass loop moving slower. Also in this case, in the limit $c \rightarrow \infty$ $T_+ - T_- \rightarrow 0$. It should be noticed that eq. (5.16) is a direct consequence of the equivalence principle. Indeed, being the orbit radius equal, the gravitoelectric parts of the periods would not cancel out if the (gravitational mass)-to-(inertial mass) m_g/m_i ratio was not equal for all particles. It is clearly pointed out by eq. (5.8) which holds only for those charges whose charge-to-mass ratio is equal.

Chapter 6

Satellite gravitational orbital perturbations and the gravitomagnetic clock effect

6.1 Introduction

In [Gronwald *et al.*, 1997; Lichtenegger *et al.*, 2000] it has been shown that, in order to make feasible the detection of the gravitomagnetic clock effect, for an orbit radius of 7,000 km the radial and azimuthal locations of the satellites must be known at a level of accuracy of $\delta r \leq 10^{-2}$ cm and $\delta\phi \leq 10^{-2}$ mas per revolution. Some studies conducted up to now on the feasibility and the error budget of such an experiment can be found in [Gronwald *et al.*, 1997; Lichtenegger *et al.*, 2000; 2001].

In this chapter we shall investigate in a quantitative manner the systematic errors induced on the radial and azimuthal locations by the solid Earth and ocean tidal perturbations and by the static part of the geopotential [Iorio, 2001b; 2001d]. The chapter is organized as follows. In section 2 and 3 the radial and azimuthal perturbations, respectively, induced by the most relevant tidal constituents are investigated. In section 4 the radial and azimuthal perturbations generated by the static part of the geopotential are worked out. section 5 is devoted to the conclusions.

6.2 The radial error induced by the solid Earth and ocean tides

According to [Williamson *et al.*, 1972; Christodoulidis *et al.*, 1988], the position perturbations in the radial direction can be expressed in general as

$$\Delta r = \sqrt{\Delta a^2 + \frac{1}{2} [(e\Delta a + a\Delta e)^2 + (ae\Delta M)^2]}. \quad (6.1)$$

In eq. (6.1) the perturbation amplitudes are the rss values of the perturbations and small eccentricity approximations have been extensively applied.

Since the difference in the proper orbital periods to be investigated is integrated over 2π with respect to the azimuthal angle ϕ , as viewed by an inertial observer fixed with the distant quasars, we shall consider only the long period perturbations averaged over an orbital revolution. This is accomplished by assuming those values for the indices l, p, q [Dow, 1988; Casotto, 1989] which satisfy the relation $l - 2p + q = 0$. Since the tidal perturbations on the semimajor axis a are proportional just to $l - 2p + q$, all the terms in $(\Delta a)^2$ and Δa of eq. (6.1) vanish and it reduces to

$$\Delta r = \sqrt{\frac{1}{2} [(a\Delta e)^2 + (ae\Delta M)^2]}. \quad (6.2)$$

For $e = 0$ eq. (6.2) becomes

$$\Delta r_{\text{tides}} = \frac{1}{\sqrt{2}} a \Delta e_{\text{tides}}. \quad (6.3)$$

For a constituent characterized by a given set of indices $\{l, m, p, q\}$, the first order tidal perturbation amplitude for the eccentricity turns out to be¹

$$\Delta e_{lmpq} \propto -\frac{(l - 2p) F_{lmp} G_{lpq}}{e}, \quad (6.4)$$

where F_{lmp} and G_{lpq} are the inclination and the eccentricity functions, respectively, as can be found in [Kaula, 1966].

Eq. (6.4) allows one to obtain a preliminary insight into those perturbations which, for a given set of indices l, m, p, q , vanish. Notice that, for $e = 0$, eq. (6.4)

¹This holds for $l - 2p + q = 0$. Notice that for the eccentricity there are no second order, indirect perturbations due to the oblateness of the Earth [Balmino, 1974; Dow, 1988; Casotto, 1989], contrary to the node, the perigee and the mean anomaly.

could become singular. Concerning this problem it must be considered that, since $G_{lpq} \propto e^{|q|}$, the behavior of $\frac{G_{lpq}}{e} \propto e^{|q|-1}$ is crucial. If $|q| - 1 \equiv k > 0$, i. e. $q > 1$ or $q < -1$, then for a circular orbit $\frac{G_{lpq}}{e} = 0$ and the perturbation vanishes. If $|q| - 1 = 0$, i.e. $q = \pm 1$, then $\frac{G_{lpq}}{e} = \text{const}$. Problems may arise only if $q = 0$, but we shall see that, in general, in the cases in which q takes such value, $l - 2p = 0$ also holds so that the perturbations identically vanish with no regards to the eccentricity or the inclination of the satellite.

Let us start with the tidal perturbations of even degree. For $l = 2n$, $p = 0, \dots, l$ and $l - 2p + q = 0$, the allowable values for q satisfy the above stated conditions so that we can conclude that there are no radial tidal perturbations of even degree. Since for the solid Earth tides we consider only the $l = 2$ constituents, this result rules out their possible influence on the radial error budget in the gravitomagnetic clock experiment.

Now we shall consider the odd degree case. For $l = 3$ there are no problems because q never vanishes. Moreover, for $p = 1$, $q = -1$ and $p = 2$, $q = 1$ $\frac{G_{lpq}}{e} = 1$ and $l - 2p = \pm 1$ while for the other sets of indices the perturbations vanish because $\frac{G_{lpq}}{e} = 0$. When we consider the inclination functions corresponding to the indices for which $\frac{G_{lpq}}{e}$ and $l - 2p$ differ from zero, i. e. F_{3m1} and F_{3m2} , and evaluate them for $i = 0$ we find that only $F_{311}(i = 0) = -\frac{3}{2}$.

So we can conclude that the radial direction is perturbed only by the $l = 3$, $m = 1$, $p = 1$, $q = -1$ ocean tides.

The full expression for the eccentricity perturbation amplitude due to ocean tides [Dow, 1988; Casotto, 1989], in our case, is given by²

$$\Delta e_{lmpqf} = \frac{4\pi G \rho_w}{na\dot{\gamma}_{lmpqf}^+} \left(\frac{R_\oplus}{a}\right)^{l+2} \left(\frac{1+k'_l}{2l+1}\right) C_{lmf}^+ \left[-\frac{(l-2p)F_{lmp}G_{lpq}}{e}\right]. \quad (6.5)$$

Recall that $\dot{\gamma}_{lmpqf}^+$ has to be evaluated on the chosen reference orbit.

For $l = 3$, $m = 1$, $p = 1$, $q = -1$, and by putting $\dot{\gamma}_{lmpqf}^+ = \frac{2\pi}{P_{\text{pert}}}$, eq. (7.1) becomes

$$\Delta r_{311-1f} = (8.80 \times 10^{25} \text{ cm}^{7/2} \text{ s}^{-1}) \times a^{-7/2} \times P_{\text{pert}} \times C_{lmf}^+. \quad (6.6)$$

Among the tesseral tides, the K_1 (165.555) is far the most important in perturbing the near Earth satellites' orbits [Iorio, 2001; Iorio and Pavlis, 2001]. So it seems

²Here we shall consider only the prograde waves [Schwiderski, 1980].

reasonable to calculate eq. (6.6) for it in order to obtain an upper bound in the order of magnitude of the tidally induced perturbations on Δr . For such a constituent

$$C_{31}^+(K_1) = 0.95 \text{ cm}, \quad (6.7)$$

and $\dot{\gamma}_{311-1}^+(K_1) = \dot{\omega} + \dot{\Omega}$. If we assume as reference orbit a secularly precessing ellipse [Kaula, 1966], we obtain:

$$P_{\text{pert}} = -\frac{4\pi}{3} \frac{1}{C_{20} R_{\oplus}^2 \sqrt{GM_{\oplus}}} a^{7/2} = (4.7639 \times 10^{-25} \text{ cm}^{-7/2} \text{s}) \times a^{7/2}. \quad (6.8)$$

Eqs. (6.6)-(6.8) tell us the important feature that for $K_1 l = 3, m = 1, p = 1, q = -1$ the perturbation amplitude is independent of the satellite's semimajor axis. For $a = 7,000$ km and $C_{20} = -0.00108261$ we obtain $P_{\text{pert}} = 50$ days. By using eqs. (6.7)-(6.8) in eq. (6.6) we obtain $\Delta r_{311-1}(K_1) = 39.8$ cm. According to EGM96 model [Lemoine *et al.*, 1998], the percent error in $C_{31}^+(K_1)$ amounts to 5.2%; this yields $\delta r_{311-1}(K_1) \simeq 2$ cm. Despite the amplitude of this long period mismodelled perturbation is 2 orders of magnitude greater than the maximum allowable error $\delta r_{\text{max}} \sim 10^{-1}$ cm, it must be noticed that its period P_{pert} amounts to only 50 days. This implies that if an observational time span T_{obs} which is an integer multiple of P_{pert} , i. e. some months, is adopted the tidal perturbative action of K_1 can be averaged out.

6.3 The azimuthal error induced by the solid Earth and ocean tides

Concerning the angular variable which defines the position of the satellite on the orbit, for an equatorial, circular orbit it seems reasonable to adopt for its rate of change:

$$\dot{\phi} = \dot{\omega} + \dot{\Omega} \cos i + \dot{\mathcal{M}}. \quad (6.9)$$

In it $\dot{\omega} + \dot{\Omega} \cos i$ represents an angular velocity around the direction of the orbital angular momentum [Milani *et al.*, 1987]; it is valid for any inclination angle i . In order to account for the fact that the orbit is circular we add to it $\dot{\mathcal{M}}$. See also [Rosborough and Tapley, 1987]. About the perturbations on the latter Keplerian orbital element, it turns out that [Milani *et al.*, 1987] in $\Delta \mathcal{M}$ one has to consider also

the indirect perturbations on the mean motion n due to the cross coupling with the semimajor axis a . Since they are proportional to $l-2p+q$, they vanish when only long period perturbations are considered, as is the case here. The perturbation amplitudes on the node, the perigee and the mean anomaly are proportional to³

$$\Delta\Omega_{lmpqf} \propto \frac{1}{\sqrt{1-e^2}\sin i} G_{lpq} \frac{dF_{lmp}}{di}, \quad (6.10)$$

$$\Delta\omega_{lmpqf} \propto \frac{\sqrt{1-e^2}}{e} \frac{dG_{lpq}}{de} F_{lmp} - \frac{\cos i}{\sqrt{1-e^2}\sin i} G_{lpq} \frac{dF_{lmp}}{di}, \quad (6.11)$$

$$\Delta\mathcal{M}_{lmpqf} \propto -\frac{1-e^2}{e} \frac{dG_{lpq}}{de} F_{lmp} + 2(l+1)F_{lmp}G_{lpq}. \quad (6.12)$$

By assuming $1-e^2 = \sqrt{1-e^2} \simeq 1$ for $e \rightarrow 0$, with the aid of eqs. (6.9)-(6.12) we obtain:

$$\Delta\phi_{lmpqf} \propto 2(l+1)F_{lmp}G_{lpq}. \quad (6.13)$$

As already done in the previous section, eq. (6.13) can be used in order to forecast which perturbations will vanish.

For $l=2$ only the combination $l=2$, $p=1$, $q=0$ yields a nonzero eccentricity function: $G_{210} = (1-e^2)^{-3/2} = 1$. Among the corresponding inclination functions F_{2m1} , for $i=0$ we have $F_{201} = -1/2$. The same conclusion holds also for $l=4$ with $G_{420}(e=0) = 1$ and $F_{402}(i=0) = 3/8$. So we can conclude that for $l=2,4$ only the zonal tides, both solid and ocean, cause nonvanishing perturbations on the satellite's azimuthal variable.

Concerning the odd degree perturbations, they all vanish since for $l=3,5$, q is always nonzero, so that, since $G_{lpq} \propto e^{|q|}$, for circular orbits all the eccentricity functions vanish. The conclusion is that the odd part of the ocean tidal spectrum does not induce systematic errors in the satellite's azimuthal variable.

For a given constituent of degree l , order m and frequency f the full expressions for the solid Earth and ocean tidal perturbation amplitude (progressive waves only) are, respectively:

$$\Delta\phi_{lmpqf}^{\text{solid}} = \frac{g}{na^2\dot{\gamma}_{lmpqf}} \left(\frac{R_{\oplus}}{a}\right)^{l+1} A_{lm} k_{lmf}^{(0)} H_l^m [2(l+1)F_{lmp}G_{lpq}], \quad (6.14)$$

³The second order, indirect perturbations will not be considered here since it can be demonstrated that they vanish in this case.

$$\Delta\phi_{lmpqf}^{\text{ocean}} = \frac{4\pi G \rho_w}{na\gamma_{lmpqf}^+} \left(\frac{R_{\oplus}}{a}\right)^{l+2} \left(\frac{1+k'_l}{2l+1}\right) C_{lmf}^+ [2(l+1)F_{lmp}G_{lpq}]. \quad (6.15)$$

We shall start by considering the three most relevant $l = 2$ $m = 0$ zonal tides:

- 18.6-year (055.565); $P_{\text{pert}} = 6,798.38$ days; $k_{20}^{(0)} = 0.315$; $H_2^0 = 2.792$ cm
- 9.3-year (055.575); $P_{\text{pert}} = 3,399.19$ days; $k_{20}^{(0)} = 0.313$; $H_2^0 = 2.72 \times 10^{-2}$ cm
- S_a (056.554); $P_{\text{pert}} = 365.27$ days; $k_{20}^{(0)} = 0.307$; $H_2^0 = -4.92 \times 10^{-1}$ cm; $k'_2 = -0.3075$; $C_{lmf}^+ = 2.54$ cm

For $l = 2$ eqs. (6.14)-(6.15) becomes

$$\Delta\phi^{\text{solid}} = (-3.77 \times 10^{18} \text{ cm}^{5/2}\text{s}^{-1}) \times a^{-7/2} \times k_{20}^{(0)} \times P_{\text{pert}} \times H_2^0, \quad (6.16)$$

$$\Delta\phi^{\text{ocean}} = (-4.707 \times 10^{17} \text{ cm}^{5/2}\text{s}^{-1}) \times a^{-7/2} \times P_{\text{pert}} \times C_{lmf}^+. \quad (6.17)$$

Notice that, since for the $l = 2$ zonal tides P_{pert} does not depend on the satellite's semimajor axis but only on the astronomical arguments, $\Delta\phi_{lmpqf}$ depends on the orbit's radius through $a^{-7/2}$, contrary to $\Delta r(K_1)$, as shown in the previous section.

For $a = 7,000$ km we have:

- $\Delta\phi(18.6\text{-year}) = -4.431 \times 10^4$ mas
- $\Delta\phi(9.3\text{-year}) = -214.4$ mas
- $\Delta\phi(S_a) = 408$ mas (solid); 857.6 mas (oceanic)

The zonal tidal perturbations on the satellite's azimuthal location are particularly insidious not only because their nominal amplitudes are up to 6 orders of magnitude greater than the maximum allowable error $\delta\phi_{\text{max}} = 10^{-2}$ mas per revolution, but also because they have periods very long, so that there is no hope they average out on reasonable T_{obs} . Concerning the 18.6-year tide, by assuming an uncertainty of 1.5% on $k_{20}^{(0)}$ [Iorio, 2001], the mismodelling on its perturbation amounts to -664 mas which is, however, very far from $\delta\phi_{\text{max}}$.

6.4 Static geopotential perturbations

As can be found in [Kaula, 1966], the perturbing function of degree l and order m of the static part of the geopotential can be cast into the form:

$$V_{lm} = \frac{GM_{\oplus}R_{\oplus}^l}{a^{l+1}} F_{lmp} G_{lpq} S_{lmpq}, \quad (6.18)$$

where:

- $S_{lmpq} = \begin{bmatrix} C_{lm} \\ -S_{lm} \end{bmatrix}_{l-m \text{ odd}}^{l-m \text{ even}} \cos \psi_{lmpq} + \begin{bmatrix} S_{lm} \\ C_{lm} \end{bmatrix}_{l-m \text{ odd}}^{l-m \text{ even}} \sin \psi_{lmpq}$
- C_{lm}, S_{lm} are the unnormalized Stokes' geopotential coefficients [Lemoine *et al.*, 1998]
- $\psi_{lmpq} = (l - 2p)\omega + (l - 2p + q)\mathcal{M} + m(\Omega - \theta)$ in which θ is the sidereal angle

Concerning the preliminary analysis of the even degree perturbations, the same conclusions of the previous sections hold. All the perturbations on the radial directions vanish, $\Delta r_{\text{static}} = 0$, while for the satellite's azimuthal location only the zonal contributions are to be considered. Let us work out explicitly the perturbation due to the main even zonal coefficient C_{20} . For the precessional secular rates induced by it of a satellite we have eqs. (3.111)-(3.113). By inserting them, evaluated for $i=e=0$, into eq. (6.9) we obtain

$$\frac{d\phi}{dt} = -3\sqrt{GM_{\oplus}}C_{20}R_{\oplus}^2a^{-7/2} = (2.637 \times 10^{25} \text{ cm}^{7/2}\text{s}^{-1}) \times a^{-7/2}. \quad (6.19)$$

For a circular orbit of radius 7,000 km the azimuthal secular rate is

$$\frac{d\phi}{dt} = 1.89 \times 10^{10} \text{ mas/y}. \quad (6.20)$$

It is important to evaluate the error induced on such rate by the poor knowledge of the Earth's gravitational field. According to the EGM96 model [Lemoine *et al.*, 1998], a relative uncertainty of 7.3×10^{-8} weighs on the C_{20} coefficient. This yields $\dot{\delta\phi} \simeq 1380$ mas/y, which is equivalent to $\delta\phi \simeq 2.5 \times 10^{-1}$ mas per revolution, since $P_{orb} = \frac{2\pi}{n} = 5.82 \times 10^3$ s for $a = 7,000$ km. Such error is 1 order of magnitude greater than $\delta\phi_{\text{max}} \simeq 10^{-2}$ mas. However, it is of the utmost importance to notice that the major source of error in the azimuthal location turns out to be the Earth's GM . Indeed, $\Delta\phi^{(GM)} = \frac{P}{2na^3} \times \delta(GM) = 1.2$ mas per revolution by assuming $\delta(GM_{\oplus}) = 8 \times 10^{11} \text{ cm}^3 \text{ s}^{-2}$ [McCarthy, 1996].

Concerning the perturbations of odd degree, let us consider in detail the most important geopotential harmonic of degree $l = 3$. By reasoning as in the previous sections, it turns out that the satellite's azimuthal location is not perturbed by the $l = 3$ part of the geopotential spectrum. Concerning Δr , the perturbation corresponding to the combination $l = 3, m = 1, p = 1, q = -1$ does not vanish. The full expression for the geopotential perturbation on the eccentricity is given by

$$\Delta e_{lmpq} = \frac{GM_{\oplus}}{na^2\dot{\psi}_{lmpq}} \left(\frac{R_{\oplus}}{a}\right)^l \frac{G_{lpq}}{e} F_{lmp} [-(l - 2p)] S_{lmpq}. \quad (6.21)$$

In our case it yields

$$\Delta r_{\text{static}} = \frac{3}{2\sqrt{2}} \sqrt{GM_{\oplus}} R_{\oplus}^3 a^{-7/2} \times \frac{P_{\text{pert}}}{2\pi} \times [C_{31} \cos \psi_{311-1} + S_{31} \sin \psi_{311-1}], \quad (6.22)$$

with

$$\dot{\psi}_{311-1} \equiv \frac{2\pi}{P_{\text{pert}}} = \dot{\omega} + \dot{\Omega} - \dot{\theta}. \quad (6.23)$$

With $a = 7,000$ km we have for the period and the amplitudes of the harmonic terms

$$P_{\text{pert}} = 8.81 \times 10^4 \text{ s}, \quad (6.24)$$

$$A_{\Delta r} = (-8.481 \times 10^9 \text{ cm}) \times \begin{bmatrix} C_{31} \\ S_{31} \end{bmatrix}. \quad (6.25)$$

According to [Lemoine *et al.*, 1998] the mismodelling weighing on the Stokes' coefficients of interest amounts to $\delta C_{31} = 1.5 \times 10^{-10}$, $\delta S_{31} = 1.3 \times 10^{-10}$. This leads to a mismodelled radial perturbation

$$\delta r_{\text{static}} \simeq (1.3 \text{ cm}) \cos \psi_{311-1} + (1.15 \text{ cm}) \sin \psi_{311-1}. \quad (6.26)$$

It turns out to be 2 orders of magnitude greater than the allowable $\delta r_{\text{max}} \simeq 10^{-2}$ cm. However, it must be pointed out that such a mismodelled perturbation averages out on an observational time span T_{obs} which is an integer multiple of 1 day, its period amounting to 24.48 hr. The same conclusions can be drawn for the other larger odd degree nonvanishing radial perturbations.

6.5 Discussion and conclusions

In this chapter we have explicitly calculated, by averaging over one orbital revolution, the most relevant perturbations Δr and $\Delta\phi$ due to the dynamical and static part of the Earth's gravitational field on the radial and azimuthal locations of a satellite placed in an equatorial, circular orbit with radius of 7,000 km. Furthermore, we have compared the mismodelling induced on such perturbations by the poor knowledge of the parameters of the Earth's gravitational field to the maximum errors per revolution $\delta r_{\text{max}} \simeq 10^{-2}$ cm and $\delta\phi_{\text{max}} \simeq 10^{-2}$ mas allowable in order to detect successfully the gravitomagnetic clock effect.

Concerning the radial direction, it is affected by harmonic perturbations induced by the odd degree part, both static and dynamical, of the Earth's gravitational field.

If, from one hand, the related mismodelling is 2 orders of magnitude greater than δr_{\max} , from the other hand it must be pointed out that such mismodelled perturbations average out on not too long time spans since their periods range from 1 to 50 days.

The situation for the azimuthal angle is different. It is acted upon by the even degree zonal harmonics of the Earth's gravitational field. The zonal tides are very insidious since they induce perturbations with great amplitudes acting on very long periods, so that it is necessary to wait for several years in order to average out their mismodelled effect which are up to 4 orders of magnitude greater than $\delta\phi_{\max}$. The $l = 2$, $m = 0$ part of the geopotential induces also a secular drift on the azimuthal satellite's angle; the uncertainties in C_{20} induces on it a mismodelled rate per revolution which is 1 order of magnitude greater than $\delta\phi_{\max}$. However, the largest source of error in ϕ is the uncertainty in the Earth's GM which induce a bias of 1.2 mas per revolution. This is a hard limitation to overcome because it is independent of the particular satellite employed and is related to our knowledge of the terrestrial gravitational field.

The conclusions outlined here hold for $r = 7,000$ km; let us see how the situation changes with different values for the orbital radius. The possible scenarios turn out to be very intricate. Indeed, from one hand we have secular or semisecular mismodelled perturbations which could be decreased only by enlarging the orbit radius, and from the other hand there are the periodic mismodelled perturbations whose periods grow with the orbit radius making so much more difficult to average them out on reasonable time spans. Moreover, it should also be considered that the maximum allowable errors depend on the orbit radius and they decrease with increasing radius putting, in this way, more stringent constraints on the mismodelled gravitational perturbations. This is shown in Fig. (6.1). In Fig. (6.2) and Fig. (6.3) we show how the mismodelled perturbative amplitudes due to the 18.6-year tide and the C_{20} depend on the orbit radius. From an inspection of Fig. (6.1) and Fig. (6.2) it can be noticed that the major problems come from the azimuthal error and the perturbation induced by the 18.6-year tide: as the orbit radius grows, the mismodelled tidal perturbation is always greater than the maximum allowable error by 2 or 3 orders of magnitude. Since this important source of systematic error cannot be made harmless by varying the orbital parameters of the satellites, it should be necessary to average its effect out: but this

means to choose a time span $T_{\text{obs}} = 18.6$ years at least.

By inspecting Fig. (6.4) it can be noticed the growth of the period of the radial tidal perturbation is induced by the K_1 , $l = 3$ $p = 1$ $q = -1$. This is an important feature since its mismodelled amplitude is at cm level and is independent of the orbit radius. Moreover, δr_{max} is of the order of 10^{-2} cm, so that we could eliminate the effect of such a perturbation only by averaging it over an integer multiple of its period.

We can conclude that the present level of accuracy in the knowledge both of the Earth solid and ocean tides, and of the static part of the geopotential does not allow an easy detection of the gravitomagnetic clock effect, at least by using short arcs only.

6.6 Figures

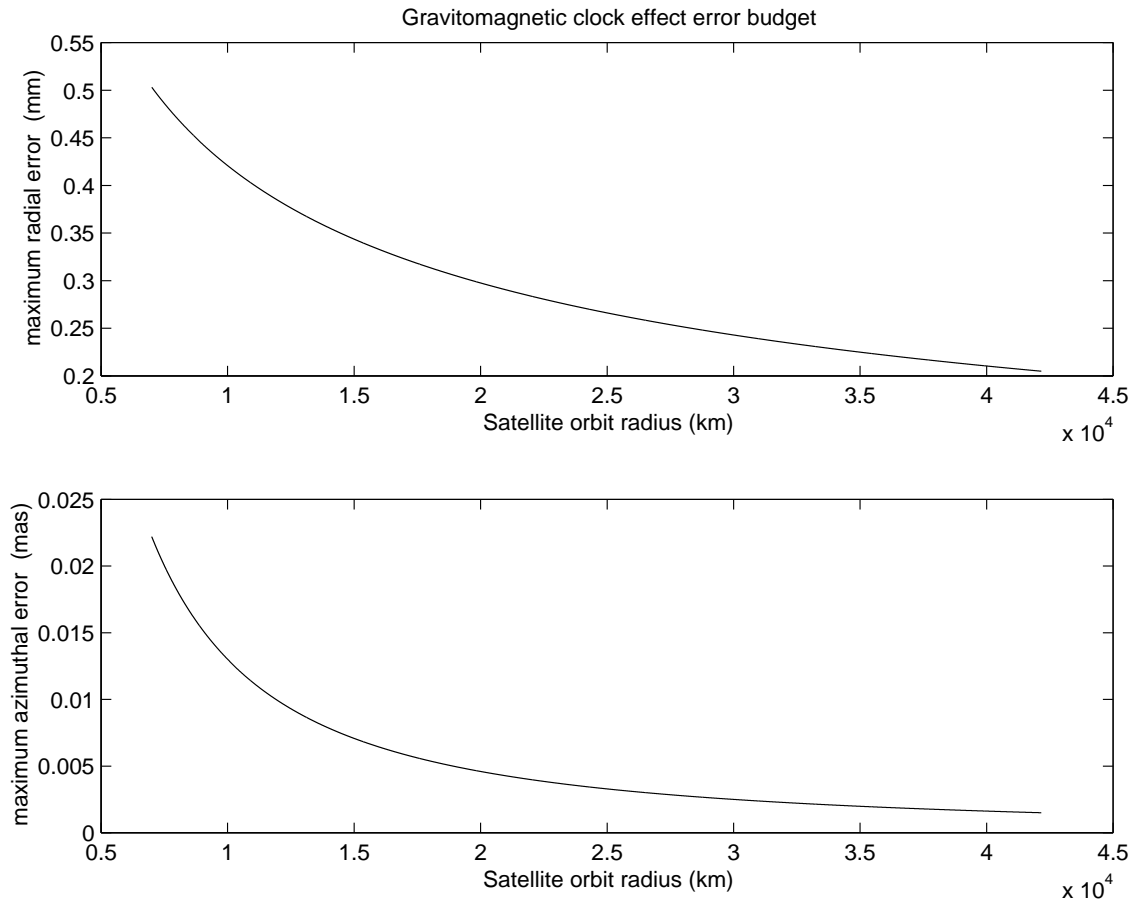


Figure 6.1: Maximum allowable errors in the radial and azimuthal locations. The values for the orbit radius span from 7,000 km to 42,160 km for a geostationary satellite.

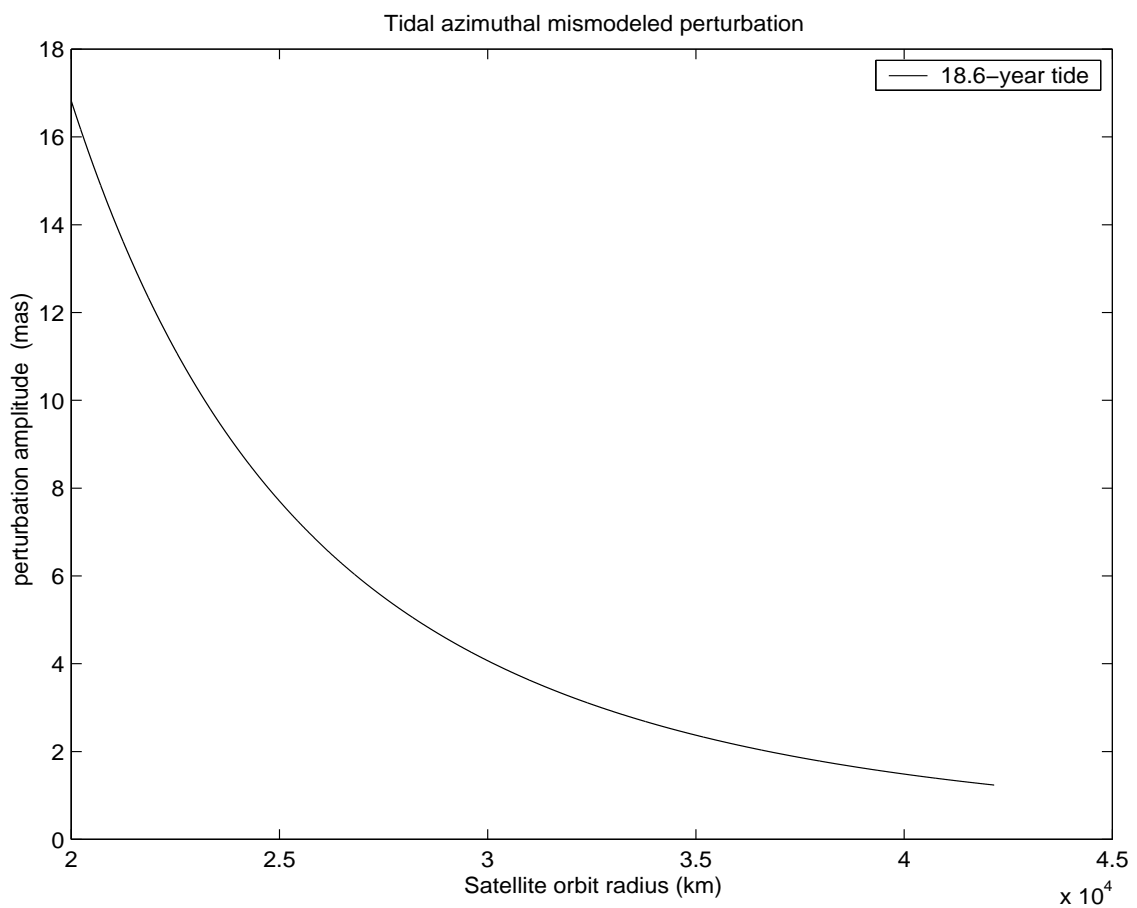


Figure 6.2: Mismodeled azimuthal perturbation induced by the 18.6-year tide.

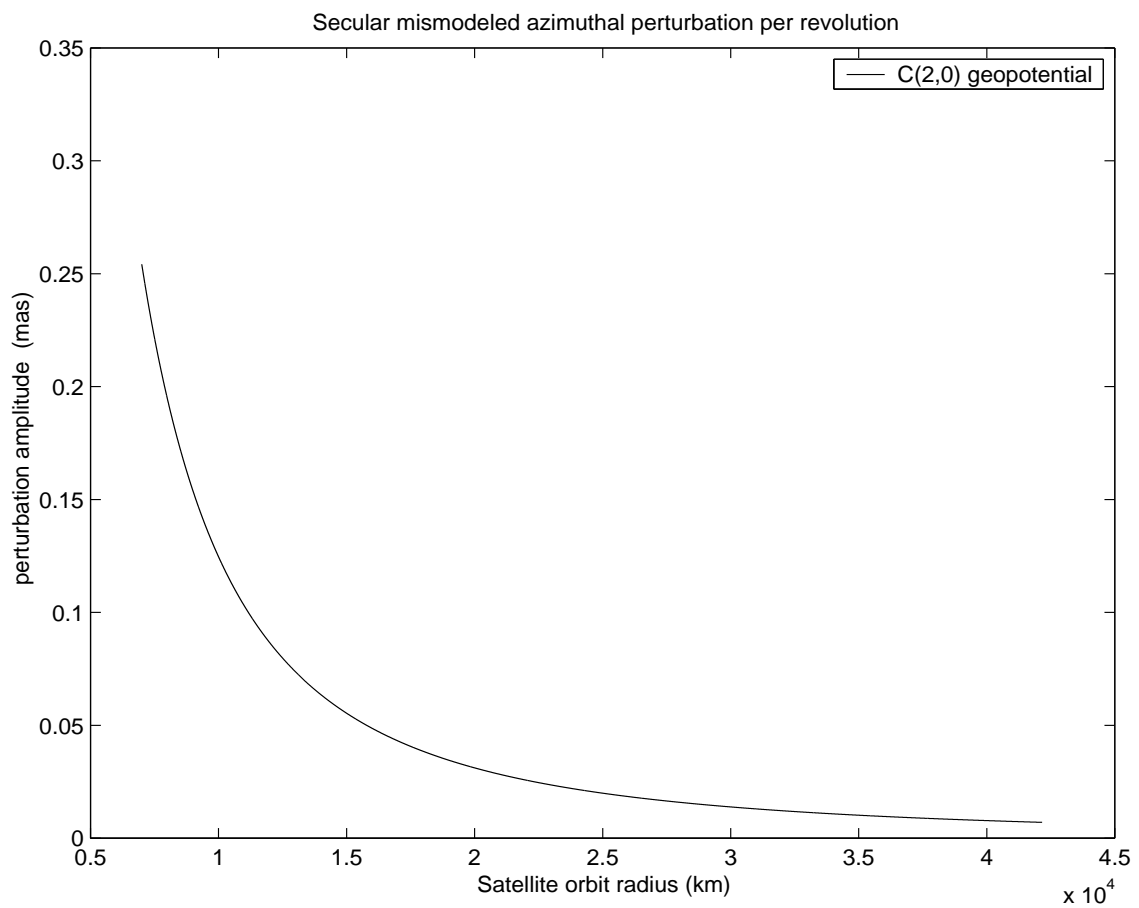


Figure 6.3: Mismodeled azimuthal rate per revolution induced by the C_{20} geopotential coefficient. The values for the orbit radius span from 7,000 km to 42,160 km for a geostationary satellite.

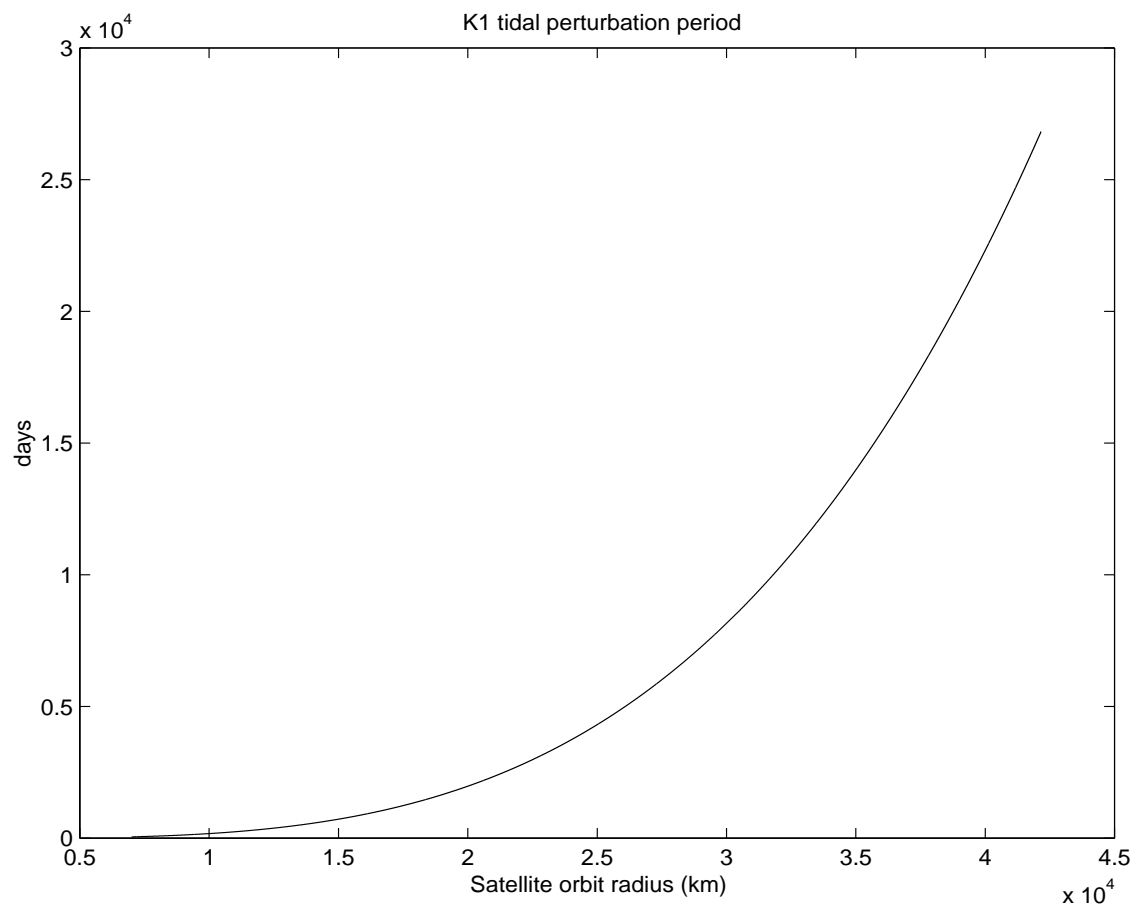


Figure 6.4: Period of the K_1 $l = 3$ $p = 1$ $q = -1$ radial tidal perturbation. The values for the orbit radius span from 7,000 km to 42,160 km for a geostationary satellite.

Chapter 7

Satellite orbital non-gravitational perturbations and the gravitomagnetic clock effect

7.1 Introduction

In the previous chapter we analyzed the gravitational static and dynamical perturbations affecting any couple of counter-orbiting near Earth satellites to be employed in order to detect the gravitomagnetic clock effect. The conclusion is that, at the present level of knowledge of the static and time-varying parts of the Earth's gravitational field [Lemoine *et al.*, 1998], the gravitational errors are larger than the required δr and $\delta\phi$. However, in the near future the new, more accurate data for the terrestrial gravitational field from the CHAMP and GRACE missions will be available and the situation could become more favorable. So, it appears important to assess the error budget due to the non-gravitational forces [Milani *et al.*, 1987] on the satellite's radial and azimuthal locations, which is the scope of this chapter [Iorio, 2001c]. We will consider throughout it a couple of identical passive, geodetic, laser-ranged spherical satellites of LAGEOS type both because Satellite Laser Ranging has reached in the last decade an astonishingly level of accuracy and because with this kind of satellites it is far simpler to model accurately enough the non-gravitational perturbations. Indeed, they depend on the physical and geometrical characteristics of the satellites and on the geometry of their orbits as well. For example, twice a year, almost six months

apart, the Sun, moving along the ecliptic, intersects the Earth's equatorial plane so that the satellite's revolutions occurring these times are affected by the phenomenon of eclipses. The radiative perturbations which are generated, directly or indirectly, by the solar electromagnetic radiation like the direct solar radiation pressure, the albedo and the Yarkovsky-Schach effect act differently on the satellite's orbit with respect to the orbital arcs described in full sunlight and in many cases such discrepancies are relevant and difficult to calculate. Moreover, the thermal forces which cause the Yarkovsky-Schach and the Rubincam effects depend on both the physical properties of the satellite and on the orientation of its spin axis with respect to an inertial frame. The terrestrial environment may cause the spin direction to change in a more or less predictable way over time spans of some years, as it is occurring to LAGEOS [*Métris et al.*, 1999].

In order to detect the gravitomagnetic time shift, which is cumulative, there is no need of very long orbital arcs: indeed, for example, the orbital period of LAGEOS amounts to 1×10^{-1} days only, so that $10^2 - 10^3$ revolutions [*Lichtenegger et al.*, 2000] would correspond to arcs $10^1 - 10^2$ days long¹. We could take advantage of this fact by choosing the arcs so to avoid the eclipses effects; moreover, over such short time spans it would be possible to consider the satellite's spin axis direction as fixed in the inertial space. Indeed, many thermal effects vanish for a suitable fixed spin axis direction.

The basic assumptions of this study are the following:

- In order to simplify the calculations we will consider a couple of LAGEOS type satellites with semimajor axis $a = 12,270$ km, as for LAGEOS, zero eccentricity e and inclination i and orbital period $P = 1.35 \times 10^4$ s
- The physical parameters of the satellites like area-to-mass ratio S/m , reflectivity and drag coefficients C_R and C_D , etc. are assumed to be equal to those of LAGEOS
- We will assume that their spins are aligned with the Earth's spin axis assumed as z axis of a terrestrial equatorial inertial frame

¹However, as pointed out in the previous chapter, short arcs would not allow one to average out many gravitational perturbations

- Only orbital arcs in full sunlight will be considered: the eclipses effects will be neglected
- The perturbations on r and φ will be averaged over an orbital revolution
- The perturbations which will be considered are the direct solar radiation pressure, the Earth's albedo, the Poynting-Robertson effect, the direct Earth IR radiation pressure, the anisotropic thermal radiation or Yarkovsky-Schach effect, the thermal trust or Rubincam effect, the atmospheric drag and the effect of the Earth's magnetic field.

The chapter is organized as follows: in section 2 and section 3 the perturbations on r and φ , respectively, are worked out, while section 4 is devoted to the conclusions.

7.2 The radial position

The radial position of a satellite in a perturbed circular orbit may change due to variations both in its semimajor axis a and its eccentricity e according to [*Christodoulidis et al.*, 1988]

$$\Delta r = \sqrt{(\Delta a)^2 + \frac{1}{2}(a\Delta e)^2}. \quad (7.1)$$

The perturbations on a are calculated with [*Milani et al.*, 1987]

$$\dot{a} = \frac{2}{n}T, \quad (7.2)$$

where T is the along-track disturbing acceleration. Concerning the eccentricity, since we are dealing with circular orbits we will use the components of the eccentricity vector $h = e \cos \omega$, $k = e \sin \omega$ and [*Milani et al.*, 1987]

$$\dot{h} \equiv \dot{e} \cos \omega + \mathcal{O}(e) = \frac{1}{na} [-R \cos(\omega + f) + 2T \sin(\omega + f)] + \mathcal{O}(e), \quad (7.3)$$

$$\dot{k} \equiv \dot{e} \sin \omega + \mathcal{O}(e) = \frac{1}{na} [R \sin(\omega + f) + 2T \cos(\omega + f)] + \mathcal{O}(e), \quad (7.4)$$

where f is the true anomaly and R is the radial component of the perturbing acceleration. For a circular orbit, from eq. (7.3) and eq. (7.4) it follows

$$\dot{e} = \sqrt{(\dot{h})^2 + (\dot{k})^2}. \quad (7.5)$$

7.2.1 The radiative perturbations

The perturbing acceleration due to direct solar radiation pressure can be approximately written as [Lucchesi, 2001]

$$\mathbf{w}_\odot = -w_\odot \hat{s}, \quad (7.6)$$

where \hat{s} is the unit vector from the Earth to the Sun and

$$w_\odot = \frac{S}{m} \frac{I_0}{c} C_R. \quad (7.7)$$

In eq. (7.6) the term $(d_\odot/r_\odot)^2$, in which d_\odot is the semimajor axis of the Earth orbit around the Sun and r_\odot is its instantaneous distance, has been set equal to one. I_0 is the solar constant. For LAGEOS type satellites eq. (7.7) amounts to almost 3.6×10^{-7} cm s⁻².

Concerning the semimajor axis, it turns out that if the total solar radiation force acting on the spacecraft can be expressed in the general form $\mathbf{F}(\hat{s})$, no long-term effect in a will appear to any order in e [Milani *et al.*, 1987]. So, $\langle \dot{a} \rangle_{2\pi} = 0$.

Regarding the eccentricity, it can be proved that it is affected, at zero order in e , by long-term periodic perturbations with an almost yearly period [Lucchesi, 2001]. The amplitudes for the components of the eccentricity vector are:

$$\langle \dot{h} \rangle_{2\pi} \propto \frac{3}{2} \frac{w_\odot}{na}, \quad (7.8)$$

$$\langle \dot{k} \rangle_{2\pi} \propto \frac{3}{2} \frac{w_\odot}{na}, \quad (7.9)$$

so that, over an orbital revolution, the radial position of the satellite changes of almost 11 cm [Milani *et al.*, 1987].

Assuming that the solar constant is known at 0.3% [Ciufolini *et al.*, 1997], the major source of uncertainty in the satellite's radial position due to the direct solar radiation pressure would reside in the C_R satellite's coefficient. Assuming a global 0.5% mismodelling, the systematic error would amount to $\delta r_{\text{SRP}} = 5 \times 10^{-2}$ cm. This result suggests that, in order to meet the requirement of $\delta r \sim 10^{-2}$ cm, a careful analysis of the optical properties of the satellites should be conducted in accurate pre-launch controls.

For a circular and equatorial orbit the perturbations on the satellite's radial position induced by the Earth's albedo are entirely due to the changes in the eccentricity vector as well. Indeed, the along-track acceleration, which is particularly sensitive to the specular part of Earth's albedo and to its spatial and temporal variations, can be expanded in terms of long-periodical harmonics whose coefficients are proportional to $\sin i$ [Anselmo *et al.*, 1983]. Concerning the eccentricity vector, the simple analytic model by *Métris et al.*, [1997], based on an uniform mean albedo of $\bar{\mathcal{A}} = 0.3$, turns out to be adequate. The related perturbation amounts to 8×10^{-2} cm per orbit. Then, the systematic error due to the mismodelling in $\bar{\mathcal{A}}$, assumed to be 10% [Lucchesi, 2001], amounts to 8×10^{-3} cm per orbit.

It may be important to notice that a way to reduce the impact of the direct solar radiation pressure and the albedo could be the use of a couple of dense satellites with small $\frac{S}{m}$.

The Poynting-Robertson acceleration [Burns *et al.*, 1979] leaves unaffected the eccentricity while changes the semimajor axis with long-term perturbations whose nominal amplitudes are of the order of $10^{-3} - 10^{-4}$ cm per orbit. Consequently, the related systematic errors are negligible.

7.2.2 The thermal perturbations

Concerning the direct Earth IR radiation pressure, the Earth thermal emissivity \mathcal{E} can be modelled in a form of a latitude-dependent spherical harmonic expansion on a spherical Earth surface [Sehnal, 1981]

$$\mathcal{E} = \mathcal{E}_0 + \mathcal{E}_1(t) P_1(\sin \phi) + \mathcal{E}_2 P_2(\sin \phi) + \dots, \quad (7.10)$$

where ϕ is the terrestrial latitude. Regarding the effects of the first two zonal constant terms \mathcal{E}_0 and \mathcal{E}_2 , $\langle \dot{a} \rangle_{2\pi} = 0$ since it is proportional to $(e \sin i)^2$ and $\langle \dot{e} \rangle_{2\pi} = 0$ since it is proportional to $e(\sin i)^2$ [Sehnal, 1981]. The perturbations due to $\mathcal{E}_1(t)$, which shows an approximately yearly variation, vanish as well since R and T are proportional to $\sin i$ [Métris *et al.*, 1997].

The Yarkovsky-Schach effect [Afonso *et al.*, 1989] induces perturbations on the

semimajor axis which vanishes since the first non-zero term in \dot{a} is of order $\mathcal{O}(e)$ for orbital arcs in full sunlight. As far as the eccentricity vector is concerned, e would be perturbed at a level of 9×10^{-2} cm per orbit. However, such effect depends on the orientation of the satellite's spin axis $\hat{\xi}$: for a fixed direction such that $\xi_x = \xi_y = 0$, as it could be feasible over short arcs, $\langle \dot{h} \rangle_{2\pi} = \langle \dot{k} \rangle_{2\pi} = 0$ [Lucchesi, 2001].

The thermal thrust or Rubincam effect [Rubincam, 1987] depends on $\hat{\xi}$ as well; for $\xi_x = \xi_y = 0$ it vanishes because it can be proved that, in this case, R and T are proportional to $\sin i$.

7.2.3 Other perturbations

The neutral and charged drag has negligible effects on r . Indeed, by neglecting the corotation of the exosphere, it turns out that [Milani *et al.*, 1987]

$$\langle \Delta a \rangle_{2\pi} = -C_D \frac{S}{m} a^2 \varrho, \quad (7.11)$$

in which ϱ is the atmospheric density. For $\varrho = 8.4 \times 10^{-21}$ g cm⁻³ [Afonso *et al.*, 1985] we would have a decay in a of 4.2×10^{-4} cm per revolution. The same holds for the charged drag [Rubincam, 1990]. For circular orbits the eccentricity is not affected by the drag [Milani *et al.*, 1987].

If the satellites carry an electric charge, as it is the case for LAGEOS, the Earth's magnetic field acts upon them via the Lorentz force. Its effect on the semimajor axis is of course zero since the Lorentz force does not change the satellite's total mechanical energy W and, consequently, a : indeed, $W = -\frac{GM}{2a}$. Regarding the eccentricity vector, it turns out that $\langle \dot{h} \rangle_{2\pi} = \langle \dot{k} \rangle_{2\pi} = 0$ because R is constant and T is of order $\mathcal{O}(e)$.

7.3 The azimuthal position

As in [Iorio, 2001b; Lichtenegger *et al.*, 2001] and in the previous chapter, for a satellite in an equatorial and circular orbit the rate of the azimuthal angle can be

calculated by means of

$$\dot{\phi} = \dot{\omega} + \dot{\Omega} \cos i + \dot{\mathcal{M}}, \quad (7.12)$$

where

$$\dot{\mathcal{M}} = n - \frac{2}{na} R \frac{r}{a} - \sqrt{1-e^2} (\dot{\omega} + \cos i \dot{\Omega}). \quad (7.13)$$

For $e = i = 0$ eqs. (7.12)-(7.13) yield

$$\dot{\phi} = n - \frac{2}{na} R. \quad (7.14)$$

In dealing with eq. (7.14) the indirect effects on n induced by the perturbations on a must be considered as well. At the first perturbative order they are: [Milani *et al.*, 1987]

$$\Delta n = -\frac{3n}{2a} \Delta a. \quad (7.15)$$

7.3.1 The radiative perturbations

The direct solar radiation pressure does not affect ϕ because, as seen in previous section, $\langle \dot{a} \rangle_{2\pi} = 0$; moreover, $\langle R \rangle_{2\pi} = 0$.

Regarding the Earth's albedo, the indirect perturbations on n vanish because $\langle \dot{a} \rangle_{2\pi} = 0$. According to the model by Métris *et al.*, [1997] $\langle R \rangle_{2\pi} = 0$.

The non-vanishing perturbations of order $\mathcal{O}(e^0)$ induced by the Poynting-Robertson effect, which amount to almost 10^{-5} mas per revolution or less are negligible.

7.3.2 The thermal perturbations

Concerning the direct Earth IR radiation pressure, $\langle \dot{a} \rangle_{2\pi} = 0$ so that the indirect perturbations on the mean motion vanish as well. The first two constant zonal terms of the Earth IR emissivity yield non-vanishing terms of zero order in e . Indeed, it turns out that, for \mathcal{E}_0

$$\left\langle -\frac{2}{na} R \right\rangle_{2\pi}^{(0)} = -\frac{2}{na} \left(\frac{R_{\oplus}}{a} \right)^2 \mathcal{E}_0 \frac{S}{m} \frac{C_R}{c}, \quad (7.16)$$

which yields -1.6×10^{-1} mas per revolution. The systematic error induced by the mismodelling in \mathcal{E}_0 is within the limit $\delta\phi \sim 10^{-2}$ mas per revolution and could be

reduced by using satellites with small area-to-mass ratio. The bias due to \mathcal{E}_2 is negligible since its nominal perturbation amounts to 1×10^{-3} mas per revolution. As in for r , also in this case $\mathcal{E}_1(t)$ does not contribute since R is proportional to $\sin i$.

The Yarkovsky-Schach effect does not affect the azimuthal position since $\langle \dot{a} \rangle_{2\pi} = 0$ and it turns out that R averages out over an orbital revolution. The same holds for the Rubincam effect which is not present when $\xi_z = \pm 1$ and $i = 0$.

7.3.3 Other perturbations

The indirect perturbation on n due to the drag shift experienced by the semimajor axis is negligible because it amounts to 6×10^{-4} mas per revolution, while

$$\left\langle -\frac{2}{na}R \right\rangle_{2\pi} = C_D \frac{S}{m} nae \langle \sin E \rangle_{2\pi} = 0, \quad (7.17)$$

where E is the eccentric anomaly.

The effect of the Earth's magnetic field is completely negligible since it is of the order of 10^{-5} mas per revolution.

7.4 Conclusions

In the context of the gravitomagnetic clock effect, by considering a couple of identical SLR satellites of LAGEOS type with $e = i = 0$ and $\xi_x = \xi_y = 0$, $\xi_z = \pm 1$ over short orbital arcs in full sunlight, it turns out that some non-gravitational perturbations on r and ϕ vanish.

Regarding the radial position, the largest perturbations are due to the direct solar radiation pressure which would change the satellite's distance of almost 10^1 cm per revolution and the Earth's albedo which would induce a change of 8×10^{-2} cm per revolution. However, their systematic errors induced by the mismodelling in the optical properties of the satellites and the Earth's albedo should fall below the cutoff $\delta r \sim 10^{-2}$ cm. The influence of the other non-vanishing perturbations, like

Poynting-Robertson effect and neutral and charged drag, is negligible. The thermal perturbations vanish.

The azimuthal angle is perturbed by the Earth's IR direct radiation pressure at a level of 10^{-1} mas per revolution. The other non-vanishing perturbations are negligible.

It should be pointed out that all the non-vanishing perturbations are proportional to $\frac{S}{m}$. This means that the impact of their systematic errors could be reduced by using particularly dense satellites with small area-to-mass ratio.

The results of the present chapter suggest that for a suitable choice of the satellites to be employed and of their orbital geometry it would be possible to keep the non-gravitational perturbations within the required constraints in order to make feasible the measurement of the gravitomagnetic clock effect. As far as the systematic errors induced by the forces acting upon the satellites are concerned, the major problems come from the Earth's gravitational environment. Improvements in satellite tracking accuracy of almost two orders of magnitude are needed as well.

Chapter 8

On the possibility of measuring the PPN parameters β and γ with LAGEOS and LAGEOS II

In order to test general relativity versus alternative metric theories of gravitation, following a method introduced by Eddington (1922), Robertson (1962) and Schiff (1967), one can expand the spacetime metric (which describes the gravitational interaction) at the order beyond Newtonian theory (post-Newtonian) and then multiply each post-Newtonian term by a dimensionless parameter, the PPN parameters, to be experimentally determined. Using this method, Nordtvedt and Will [Will, 1993] have developed the PPN (Parameterized-Post-Newtonian) formalism, a powerful and useful tool for testing general relativity and alternative metric theories. Therefore, the PPN formalism is a post-Newtonian parameterized expansion of the metric tensor \mathbf{g} and of the energy-momentum tensor \mathbf{T} in terms of small known classical potentials.

In the slow-motion and weak-field approximation, at the so-called post-Newtonian limit, the structure of known metric theories of gravity is identical apart from the numerical values of the PPN parameters which appear in the expansion of the metric coefficients [Will, 1993; Ciufolini and Wheeler, 1995; Will, 2001]. Especially meaningful are the parameters β and γ , i.e the usual Eddington-Robertson-Schiff parameters used to describe the “classical” tests of General Relativity. γ measures how much space curvature is produced by unit rest mass and in the standard parameterized post-Newtonian gauge β accounts for the level of nonlinearity in the superposition

law for gravity [Misner *et al.*, 1973]. In general relativity $\beta = 1$ and $\gamma = 1$.

To-day a very accurate measurement of γ was performed by using the Viking time delay [Reasenberg *et al.*, 1979]: the results was $\gamma = 1.000 \pm 2 \times 10^{-3}$. The quoted uncertainty allows for possible systematic errors. A more recent measurement based on the time delay of the NEAR spacecraft [Elliott *et al.*, 1998] claims an uncertainty $\leq 10^{-3}$. Other recent measurements exploit the gravitational bending of the electromagnetic waves at various wavelength [Robertson and Carter, 1984; Robertson *et al.*, 1991; Fræschlé *et al.*, 1997] obtaining an uncertainty of the order of 10^{-3} ; e.g., according to the VLBI radio analysis by [Lebach *et al.*, 1995] $\gamma = 0.9996 \pm 1.7 \times 10^{-3}$, while in [Fræschlé *et al.*, 1997] $\gamma = 0.997 \pm 3 \times 10^{-3}$ is quoted based on the astrometric observations of the electromagnetic waves deflection in the visible. An improvement in the accuracy of two orders of magnitude [Fræschlé *et al.*, 1997] is expected from the future GAIA astrometric mission [GAIA, 2000]. Lunar laser ranging (LLR) measurements of the geodetic precession yields for γ an accuracy of 10^{-2} [Williams *et al.*, 1996]. However a careful discussion of the different terms in the lunar motion yields eventually $\gamma = 1.000 \pm 5 \times 10^{-3}$ as the present LLR result [Fræschlé *et al.*, 1997].

The value of the parameter β , which cannot be measured independently, can be obtained from the measured values of γ and of some combinations of γ and β : $\eta = 4\beta - \gamma - 3$ and $\frac{2+2\gamma-\beta}{3}$ are the most accurately determined. General relativity predicts $\eta = 0$ and $\frac{2+2\gamma-\beta}{3} = 1$. For β in [Anderson and Williams, 2001] by using LLR data $\delta\beta = 4.7 \times 10^{-4}$ is reported.

The combination η measures the possible violation of the strong equivalence principle, i.e. the so-called Nordvedt effect [Nordvedt, 1968a; 1968b; 1968c; 1991]. η has been measured by analyzing the motion of the Moon via LLR data analyses [Shapiro *et al.*, 1976; Williams *et al.*, 1996; Anderson and Williams, 2001]. The most recent determination of η by LLR is $\eta = 0.0002 \pm 8 \times 10^{-4}$ [Anderson and Williams, 2001].

The combination $\frac{2+2\gamma-\beta}{3}$ is related to the well known pericenter shift of a test body induced by the Schwarzschild's gravitoelectric part of the metric for a static, spherically symmetric distribution of mass-energy [Misner *et al.*, 1973; Ciufolini and Wheeler, 1995]. This effect has been accurately measured for the Mercury perihelion

shift in the field of the Sun by means of the echo delays of radar signals transmitted from Earth to Mercury [Shapiro *et al.*, 1972] yielding $\frac{2+2\gamma-\beta}{3} = 1.005 \pm 7 \times 10^{-3}$. Inclusion of the probable contribution of systematic errors raises the uncertainty to about 2×10^{-2} . In this case the major sources of systematic error are the poorly-known variation in topography on the planet's surface and the uncertainties in the radar scattering law [Shapiro, 1990; Pitjeva, 1993].

Unfortunately, the interpretation of the perihelion advance of Mercury as a test of general relativity is complicated by the uncertainty in the mass quadrupole moment of the Sun which also contributes to the perihelion advance. From the expression of the perihelion precession and from the 1976 experimental uncertainties in $\dot{\omega}$, one can easily calculate that for Mercury orbiting the Sun, any value of $J_{2\odot}$ larger than about 3×10^{-6} would disagree with the general relativistic prediction of 42.98 arcseconds/century; indeed, according to some authors measured values of $J_{2\odot}$ may be as large as $\sim 5.5 \times 10^{-6}$ (for a comprehensive discussion see [Ciufolini and Wheeler, 1995; Pireaux *et al.*, 2001]). Laboratory experiments have been also proposed [Cacciani *et al.*, 1989] to measure the solar mode $l = 1$, to get informations on the rotation of the core of the Sun from the $l = 1$ rotational frequency splitting. Nevertheless, according to more recent determinations of $J_{2\odot}$ using the analysis of the Sun's pressure modes, both from the ground-based network of observatories and the space based SOHO, $J_{2\odot} = (2.3 \pm 0.1) \times 10^{-7}$ [Shapiro, 1999]; in [Godier and Rozelot, 2000] a theoretical estimate of $J_{2\odot} = (2.0 \pm 0.4) \times 10^{-7}$ is reported. Thus, according to these values of $J_{2\odot}$ the observed perihelion advance of Mercury is well in agreement with the general relativistic predictions.

In order to measure $J_{2\odot}$, among other astrodynamical and relativistic parameters, several space missions have been proposed using a variety of techniques: the most recent and promising are SORT, IPLR and ASTROD [Ni, 2001]. In [Ciufolini and Matzner, 1992] a measurement of the LAGEOS laser ranged satellite perigee shift in the field of the Earth is quoted, but the accuracy amounts only to 2×10^{-1} . More accurate measurements of $\frac{2+2\gamma-\beta}{3}$ might be performed in the future by means of an ESA Mercury orbiter [Balogh *et al.*, 2000; Milani *et al.*, 2001]. By detecting the relativistic perigee rate of the proposed LARES laser ranged satellite only [Ciufolini,

1998] it might be possible to reach a 3×10^{-4} level of accuracy of the order $10^{-3} - 10^{-4}$ over a long enough time span.

In this chapter we explore the possibility of accurately measuring $\frac{2+2\gamma-\beta}{3}$ by using some suitable combinations of the orbital residuals of the presently (or proposed) existing spherical geodetic laser ranged satellites with particular emphasis to LAGEOS and LAGEOS II in order to exploit the relevant experience obtained with the gravitomagnetic measurements in [*Ciufolini et al.*, 1996; 1997; 1998]. So, by combining the accurate determinations of the Nordtvedt parameter η and of $\frac{2+2\gamma-\beta}{3}$ from SLR it should be possible to obtain independent and precise values for γ and β .

This chapter is organized as follows: in section 1 we compare the present experimental accuracy in satellite laser-ranging measurements with the relativistic expressions of the perigee shift of the two LAGEOS satellites. In section 2 we analyze some of the most important sources of systematic errors: the even zonal harmonics of the static part of the geopotential, the Earth solid and ocean tidal perturbations, the direct solar radiation pressure and the mismodelling of the inclination. In section 3 we simulate the LAGEOS combined residuals curve over different observational time spans T_{obs} and for different satellite orbital arc lengths Δt in order to estimate the experimental error in the recovery of the solve-for least square parameter which accounts for the investigated relativistic effect. Section 4 is devoted to the conclusions.

8.1 The relativistic perigee precession of LAGEOS type satellites

As known, in the slow-motion and weak-field approximation, the Schwarzschild metric generated by a static, spherically symmetric distribution of mass-energy induces an additional post-Newtonian “gravitoelectric” force which acts on the orbit of a test body by shifting its pericenter; in the PPN formalism the pericenter rate can be written as

$$\dot{\omega}_{\text{GR}} = \frac{3nGM}{c^2a(1-e^2)} \times \frac{2+2\gamma-\beta}{3}. \quad (8.1)$$

In the following we define $\nu \equiv \frac{2+2\gamma-\beta}{3}$. General Relativity predicts that the perigee shifts for LAGEOS and LAGEOS II amount to 3,312.35 mas/y and 3,387.46 mas/y, respectively.

Following [Ciufolini, 1996] the actual experimental precision allows for detecting such rates for both LAGEOS. Indeed, for the perigee the observable quantity is $r \equiv ea\dot{\omega}$ and at present its measurement error amounts to about $\delta r_{\text{exp}} \leq 1$ cm for the two LAGEOS, over several orbits and for a given set of force models (i.e. not including modelling errors). Since the LAGEOS eccentricity is $e_I = 4.5 \times 10^{-3}$ the accuracy in detecting the perigee is $\delta\omega_{\text{exp}}^I = \delta r_{\text{exp}}/(e_I a_I) \simeq 37$ mas. So, over 1 year the relative accuracy of the measurement of the relativistic perigee shift would be $\sim 1 \times 10^{-2}$. For LAGEOS II this measurement accuracy is better than that of LAGEOS indeed the LAGEOS II eccentricity is $e_{II} = 1.4 \times 10^{-2}$, so that $\delta\omega_{\text{exp}}^{II} \simeq 12$ mas; this may yield an accuracy of about 3×10^{-3} over 1 year. These considerations rule out the possibility of directly using the perigee of the other existing spherical geodetic laser-ranged satellites Etalon-1, Etalon-2, Ajisai, Stella, Westpac-1 because their eccentricities are even smaller than that of LAGEOS. On the contrary, Starlette has an eccentricity of the order of 2×10^{-2} ; however, since it orbits at a lower altitude it is more sensitive than the LAGEOS satellites to atmospheric drag and to Earth's zonal harmonics, so that it would be difficult to process its data at an acceptable level of accuracy. Accordingly, we will focus on the perigee of LAGEOS and especially of LAGEOS II in order to accurately detect the gravitoelectric relativistic shift in the gravitational field of Earth.

8.2 The systematic errors

The most important source of systematic error in such measurements is represented by the mismodelling induced by the even zonal harmonics of the Earth gravitational field [Kaula, 1966] on the classical perigee precession. By using the covariance matrix of the EGM96 Earth gravity model [Lemoine *et al.*, 1998] and adding the correlated terms in a root-sum-square fashion up to degree $l = 20$ we obtain for LAGEOS a systematic error $\delta\nu/\nu_{\text{zonals}} = 8.1 \times 10^{-3}$, whereas for LAGEOS II we have $\delta\nu/\nu_{\text{zonals}} = 1.5 \times 10^{-2}$.

Since the major source of uncertainty lies in the first two even zonal harmonics δJ_2 and δJ_4 , following [Ciufolini, 1996] for the Lense-Thirring LAGEOS experiment, we search for suitable combinations of orbital residuals of the existing SLR satellites in order to eliminate most static and dynamical even zonal terms of the geopotential. In Tab.?? we report the most promising combinations: their general form is

$$\delta\dot{\omega}^{\text{II}} + \sum_{j=1}^N c_j \delta\dot{\Omega}^j + c_{N+1} \delta\dot{\omega}^{\text{I}} = x_{\text{GR}} \nu, \quad (8.2)$$

in which N is the number of the nodes of different SLR satellites employed, x_{GR} is the slope, in mas/y, of the relativistic trend to be measured and $\delta\nu/\nu_{\text{zonals}}$ is the systematic error induced by the even zonal harmonics up to degree $l = 20$ calculated with EGM96 covariance matrix. It is important to stress that the use of LAGEOS, due to their altitude, makes our measurement substantially insensitive to the errors in the zonal harmonics of degree $l > 20$, so that our estimates of $\delta\nu/\nu_{\text{zonals}}$ presented here are valid even in the case that the EGM96 covariance matrix for higher degrees $l > 20$ would not be accurate enough.

In addition to LAGEOS and LAGEOS II, we have only considered Ajisai since it is well tracked, contrary to, e.g., the Etalons, and it would be less demanding than the other satellites to reduce its laser ranged data to a level of accuracy comparable to that of LAGEOS and LAGEOS II. Moreover, the other SLR satellites orbit at lower altitudes, therefore they are more sensitive to the higher degree terms of the geopotential. Consequently, as confirmed by numerical calculations, the inclusion in their data in the combined residuals would increase $\delta\nu/\nu_{\text{zonals}}$.

Note that the systematic error induced by the mismodelled secular rates of the even zonal harmonics of the geopotential is really critical because it can be considered as an unavoidable part of the total error in the experiment. Indeed, the resulting aliasing trend cannot be removed from the data and nothing can be done about it apart from assessing as more reliably as possible the related error.¹

It is important to point out that the values quoted in Tab.8.1 for $\delta\nu/\nu_{\text{zonals}}$ will be

¹About combination 3, it should be noted that in order to obtain more reliable and accurate estimates of the systematic error due to the even zonal harmonics of the geopotential it should be better to extend the calculations to higher degrees than $l = 20$ due to the sensitivity of Ajisai to such higher degree terms.

reduced in the near future when the data from the CHAMP mission will be released.

In regard to the evaluation of the impact of other sources of systematic errors in this chapter we consider in detail only the combination 1 of Tab. 8.1 so to exploit the background acquired with the Lense-Thirring LAGEOS experiment [*Ciufolini et al.*, 1996; 1997; 1998]. Moreover, reducing the Ajisai's data to an acceptable level of accuracy for our measurement would neither be a trivial nor an immediate task to be performed and the inclusion of the perigee of LAGEOS would raise the experimental error. For example, for combination 2 of Tab. 8.1, over 1 year, the impact of the error in measuring the perigee rate of LAGEOS amounts to $2.5 \times (3.1 \times 10^{-3}) = 7.7 \times 10^{-3}$ while for combination 3 it is $1.370 \times (4.7 \times 10^{-3}) = 6.4 \times 10^{-3}$.

8.2.1 Tides and other disturbing harmonics

In Fig.8.1 we show a preliminary estimate of the impact of the most effective harmonic orbital perturbations on the considered combination

$$\delta\omega^{\text{II}} - 0.87 \delta\Omega^{\text{II}} - 2.86 \delta\Omega^{\text{I}} = \nu 3,387.46 \times T_{\text{obs}}. \quad (8.3)$$

The harmonic, long-period perturbations, according to their periods P and to the adopted observational time span T_{obs} , may turn out to be less insidious than the mismodelled linear perturbations due to the zonal harmonics of the geopotential since, if $P < T_{\text{obs}}$ and $T_{\text{obs}} = nP$, $n = 1, 2, \dots$ they average out; if their periods are shorter than the time span they can be viewed as empirically fitted quantities which can be subsequently removed from the signal. With a very conservative approach, we have tried to assess their impact by comparing the averages, over different time spans, of the entire set of the harmonic perturbations with the general relativistic linear trend over the same observational periods. This approach is equivalent to that followed in chapter 4 and in [*Iorio and Pavlis*, 2001; *Pavlis and Iorio*, 2001].

For different time spans T_{obs} , we have simulated with MATLAB the time series of the mismodelled harmonic part of the signal by including the solid Earth and ocean tides as worked out in chapter 3 and in [*Iorio*, 2001a], the $l = 3$ Earth's zonal harmonic perturbation of the perigee of LAGEOS II and the solar radiation pressure.

² Subsequently, at fixed T_{obs} , we have performed 5,000 runs by varying the initial phases so to account for the different cases occurring in the real world, and for each run at fixed T_{obs} we have calculated $\langle \delta\Omega^{\text{I}} \rangle_{T_{\text{obs}}}$, $\langle \delta\Omega^{\text{II}} \rangle_{T_{\text{obs}}}$ and $\langle \delta\omega^{\text{II}} \rangle_{T_{\text{obs}}}$ in mas. We have then inserted them in eq. (8.3) and we have taken the ratios of the averages of the long-periodic systematic errors obtained in this way with the general relativistic shift for the given time span. In this way we have obtained a vector of 5,000 figures, for any given T_{obs} , depending on the initial phases. Such values turn out to be normally distributed, so that we have chosen their standard deviation to represent $\delta\nu/\nu_{\text{harmonics}}$ for the various T_{obs} chosen. Note that over 5 years we have $\delta\nu/\nu_{\text{harmonics}} = 1.4 \times 10^{-3}$ while over 8 years we have $\delta\nu/\nu_{\text{harmonics}} = 6.7 \times 10^{-4}$.

8.2.2 Errors in the inclination

As in the case of the Lense-Thirring experiment [Ciufolini *et al.*, 1996; 1997], the analyzed combined residuals are not only affected by the errors in the higher degree even zonal harmonics of the geopotential but also by the error in the knowledge of the inclination of the satellites

$$\delta\nu_{\text{inclination}} = \frac{\partial\dot{\omega}^{\text{II}}}{\partial i}\delta i^{\text{II}} - 0.87 \frac{\partial\dot{\Omega}^{\text{II}}}{\partial i}\delta i^{\text{II}} - 2.86 \frac{\partial\dot{\Omega}^{\text{I}}}{\partial i}\delta i^{\text{I}}, \quad (8.4)$$

in which, by just considering the even zonal harmonic J_2 , $\frac{\partial\dot{\omega}^{\text{II}}}{\partial i} = -16 \text{ rad/y}$, $\frac{\partial\dot{\Omega}^{\text{II}}}{\partial i} = 5.3 \text{ rad/y}$ and $\frac{\partial\dot{\Omega}^{\text{I}}}{\partial i} = 6 \text{ rad/y}$.

An assessment of eq. (8.4) requires an inspection of the residuals of the inclination over the considered time span. To this aim, as done for tides and other harmonic perturbations, for different time spans T_{obs} , we have simulated with MATLAB the time series of the mismodelled part of the inclinations of LAGEOS and LAGEOS II by including the solid Earth and ocean tides and the solar radiation pressure and randomly varying the initial phases of these harmonic perturbations. Subsequently, with fixed T_{obs} , we have performed 5,000 runs by varying the initial phases and for each of these runs we have calculated $\langle \delta i^{\text{I}} \rangle_{T_{\text{obs}}}$ and $\langle \delta i^{\text{II}} \rangle_{T_{\text{obs}}}$ in mas; we then have

²In the present error budget we have neglected other subtle non-gravitational perturbations acting on LAGEOS orbits (Earth's albedo, Earth's direct IR radiation pressure, thermal effects) whose effects on the perigee of LAGEOS II are currently under detailed investigation. Anyway, their impact on our measurement should be at the level of 10^{-3} or less on long enough time span.

inserted them in eq. (8.4) and we have taken the ratios of such values to the general relativistic shift for the given time span. In this way we have obtained a vector of 5,000 figures, for any given T_{obs} , depending on the initial phases, which represent the systematic errors induced by the mismodelling in the inclination. Such values turn out to be normally distributed, so that we have taken their standard deviation to represent $\delta\nu_{\text{incli}}$ corresponding to the various T_{obs} chosen. The results are shown in Fig.8.2. Note that over 5 years we have $\delta\nu/\nu_{\text{incli}} = 1.4 \times 10^{-3}$ while over 8 years we have $\delta\nu/\nu_{\text{incli}} = 7.6 \times 10^{-4}$.

When the real data will be available we can get the inclination modelling errors from the orbital residuals of our data reductions with GEODYN-SOLVE and then use eq. (8.4) to correct for the corresponding modelling error in nodal and perigee rates due to these inclination errors.

8.3 Numerical simulations

In order to get an insight into the least-squares formal error we have simulated the combined residuals curve and subsequently we have fitted it with a straight line only, as done in the case of the gravitomagnetic experiment in chapter 4 and in [*Pavlis and Iorio, 2001; Iorio and Pavlis, 2001*]. We have constructed the simulated data by including a linear trend with a slope of 3,387.46 mas/y, as predicted by General Relativity, the most relevant tidal and radiative perturbations and a noise. It consists of a random, white part and a non-zero average part. The first component has been used in order to reproduce the actual level of uncertainty in LAGEOS data as used in the Lense-Thirring experiment [*Ciufolini et al., 1998*]. The amplitude of the latter has been chosen in order to account for the systematic error due to the even zonal harmonics of degree $l \geq 6$. By then varying the time span T_{obs} and the satellites' orbital arc length Δt we have fitted the simulated data with a straight line only without including any periodical perturbation in the least-square fitted quantities. More precisely, for given T_{obs} and Δt , we have performed 100 runs by varying the initial phases of the harmonics and the features of the random part of the noise. Subsequently, we have taken the averaged values for the recovered ν and $\delta\nu/\nu$. Fig.8.3

summarizes the results. For $T_{\text{obs}} = 8$ years and $\Delta t = 7$ days the formal error amounts to $\sim 5 \times 10^{-4}$

8.4 Discussion and conclusions

In Tab.8.2 we summarize the results obtained for a 8 years long time span with 7 days arc lengths. In assessing the total systematic error we have accounted for the fact that the gravitational errors are not independent simply by summing them up. Then, we have added them and the other independent sources of errors in a root-sum-square fashion. In the first column we quoted the kind of error. In the second column there are the sources, in this paper, of the quoted numbers in the third column. Note that the error in the LAGEOS II perigee refers to 1 year only by assuming an error of 1 cm in its radial position. Moreover, the estimate of the statistical formal error has been obtained by considering the noise level in the LAGEOS data of 1998 Lense-Thirring experiment; in the near future and for longer time spans these uncertainties will be reduced. Moreover, it is important to emphasize that the data from the CHAMP and GRACE missions will soon yield a notable reduction of the systematic error due to the higher degree static even zonal harmonics of the geopotential and of the solid and ocean tides systematic errors as well. In particular, a very significant reduction of the systematic errors will take place due to the static part of the geopotential, which has turned out to be the most important source of uncertainty.

The results obtained for the combination 1 examined here together with those released in [*Anderson and Williams, 2001*] for the combination η would allow to measure $\beta = \frac{2}{7}\eta + \frac{3}{7}\nu + \frac{4}{7}$ independently of other measurements of γ with $\sim 3.4 \times 10^{-3}$ accuracy over 8 years; this result, which is of the same order of magnitude of that obtained with the radar ranging technique [*Shapiro, 1990*], should be compared with the most recent $\delta\beta = 4.7 \times 10^{-4}$ obtained from the LLR data [*Anderson and Williams, 2001*]. The parameter γ , given by $\gamma = \frac{1}{7}\eta + \frac{12}{7}\nu - \frac{5}{7}$, could be measured less precisely over the same time span: $\delta\gamma \sim 1.3 \times 10^{-2}$.

However, in the recent years it has been done a lot of work in predicting what it can be got from the gravity modelling efforts that will include the CHAMP and GRACE

data [Pavlis, 2001]. In Tab.8.3, in a very conservative and pessimistic approach, we sketch a tentative error budget that we expect to be realized within a year or two from now. If these pessimistic predictions will be confirmed, the accuracy of the measurement of β and γ will increase to $\delta\beta \sim 3 \times 10^{-4}$ and $\delta\gamma \sim 8 \times 10^{-4}$. A very important point to stress is that we do not need to wait for 8 years after we get the new gravity models from CHAMP and GRACE. Indeed we already have the required SLR data (suffice it to say that by next summer we will have 10 years of LAGEOS and LAGEOS II data) to do the analysis immediately after we receive the new models. So the results could be produced within a few days after that.

8.5 Tables

Table 8.1: PPN combined residuals.

	Ω^{II}	Ω^{I}	Ω^{AJ}	ω^{I}		
κ	c_1	c_2	c_3	c_4	x_{GR} (mas/y)	$\delta\nu/\nu_{\text{zonals}}$
1	-0.868	-2.855	0	0	3,387.46	6.59×10^{-3}
2	-2.514	-4.372	0	2.511	11,704.92	1.1×10^{-3}
3	-1.962	-3.693	0.0366	1.370	7,928.51	8.1×10^{-4}

Table 8.2: Preliminary error budget: $T_{\text{obs}} = 8$ years, $\Delta t = 7$ days.

Even zonal harmonics	6.59×10^{-3}
J_3 geopotential	3.2×10^{-4}
Tides	4.4×10^{-4}
Non-gravitational effects	3.6×10^{-4}
Measurement error in LAGEOS II perigee	3×10^{-3}
Total systematic error	8×10^{-3}
Formal statistical error	5.7×10^{-4}

Table 8.3: Tentative future error budget.

Even zonal harmonics	1×10^{-4}
J_3 geopotential	1×10^{-5}
Tides	1×10^{-4}
Non-gravitational effects	3×10^{-4}
Measurement error in LAGEOS II perigee	3×10^{-4}
Total systematic error	4.7×10^{-4}
Formal statistical error	5×10^{-5}

8.6 Figures

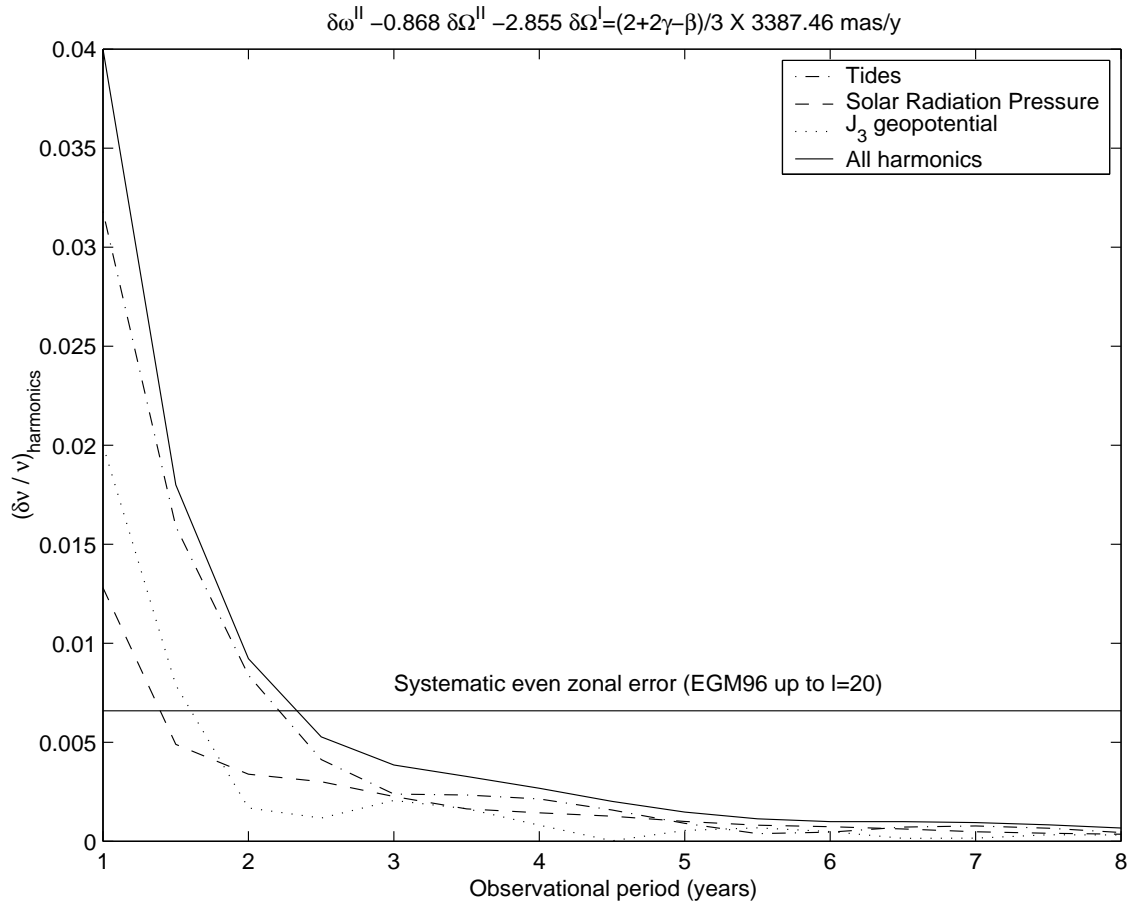


Figure 8.1: Systematic errors induced by the major harmonic perturbations

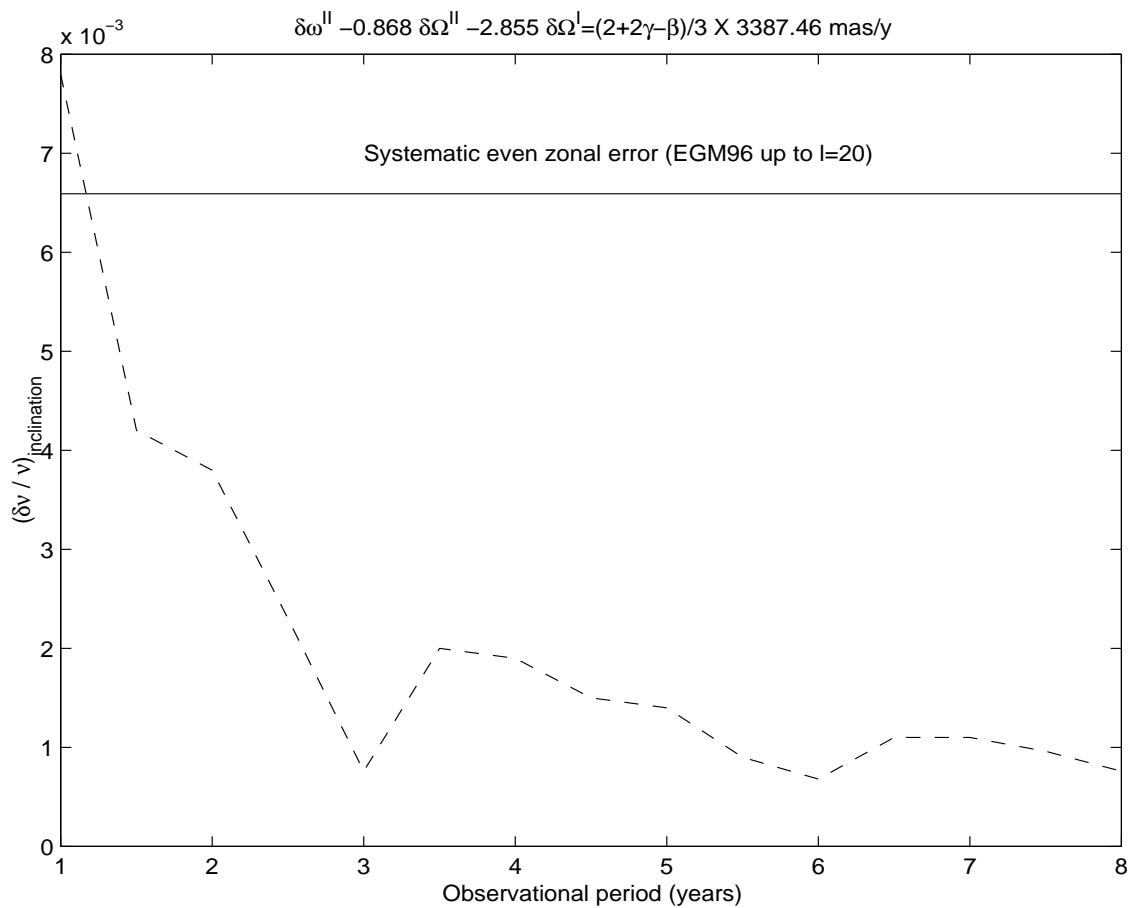


Figure 8.2: Systematic relative error induced by the mismodelling in the inclinations.

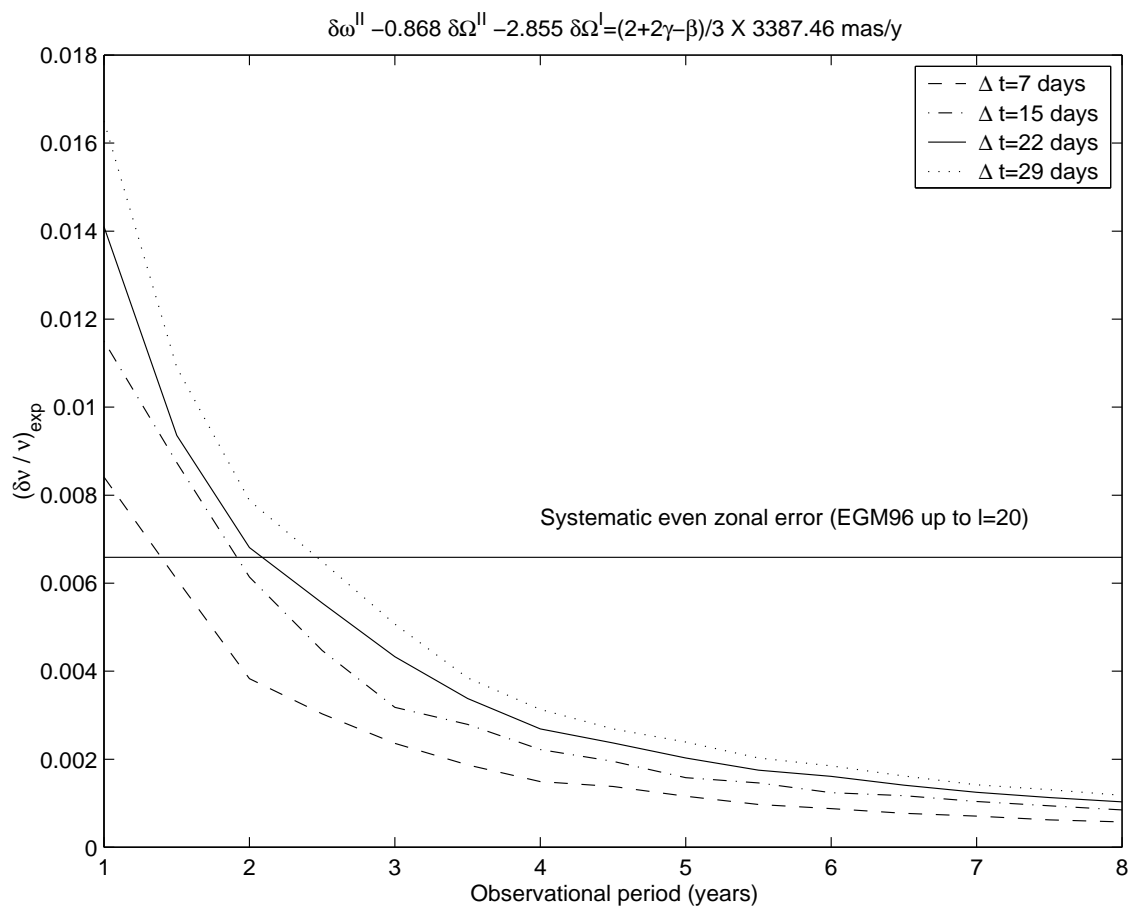


Figure 8.3: Simulated measurement errors over different time spans and arc lengths. Straight line fit only.

Chapter 9

The LARES mission revisited: some alternative scenarios

9.1 Introduction

In order to measure the Lense-Thirring drag with an accuracy of few percent, in [Ciufolini, 1986] it was proposed to launch a passive geodetic laser-ranged satellite - the former LAGEOS III - with the same orbital parameters of LAGEOS apart from its inclination which should be supplementary to that of LAGEOS.

This orbital configuration would be able to cancel out exactly the classical nodal precessions provided that the observable to be adopted is the sum of the residuals of the nodal precessions of LAGEOS III and LAGEOS

$$\delta\dot{\Omega}^{\text{III}} + \delta\dot{\Omega}^{\text{I}} = 62\mu_{\text{LT}}. \quad (9.1)$$

Later on the concept of the mission slightly changed. The area-to-mass ratio of LAGEOS III was reduced in order to make less relevant the impact of the non-gravitational perturbations and the eccentricity was enhanced in order to be able to perform other general relativistic tests [Ciufolini, 1998]: the LARES was born. The most recent error budget of the LARES Lense-Thirring experiment claim an accuracy of the order of 3%. Unfortunately, at present we do not know if the LARES mission will be approved by any space agency.

In this chapter we investigate the possibility of further reducing the error in this

important proposed mission. This chapter is organized as follows. In section 2 we analyze in detail the impact of the unavoidable injection errors in the orbital parameters of LARES on the systematic error induced by the mismodelling in the even zonal harmonics of the geopotential according to the most recently released Earth gravity model. Moreover, in section 3 we propose an alternative configuration which should be able to reduce this error by one order of magnitude. It adopts as observable a suitable combination of the orbital residuals of the nodes of LAGEOS, LAGEOS II and LARES, and the perigees of LAGEOS II and LARES. It presents also the important advantage that it is almost insensitive to the errors in the inclination of LARES, contrary to the original LAGEOS/LARES only configuration. The negative implications of placing the LARES in a low-altitude polar orbits are examined in section 4. Section 5 is devoted to the conclusions.

9.2 The impact of the even zonal harmonics of the geopotential on the original LARES mission

Let us calculate the systematic error induced by the mismodelling in the even degree zonal coefficients J_2, J_4, \dots of the geopotential on the sum of the classical precessions of the nodes of LAGEOS and LARES (See Appendix A and Appendix B). It is important to stress that it is the major source of systematic error and it cannot be eliminated in any way. We will use the covariance matrix of the Earth gravity field model EGM96 [Lemoine *et al.*, 1998] by summing up in a root sum square fashion the correlated contributes up to degree $l = 20^1$. The relative error obtained by using the nominal values amounts to

$$\frac{\delta\mu_{\text{LT}}}{\mu_{\text{LT zonals}}} = 3 \times 10^{-3}. \quad (9.2)$$

It is not equal to zero because we have assumed $e_{\text{LR}} = 0.04$ while $e_{\text{LAGEOS}} = 0.0045$. If it was $e_{\text{LR}} = e_{\text{LAGEOS}}$, then the classical nodal precessions would be exactly equal in value and opposite in sign and would cancel out. Notice that the coefficients with which $\delta\dot{\Omega}^{\text{III}}$ and $\delta\dot{\Omega}^{\text{I}}$ enter the combination of eq. (9.1) do not depend on any orbital parameters: they are constants equal to 1. Moreover, eq. (9.1) is affected by all the

¹It is important to notice that using satellites of the LAGEOS family allows one to obtain reliable estimates with EGM96. Indeed, the LAGEOS' orbits are not affected by the terms of degree $l > 20$, for which the EGM96 covariance matrix elements are determined less accurately.

classical nodal precessions, including those induced by J_2 and J_4 which, instead, are cancelled out *a priori* in the combination used in the LAGEOS experiment [Ciufolini, 1996]. They are the most effective in aliasing the Lense-Thirring precessional rates.

Now we will focus on the sensitivity of $\frac{\delta\mu_{LT}}{\mu_{LT} \text{ zonals}}$ to the unavoidable orbital injection errors in the possible orbital parameters of LARES. For a former analysis see [Casotto *et al.*, 1990]. It is particularly interesting to consider the impact of the errors in the inclination and the semimajor axis. The ranges of variation for them have been chosen in a very conservative way in order to take into account low-precision and low-costs injection scenarios.

From Fig.9.1 it is interesting to notice that the minimum value of the systematic zonal error, which amounts to 2.1×10^{-3} , does not correspond to $i_{LR} = 70$ deg but it is obtained for a slightly smaller value. It is possible to show that for $e_{LR} = e_{\text{LAGEOS}}$ the minimum is 0 and that it is attained at $i_{LR} = 70$ deg. The maximum error amounts to 1.6×10^{-2} . This suggests that the original LARES project is rather sensitive to small departures of i_{LR} from its nominal value. Fig. 9.2 shows that even more relevant is the sensitivity to the LARES semimajor axis. Also in this case the minimum is attained at a value of a_{LR} smaller than the nominal $a_{LR} = 12,270$ km. For $e_{LR} = e_{\text{LAGEOS}}$ the minimum error amounts to 0 and it is obtained for $a_{LR} = 12,270$ km, as expected. In obtaining Fig. 9.2 we have accounted for the dependence of the nodal Lense-Thirring precession on a by varying, accordingly, the slope of the general relativistic trend. The sensitivity to eccentricity variations is less relevant: indeed, by varying it from 0.03 to 0.05 the relative systematic zonal error passes from 1.6×10^{-3} to 4.6×10^{-3} .

9.3 An alternative LARES scenario

Here we will look for an alternative observable involving the orbital elements of LARES which

- yields a smaller value for the systematic error due to the mismodelled even zonal harmonics of the geopotential than that of the simple sum of the nodes of LAGEOS and LARES
- is less sensitive to the departures of the possible orbital elements of LARES from

the nominal values. The first requirement could be implemented by setting up a suitable orbital combination which cancels out the contributions of as many mismodelled even zonal harmonics as possible, following the strategy of the LAGEOS experiment outlined in [Ciufolini, 1996]. To this aim we will consider only the satellites of the LAGEOS family both because they are the best laser-ranged tracked targets and because the gravitational and non-gravitational perturbations affecting their orbits have been extensively and thoroughly analyzed.

Our result is

$$\delta\dot{\Omega}^{\text{LAGEOS}} + c_1\delta\dot{\Omega}^{\text{LAGEOS II}} + c_2\delta\dot{\Omega}^{\text{LARES}} + c_3\delta\dot{\omega}^{\text{LAGEOS II}} + c_4\delta\dot{\omega}^{\text{LARES}} = 61.8\mu_{\text{LT}}, \quad (9.3)$$

with

$$c_1 = 6 \times 10^{-3}, \quad (9.4)$$

$$c_2 = 9.83 \times 10^{-1}, \quad (9.5)$$

$$c_3 = -1 \times 10^{-3}, \quad (9.6)$$

$$c_4 = -2 \times 10^{-3}. \quad (9.7)$$

It is important to notice that the coefficients given by eqs. (9.4)-(9.7) depend on the orbital parameters of the satellites entering the combination and, among them, of LARES. The values released here are calculated for the nominal LARES parameters, as is the case for the slope in mas/y of the general relativistic trend. The observable of eq. (9.3) allows one to cancel out the static and dynamical contributions of the first four even zonal harmonics. The relative systematic error due to the J_{2n} , $n \geq 5$, according to EGM96 up to degree $l = 20$, amounts to:

$$\frac{\delta\mu_{\text{LT}}}{\mu_{\text{LT}} \text{ zonals}} = 2 \times 10^{-4}, \quad (9.8)$$

which is one order of magnitude better than the result of eq. (9.2).

Fig. 9.3 and Fig. 9.4 show the important achievements realized in reducing the sensitivity of the proposed combined residuals to the orbital injection errors in the LARES orbital elements. In obtaining Fig. 9.3 and Fig. 9.4 we have accounted for the dependence on a_{LR} and i_{LR} of both the coefficients and the Lense-Thirring precessions: it turns out that the variations in the slope of the general relativistic trend are very

smooth with respect to the nominal value of 61.8 mas/y amounting to few mas/y. Now the values of the zonals' error are much more close to the nominal one given by eq. (9.8). Also in this case, the minima are attained at slightly different values of the LARES orbital elements with respect to the nominal ones. It is interesting to notice in Fig. 9.3 that over a 3% variation of i_{LARES} the error due to the mismodeled zonal harmonics remain almost constant, while over a 5% variation of a_{LARES} it changes of 1 order of magnitude, as it turns out from Fig. 9.4.

It is worthwhile noting that the time-varying gravitational and non-gravitational orbital perturbations which affect the proposed combined residuals are depressed by the small values of the coefficients with which some orbital elements enter the combination. Moreover, the observational error in the LAGEOS II and LARES perigees, which are difficult to measure for low eccentric satellites as LAGEOS due to the small value of their eccentricity, would have an impact of the order of 1×10^{-4} by assuming an uncertainty of 1 cm over 1 year in the satellite's position.

9.4 The POLARES

In order to cope with practical launching costs it is currently under consideration the possibility of inserting the new LAGEOS-like satellite in a low altitude polar orbit with $i = 90$ deg and $a = 8,378$ km obtaining so the POLARES. If it was possible to obtain exactly such nominal values we should be able even to use the POLARES node only because the classical nodal precession would vanish. However, the unavoidable injection errors in the POLARES inclination in this case, would be greatly and fatally enhanced by the too low altitude in the sense that the systematic error due to the even zonal harmonics would blow up even for tiny departures from the nominal values.

This is clearly shown by Fig. 9.5. As expected, for $i_{\text{PL}} = 90$ deg the systematic zonal error vanishes. It can be shown that even by including the POLARES in some combination the situation would remain unfavorable.

9.5 Conclusions

If analyzed from the point of view of the impact of the systematic error induced by the mismodelling in the even zonal harmonics of the geopotential, which is the most important source of systematic error, the original LARES mission seems to be affected by a certain sensitivity to the unavoidable departures of the LARES orbital parameters from their nominal values due to orbital injection errors. In such a refined experiment, which would compete with the ambitious Stanford GP-B mission and its claimed global 1% accuracy level, it could be a serious drawback. It could be enhanced if LARES will be finally put in orbit with a low-cost launcher which, inevitably, would induce relatively large injection errors.

The adoption of the alternative combined residuals proposed here, including also the node of LAGEOS II and the perigees of LAGEOS II and LARES, would reduce by one order of magnitude the systematic error due to the even zonal harmonics of the geopotential passing from 0.3% to 0.02%, and would reduce greatly the sensitivity of such result to errors in the LARES orbital parameters. This would yield to less stringent requirements on the quality and the costs of the launcher to be adopted. It is very important to notice that the estimates presented here are based on the most recent Earth gravity model EGM96. When the new data on the terrestrial gravitational field from the CHAMP and GRACE missions will be available, the systematic zonal error will greatly reduce. The impact of the errors related to the quality of laser data will further reduce in the near future as well. Preliminary estimates of the standard statistical error in the solve-for least square parameter μ_{LT} , based on the present models of the time-dependent LAGEOS perturbations worked out in chapter 3 and the noise level reported in the Lense-Thirring LAGEOS experiment, yield a value of the order of 10^{-3} . If confirmed by further analysis of the impact of the time-dependent gravitational and non-gravitational perturbations, this result is very important because the total error of this improved version of the LARES mission would be $\leq 1\%$.

The possibility of injecting LARES in a polar low orbit at 2,000 km of altitude should be discarded because even small deviations from the projected inclination

would lead to an error due to the even zonal harmonics of the geopotential of some percent.

9.6 Figures

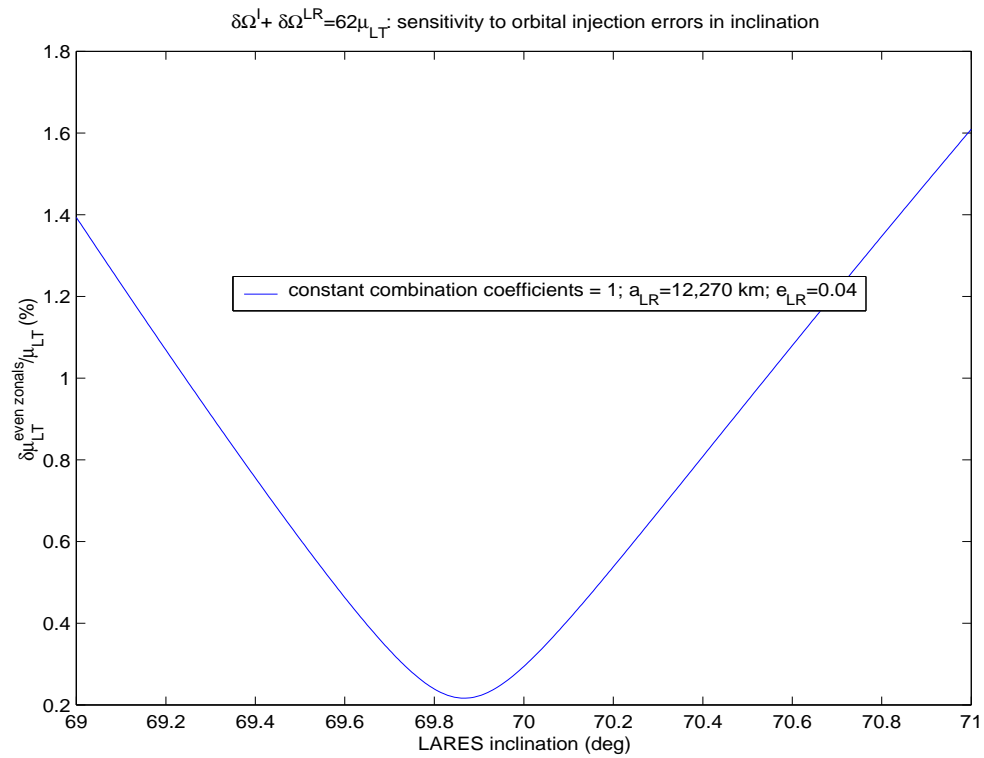


Figure 9.1: Influence of the injection errors in the LARES inclination on the zonals' error.

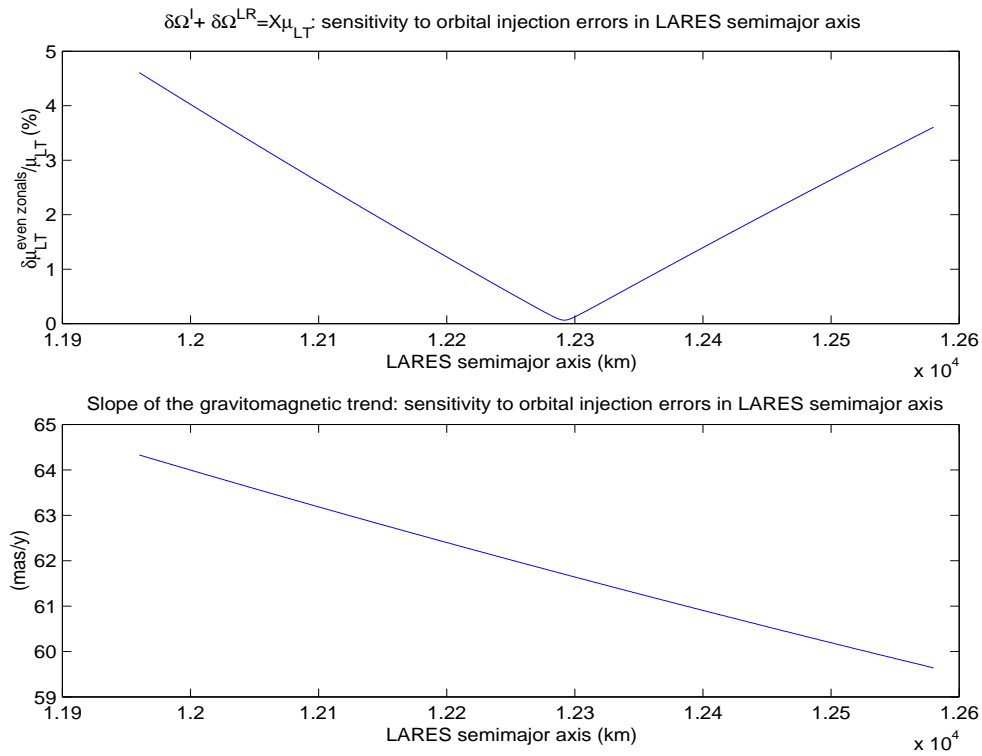


Figure 9.2: Influence of the injection errors in the LARES semimajor axis on the zonals' error.

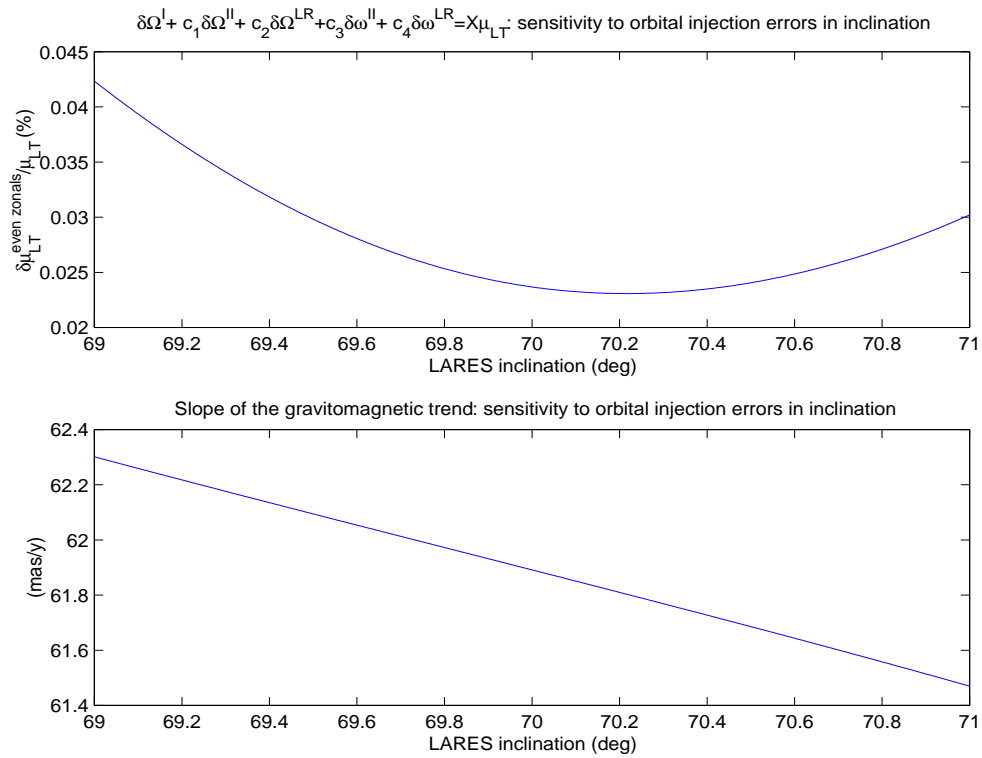


Figure 9.3: Alternative combined residuals: influence of the injection errors in the LARES inclination on the zonals' error.

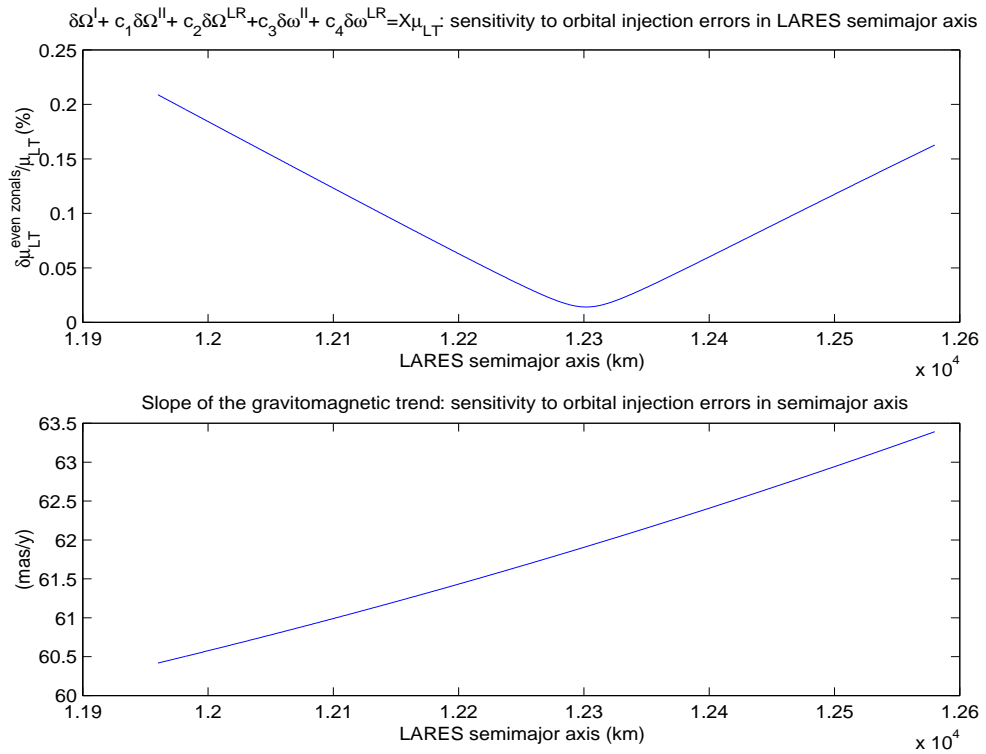


Figure 9.4: Alternative combined residuals: influence of the injection errors in the LARES semimajor axis on the zonals' error.

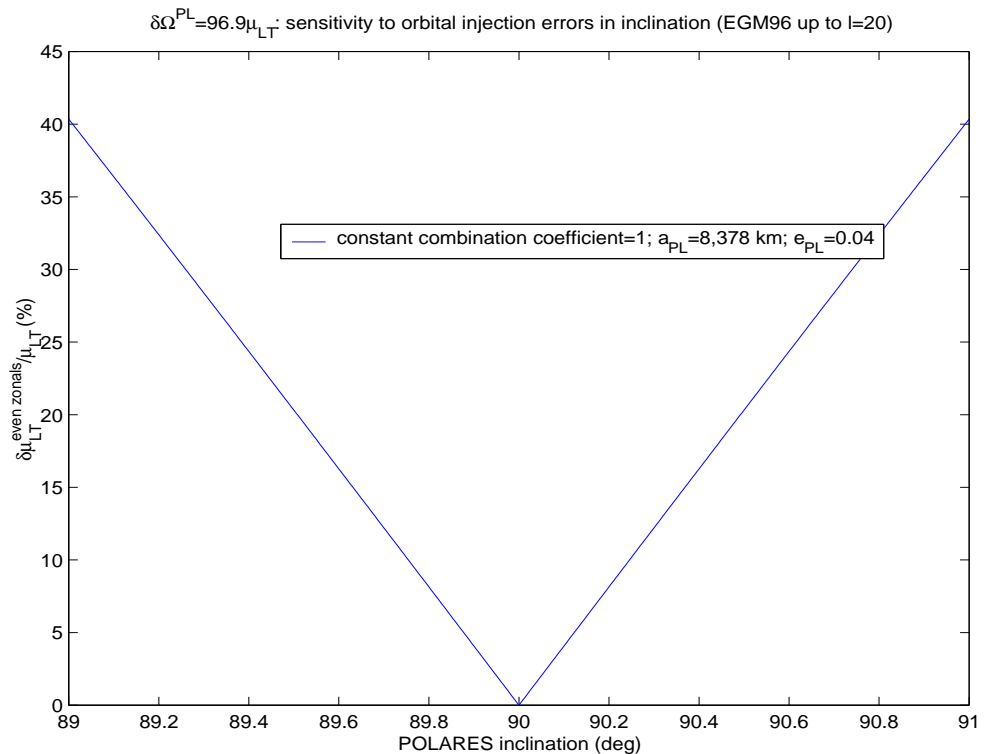


Figure 9.5: Influence of the injection errors in the POLARES inclination on the zonals' error of the node only.

Chapter 10

Conclusions and recommendations for future work

The general relativistic features considered in this work are:

- The gravitomagnetic LAGEOS experiment devoted to the measurement of the Lense-Thirring drag of inertial frames, currently carried on by analyzing the combined residuals of the nodes of LAGEOS and LAGEOS II and the perigee of LAGEOS II. The role of the proposed LARES in a new context is also taken into account
- The gravitomagnetic clock effect experiment whose feasibility in a space-based mission is, at present, under investigation by the scientific community
- The pericenter shift of a test particle due to the Schwarzschild's gravitoelectric part of the gravitational field of a central, static body and the possibility of measuring it at a 10^{-3} level in the field of the Earth with LAGEOS, LAGEOS II, and, perhaps, other SLR satellites

10.1 Summary of the obtained results

These effects, can be thought as consequences of post-Newtonian corrections of order $\mathcal{O}(c^{-2})$ to the main central Newtonian monopole acceleration so that they can be treated as classical perturbations in a flat spacetime. Concerning the gravitomagnetic

effects, in such an approximation the equations of motion of a test particle look like those of an electrically charged particle acted upon by the Lorentz force.

- In this spirit in chapter 2 we have derived the Lense-Thirring effect on the Keplerian elements of a test particle in the field of a central spherical body. The well known Lense-Thirring formulas for the gravitomagnetic rates of the node and the pericenter has been obtained. The approach followed here has allowed for working out the corrections induced by departures from sphericity of the central body as well. It has turned out that, for an axially symmetric body, it yields small additive rates for the node and the pericenter, but, in the case of the LAGEOS experiment, they are too small to be detected.

Detecting the Lense-Thirring drag of inertial frames and the gravitomagnetic clock effect in the weak field of the Earth by means of space-based missions is very difficult because of lots of other competing forces which are much more larger than the relativistic signals. So, when such an experiment is carried out or planned it is of the utmost importance to assess as more reliably as possible the error budget in order to have a reliable estimate of the uncertainty in the obtained or expected results. In such kind of measurements the major source of uncertainty is not represented by the statistical, formal error but by the systematic errors arising from the mismodelling in the various gravitational and non-gravitational other forces of the terrestrial space environment which may alias the detection of the relativistic effects of interest.

Concerning the Lense-Thirring effect, whose observable in the LAGEOS experiment is a linear trend with a slope of 60.2 mas/y, the systematic errors fall in two main categories. The first one is represented by the mismodelling in the classical nodal and apsidal precessions due to the errors in the spherical harmonics in terms of which the terrestrial gravitational field is expanded, especially the higher degree even zonal coefficients J_6, J_8, \dots not cancelled out by the combination of residuals. They induce an aliasing trend whose impact on the measurement of the Lense-Thirring signal is 12.92% by using the most recent Earth's gravity model EGM96. There are other secular mismodelled effects of non-gravitational origin, but they are far less relevant. The other category is represented by the periodic mismodelled signals like the solid Earth and ocean orbital tidal perturbations and the solar radiation pressure perturbations.

- In chapter 3 we have worked out in great detail the orbital perturbations due to the solid and ocean Earth tides on the Keplerian elements of LAGEOS and LAGEOS II. Our goal was to determine those perturbations whose periods and amplitudes are very large and which, consequently, could induce relevant bias in the determination of the Lense-Thirring trend over time spans some years long. The perigee of LAGEOS II has turned out to be very sensitive to the $l = 3$ ocean tidal perturbations.

- In chapter 4 we have analyzed in detail the impact of the tidal errors in the LAGEOS' orbital elements involved by simulating with MATLAB the combined residuals and analyzing the results with different approaches. According to our results, they affect the gravitomagnetic trend at a 4.2% level over 4 years and 2-1.5% over 7 years. Another source of systematic error which has been investigated in chapter 4 by using the results obtained in chapter 3 for the tidal perturbations is the mismodelling in the inclinations of both LAGEOS. Its impact amounts to almost 3.8% over 4 years and 1.5% over 8 years.

- The analogy with the electromagnetic case has been exploited in deriving in a simple and more intuitive way the gravitomagnetic clock effect in chapter 5. A system of two point charged test particles following counter-orbiting circular paths in the equatorial plane of a central, spherical charged body has been considered. Subsequently, a magnetic field orthogonal to the orbital plane has been switched on. It has induced a time shift in the orbital periods of the two charges which is completely analogous to the gravitomagnetic time difference in the general relativistic weak-field and slow-motion approximation: indeed, the expressions obtained here differ from the fully general relativistic difference in the proper times by terms of order $\mathcal{O}(c^{-4})$.

- Regarding the gravitomagnetic clock effect, we have analyzed in chapter 6 and 7 the systematic errors in the radial and the azimuthal positions induced by various gravitational and non-gravitational perturbing forces. It turns out that, with certain assumptions on the kind of satellites to be used, the errors due to the non-gravitational perturbations should remain within the limits $\delta r \sim 10^{-2}$ cm and $\delta\phi \sim 10^{-2}$ mas per revolution which would make the measurement of the gravitomagnetic clock effect feasible. Such result holds for short orbital arcs so to avoid the effects of the eclipses and the possible consequences of the satellite's spin axis motion. However, the major

problems would arise from the gravitational perturbations. For example, the uncertainty in the GM value of the Earth would induce an error of 1.2 mas per revolution in the azimuthal position. Moreover, the errors in tides and geopotential would affect the satellites' orbits to a level which rules out the possibility of detecting the gravitomagnetic effect. Since many of these mismodelled perturbations are periodic it would be possible to overcome the impact of their errors by adopting time spans sufficiently long to average them out. Unfortunately, many of such perturbations are secular or semisecular, so that it would be necessary to adopt orbital arcs of some years in order to cancel out their effects.

- As an example of the level of maturity reached by the SLR technique and of its opportunities in the field of fundamental research, we have sketched in chapter 8 a possible use of the laser-ranged data to some existing geodetic satellites, with particular emphasis to LAGEOS and LAGEOS II, in measuring accurately in the field of the Earth a suitable combination of the Post Newtonian parameters β and γ . Such combination is sensible to the gravitoelectric shift of the pericenter of a test particle. For it, to date, there exist only the well known classical measurements in the field of the Sun of the Mercury's perihelion precession; their relative accuracy amounts to $10^{-2} - 10^{-3}$. By considering a suitable combination of orbital residuals of LAGEOS and LAGEOS II, and following an approach similar to that employed in the gravitomagnetic LAGEOS experiment, it should be possible to reach a relative accuracy level of about 8×10^{-3} over 8 years in the field of the Earth as well. By using other residual combinations it would be possible to reach the 10^{-4} level. Such estimates account for a detailed analysis of the systematic errors and are based on the present level of our knowledge of the terrestrial gravitational field summarized by EGM96 model. The main source of error is the aliasing trend induced by the mismodelling in the classical nodal and apsidal precessions due to the even zonal harmonics of the geopotential. The new data on the Earth gravity field from the CHAMP and GRACE missions, which will be available in the near future, will allow for a great improvement in the precision of this measurement.
- In the original LARES mission the Lense-Thirring effect would be detected by using as observable the sum of the residuals of the nodes of the existing LAGEOS

satellite and of its twin LARES. The proposed nominal orbital configuration of LARES would reduce the systematic error due to the mismodelling in the even zonal harmonics of the geopotential, which is the most important source of error, to 0.3%, according to the most recent Earth gravity model EGM96. Unfortunately, as shown in chapter 9, this observable turns out to be rather sensitive to the unavoidable departures of the LARES orbital parameters from their nominal values due to the orbital injection errors. By adopting a suitable combination of the orbital residuals of the nodes of LAGEOS, LAGEOS II and LARES and perigees of LAGEOS II and LARES it would be possible to reduce the error due to the geopotential to 0.02%. Moreover, the sensitivity to the injection errors would be greatly reduced. In view of near improvements in the time-dependent force models the total error could be reduced to less than 1%. The proposal of placing LARES in a polar 2,000 km altitude orbit should be rejected because even small departures from the polar geometry would yield large errors due to the mismodelled even zonal harmonics of the geopotential. Also this measurement could be improved with the CHAMP and GRACE data.

10.2 Recommendations for future work

It is very important to stress that in the near future, when the new and more precise data relative to the static and dynamical parts of the Earth's gravitational field from the CHAMP and GRACE missions will be available, it will be possible to reduce sensibly the uncertainties of many source of systematic errors. This is particularly true for the even zonal harmonics of the static part of the geopotential. It suffices to say that the CHAMP data should yield a covariance matrix for it two order of magnitude better than the present level. Regarding the gravitomagnetic LAGEOS experiment, this will allow one to reduce the total error from the present 12.9% to some percent. Moreover, the zonals error in the PPN measurement could reach the level of $10^{-4} - 10^{-5}$ according to the observable adopted. These improvements would extend also to the LARES project.

- So, it could be possible to proceed in the future by updating the orbit determination softwares like GEODYN II with the new data of the geopotential and,

subsequently, by reanalyzing the data of the gravitomagnetic LAGEOS experiment.

- In the framework of the gravitomagnetic LAGEOS experiment, it could be useful to look for alternative combinations of orbital residuals involving also other SLR satellites in order to reduce the systematic error due to the geopotential. It would be the follow-on of [*Casotto et al.*, 1990].
- Moreover, by exploiting the knowledge acquired with the gravitomagnetic experiment, it would be possible to implement the PPN measurement with LAGEOS as well. In this context, it should be necessary to extend the analysis of the error budget to the other scenarios proposed for such experiment, with particular emphasis to the orbital perturbations of Ajisai SLR satellite which turns out to be the most suited non-LAGEOS satellite to be employed in these measurements together with LAGEOS and LAGEOS II.
- Another possible line of action could be the search for other post-Newtonian phenomena, parameterized with other combinations of PPN parameters, which could be measured with high accuracy in the field of the Earth with SLR technique.
- From another hand, the results obtained here about the tidal orbital perturbations could be employed by performing a set of simulations with GEODYN II in order to demonstrate the capability of the strategy followed until now to recover the Lense-Thirring trend. In such simulations the value of the Lense-Thirring parameter μ_{LT} would be varied randomly from, say, -2 to +2. For a given value of μ_{LT} randomly chosen, by varying suitably in the force models the parameters of such disturbing forces which turned out to be more effective in affecting the Lense-Thirring signal it should be possible to reobtain the a priori chosen value of μ_{LT} . This approach could be followed with the present force models of GEODYN II.
- In view of the near improvements in the force models due to the CHAMP and GRACE missions it would be helpful to update the error budget of the LARES mission, especially as far as the gravitational tidal perturbations are concerned, and to extend it to the alternative configuration presented here.

Appendix A

The classical precessions of the node and the perigee

Here we show the explicitly calculated coefficients

$$\dot{\Omega}_{.2n} \equiv \frac{\partial \dot{\Omega}_{\text{class}}}{\partial (J_{2n})} \quad (A.1)$$

and

$$\dot{\omega}_{.2n} \equiv \frac{\partial \dot{\omega}_{\text{class}}}{\partial (J_{2n})} \quad (A.2)$$

of the satellites' classical nodal and apsidal precessions due to the even ($l = 2n$, $n = 1, 2, 3\dots$) zonal ($m = 0$) harmonics of the geopotential up to $l = 20$. Recall that $J_l \equiv -C_{l0}$, $l = 2n$, $n = 1, 2, 3\dots$ where the unnormalized adimensional Stokes coefficients C_{lm} of degree l and order m can be obtained from the normalized \bar{C}_{lm} with

$$C_{lm} = N_{lm} \bar{C}_{lm}. \quad (A.3)$$

In it

$$N_{lm} = \left[\frac{(2l+1)(2-\delta_{0m})(l-m)!}{(l+m)!} \right]^{\frac{1}{2}}. \quad (A.4)$$

For the general expression of the classical rates of the near Earth satellites' Keplerian orbital elements due to the geopotential \dot{a}_{class} , \dot{e}_{class} , \dot{i}_{class} , $\dot{\Omega}_{\text{class}}$, $\dot{\omega}_{\text{class}}$, \dot{M}_{class} , see [Kaula, 1966]. The coefficients $\dot{\Omega}_{.2n}$ and $\dot{\omega}_{.2n}$ are of crucial importance in the evaluation of the systematic error due to the mismodelled even zonal harmonics of the geopotential; moreover, they enter the combined residuals' coefficients c_i , $i = 1, 2\dots N$ of chapter 8 and chapter 9. See also [Ciufolini, 1996] and Appendix B. Since the

general relativistic effects investigated are secular perturbations, we have considered only the perturbations averaged over one satellite's orbital period. This has been accomplished with the condition $l - 2p + q = 0$. Since the eccentricity functions G_{lpq} are proportional to $e^{|q|}$, for a given value of l we have considered only those values of p which fulfil the condition $l - 2p + q = 0$ with $q = 0$, i.e. $p = \frac{l}{2}$. This implies that in the summations

$$\sum_{p=0}^l \frac{dF_{l0p}}{di} \sum_{q=-\infty}^{+\infty} G_{lpq} \quad (A.5)$$

and

$$\sum_{p=0}^l F_{l0p} \sum_{q=-\infty}^{+\infty} \frac{dG_{lpq}}{de} \quad (A.6)$$

involved in the expressions of the classical rates we have considered only $F_{l0\frac{l}{2}}$ and $G_{l\frac{l}{2}0}$. Moreover, in working out the $G_{l\frac{l}{2}0}$ we have neglected the terms of order $\mathcal{O}(e^k)$ with $k > 2$.

A.1 The nodal coefficients

The nodal coefficients, proportional to

$$\frac{1}{\sin i} \sum_{q=-\infty}^{+\infty} G_{lpq} \sum_{p=0}^l \frac{dF_{lmp}}{di}, \quad (A.7)$$

are

$$\dot{\Omega}_{.2} = -\frac{3}{2}n \left(\frac{R}{a}\right)^2 \frac{\cos i}{(1-e^2)^2}, \quad (A.8)$$

$$\dot{\Omega}_{.4} = \dot{\Omega}_{.2} \left[\frac{5}{8} \left(\frac{R}{a}\right)^2 \frac{(1+\frac{3}{2}e^2)}{(1-e^2)^2} (7\sin^2 i - 4) \right], \quad (A.9)$$

$$\dot{\Omega}_{.6} = \dot{\Omega}_{.2} \left[\frac{35}{8} \left(\frac{R}{a}\right)^4 \frac{(1+5e^2)}{(1-e^2)^4} \left(\frac{33}{8} \sin^4 i - \frac{9}{2} \sin^2 i + 1 \right) \right], \quad (A.10)$$

$$\dot{\Omega}_{.8} = \dot{\Omega}_{.2} \left[\frac{105}{16} \left(\frac{R}{a}\right)^6 \frac{(1+\frac{21}{2}e^2)}{(1-e^2)^6} \left(\frac{715}{64} \sin^6 i - \frac{143}{8} \sin^4 i + \frac{33}{4} \sin^2 i - 1 \right) \right], \quad (A.11)$$

$$\dot{\Omega}_{.10} = \dot{\Omega}_{.2} \left[\frac{1,155}{128} \left(\frac{R}{a}\right)^8 \frac{(1+18e^2)}{(1-e^2)^8} \left(\frac{4,199}{128} \sin^8 i - \frac{1,105}{16} \sin^6 i \right) \right]$$

$$+ \left. \frac{195}{4} \sin^4 i - 13 \sin^2 i + 1 \right) \Big] , \quad (A.12)$$

$$\begin{aligned} \dot{\Omega}_{12} = & \dot{\Omega}_{.2} \left[\frac{3,003}{256} \left(\frac{R}{a} \right)^{10} \frac{(1 + \frac{55}{2}e^2)}{(1 - e^2)^{10}} \left(\frac{52,003}{512} \sin^{10} i - \frac{33,915}{128} \sin^8 i \right. \right. \\ & \left. \left. + \frac{8,075}{32} \sin^6 i - \frac{425}{4} \sin^4 i + \frac{75}{4} \sin^2 i - 1 \right) \right] , \end{aligned} \quad (A.13)$$

$$\begin{aligned} \dot{\Omega}_{14} = & \dot{\Omega}_{.2} \left[\frac{15,015}{1,024} \left(\frac{R}{a} \right)^{12} \frac{(1 + \frac{91}{2}e^2)}{(1 - e^2)^{12}} \left(\frac{334,305}{1,024} \sin^{12} i - \frac{260,015}{256} \sin^{10} i \right. \right. \\ & \left. \left. + \frac{156,009}{128} \sin^8 i - \frac{11,305}{16} \sin^6 i + \frac{1,615}{8} \sin^4 i - \frac{51}{2} \sin^2 i + 1 \right) \right] , \end{aligned} \quad (A.14)$$

$$\begin{aligned} \dot{\Omega}_{16} = & \dot{\Omega}_{.2} \left[\frac{36,465}{2,048} \left(\frac{R}{a} \right)^{14} \frac{(1 + \frac{105}{2}e^2)}{(1 - e^2)^{14}} \left(\frac{17,678,835}{16,384} \sin^{14} i - \frac{3,991,995}{1,024} \sin^{12} i \right. \right. \\ & \left. \left. + \frac{2,890,755}{512} \sin^{10} i - \frac{535,325}{128} \sin^8 i + \frac{107,065}{64} \sin^6 i \right. \right. \\ & \left. \left. - \frac{2,793}{8} \sin^4 i + \frac{133}{4} \sin^2 i - 1 \right) \right] , \end{aligned} \quad (A.15)$$

$$\begin{aligned} \dot{\Omega}_{18} = & \dot{\Omega}_{.2} \left[\frac{692,835}{32,768} \left(\frac{R}{a} \right)^{16} \frac{(1 + 68e^2)}{(1 - e^2)^{16}} \left(\frac{119,409,675}{32,768} \sin^{16} i - \frac{30,705,345}{2,048} \sin^{14} i \right. \right. \\ & \left. \left. + \frac{6,513,255}{256} \sin^{12} i - \frac{1,470,735}{64} \sin^{10} i + \frac{760,725}{64} \sin^8 i \right. \right. \\ & \left. \left. - \frac{28,175}{8} \sin^6 i + \frac{1,127}{2} \sin^4 i - 42 \sin^2 i + 1 \right) \right] , \end{aligned} \quad (A.16)$$

$$\begin{aligned} \dot{\Omega}_{20} = & \dot{\Omega}_{.2} \left[\frac{1,616,615}{65,536} \left(\frac{R}{a} \right)^{18} \frac{(1 + \frac{171}{2}e^2)}{(1 - e^2)^{18}} \left(\frac{1,641,030,105}{131,072} \sin^{18} i \right. \right. \\ & \left. \left. - \frac{1,893,496,275}{32,768} \sin^{16} i + \frac{460,580,175}{4,096} \sin^{14} i - \frac{30,705,345}{256} \sin^{12} i \right. \right. \\ & \left. \left. + \frac{19,539,765}{256} \sin^{10} i - \frac{1,890,945}{64} \sin^8 i + \frac{108,675}{16} \sin^6 i - \frac{1,725}{2} \sin^4 i \right) \right] , \end{aligned}$$

$$+ \left. \frac{207}{4} \sin^2 i - 1 \right) \Big] . \quad (A.17)$$

A.2 The perigee coefficients

The coefficients of the classical perigee precession are much more involved because they are proportional to

$$- \left(\frac{\cos i}{\sin i} \right) \sum_{q=-\infty}^{+\infty} G_{lpq} \sum_{p=0}^l \frac{dF_{lmp}}{di} + \frac{(1-e^2)}{e} \sum_{q=-\infty}^{+\infty} \frac{dG_{lpq}}{de} \sum_{p=0}^l F_{lmp}. \quad (A.18)$$

We can pose $\dot{\omega}_{.2n} = \dot{\omega}_{.2n}^a + \dot{\omega}_{.2n}^b$.

The first set is given by

$$\dot{\omega}_{.2}^a = \frac{3}{2} n \left(\frac{R}{a} \right)^2 \frac{\cos^2 i}{(1-e^2)^2}, \quad (A.19)$$

$$\dot{\omega}_{.4}^a = \dot{\omega}_{.2}^a \left[\frac{5}{8} \left(\frac{R}{a} \right)^2 \frac{(1+\frac{3}{2}e^2)}{(1-e^2)^2} (7 \sin^2 i - 4) \right], \quad (A.20)$$

$$\dot{\omega}_{.6}^a = \dot{\omega}_{.2}^a \left[\frac{35}{8} \left(\frac{R}{a} \right)^4 \frac{(1+5e^2)}{(1-e^2)^4} \left(\frac{33}{8} \sin^4 i - \frac{9}{2} \sin^2 i + 1 \right) \right], \quad (A.21)$$

$$\dot{\omega}_{.8}^a = \dot{\omega}_{.2}^a \left[\frac{105}{16} \left(\frac{R}{a} \right)^6 \frac{(1+\frac{21}{2}e^2)}{(1-e^2)^6} \left(\frac{715}{64} \sin^6 i - \frac{143}{8} \sin^4 i + \frac{33}{4} \sin^2 i - 1 \right) \right], \quad (A.22)$$

$$\begin{aligned} \dot{\omega}_{.10}^a &= \dot{\omega}_{.2}^a \left[\frac{1,155}{128} \left(\frac{R}{a} \right)^8 \frac{(1+18e^2)}{(1-e^2)^8} \left(\frac{4,199}{128} \sin^8 i - \frac{1,105}{16} \sin^6 i \right. \right. \\ &\quad \left. \left. + \frac{195}{4} \sin^4 i - 13 \sin^2 i + 1 \right) \right], \end{aligned} \quad (A.23)$$

$$\begin{aligned} \dot{\omega}_{.12}^a &= \dot{\omega}_{.2}^a \left[\frac{3,003}{256} \left(\frac{R}{a} \right)^{10} \frac{(1+\frac{55}{2}e^2)}{(1-e^2)^{10}} \left(\frac{52,003}{512} \sin^{10} i - \frac{33,915}{128} \sin^8 i \right. \right. \\ &\quad \left. \left. + \frac{8,075}{32} \sin^6 i - \frac{425}{4} \sin^4 i + \frac{75}{4} \sin^2 i - 1 \right) \right], \end{aligned} \quad (A.24)$$

$$\dot{\omega}_{.14}^a = \dot{\omega}_{.2}^a \left[\frac{15,015}{1,024} \left(\frac{R}{a} \right)^{12} \frac{(1+\frac{91}{2}e^2)}{(1-e^2)^{12}} \left(\frac{334,305}{1,024} \sin^{12} i - \frac{260,015}{256} \sin^{10} i \right. \right. \quad (A.25)$$

$$+ \left. \frac{156,009}{128} \sin^8 i - \frac{11,305}{16} \sin^6 i + \frac{1,615}{8} \sin^4 i - \frac{51}{2} \sin^2 i + 1 \right) \Big], \quad (A.25)$$

$$\begin{aligned} \dot{\omega}_{.16}^a &= \dot{\omega}_{.2}^a \left[\frac{36,465}{2,048} \left(\frac{R}{a} \right)^{14} \frac{(1 + \frac{105}{2}e^2)}{(1 - e^2)^{14}} \left(\frac{17,678,835}{16,384} \sin^{14} i - \frac{3,991,995}{1,024} \sin^{12} i \right. \right. \\ &+ \left. \frac{2,890,755}{512} \sin^{10} i - \frac{535,325}{128} \sin^8 i + \frac{107,065}{64} \sin^6 i \right. \\ &\left. - \left. \frac{2,793}{8} \sin^4 i + \frac{133}{4} \sin^2 i - 1 \right) \right], \end{aligned} \quad (A.26)$$

$$\begin{aligned} \dot{\omega}_{.18}^a &= \dot{\omega}_{.2}^a \left[\frac{692,835}{32,768} \left(\frac{R}{a} \right)^{16} \frac{(1 + 68e^2)}{(1 - e^2)^{16}} \left(\frac{119,409,675}{32,768} \sin^{16} i - \frac{30,705,345}{2,048} \sin^{14} i \right. \right. \\ &+ \left. \frac{6,513,255}{256} \sin^{12} i - \frac{1,470,735}{64} \sin^{10} i + \frac{760,725}{64} \sin^8 i \right. \\ &\left. - \left. \frac{28,175}{8} \sin^6 i + \frac{1,127}{2} \sin^4 i - 42 \sin^2 i + 1 \right) \right], \end{aligned} \quad (A.27)$$

$$\begin{aligned} \dot{\omega}_{.20}^a &= \dot{\omega}_{.2}^a \left[\frac{1,616,615}{65,536} \left(\frac{R}{a} \right)^{18} \frac{(1 + \frac{171}{2}e^2)}{(1 - e^2)^{18}} \left(\frac{1,641,030,105}{131,072} \sin^{18} i \right. \right. \\ &- \left. \frac{1,893,496,275}{32,768} \sin^{16} i + \frac{460,580,175}{4,096} \sin^{14} i - \frac{30,705,345}{256} \sin^{12} i \right. \\ &+ \left. \frac{19,539,765}{256} \sin^{10} i - \frac{1,890,945}{64} \sin^8 i + \frac{108,675}{16} \sin^6 i - \frac{1,725}{2} \sin^4 i \right. \\ &+ \left. \left. \frac{207}{4} \sin^2 i - 1 \right) \right]. \end{aligned} \quad (A.28)$$

The second set is given by

$$w_{.2} = -\frac{3}{2}n \left(\frac{R}{a} \right)^2, \quad (A.29)$$

$$\dot{\omega}_{.2}^b = w_{.2} \left\{ \left[\frac{1}{(1 - e^2)^2} \right] \left(\frac{3}{2} \sin^2 i - 1 \right) \right\}, \quad (A.30)$$

$$\dot{\omega}_{.4}^b = w_{.2} \left\{ \frac{5}{8} \left(\frac{R}{a} \right)^2 \left[\frac{3}{(1 - e^2)^3} + 7 \frac{(1 + \frac{3}{2}e^2)}{(1 - e^2)^4} \right] \left(\frac{7}{4} \sin^4 i - 2 \sin^2 i + \frac{2}{5} \right) \right\}, \quad (A.31)$$

$$\begin{aligned}
\dot{\omega}_{.6}^b &= w_{.2} \left\{ \frac{35}{8} \left(\frac{R}{a} \right)^4 \left[\frac{10}{(1-e^2)^5} + 11 \frac{(1+5e^2)}{(1-e^2)^6} \right] \left(\frac{33}{48} \sin^6 i \right. \right. \\
&\quad \left. \left. - \frac{9}{8} \sin^4 i + \frac{1}{2} \sin^2 i - \frac{1}{21} \right) \right\}, \tag{A.32}
\end{aligned}$$

$$\begin{aligned}
\dot{\omega}_{.8}^b &= w_{.2} \left\{ \frac{105}{16} \left(\frac{R}{a} \right)^6 \left[\frac{21}{(1-e^2)^7} + 15 \frac{(1+\frac{21}{2}e^2)}{(1-e^2)^8} \right] \left(\frac{715}{512} \sin^8 i \right. \right. \\
&\quad \left. \left. - \frac{143}{48} \sin^6 i + \frac{33}{16} \sin^4 i - \frac{1}{2} \sin^2 i + \frac{1}{36} \right) \right\}, \tag{A.33}
\end{aligned}$$

$$\begin{aligned}
\dot{\omega}_{.10}^b &= w_{.2} \left\{ \frac{1,155}{128} \left(\frac{R}{a} \right)^8 \left[\frac{36}{(1-e^2)^9} + 19 \frac{(1+18e^2)}{(1-e^2)^{10}} \right] \left(\frac{4,199}{1,280} \sin^{10} i \right. \right. \\
&\quad \left. \left. - \frac{1,105}{128} \sin^8 i + \frac{195}{24} \sin^6 i - \frac{13}{4} \sin^4 i + \frac{1}{2} \sin^2 i - \frac{1}{55} \right) \right\}, \tag{A.34}
\end{aligned}$$

$$\begin{aligned}
\dot{\omega}_{.12}^b &= w_{.2} \left\{ \frac{3,003}{256} \left(\frac{R}{a} \right)^{10} \left[\frac{55}{(1-e^2)^{11}} + 23 \frac{(1+\frac{55}{2}e^2)}{(1-e^2)^{12}} \right] \left(\frac{52,003}{6,144} \sin^{12} i \right. \right. \\
&\quad \left. \left. - \frac{6,783}{256} \sin^{10} i + \frac{8,075}{256} \sin^8 i - \frac{425}{24} \sin^6 i + \frac{75}{16} \sin^4 i \right. \right. \\
&\quad \left. \left. - \frac{1}{2} \sin^2 i + \frac{1}{78} \right) \right\}, \tag{A.35}
\end{aligned}$$

$$\begin{aligned}
\dot{\omega}_{.14}^b &= w_{.2} \left\{ \frac{15,015}{1,024} \left(\frac{R}{a} \right)^{12} \left[\frac{91}{(1-e^2)^{13}} + 27 \frac{(1+\frac{91}{2}e^2)}{(1-e^2)^{14}} \right] \left(\frac{334,305}{14,336} \sin^{14} i \right. \right. \\
&\quad \left. \left. - \frac{260,015}{3,072} \sin^{12} i + \frac{156,009}{1,280} \sin^{10} i - \frac{11,305}{128} \sin^8 i + \frac{1,615}{48} \sin^6 i \right. \right. \\
&\quad \left. \left. - \frac{51}{8} \sin^4 i + \frac{1}{2} \sin^2 i - \frac{1}{105} \right) \right\}, \tag{A.36}
\end{aligned}$$

$$\begin{aligned}
\dot{\omega}_{.16}^b &= w_{.2} \left\{ \frac{36,465}{2,048} \left(\frac{R}{a} \right)^{14} \left[\frac{105}{(1-e^2)^{15}} + 31 \frac{(1+\frac{105}{2}e^2)}{(1-e^2)^{16}} \right] \left(\frac{17,678,835}{262,144} \sin^{16} i \right. \right. \\
&\quad \left. \left. - \frac{570,285}{2,048} \sin^{14} i + \frac{963,585}{2,048} \sin^{12} i - \frac{107,065}{256} \sin^{10} i + \frac{107,065}{512} \sin^8 i \right) \right\}
\end{aligned}$$

$$- \left. \frac{931}{16} \sin^6 i + \frac{133}{16} \sin^4 i - \frac{1}{2} \sin^2 i + \frac{1}{136} \right) \} , \quad (A.37)$$

$$\begin{aligned} \dot{\omega}_{.18}^b &= w_{.2} \left\{ \frac{692,835}{32,768} \left(\frac{R}{a} \right)^{16} \left[\frac{136}{(1-e^2)^{17}} + 35 \frac{(1+68e^2)}{(1-e^2)^{18}} \right] \left(\frac{39,803,225}{196,608} \sin^{18} i \right. \right. \\ &- \left. \frac{30,705,345}{32,768} \sin^{16} i + \frac{930,465}{512} \sin^{14} i - \frac{490,245}{256} \sin^{12} i + \frac{152,145}{128} \sin^{10} i \right. \\ &- \left. \left. \frac{28,175}{64} \sin^8 i + \frac{1,127}{12} \sin^6 i - \frac{21}{2} \sin^4 i + \frac{1}{2} \sin^2 i - \frac{1}{171} \right) \right\} , \quad (A.38) \end{aligned}$$

$$\begin{aligned} \dot{\omega}_{.20}^b &= w_{.2} \left\{ \frac{1,616,615}{65,536} \left(\frac{R}{a} \right)^{18} \left[\frac{171}{(1-e^2)^{19}} + 39 \frac{(1+\frac{171}{2}e^2)}{(1-e^2)^{20}} \right] \left(\frac{328,206,021}{524,288} \sin^{20} i \right. \right. \\ &- \left. \frac{210,388,475}{65,536} \sin^{18} i + \frac{460,580,175}{65,536} \sin^{16} i - \frac{30,705,345}{3,584} \sin^{14} i \right. \\ &+ \left. \frac{6,513,255}{1,024} \sin^{12} i - \frac{378,189}{128} \sin^{10} i + \frac{108,675}{128} \sin^8 i \right. \\ &- \left. \left. \frac{575}{4} \sin^6 i + \frac{207}{16} \sin^4 i - \frac{1}{2} \sin^2 i + \frac{1}{210} \right) \right\} . \quad (A.39) \end{aligned}$$

A.3 The mismodelled classical precessions of the SLR satellites

The results obtained in the previous sections can be used in working out explicitly the contributions of the mismodelled classical nodal and apsidal precessions up to degree $l = 20$ of the existing spherical passive laser-ranged geodetic satellites and of LARES. They are of the form $\delta\dot{\Omega}_{(2n)} = \dot{\Omega}_{.2n} \times \delta J_{2n}$, $n = 1, 2, \dots, 10$ and $\delta\dot{\omega}_{(2n)} = \dot{\omega}_{.2n} \times \delta J_{2n}$, $n = 1, 2, \dots, 10$. The coefficients $\dot{\Omega}_{.2n}$ and $\dot{\omega}_{.2n}$ are worked out in section A.2 and the values employed for $\delta J_{2n} = \sqrt{4n+1} \times \delta \bar{C}_{2n,0}$, $n = 1, 2, \dots, 10$ are those quoted in EGM96 model.

In Tab. A.3 we quote the orbital parameters of the other spherical passive geodetic laser-ranged satellites: Ajisai, Stella, Starlette, WESTPAC1, ETALON1 and ETALON2. It is worth noting that the perigees of many of them, except for Starlette, cannot be

Table A.1: Mismodelled classical nodal precessions $|\delta\dot{\Omega}_{(2n)}|$ and predicted Lense-Thirring nodal precessions $\dot{\Omega}_{LT}$ of the existing spherical passive geodetic laser-ranged satellites and of LARES. L1=LAGEOS, L2=LAGEOS II, LR=LARES, Aj=Ajisai, Stl=Stella, Str=Starlette, WS=WESTPAC1, E1=ETALON1, E2=ETALON2. All the values are in mas/y.

$2n$	L1	L2	LR	Aj	Stl	Str	WS	E1	E2
2	33.4	61	33.4	296.8	94.6	382.3	87.1	3.2	3.1
4	48.3	17.4	48.7	51.5	519	59.5	479.2	0.8	0.8
6	17	26.1	17.3	809.7	912.2	1,397.7	847.9	0.03	0.03
8	1.9	10.3	2	366.3	1,487.2	674.4	1,399.7	0.005	0.004
10	2.1	3.1	2.2	823.5	1,855	1,933.4	1,781.8	0.001	$\mathcal{O}(10^{-4})$
12	1.6	2.5	1.7	647.5	2,144.6	1,636.4	2,126.6	$\mathcal{O}(10^{-5})$	$\mathcal{O}(10^{-5})$
14	0.6	0.007	0.6	542.6	1,963.4	1,780.9	2,049.4	$\mathcal{O}(10^{-7})$	$\mathcal{O}(10^{-7})$
16	0.09	0.2	0.1	517.2	1,204.6	1,787.9	1,376.8	$\mathcal{O}(10^{-7})$	$\mathcal{O}(10^{-7})$
18	0.007	0.03	0.008	117.9	512.4	580	717	$\mathcal{O}(10^{-8})$	$\mathcal{O}(10^{-8})$
20	0.01	0.01	0.01	247.6	79.5	1,177	309	$\mathcal{O}(10^{-10})$	$\mathcal{O}(10^{-9})$
$\dot{\Omega}_{LT}$	30.7	31.6	30.8	116.7	152.8	144.4	151.5	3.4	3.4

Table A.2: Mismodelled classical perigee precessions $|\delta\dot{\omega}_{(2n)}|$ and predicted Lense-Thirring perigee precessions $\dot{\omega}_{LT}$ of the existing spherical passive geodetic laser-ranged satellites and of LARES. L1=LAGEOS, L2=LAGEOS II, LR=LARES, Aj=Ajisai, Stl=Stella, Str=Starlette, WS=WESTPAC1, E1=ETALON1, E2=ETALON2. All the values are in mas/y.

$2n$	L1	L2	LR	Aj	Stl	Str	WS	E1	E2
2	20.2	42.3	20.3	246	280.9	320.7	282.9	0.3	0.5
4	17.5	122.7	17.6	1,306	1,354.7	1,924.4	1,395.2	1	1
6	48.5	18.2	49.2	197.7	1,833.9	429.1	2,001.2	0.2	0.2
8	41.9	43.1	42.6	3,204.2	1,656.5	6,355.8	2,166.8	0.03	0.03
10	17.5	19.5	18	1,374.1	344.8	2,805.1	707.4	$\mathcal{O}(-5)$	$\mathcal{O}(-4)$
12	2.9	5.3	3	4,017.3	4,503.1	10,862.2	2,627.9	$\mathcal{O}(-4)$	$\mathcal{O}(-4)$
14	1.9	6.2	2	3,759.6	11,217.4	10,774.7	8,341.3	$\mathcal{O}(-5)$	$\mathcal{O}(-5)$
16	1.2	0.2	1.3	2,216.2	12,651.8	8,395.8	10,288.4	$\mathcal{O}(-6)$	$\mathcal{O}(-6)$
18	0.4	0.4	0.4	2,324.6	12,244.5	9,086.4	10,557.4	$\mathcal{O}(-8)$	$\mathcal{O}(-8)$
20	0.07	0.1	0.08	510.5	11,961.1	3,043.3	10,880	$\mathcal{O}(-8)$	$\mathcal{O}(-8)$
$\dot{\omega}_{LT}$	31.5	-57.5	-31.6	-225	68.5	-279.7	63.3	-4.3	-4.2

employed for any relativistic tests due to the notable smallness of their eccentricities.

Table A.3: Orbital parameters of the other existing spherical passive geodetic laser-ranged satellites. a is in km, i in deg and n in s^{-1} .

	Ajisai	Stella	Starlette	WESTPAC1	ETALON1	ETALON2
a	7,870	7,193	7,331	7,213	25,498	25,498
e	0.001	0	0.0204	0	0.00061	0.00066
i	50	98.6	49.8	98	64.9	65.5
n	9.05×10^{-4}	1.03×10^{-3}	1×10^{-3}	1.03×10^{-3}	1.58×10^{-4}	1.58×10^{-4}

Appendix B

The systematic zonal error

Here we expose how to calculate the systematic error due to the mismodelled even zonal harmonics of the geopotential for the combinations involving the residuals of the nodes and the perigees of various satellites.

In general, if we have an observable q which is a function $q = q(x_j)$, $j = 1, 2 \dots M$ of M correlated parameters x_j the error in it is given by

$$\delta q = \left[\sum_{j=1}^M \left(\frac{\partial q}{\partial x_j} \right)^2 \sigma_j^2 + 2 \sum_{h \neq k=1}^M \left(\frac{\partial q}{\partial x_h} \right) \left(\frac{\partial q}{\partial x_k} \right) \sigma_{hk}^2 \right]^{\frac{1}{2}} \quad (B.1)$$

in which $\sigma_j^2 \equiv C_{jj}$ and $\sigma_{hk}^2 \equiv C_{hk}$ where $\{C_{hk}\}$ is the $M \times M$ square matrix of covariance of the parameters x_j .

In our case the observable q is any residuals' combination

$$q = \sum_{i=1}^N c_i f_i(x_j), \quad j = 1, 2 \dots 10, \quad (B.2)$$

where x_j , $j = 1, 2 \dots 10$ are the first ten even zonal geopotential's coefficients $J_2, J_4 \dots J_{20}$, the f_i , $i = 1, 2 \dots N$ are the residuals of the precessions of the nodes $\delta\dot{\Omega}$ and the perigee $\delta\dot{\omega}$, the c_i , $i = 1, 2 \dots N$ are the coefficients of the residuals entering the combinations, and N is the number of orbital nodal or apsidal residuals entering the combination. Recall that the coefficients c_i may be either constant or depend on the orbital elements of the satellites entering the combinations through the coefficients $\dot{\Omega}_{2n}$ and $\dot{\omega}_{2n}$ worked out in Appendix A. Since

$$\frac{\partial q}{\partial x_j} = \sum_{i=1}^N c_i \frac{\partial f_i}{\partial x_j}, \quad j = 1, 2 \dots 10, \quad (B.3)$$

by putting eq. (B.3) in eq. (B.1) one obtains, in mas/y

$$\delta q = \left[\sum_{j=1}^{10} \left(\sum_{i=1}^N c_i \frac{\partial f_i}{\partial x_j} \right)^2 \sigma_j^2 + 2 \sum_{h \neq k=1}^{10} \left(\sum_{i=1}^N c_i \frac{\partial f_i}{\partial x_h} \right) \left(\sum_{i=1}^N c_i \frac{\partial f_i}{\partial x_k} \right) \sigma_{hk}^2 \right]^{\frac{1}{2}}. \quad (B.4)$$

The covariance matrix is that of EGM96. The percent error, for a given general relativistic trend and for a given combination, is obtained by taking the ratio of eq. (B.4) to the slope in mas/y of the general relativistic trend for the residual combination considered.

The validity of eq. (B.4) has been checked by calculating with it the systematic error due to the even zonal harmonics of the geopotential of the gravitomagnetic LAGEOS experiment; indeed the result

$$\delta \mu_{LT} = 12.92\% \mu_{LT} \quad (B.5)$$

claimed in [*Ciufolini et al.*, 1998] has been obtained again.

Appendix C

Some useful parameters used in the text

The data employed for the terrestrial space environment and the LAGEOS satellites are in the following table. In it ε is the angle between the ecliptic and the equatorial plane, I_0 is the solar constant, \bar{A} is the mean Earth albedo, R_{\oplus} is the Earth mean equatorial radius, G is the Newtonian gravitational constant, GM_{\oplus} and $\delta(GM_{\oplus})$ are the Newtonian gravitational constant times the Earth's mass and its error according to IERS standard, J_2 , J_4 , δJ_2 and δJ_4 are the first two even zonal geopotential's coefficients and their errors according to EGM96, J_{\oplus} is the Earth's angular momentum, ω_{\oplus} is the mean Earth angular velocity.

a , e , i and n are the semimajor axis, the eccentricity, the inclination of the orbits and the mean motion of the satellite, respectively, P is the satellite's orbital period, $P[X]$ is the period of the Keplerian element X , r and m are the satellites' radius and mass, S/m is the satellite area-to-mass ratio, respectively, C_R is its reflectivity constant, ϵ is its IR emissivity, δ is its thermal lag angle, T_0 is the average temperature of its retroreflectors, ΔT is the temperature difference between the hotter and cooler poles of the retroreflectors, C_D is its drag coefficient, q is its electric charge.

The conversion factor from rad/s to mas/y is $1 \text{ rad/s} = 6.509 \times 10^{15} \text{ mas/y}$.

Table C.1: Earth's and LAGEOS parameters used in the text.

Parameter	Numerical value	Units
ε	23.44	deg
I_0	1.38×10^6	$\text{erg s}^{-1} \text{ cm}^2$
$\bar{\mathcal{A}}$	0.3	
R_{\oplus}	$6,378 \times 10^5$	cm
G	6.67259×10^{-8}	$\text{cm}^3 \text{ g}^{-1} \text{ s}^{-2}$
GM_{\oplus}	3.986×10^{20}	$\text{cm}^3 \text{ s}^{-2}$
$\delta(GM_{\oplus})$	8×10^{11}	$\text{cm}^3 \text{ s}^{-2}$
J_2	1.0826×10^{-3}	-
J_4	-1.6194×10^{-6}	-
δJ_2	7.9626×10^{-11}	-
δJ_4	3.126×10^{-10}	-
J_{\oplus}	5.9×10^{40}	$\text{g cm}^2 \text{ s}^{-1}$
ω_{\oplus}	7.29×10^{-5}	rad s^{-1}
G/c^2	7.42×10^{-29}	cm g^{-1}
$(GJ_{\oplus})/c^2$	4.37×10^{12}	$\text{cm}^3 \text{ s}^{-1}$
$(GM_{\oplus})/c^2$	4.43×10^{-1}	cm
a_{LAGEOS}	1.2270×10^9	cm
$a_{\text{LAGEOS II}}$	1.2163×10^9	cm
a_{LARES}	1.2270×10^9	cm
e_{LAGEOS}	0.0045	-
$e_{\text{LAGEOS II}}$	0.014	-
e_{LARES}	0.04	-
i_{LAGEOS}	110	deg
$i_{\text{LAGEOS II}}$	52.65	deg
i_{LARES}	70	deg
n_{LAGEOS}	4.643×10^{-4}	s^{-1}
$n_{\text{LAGEOS II}}$	4.710×10^{-4}	s^{-1}
n_{LARES}	4.643×10^{-4}	s^{-1}
P_{LAGEOS}	1.353×10^4	s
$P_{\text{LAGEOS II}}$	1.334×10^4	s
$P[\Omega]_{\text{LAGEOS}}$	9.017×10^7	s
$P[\Omega]_{\text{LAGEOS II}}$	-4.917×10^7	s
$P[\omega]_{\text{LAGEOS}}$	-1.475×10^8	s
$P[\omega]_{\text{LAGEOS II}}$	7.100×10^7	s
r	30	cm
m	4.11×10^5	g
S/m	6.87×10^{-3}	$\text{cm}^2 \text{ g}^{-1}$
C_R	1.13	-
ϵ	0.4	-
δ	55	deg
T_0	316	K
ΔT	21	K
C_D	4.9	-
q	-3×10^{-11}	C

Acknowledgements

I am particularly grateful to L. Guerriero who supported me at Bari. I am profoundly indebted to I. Ciufolini, who directed my attention to the interesting field of gravitomagnetism. I wish to warmly thank E. C. Pavlis for his patience and helpful discussions and B. Mashhoon for the useful material supplied to me and for his kind attention to my researches. Special thanks also to F. Vespe and N. Cufaro-Petroni for their collaboration and help. Thanks also to R. Eanes, R. Ray, A. Sengoku, V. Dehant, H. Schuh, L. Petrov, F. Roosbeek, A. Paolozzi, D. Lucchesi. I am very grateful also to A. Refice and F. Bovenga for their help with software matters. I am glad to thank my family as well who lovely helped and supported me in this demanding work.

Bibliography

[*Adler and Silbergleit*, 2000] Adler, R. J., and A. S. Silbergleit, A General Treatment of Orbiting Gyroscope Precession, *Int. J. of Th. Phys.*, 39(5), 1291-1316, 2000.

[*Afonso et al.*, 1985] Afonso G., Barlier F., Berger C., Mignard F., Walch J.J., Re-assessment of the charge and neutral drag of LAGEOS and its geophysical implications, *J. Geophys. Res.*, 90, 9381-9398, 1985.

[*Afonso et al.*, 1989] Afonso G., Barlier F., Carpino M., Farinella P., Mignard F., Milani A., Nobili A. M., Orbital effects of LAGEOS seasons and eclipses, *Ann. Geophys.*, 7, 501-514, 1989.

[*Allison and Ashby*, 1993] Allison, T., and N. Ashby, Canonical planetary equations for velocity-dependent forces, and the Lense-Thirring precession, *Celest. Mech.*, 57, 537-585, 1993.

[*Anderson and Williams*, 2001] Anderson, J.D., and J.G. Williams, Long-range tests of the equivalence principle, *Class. and Quant. Grav.*, 18(13), 2447-2456, 2001.

[*Anselmo et al.*, 1983] Anselmo L., Farinella P., Milani A., Nobili A. M., Effect of the Earth-reflected Sunlight on the Orbit of the LAGEOS Satellite, *Astron. Astrophys.*, 117, 3-8, 1983.

[*Arnold*, 1983] Arnold, V. I., *Geometrical Methods in the Theory of Ordinary Differential Equations*, 334 pp., Springer Verlag, 1983.

[*Arnold*, 1989] V. I. Arnold, *Mathematical Methods of Classical Mechanics*, Springer Verlag, 1989.

[Balmino, 1974] Balmino, G., The Use of Artificial Satellites for Geodesy and Geodynamics, edited by G. Veis, National Technical University, Athens, 1974.

[Balogh et al., 2000] Balogh, et al., BepiColombo An Interdisciplinary Cornerstone Mission to the Planet Mercury, *ESA-SCI, 1*, pp. 21-24 and pp. 35-38, 2000.

[Bard, 1974] Bard, Y., 1974. *Nonlinear Parameter Estimation*, 341 pp., Academic Press, New York, 1974.

[Bertotti and Carpino, 1989] Bertotti, B., and M. Carpino, Supplementary satellites and tidal perturbations in *Measurement of the Gravitomagnetic Field Using a Pair of Laser Ranged Satellites*, ASI final report, pp. 105-121, Frascati, 1989.

[Bertotti and Farinella, 1990] Bertotti B., Farinella P., *Physics of the Earth and the Solar System*, Kluwer Academic Publishers, Dordrecht, 1990.

[Bretagnon and Francou, 1988] Bretagnon, P., and G. Francou, Planetary theories in rectangular and spherical variables, *Astron. Astrophys.*, *202*, 309-315, 1988.

[Buellesfeld, 1985] Buellesfeld, F. J., Ein Beitrag zur harmonischen Darstellung des gezeiterzeugenden Potentials, Deutsche Geodätische Kommission, Reihe C, Heft 314, München, Germany, 1985.

[Burns et al., 1979] Burns, J. A., P. L. Lamy, and S. Soter, Radiation forces on small particles in the solar system, *Icarus*, *40*, 1-48, 1979.

[Cacciani et al., 1989] Cacciani, A., et al., An experiment to measure the solar $l = 1$ rotational frequency splitting, in: Osaki, Y., and H. Shibahashi (Eds.) *Proc. Oji Int. Seminar on Progress of Seismology of the Sun and the Stars*, Hakone, Japan, 11-14 December 1989, Lecture Notes in Physics, 1989.

[Cartwright and Tayler, 1971] Cartwright, D. E., and R. J. Tayler, New computations of the tide generating potential, *Geophys. J. R. Astron. Soc.*, *23*, 45-74, 1971.

[Cartwright and Edden, 1973] Cartwright, D. E., and A. C. Edden, Corrected tables of tidal harmonics, *Geophys. J. R. Astron. Soc.*, *33*, 253-264, 1973.

[Cartwright, 2000] Cartwright, D. E., *Tides A Scientific History*, 292 pp., Cambridge, 2000.

[Casotto, 1989] Casotto, S., Ocean tide models for TOPEX precise orbit determination, Ph. D. thesis, The University of Texas, Austin, 1989.

[Casotto et al., 1990] Casotto, S, I. Ciufolini, F. Vespe, and G. Bianco, Earth satellites and Gravitomagnetic Field, *Il Nuovo Cimento*, 105B(5), 589-599, 1990.

[Chapront-Touzé, 1988] Chapront-Touzé, M., and J. Chapront, ELP2000-85: a semi-analytical lunar ephemeris adequate for historical times, *Astron. Astrophys.*, 190, 342-352, 1988.

[Cheng, 1995] Cheng, M. K., C. K. Shum and B. D. Tapley, Global constraint on the modeling of mass transport within the Earth system from long-term SLR observations, in *Proc. IUGG, XII General Assembly*, Boulder, Colorado, July 1995.

[Christodoulidis, 1978] Christodoulidis, D., Satellite Contributions to the Tidal Studies, 34 pp., Lehrstuhl für Astronomische und Physikalische Geodäsie, Technische Universität München, 1978.

[Christodoulidis et al., 1988] Christodoulidis, D., D. E. Smith, R. G. Williamson and S. M. Klosko, Observed tidal braking in the Earth/Moon/Sun system, *J. Geophys. Res.*, 93(B6), 6216-6236, 1988.

[Ciufolini, 1986] Ciufolini, I., Measurement of Lense-Thirring drag on high-altitude laser ranged artificial satellite, *Phys. Rev. Lett.*, 56(4), 278-281, 1986.

[Ciufolini, 1987] Ciufolini I., The LAGEOS Lense-Thirring precession and the LAGEOS non-gravitational nodal perturbations-I, *Celest. Mech.*, 40, 19-33, 1987.

[Ciufolini, 1989] Ciufolini, I., A comprehensive introduction to the LAGEOS gravitomagnetic experiment: from the importance of the gravitomagnetic field in physics to preliminary error analysis and error budget, *Int. J. of Mod. Phys. A*, 4(13), 3083-3145, 1989.

[Ciufolini and Matzner, 1992] Ciufolini, I., and R. Matzner, Non-Riemannian theories of gravity and lunar and satellite laser ranging, *Int. J. of Mod. Phys.*, 7(4), 843-852, 1992.

[Ciufolini and Wheeler, 1995] Ciufolini, I., and J. A. Wheeler, *Gravitation and Inertia*, 498 pp., Princeton University Press, New York, 1995.

[Ciufolini, 1996] Ciufolini, I., On a new method to measure the gravitomagnetic field using two orbiting satellites, *Il Nuovo Cimento*, 109A(12), 1709-1720, 1996.

[Ciufolini et al., 1996] Ciufolini I., D. Lucchesi, F. Vespe and A. Mandiello, Measurement of dragging of inertial frames and gravitomagnetic field using laser-ranged satellites, *Il Nuovo Cimento* 109A(5), 575-590, 1996.

[Ciufolini et al., 1997] Ciufolini, I., F. Chieppa, D. Lucchesi, and F. Vespe, Test of Lense-Thirring orbital shift due to spin, *Class. Quantum Grav.*, 14(10), 2701-2726, 1997.

[Ciufolini et al., 1998] Ciufolini, I., E. Pavlis, F. Chieppa, E. Fernandes-Vieira, and J. Pérez-Mercader, Test of General Relativity and Measurement of the Lense-Thirring Effect with Two Earth Satellites, *Science*, 279, 2100-2103, 1998.

[Ciufolini, 1998] Ciufolini, I., Accurate Test of the Relativistic Perigee Precession and Measurement of the Relativistic Parameters β and γ using LARES, in *LARES Phase-A Study*, pp. 39-40, Rome, 1998.

[Ciufolini and Matzner, 1998] Ciufolini, I., and R. Matzner, Phenomena Due to the Rotation of a Mass and the Gravitomagnetic Field in Einstein's General Relativity, in *LARES Phase-A Study*, pp. 2-5, Rome, 1998.

[Ciufolini, 2000] Ciufolini, I., The 1995-99 measurements of the Lense-Thirring effect using laser-ranged satellites, *Class. Quantum Grav.*, 17,(12), 2369-2380, 2000.

[Cohen and Mashhoon, 1993] Cohen, J. M., and B. Mashhoon, Standard clocks, interferometry, and gravitomagnetic, *Physics Letters A*181, 353-358, 1993.

[Dahlen, 1972] Dahlen, F. A., Elastic Dislocation Theory for a Self-Gravitating Elastic Configuration with an Initial Static Stress Field, *Geophys. J. R. Astr. Soc.*, 28, 357-383, 1972.

[Defant, 1961] Defant, A., *Physical Oceanography*, vol. 2, 598 pp., Pergamon Press, New York, 1961.

[Dehant et al., 1999] Dehant, V., P. Defraigne, and J. M. Wahr, Tides for a convective Earth, *J. Geophys. Res.*, 104(B1), 1035-1058, 1999.

[Doodson, 1921] Doodson, A. T., The harmonic development of tide generating potential, *Proc. R. Soc. A.*, 100, 305-329, 1921.

[Dow, 1988] Dow, J. M., Ocean Tides and Tectonic Plate Motions from Lageos, Ph. D. thesis, München, 1988.

[Draper and Smith, 1981] Draper, N. R., and H. Smith, *Applied Regression Analysis*, 709 pp., 2nd edition, Wiley Series in Probability and Mathematical Statistics, Wiley, 1981.

[Dronkers, 1964] Dronkers, J. J., *Tidal Computations*, 518 pp., North-Holland Publishing Company, Amsterdam, 1964.

[Dziewonski and Anderson, 1981] Dziewonski, A. D., and D. L. Anderson, Preliminary reference Earth model, *Phys. Earth Planet Inter.*, 25, 297-356, 1981.

[Eanes et al., 1983] Eanes, R. J., B. Schutz, and B. D. Tapley, Earth and Ocean Tide Effects on Lageos and Starlette, in *Proceedings of the Ninth International Symposium on Earth Tides*, pp. 239-249, ed. J. T. Kuo, E. Schweizerbart'sche Verlagbuchhandlung, Stuttgart, 1983.

[Eanes, 1995] Eanes, R. J., and S. V. Bettadpur, Temporal variability of Earth's gravitational field from satellite laser ranging observations, XXI General Assembly, IUGG, Boulder, Colorado, July 1995.

[Einstein, 1975] A. Einstein, *The meaning of Relativity*, 5th ed. Princeton University Press, New York, 1975.

[Elliott *et al.*, 1998] Elliott, A. A., R. W. Hellings, and J. K. Miller, PPN Gamma Results from the NEAR Conjunction, AAS 191st Meeting, Washington, DC, Session 48, no. 09, January 1998.

[Everitt *et al.*, 2001] Everitt, C.W.F., and other members of the Gravity Probe B team, Gravity Probe B: Countdown to Launch, in: Lämmerzahl, C., C.W.F. Everitt, and F.W. Hehl (Eds.), *Gyros, Clocks, Interferometers...:Testing Relativistic Gravity in Space*, Lecture Note in Physics 562, 507 pp., Springer Verlag, Berlin, 2001.

[Farrell, 1972] Farrell, W. E., Deformation of the Earth by surface load, *Rev. Geophys. Space Phys.*, 10, 761-797, 1972.

[Felsentreger and Marsh, 1978] Felsentreger, T. L., and J. G. Marsh, Tidal Perturbations on the Satellite 1967-92A, *J. Geophys. Res.*, 83(B4), 1837-1842, 1978.

[Fræschlé *et al.*, 1997] Fræschlé, M., F. Mignard, and F. Arenou, Determination of the PPN parameter γ with the Hipparcos data, ESA SP-402, 1997.

[GAIA, 2000] GAIA Science Advisory Group. GAIA: Composition, formation and evolution of the galaxy. Results of the Concept and Technology Study. Draft version available on as <http://astro.estec.esa.nl/GAIA> march-report.pdf, version 1.6, 2000.

[Gilbert and Dziewonski, 1975] Gilbert, F., and A. M. Dziewonski, An application of normal mode theory to the retrieval of structure parameters and source mechanisms for seismic spectra, *Philos. Trans. R., Soc. London, Ser. A*, 278, 187-269, 1975.

[Gill, 1982] Gill, A., *Atmosphere-Ocean Dynamics*, International Geophysics Series, vol. 30, 662 pp., Academic Press, New York, 1982.

[Goad and Douglas, 1978] Goad, C. C., and B. C. Douglas, Lunar Tidal Acceleration Obtained From Satellite-Derived Ocean Tide Parameters, *J. Geophys. Res.*, 83(B5), 2306-2310, 1978.

[*Godier and Rozelot*, 2000] Godier, S., and J.-P. Rozelot, The solar oblateness and its relationship with the structure of the tachocline and of the Sun's subsurface, *Astron. and Astrophys.*, 355, 365-374, 2000.

[*Godin*, 1972] Godin, G., *The analysis of tides*, 263 pp., Liverpool University Press, Liverpool, 1972.

[*Graffarend and Joos*, 1992] Graffarend, E.W., and G., Joos, in: Linkwitz, K., and U. Hangleiter (Eds.), Relativistic computation of geodetic satellite orbits, *Proceedings of the 21nd International Workshop on High Precision Navigation*, 19-29, Dümmeler Verlag, Bonn, 1992.

[*Gronwald et al.*, 1997] Gronwald, F., E. Gruber, H. Lichtenegger, and R. A. Puntigam, Gravity Probe C(lock) - Probing the gravitomagnetic field of the Earth by means of a clock experiment, *ESA SP-420*, 29-37, 1997.

[*Hartmann and Wenzel*, 1995] Hartmann, T., and H. G. Wenzel, Catalogue HW95 of the tide generating potential, *Bull. Info. Marées Terrestres*, 123, 9278-9301, 1995.

[*Hendershott and Munk*, 1970] Hendershott, M. C., and W. Munk, Tides, *A. Rev. Fluid Mech.*, 21, 205-224, 1970.

[*Hendershott*, 1972] Hendershott, M. C., The effects of solid earth deformations on global ocean tides, *Geophys. J. R. Astr. Soc.*, 29, 399-402, 1972.

[*Hendershott*, 1973] Hendershott, M. C., Ocean Tides, *EOS Trans., American Geophys. Union* 54, No 2, pp. 76-86, 1973.

[*Iorio*, 2001a] Iorio, L., Earth tides and Lense-Thirring effect, *Celest. Mech.*, 79(3), 201-230, 2001.

[*Iorio*, 2001b] Iorio, L., Satellite gravitational orbital perturbations and the gravitomagnetic clock effect, *Int. J. of Mod. Phys. D*, 10(4), 465-476, 2001.

[*Iorio*, 2001c] Iorio, L., Satellite non-gravitational orbital perturbations and the detection of the gravitomagnetic clock effect, *Class. and Quantum Grav.*, 18(20), 4303-4310, 2001.

[Iorio, 2001d] Iorio L., Solid and ocean Earth tides and the detection of some gravito-magnetic effects, in: Pascual-Sánchez, J.F., L. Floría, A. San Miguel, and F. Vicente (Eds.), *Proceedings of the XXIII Spanish Relativity Meeting on Reference Frames and Gravitomagnetism*, World Scientific, Singapore, 179-184, 2001.

[Iorio, 2001e] Iorio, L., An alternative derivation of the Lense-Thirring drag on the orbit of a test body, *Il Nuovo Cimento B*, 116(7), 777-789, 2001.

[Iorio and Pavlis, 2001] Iorio, L., and E. C. Pavlis, Tidal Satellite Perturbations and the Lense-Thirring Effect, *J. of the Geod. Soc. of Japan*, 47(1), 169-173, 2001.

[Jackson, 1962] J. D. Jackson, *Classical Electrodynamics*, 641 pp., Wiley, New York, 1962.

[Jentzsch, 1997] Jentzsch, G., Earth tides and Ocean Tidal Loading, in Wilhelm, H., W. Zürn, and H. G. Wenzel, *Tidal Phenomena*, 398 pp., Springer, Heidelberg, 1997.

[Kaula, 1966] Kaula, W. M., *Theory of Satellite Geodesy*, 124 pp., Blaisdell Publishing Company, Waltham, 1966.

[Lambeck *et al.*, 1974] Lambeck, K., A. Cazenave, and G. Balmino, Solid Earth and Ocean Tides Estimated from Satellite Orbit Analyses, *Rev. Geophys. Space Phys.*, 12, 421-434, 1974.

[Lambeck, 1977] Lambeck, K., Tidal dissipations in the oceans: astronomical, geophysical and oceanographic consequences, *Phil. Trans. R. Soc. Lond. A.*, 287, 545-594, 1977.

[Lämmerzahl *et al.*, 2001] Lämmerzahl, C., C.W.F. Everitt, and F.W. Hehl (Eds.), *Gyros, Clocks, Interferometers...: Testing Relativistic Gravity in Space*, Lecture Note in Physics 562, 507 pp., Springer Verlag, Berlin, 2001.

[Landau and Lifshitz, 1979] L. D. Landau, E. M. Lifshitz, *The Classical Theory of Fields*, 402 pp., Oxford University Press, 1979.

[Lebach *et al.*, 1995] Lebach, D. E., et al., Measurement of the solar Gravitational Deflection of Radio Waves using Very-Long-Baseline Interferometry, *Phys. Rev. Lett.*, 75, 1439-1442, 1995.

[Lemoine *et al.*, 1998] Lemoine, F. G., et al., The Development of the Joint NASA GSFC and the National Imagery Mapping Agency (NIMA) Geopotential Model EGM96, NASA/TP-1998-206861, 1998.

[Lense and Thirring, 1918] Lense, J., and H. Thirring, Über den Einfluss der Eigen-rotation der Zentralkörper auf die Bewegung der Planeten und Monde nach der Einsteinschen Gravitationstheorie, *Phys. Z.*, 19, 156-163, 1918, translated by Mashhoon, B., F. W. Hehl, and D. S. Theiss, On the Gravitational Effects of Rotating Masses: The Thirring-Lense Papers, *Gen. Rel. Grav.*, 16, 711-750, 1984.

[Lichtenegger *et al.*, 2000] Lichtenegger, H. I. M., F. Gronwald, and B. Mashhoon, On detecting the gravitomagnetic field of the earth by means of orbiting clocks, *Adv. Space Res.* 25(6), 1255-1258, 2000.

[Lichtenegger *et al.*, 2001] Lichtenegger, H. I. M., W. Hausleitner, F. Gronwald, and B. Mashhoon, Some aspects on the observation of the gravitomagnetic clock effect, to appear in *Adv. Space Res.*, gr-qc/0101089, 2001.

[Love, 1926] Love, A. E. H., A Treatise on the Mathematical Theory of Elasticity, 643 pp., 4 th ed., Dover, Mineola, New York, 1926.

[Lucchesi, 2001] Lucchesi, D., Reassessment of the error modelling of non-gravitational perturbations on LAGEOS II and their impact in the Lense-Thirring determination. Part I, *Planetary Space Sci.* 40, 447-463, 2001.

[Mashhoon, 1993] Mashhoon, B., On the Gravitational Analogue of Larmor Theorem, *Phys. Lett. A*, 173, 347-354, 1993.

[Mashhoon *et al.*, 1999] Mashhoon, B., F. Gronwald, and D. S. Theiss, On Measuring Gravitomagnetism via Spaceborne Clocks: A Gravitomagnetic Clock Effect, *Annalen Phys.*, 8(2), 135-152, 1999.

[Mashhoon *et al.*, 2001] Mashhoon, B., F. Gronwald, and H. I. M. Lichtenegger, Gravitomagnetism and the Clock Effect, in: Lämmerzahl, C., C.W.F. Everitt, and F.W. Hehl (Eds.), *Gyros, Clocks, Interferometers...: Testing Relativistic Gravity in Space*, Lecture Note in Physics 562, 83-108, Springer Verlag, Berlin, 2001.

[Mashhoon, 2001] Mashhoon, B., Gravitoelectromagnetism, in: Pascual-Sánchez, J.F., L. Floría, A. San Miguel, and F. Vicente (Eds.), *Proceedings of the XXIII Spanish Relativity Meeting on Reference Frames and Gravitomagnetism*, World Scientific, Singapore, 121-132, 2001.

[Mathews *et al.*, 1995] Mathews, P. M., B. A. Buffet, and I. I. Shapiro, Love numbers for a rotating spheroidal Earth: New definitions and numerical values, *Geophys. Res. Lett.*, 22(5), 579-582, 1995.

[McCarthy, 1996] McCarthy, D. D., IERS conventions (1996), 95 pp., IERS Technical Note 21, U. S. Naval Observatory, 1996.

[Melchior, 1983] Melchior, P., *The Tides Of The Planet Earth*, 609 pp., Pergamon Press, New York, 1983.

[Métris *et al.*, 1997] Métris, G., D. Vokrouhlický J. C. Ries and R. Eanes, LAGEOS Eccentricity Excitations, *J. Geophys. Res.*, 102, 2711-2729, 1997.

[Métris *et al.*, 1999] Métris, G., D. Vokrouhlický, J. C. Ries, and R. J. Eanes, LAGEOS spin axis and non-gravitational excitations of its orbit, *Adv. Space Res.*, 23(4), 721-725, 1999.

[Milani *et al.*, 1987] Milani, A., P. Farinella and A. M. Nobili, *Non-Gravitational Perturbations and Satellite Geodesy*, 125 pp., Adam Hilger, Bristol, 1987.

[Milani *et al.*, 2001] Milani, A., A. Rossi, D. Vokrouhlický, D. Villani, and C. Bonanno, Gravity field and rotation state of Mercury from the BepiColombo Radio Science Experiment, *Planetary Space Sci.* 49, 1579-1596, 2001.

[Misner *et al.*, 1973] Misner, C. W., K. S. Thorne and J. A. Wheeler, *Gravitation*, 1279 pp., Freeman, San Francisco, 1973.

[Montenbruck and Gill, 2000] Montenbruck, O., and E. Gill, *Satellite Orbits: Models, Methods, Applications*, 383 pp., Springer, Berlin, 2000.

[Neumann, 1966] Neumann, G., and W. J. Pierson jr., *Principles Of Physical Oceanography*, 545 pp., Prentice-Hall, Englewood Cliffs, N. Y., 1966.

[Ni, 2001] Ni, Wei-Tou, Testing Relativistic Gravity and Measuring Solar System Parameters via Optical Space Missions, in: Lämmerzahl, C., C.W.F. Everitt, and F.W. Hehl (Eds.), *Gyros, Clocks, Interferometers...:Testing Relativistic Gravity in Space*, Lecture Note in Physics 562, 330-343, Springer Verlag, Berlin, 2001.

[Nordvedt, 1968a] Nordvedt, K., Equivalence Principle for Massive Bodies. I. Phenomenology, *Phys. Rev.*, 169, 1014-1016, 1968.

[Nordvedt, 1968b] Nordvedt, K., Equivalence Principle for Massive Bodies. II. Theory, *Phys. Rev.*, 169, 1017-1025, 1968.

[Nordvedt, 1968c] Nordvedt, K., Testing Relativity with Laser Ranging to the Moon, *Phys. Rev.*, 170, 1186-1187, 1968.

[Nordvedt, 1991] Nordvedt, K., Lunar laser ranging reexamined. The non-null relativistic contribution, *Phys. Rev. D*, 43, 3131-3135, 1991.

[Pagiatakis, 1990] Pagiatakis, S. D., The response of a realistic earth to ocean tide loading, *Geophys. J. Int.*, 103, 541-560, 1990.

[Pavlis, 2001] Pavlis, E. C., Geodetic Contributions to Gravitational Experiments in Space, to appear in: Cianci, R. (Ed.), *Recent Developments in General Relativity*, Springer Verlag, Milan, 2001.

[Pavlis and Iorio, 2001] Pavlis, E. C., and L. Iorio, The impact of tidal errors on the determination of the Lense-Thirring effect from satellite laser ranging, to be published in *Int. J. of Mod. Phys. D*, 2001.

[Pekeris and Akkad, 1969] Pekeris, C. L., and Y. Akkad, Solution of Laplace' s equations for M_2 tide in the world oceans, *Phil. Trans. R. Soc.*, 265, 413-436, 1969.

[Pireaux *et al.*, 2001] Pireaux, S., J.-P. Rozelot, and S. Godier, Solar quadrupole moment and purely relativistic gravitation contributions to Mercury's perihelion advance, astro-ph/0109032, submitted to *Astrophysics and Space Sciences*, 2001.

[Pitjeva, 1993] Pitjeva, E.V., Experimental testing of relativistic effects, variability of the gravitational constant and topography of Mercury surface from radar observations 1964-1989, *Celest. Mech.*, 55, 313-321, 1993.

[Priestley, 1981] Priestley, M. B., *Spectral analysis and time series*, Vol. 1-2, Academic Press, 1981.

[Radicchio, 1998] Radicchio, M., Misure di Relatività Generale e Fisica della Gravità: Studio delle Perturbazioni Gravitazionali del Perigeo del Lares, Degree thesis, Bari, 1998.

[Reasenberg, 1979] Reasenberg, R. D., *Viking* Relativity Experiment: Verification of Signal Retardation by Solar Gravity, *Astrophys. Jou.*, 234, 124-B5, L219-L221, 1979.

[Robertson and Carter, 1984] Robertson, D. S., and W. E. Carter, Relativistic deflection of radio signals in the solar Gravitational field measured with VLBI, *Nature*, 310, 572-574, 1984.

[Robertson *et al.*, 1991] Robertson, D. S., W. E. Carter, and W. H. Dillinger, New measurement of solar gravitational deflection of radio signals using VLBI, *Nature*, 349, 768-770, 1991.

[Roosbeek, 1996] Roosbeek, F., RATGP95: a harmonic development of the tide-generating potential using an analytical method, *Geophys. J. Int.*, 126, 197-204, 1996.

[Rosborough and Tapley, 1987] Rosborough, G. W., and B. D. Tapley, Radial, transverse and normal satellite position perturbations due to the geopotential, *Celest. Mech.*, 40, 409-421, 1987.

[Rubincam, 1987] Rubincam D. P., LAGEOS Orbit Decay Due to Infrared Radiation From Earth, *J. of Geophys. Res.*, 92, 1287-1294, 1987.

[*Rubincam*, 1990] Rubincam D. P., Drag on the LAGEOS Satellite, *J. of Geophys. Res.*, 95, 4881-4886, 1990.

[*Scheeres and Hu*, 2001] Scheeres, D.J., and W. Hu, Secular motion in a 2nd degree and order-gravity field with no rotation, *Celest. Mech. & Dyn. Astr.*, 79(3), 183-200, 2001.

[*Schneider*, 1988] Schneider M., Satellitengeodäsie, Bi. Inst., Wiss.-Verlag, Mannheim; Wien; Zürich, 1988.

[*Schwiderski*, 1980] Schwiderski, E. W., On charting global ocean tides, *Rev. Geophys. Space Phys.*, 18(1), 243-268, 1980.

[*Schwiderski*, 1981] Schwiderski, E. W., Global ocean tides: atlas of ocean tidal charts and maps, Tech. Rep. 2-10, Nav. Surface Weapons Cent., Dahlgren, Va., 1981.

[*Schwintzer*, 1997] Schwintzer, P., Satellite Orbit Perturbations Induced by Tidal Forces, in Wilhelm, H., W. Zürn, and H. G. Wenzel, *Tidal Phenomena*, 398 pp., Springer, Heidelberg, 1997.

[*Sehnal*, 1981] Sehnal L., Effects of the terrestrial infrared radiation pressure on the motion of an artificial satellite, *Celest. Mech.*, 25, 169-179, 1981.

[*Shapiro et al.*, 1972] Shapiro, I. et al., Mercury's Perihelion Advance: Determination By Radar, *Phys Rev. Lett.*, 28(24), 1594-1597, 1972.

[*Shapiro et al.*, 1976] Shapiro, I., C. Counselman, and R. King, Verification of the Principle of Equivalence for Massive Bodies, *Phys Rev. Lett.*, 36, 555-558, 1976.

[*Shapiro*, 1990] Shapiro, I., Solar system tests of general relativity: recent results and present plans, in: Ashby, N., D. Bartlett, and W. Wyss (Eds.), *Proceedings of the 12th International Conference on General Relativity and Gravitation*, University of Colorado at Boulder, 1989, Cambridge University Press, Cambridge, 313-330, 1990.

[*Shapiro*, 1999] Shapiro, I., A century of relativity, *Rev. Mod. Phys.*, 71(2), S41-S53, 1999.

[Shum *et al.*, 1995] Shum, C. K., J. C. Ries, and B. D. Tapley, The accuracy and applications of satellite altimetry, *Geophys. J. Int.*, 121, 321-336, 1995.

[Smith, 1974] Smith, M. L., The Scalar Equations of Infinitesimal Elastic-Gravitational Motion for a Rotating Slightly Elliptical Earth, *Geophys. J. R. Astr. Soc.*, 37, 491-526, 1974.

[Soffel, 1989] Soffel, M. H., *Relativity in Astrometry, Celestial Mechanics and Geodesy*, 208 pp., Springer, Berlin, Heidelberg, 1989.

[Sterne, 1960] Sterne, T. E., *An Introduction to Celestial Mechanics*, 206 pp., Interscience, New York, 1960.

[Tamura, 1987] Tamura, Y., A harmonic development of the tide-generating potential, *Bull. Info. Marées Terrestres*, 99, 6813-6855, 1987

[Tapley *et al.*, 1989] Tapley, B. D., J. C. Ries, R. J. Eanes, and M. Watkins, Simulation of an Experiment to Measure the Lense-Thirring Precession Using A Second Lageos Satellite, *Appendix A-1, Report No. CSR-89-3*, 104 pp., Center for Space Research, The University of Texas at Austin, Austin, Texas, 1989.

[Tapley, 1995] B. D. Tapley, The accuracy and applications of satellite altimetry, *Geophys. J. Int.*, 121, 321-336, 1995.

[Tartaglia, 2000a] A. Tartaglia, Geometric treatment of the gravitomagnetic clock effect, *Gen. Rel. and Grav.*, 32,(9), 1745-1756, 2000.

[Tartaglia, 2000b] A. Tartaglia, Detection of the gravitomagnetic clock effect, *Class. Quant. Grav.*, 17,(4) 783-792, 2000.

[Teyssandier, 1977a] P. Teyssandier, Rotating nonspherical masses and their effects on the precessions of a gyroscope, *Phys. Rev. D16*, 946-952, 1977.

[Teyssandier, 1977b] P. Teyssandier, Rotating stratified ellipsoids of revolution and their effects on the dragging of inertial frames, *Phys. Rev. D18*, 1037-1046, 1978.

[Tribble, 1995] Tribble A. C., *The Space Environment*, 204 pp., Princeton University Press, Princeton, 1995.

[Varga, 1998] Varga, P., Earth tidal phase lag and the tidal development of the Earth-Moon system, *Proceedings of the Thirteenth International Symposium on Earth Tides*, pp. 297-305, ed. B. Ducarme, P. Paquet, Observatoire Royal de Belgique, Brussels, 1998.

[Vespe, 1999] Vespe, F., The perturbations of Earth penumbra on LAGEOS II perigee and the measurement of Lense-Thirring gravitomagnetic effect, *Adv. Space Res.*, 23(4), 699-703, 1999.

[Vinti, 1998] J. P. Vinti, *Orbital and Celestial Mechanics*, 409 pp., edited by G. J. Der and N. L. Bonavito Progress in Astronautics and Aeronautics, Volume 177, 1998.

[Vladimirov et al., 1987] Y. Vladimirov, N. Miskievich, J. Horsky, *Space Time Gravitation*, 215 pp., Mir Publishers, Moscow, 1987.

[Wahr, 1981a] Wahr, J. M., A normal mode expansion for the forced response of a rotating earth, *Geophys. J. R. Astron. Soc.*, 64, 651-675, 1981a.

[Wahr, 1981b] Wahr, J. M., Body tides on an elliptical, rotating, elastic and oceanless earth, *Geophys. J. R. Astr. Soc.*, 64, 677-703, 1981b.

[Wang, 1994] Wang, R., Effect of rotation and ellipticity on Earth tides, *Geophys., J. Int.*, 117, 562-565, 1994.

[Wang, 1997] Wang, R., Tidal Response of the Solid Earth, in Wilhelm, H., W. Zürn, and H. G. Wenzel, *Tidal Phenomena*, 398 pp., Springer, Heidelberg, 1997.

[Will, 1993] Will, C M., *Theory and Experiment in Gravitational Physics*, 2nd edition, Cambridge University Press, Cambridge, 1993.

[Will, 2001] Will, C M., The Confrontation between General Relativity and Experiment, *Living Rev. Relativity* 2001-4 (January, 2001), [Article in Online Journal] cited on: 09 Aug 2001, <http://www.livingreviews.org/Articles/Volume4/2001-4will>.

[Williams *et al.*, 1996] Williams, J. G., X.X. Newhall, and J. O. Dickey, Relativity parameters determined from lunar laser-ranging, *Phys. Rev. D*53(12), 6730-6738, 1996.

[Williamson and Douglas, 1972] Williamson, R. G., and B. C. Douglas, HAP user's guide, *Rep. NAS-11726-163*, Wolf Res. and Dev. Corp., Riverdale, Md., 1972.

[Xi, 1987] Xi, Q., A new complete development of the tide-generating potential for the epoch J2000.0, *Bull. Info. Marées Terrestres*, 99, 6766-6812, 1987.

[Zahel, 1997] Zahel, W., Ocean Tides, in Wilhelm, H., W. Zürn, and H. G. Wenzel, *Tidal Phenomena*, 398 pp., Springer, Heidelberg, 1997.

WEB resources

- <http://wugrav.wustl.edu/People/CLIFF/tegp.html>, the experimental gravity web page.
- <http://www.livingreviews.org/Articles/Volume4/2001-4will/index.html>, recent review of the current status of the empirical basis of General Relativity.
- <http://www.laeff.esa.es/eng/laeff/activity/lageos3.html>
- <http://w3.ing.uniroma1.it/tildespacedpt/lares.html>, on LAGEOS III-LARES project.
- <http://earth.agu.org/revgeophys/marsha01/node1.html>, on the force models acting on LAGEOS satellites.
- <http://einstein.stanford.edu/index.html>
- <http://www.nas.edu/ssb/gpbexe.html>, on the GP-B mission.
- <http://op.gfz-potsdam.de/champ/>
- <http://op.gfz-potsdam.de/grace/>, on the CHAMP and GRACE missions.
- <http://ilrs.gsfc.nasa.gov/>, the International Laser Ranging Service web site.
- <http://www.ee.surrey.ac.uk/SSC/SSHP/>, small satellites web site.
- <http://cddisa.gsfc.nasa.gov/926/egm96/egm96.html>, the EGM96 Earth gravity model.
- <http://co-ops.nos.noaa.gov/restles1.html>, on the phenomenon of Earth tides.
- [http://www.astro.oma.be/D1/EARTH\\$_TIDES/wgtide.html](http://www.astro.oma.be/D1/EARTH$_TIDES/wgtide.html), home page of the Working Group of Theoretical Tidal Model of the Earth Tide Commission.
- <http://www.ill.fr/tas/matlab/doc/mfit.html>, useful collection of MATLAB least squares programs and other routines.